Universitat Autònoma de Barcelona

Use of 234Th:238U disequilibrium to estimate particulate organic carbon export in the upper ocean

Viena Puigcorbé Lacueva

USE OF ^{234}Th:^{238}U DISEQUILIBRIUM TO ESTIMATE PARTICULATE ORGANIC CARBON EXPORT IN THE UPPER OCEAN

VIENA PUIGCORBÉ LACUEVA

TESI DOCTORAL 2016

DIRECTORS
DR. PERE MASQUÉ BARRI
DRA. CLAUDIA BENITEZ-NELSON

UNIVERSITAT AUTÒNOMA DE BARCELONA
INSTITUT DE CIÈNCIA I TECNOLOGIA AMBIENTALS

UNIVERSITAT AUTÒNOMA DE BARCELONA

INSTITUT DE CIÈNCIA I TECNOLOGIA AMBIENTALS

TESI DOCTORAL

Doctorat en ciencia i Tecnologia ambientals

Setembre 2016

Use of ^{234}Th:^{238}U disequilibrium to estimate particulate organic carbon export in the upper ocean

Viena Puigcorbé Lacueva

Directors:

Dr. Pere Masqué Barri

Dra. Claudia Benitez-Nelson

Aquesta Tesi doctoral ha estat finançada mitjançant una Beca del Programa de Formación de Personal Universitario (FPU) del Ministerio de Educación, Cultura y Deporte (AP2009-4733), des de l'any 2010 fins al 2014.

El finançament econòmic també ha provingut dels següents projectes d'investigació, així com del grup de recerca consolidat MERS (2014 SGR-1356) de la Generalitat de Catalunya.

- Export and remineralisation rates of particulate organic carbon in Southern Ocean eddies
  Ministerio de Ciencia e Innovación (CTM2011-14027-E)

- Radionúclidos artificiales en el Océano Atlántico 4 décadas después de GEOSECS.
  Ministerio de Ciencia e Innovación (CTM2010-10267-E)

- Nitrogen fixation and its coupling with denitrification in the Eastern Tropical North Pacific.
  Ministerio de Educación y Ciencia (CTM2007-31241-E)

- Carbon export: New approaches for understanding organic carbon uptake.
  Marie Curie International Incoming Fellowships, FP7-PEOPLE-2007-4-2-IIF

Coberta dissenyada per Xavi Alsina

Man cannot discover new oceans
unless he has the courage to lose sight of the shore

Andre Gide

AGRAÏMENTS/ACKNOWLEDGMENTS

Ha estat un camí llarg però finalment aquesta tesi doctoral és una realitat. Avui escric aquestes línies recordant la multitud de bons moments viscuts al costat de persones que han fet que no només aquesta tesi hagi arribat a bon port, sinó que també han fet que gaudís del camí fent que el trajecte fos d'allò més excitant, divertit i gratificant.

First of all I want to thank my PhD supervisors, Pere and Claudia. I started to work with both of you when I was still doing my Bachelors. I was sent to participate on my first research cruise and I instantaneously fell in love with the world of oceanographic research. Since then, there have been many more expeditions, but I am still passionate about going to sea; no matter what regions, there is always something new to explore. I think part of that enthusiasm is due to having you as supervisors, since both of you are extremely active and exited about a wide variety of topics. You have fed my passion of going to sea and always supported me, even when you probably thought it was not the smartest decision if one was planning to finish a PhD thesis, and for that I will be eternally grateful. I know the academic world is competitive and papers seem to be the only thing that matters nowadays, but you have always been patient and supportive, clearly valuing other aspects of research that had a much deeper impact on me as a person. Thanks for giving me the opportunity to work with you, for all the support, knowledge and advice provided. It has been a great pleasure and hopefully it will not finish here.

Em sento extremadament afortunada per haver tingut els companys de grup que he tingut. Heu estat una peça clau del meu dia a dia, heu fet de tots aquests anys un record inoblidable. Gràcies a vosaltres he tirat endavant quan el que em venien ganes de fer era plegar veles i triar l'opció cocotero. Moltes gràcies pel recolzament, per tots els moments fantàstics compartits i per la vostra amistat. Sé que acabar el doctorat no implicarà perdre el contacte amb vosaltres perquè sou molt més que companys de laboratori. Vull començar donant les gràcies al Jordi perquè tu vas ser el que em vas iniciar en el món de la radioactivitat ambiental i ets el culpable que els radioisòtops es convertissin en la meva passió aquell curs 2005/06 (si si, ara fa 10 anys!!!). Sempre has estat disponible i ajudant quan ha fet falta, amb la millor de les actituds i amb bon humor. Gràcies per ser un jefe que aporta tan bon ambient al grup, amb tanta motivació i tan involucrat en tot, fins i tot quan ja no queden més minuts lliures per res. Moltes gràcies Joan Manuel per tot el suport que m'has donat durant tots aquests anys, en el lab (amb les depos i mesurant discs de Pb-Po del dret i del revés tantes vegades com ha fet falta amb molta paciència), com preparant campanyes com fins i tot participant-ne en una. Saps que sense tu donant un cop de mà quan fes falta, arribar fins aquí

hagués estat molt més dur. Valentí, vam començar junts però em vas avançar ben avançada, eh. Ets un crack. Fer aquest camí amb tu ha estat fantàstic i només m'enduc bons records. Encara que estiguem lluny lluny lluny sempre estàs a prop quan més falta fa i estic molt agraïda i feliç de poder comptar amb tu com a company de feina i com a amic. Muntsa, quins inicis més intensos que vam tenir. Vas començar en el món de la recerca oceanogràfica ben forta: anant a una campanya de dos mesos al Southern Ocean. Si t'he de ser sincera, patia una mica perquè gairebé no et coneixia i 64 dies al Southern Ocean no tothom els porta bé, però com dic, patia perquè encara no et coneixia. Tu t'hi vas llençar de cap i el resultat va ser espectacular. Ets treballadora i aplicada i, al mateix temps, divertida i relaxada. Anar de campanya amb tu va ser un veritable plaer i passar gairebé 6 mesos voltant de punta a punta (literalment) del món amb tu és un dels millors records que tinc d'aquest doctorat. Gràcies per fer-ho tot tan fàcil, per ser tan positiva i per tota la motivació i ànims que em dónes. Potser semblava que no però el "Ho fas molt bé, Viena!" em donava moltes forces. Ara una campanya més ens portarà a les dues a l'Antàrtida i estic feliç de tenir-te altre cop de companya d'aventures navegant pel Southern Ocean altre cop, tal com vam començar. Giada, al final tú también me adelantaste, eh. Admiro tu hacer y tu determinación. Poquito a poco te hiciste tu hueco hasta convertirte en una parte vital del LRA y hoy escribo estas línias justo el día que defiendes tu tesis. Preparando tu regalo recordé todos los momentos compartidos, quizás más fuera del laboratorio que dentro, pero buenos momentos en cualquier caso. Gracias porque a veces, sin decir nada decías mucho, por compartir el spring final de nuestras tesis i darme fuerzas para seguir tu ejemplo y llegar al día de hoy donde yo también cruzo la línia de la meta. Maxi, llegaste al lab lleno de energía contagiosa y le diste un giro al LRA. Hasta conseguiste que fueramos de ruta por tus tierras y fuera una de las escapadas del LRA más memorables. Los primeros meses no sólo eras compañero de trabajo sino que eras mi vecino. Siento haberte fallado en alguno de esos momentos de "salimos a tomar una cerveza?", pero las que nos tomamos desahogándonos de nuestras inquietudes y preocupaciones de la vida del PhD fueron sanadoras. Gracias por esos "Aupa equipo!" y "Power!" que se han convertido en un "himno" para los del LRA, por los bolis bic en las rótulas y por todas las risas que has traído al grupo. Ariane, amb tu no només he compartit despatx, aquests darrers mesos hem compartit pis, però també alegries i penes. Recordo que quan vas entrar em deien que tu i jo ens enganxaríem perquè les dues tenim caràcter però tot el contrari, t'admiro perquè ets treballadora, molt positiva i tens caràcter però el treus quan toca, ets clara i no vas amb segones, ets súper vital i activa i ho contagies. Viure amb tu a Perth em va encantar, m'ho vaig passar molt bé i em va ajudar un munt tenir-te allà. Moltes gràcies, mi llave, per les vivències compartides, per saber escoltar i dir les coses com són. Espero veure't de nou per casa aviat. Almudena, con tu acento andalús y tu calidez nos enamoraste a todos e hiciste del LRA un sitio

más cálido. Gracias por tu alegría y buen humor, por siempre estar dispuesta a echar una mano y animarme cuando me has visto tocada. Espero que vengas a visitarme a Australia. La última incorporación del LRA, Sarah, con quien a pesar del poquito tiempo compartido, hemos podido explorar cuevas a 45 m de profundidad y subir a la copa de un árbol de unos 60 m (bueno, eso tú, yo animaba desde abajo). Aún con ese poquito que hemos compartido me ha quedado claro que eres una curranta, generosa y detallista y muy buena cocinera. Te deseo lo mejor en el doctorado que acabas de iniciar. Disfrútalo al máximo!

També vull donar les gràcies aquells companys del LRA que ja portaven un temps quan vaig aterrar-hi. A l'Eli, que va ser la meva mentora en el món de les campanyes oceanogràfiques i del ^{234}Th i el ^{210}Po-^{210}Pb. Gràcies per establir les bases a partir de les quals aquesta tesi ha anat creixent i per contagiar-me una mica la teva organització i ben fer, de no ser així això hauria pogut ser un desastre. Ester, vaig arribar que tu ja acabaves però encara vam tenir l'oportunitat d'anar juntes de campanya. Va ser en aquella FAMOSO 1 on et vaig conèixer una mica més, sempre divertida, treballadora i disposada a ajudar amb el que faci falta. Estic segura que, per més temps que passi i encara que marxis fora, el teu vincle amb el LRA es mantindrà perquè n'ets una part essencial. Gràcies per l'alegria que transmets, per ser tan energètica, protectora i bona persona. Núria, amb tu vaig fer una de les primeres campanyes (la FAMOSO 2) i ara fa un any vam fer juntes la que seria la meva última campanya com a doctorant (pensava que no arribaria mai aquesta campanya jeje). M'has acompanyat al llarg de tots aquests anys i t'agreixo molt el suport i els consells que m'has donat des que vaig trepitjar el LRA per primera vegada, intentant que no em compliqui i que vagi al que he d'anar. Ara estàs a Suïssa però és com si no haguessis marxat (sobretot quan escolto els missatges de veu llarguíssims que ens enviem i que sempre em fan riure tant). Gràcies pel suport, les confidències i els bons moments que hem compartit, tant dins com fora del lab. Carolina, gràcies per fer que tots aquells números que se'm resistien cobressin sentit. Vas fer que la física de les radiacions fos molt més atractiva del que semblava a primer cop d'ull i si he acabat aquí és, en gran part, gràcies a tu. César y Patri, coincidimos durante los primeros años de mi incorporación al grupo y seguisteis caminos distintos pero también quiero agradeceros los ratos compartidos en el LRA. Teresa, empezamos juntas y juntas estamos terminando. Gracias por hacerme sentir acompañada en este tramo final. Muchos ánimos y suerte con todo! Sou uns quants els que heu passat pel grup durant un temps més o menys llarg, enriquint-lo i fent-lo créixer: María, contigo me inicié en el mundo de la radioquímica. Gracias por todo lo que me enseñaste, por la paciencia y por esos abrazo que son abrazos de verdad. Mercè, quatre campanyes juntes, que es diu ràpid. Hem creuat mig Atlàntic i, si ens arriben a donar més CTDs, el buidem. Gràcies pel teu esperit de

superació i la teva curiositat contagiosa. Karina, Oriol, Esther, Marta, Yi, Marc, Xènia, Aaron i Marc, gràcies per haver passat pel laboratori deixant bons moments per recordar.

Gràcies a la resta de companys del grup de Física de les Radiacions, en especial al Lluís Font, perquè els petits gests són realment importants, i també als técnics, en especial al Manel, que m'han donat suport construint i arreglant diversitat d'instruments, sempre aportant noves idees per intentar millorar tant com es pugui. Gràcies al Jordi Mompart perquè sempre té un somriure.

I would need an additional volume of this thesis to express my gratitude to all the people that have been on oceanographic expeditions with me and that, in one way or another, have had an impact on my research and on myself. I want to acknowlegde all the colleagues and the crew members of all those expeditions because spending so much time at sea can be complicated, but I always had great people around that made my life on the ships so memorable.

In particular, I want to thank Debora, Jason, Paulina and Efrain, from the GoCal4 expedition, to make of my baptisme in oceanographic expeditions such a successful experience. A los participantes de las campañas FAMOSO, a los que no puedo mencionar uno por uno porque la lista es extensísima, con los que siempre fue un placer trabajar y pasar las tormentas en Palamós. To the participants of the R/V Pelagia cruises, in particular to Michiel, Micha, Loes, Sven, Patrick and Steven, you are all amazing scientist but additionally you are among the kindest people I have worked with. Also to Gabriel, because even though you were not on those cruises, we met because of them, we have a paper together (thanks for the opportunity) and we have been friends since that first meeting. To Eddy Pump group (and the red mafia) that worked tireless in the most multidisciplinary cruise I have ever been, but also knew how to enjoy the not-so-great weather conditions of the Southern Ocean during two entire months. Thanks also to the participants of the IceArc expedition, for the most special expedition I had from a personal side. The Arctic marked me and since then I fell in love with it. To the PS94 crew, with whom I finally got baptised after crossing the Artic Cercle for the second time. It was great to have the oportunity to go back to sea with some of you and to meet such a nice group of people with whom I am sure collaborations will arise easily. And last, but not least, to the Survivors family, because we kept calm under a complicated cruise and managed to achieve our goals with a smile and good mood, always finding the positive side.

Michiel, you deserve a special thank you because you have done so much for this thesis and for me. I had the great pleasure to work closely with you and you became a role model for me. Working with you has always been motivating and you can be sure that your passion for research has had an impact on me. If I have spent more than a year at sea it is because you facilitated many collaborations and research opportunities for me. All of them have allowed me to grow in this scientific world and for that I am grateful and I feel extremely lucky. Thank you also because, from a personal side, you are a caring person, good listener and you always gave me good advices and supported me when I had to make difficult decisions.

I want to warmly acknowledge Ingrid Stimac. You have been such a great support helping me with the logistics to join the Polarstern and Pelagia cruises, but also because of all the analyses and beta counting you have taken care of during all these years. Great part of the data here presented is thanks to your contribution. You have always been kind, helpful and extremely efficient and it is a pleasure to work with you.

Many thanks to Tom Church and Silvain Rigaud, for sharing their expertise and for their collaboration when I was beginning to explore the intricacies of the $^{210}Pb/^{210}Po$ world, and to Stephanie Morris, Ken Buesseler and Kanchan Maiti for sharing their data and knowledge whenever requested, for doing it quickly and being always helpful and willing to discuss whatever is necessary.

To all the coauthors of the papers here presented I want to say a big thank you! Thanks because you have been patient, provided really useful feedback and made this thesis possible. I am really glad I had the chance to closely collaborate with all of you and I hope there will be more papers to come where we can work together again. Many thanks also to those that have counted on me to contribute in their publications.

Gracias a todos aquellos que habéis convivido conmigo durante este periodo, especialmente a Fede y Bea, que habéis sufrido conmmigo la recta final de esta tesis y me habéis apoyado y animado en todo momento con mucha paciencia. Gracias también a Fer, porque llegaste hace poco pero en nada le diste un giro a la casa, haciendo que los últimos días fueran de lo más entretenidos.

Thank you Shane because you lived with me part of this thesis and you were always supportive and made things easy for me. You are also passionate about the ocean and showed real interest and enthusiasm for what I was doing, never complaining when I asked for help with my English and

always motivating me to work hard and to do whatever was necessary to achieve my goals, even if it meant spending a lot of time at sea.

Dani, ja acabem! Moltes gràcies per tots els cafès compartits. Sempre és un plaer quedar amb tu, parlar de mil temes diferents i compartir inquietuds. No sé quin camí seguiràs un cop doctorat, però de debó espero que segueixis en ciència perquè ets molt bo i quan expliques el que fas trasnmets una passió que deixa veure clarament que t'encanta. En qualsevol cas, facis el que facis, espero seguir compartint molts més moments amb tu.

Gracias Pablo y Hortencia, porque hay vida fuera de la tesis y compartirla con vosotros es siempre un lujo. Grandes amigos, mejores personas! Tenemos pendientes un sinfín de viajes!

Gràcies Alba perquè sempre es pot comptar amb tu. Ets una de les persones més fortes i treballadores que conec i a més m'ho passo molt bé amb tu! Aquesta tesi no seria la que és sense tu, literalment. Saps que t'estic infinitament agraïda per les hores que m'has dedicat, per la teva paciència inesgotable, bon humor, però sobretot per la teva amistat. Ets una gran amiga i t'estimo molt, encara que mai t'ho digui.

Gràcies als meus pares perquè sempre m'heu donat suport en totes les decisions que he pres i m'heu animat a tirar endavant, a esforçar-me pel que vull, sense posar límits de cap mena i donant-me forces quan més m'han fet falta.

Ich war nicht sicher, ob ich diese Zeilen schreiben würde, doch du verdienst es definitiv, in dieser Arbeit erwähnt zu werden, da du mit mir die letzten Jahre dieser Doktorarbeit geteilt hast und hätte ich die Zielgerade gerne mit dir zusammen überquert. Ich weiß, dass es nicht immer einfach war, was du durchmachen musstest, aber du hieltest mich immer zum Weitermachen an und hast mich unterstützt, wenn Unsicherheiten überhand nahmen. Du warst geduldig und verständnisvoll, aber vor allem machtest du mich wirklich sehr glücklich. Ich bin dankbar für die Zeit und die Erfahrungen, die wir teilten. Ich bin nicht traurig, dass es vorbei ist, ich bin glücklich, dass es passiert ist.

Gràcies a tots els que sense voler he oblidat d'incloure però que han estat al meu costat durant aquests anys. Gracias a todos los que sin querer olvidé mencionar pero que han estado a mi lado durante estos años. Thanks to all those that I forgot to mention but that have been by my side during these years.

Moltes gràcies — Muchas gracias – Many thanks

TABLE OF CONTENTS

LIST OF FIGURES

LIST OF TABLES

ABSTRACT

The particulate export of photosynthetically fixed carbon from the surface ocean to the ocean interior by marine plankton is a key component of the biological carbon pump and, by extension, of the global carbon cycle as it helps to maintain atmospheric CO_2 levels lower than would occur with out this process (Feely et al., 2001; Khatiwala et al., 2009; Parekh et al., 2006). Particle cycling and export are also essential for the biogeochemical cycles of other major nutrients and chemical species of vital importance for marine biota, as well as anthropogenic metals and pollutans.

The radiotracer pair ^{238}U:^{234}Th as been commonly and extensively used to study particle export and determine the strength of the biological carbon pump in the upper ocean (Coale and Bruland, 1985; Le Moigne et al., 2013b). This thesis evaluates oceanic carbon export fluxes and the efficiency of the biologically mediated sequestration using this naturally occurring radiotracer pair in a variety of regimes under contrasting biogeochemical conditions.

First, basin-scale export variability was examined in the North Western Atlantic Ocean along a latitudinal transect (from 64ºN to the equator) with high spatial resolution, providing additional data in under sampled areas. The results agreed with previous studies carried out in the North Atlantic and were also compared with different satellite-derived export models. These models have a strong dependence on sea surface temperature and net primary productivity estimates, but they usually do not consider biological parameters that influence carbon export, such as the trophic structure, the grazing intensity, the recycling efficiency, the bacterial activity and the dissolved organic carbon export (Maiti et al., 2013). The differences observed between the satellite-derived and the ^{234}Th-derived carbon export estimates highlights the necessity to include such biological parameters at a regional scale, for which continued observing efforts are needed. This would thereby reduce uncertainty in the global carbon budget and improve carbon cycle monitoring from satellite-based platforms.

Second, the zonation of surface properties derived from the various fronts crossed along a 10ºE transect, from 44ºS to 53ºS, in the Antarctic Circumpolar Current were evaluated in relation to particle export. Our results show that, despite the contrasting food webs encountered north and south of the Antarctic Polar Front (~49ºS), the magnitude of the carbon export fluxes were similar along the transect. However, differences appeared when examining transfer efficiencies: in the northern section, which was dominated by nanophytoplankton, presented high export efficiencies and reduced transfer efficiencies in comparison to the southern section, dominated by

microphytoplankton. Thus, and although different food web regimes led to similar export of carbon, the sinking particle pools differed in their composition north and south of the Antarctic Polar Front (aggregates of small particles in the north *vs* fast-sinking large particles in the south), resulting in two different scenarios regarding the amount of exported carbon that reached greater depths.

Finally, estimates of particle flux and export efficiency were examined in a semi-enclosed basin (Gulf of California and the surrounding waters of the Eastern Tropical North Pacific), with a strong seasonality that leads to changes in the planktonic community. Export estimates were assessed using the ^{234}Th approach in combination with surface-tethered sediment traps. Data on size fractionation and high vertical resolution of *in situ* pump deployments allowed a comparison of the C/^{234}Th ratios attenuation with depth between small (1-53 μm) and large (>53 μm) particles. Results indicate that, under dominance of pico- and nanoplankton and with presence of diazotrophs, small particles play and important role in carbon export and that this export might be more efficient than that resulting from a diatom dominated planktonic community in the study area.

THESIS STRUCTURE

This dissertation is organized in six chapters:

Chapter 1 is a general introduction that provides the context for the work presented in this thesis, which aims to evaluate the particle flux and carbon export efficiency from the surface ocean through the mesopelagic zone using the naturally occurring radioisotope ^{234}Th as a particle tracer. The increase of atmospheric carbon dioxide (CO_2) due to anthropogenic emissions and the climatic consequences of such increases are briefly presented. The sources and sinks of atmospheric CO_2 are then described, followed by a short description of the importance of the oceans as a CO_2 sink. In this regard, attention is paid to the biological carbon pump as a CO_2 sequestration mechanism, highlighting the complexity and uncertainties that exist regarding its magnitude and variability. This chapter finishes with a brief description of the different methodologies that are used to estimate export fluxes and therefore determine the strength of the biological carbon pump, with special emphasis on the use of the ^{234}Th method, which is described in *Chapter 2*.

Chapter 2 consists on the description of the ^{238}U:^{234}Th approach to determine particle export fluxes, describing the sampling techniques as well as the analytical procedures used for the determination of ^{234}Th and POC in both, seawater and particulate samples.

Chapters 3 to 5 are each independent studies devoted to investigating what controls the magnitude and downward transport efficiency of export from regional to basin scales and to provide new insights into the use of the ^{238}U:^{234}Th disequilibrium as a tracer for particle export.

Chapter 3 is a basin-scale study that examines export variability across the North Atlantic derived from a high spatial resolution latitudinal transect in the western basin (0º-64ºN). This work was conducted within the framework of the international GEOTRACES Program (www.geotraces.org), whose aim is to improve the understanding of biogeochemical cycles and large-scale distribution of trace elements and their isotopes in the marine environment. This study also includes a compilation of previous work that was conducted in this area using the same methodology and discusses the necessity of basin-wide and temporal coverage to account for seasonal variability. A comparison with satellite-derived export models is also presented in this chapter in order to assess the

agreement on carbon export estimated obtained with the ^{234}Th-derived and satellite-based approaches. This chapter has been recently submitted for publication in *Deep Sea Research-I*[1].

The influence of the overlaying community structure on the particle and carbon export flux is evaluated in ***Chapter 4***. In the Antarctic Circumpolar Current the zonation due to frontal boundaries that can lead to drastic changes in the planktonic community. This work investigates the physical, biological and biogeochemical characteristics of part of the Atlantic sector of the Antarctic Circumpolar Current to study the impact of the frontal zones on the export of particulate oganic carbon from the upper ocean. A paper synthesizing our major findings has been published in *Deep Sea Research II*[2].

Chapter 5 is dedicated to the study of the export fluxes in a warm and semi-enclosed sea. The oceanographic characteristics of the study area provide an excellent opportunity to study the linkages between surface productivity and particulate export fluxes under oceanographic conditions similar to those expected in a future warmer ocean. This chapter also discusses the differences between different sampling techniques (*in situ* pumps vs sediment traps) for particulate samples and how these particles are attenuated with depth depending on the particle size. This work has been published in *Global Biogeochemical Cycles*[3].

Finally, ***Chapter 6*** includes the most relevant conclusions of this dissertation and a number of research priorities and recommendations for future studies.

---

[1] Puigcorbé V., M. Roca-Martí, P. Masqué, C. R. Benitez-Nelson, M. Rutgers v.d. Loeff, A. Bracher, S. Moreau (*submitted*). Latitudinal distributions of particulate carbon export across the North Western Atlantic Ocean. *Deep-Sea Research-I*.

[2] Puigcorbé V., M. Roca-Martí, P. Masqué, C. R. Benitez-Nelson, M. Rutgers v.d. Loeff, L.M. Laglera, A. Bracher, W. Cheah, V.H. Strass, M. Hoppema, J. Santos-Echeandía, B.P.V. Hunt, E.A. Pakhomov, C. Klaas (2016). Particulate organic carbon export across the Antarctic Circumpolar Current at 10°E: Differences between north and south of the Antarctic Polar Front. *Deep-Sea Research II*. doi: 10.1016/j.dsr2.2016.05.016

[3] Puigcorbé, V., C. R. Benitez-Nelson, P. Masqué, E. Verdeny, A. E. White, B. N. Popp, F. G. Prahl, and P. J. Lam (2015), Small phytoplankton drive high summertime carbon and nutrient export in the Gulf of California and Eastern Tropical North Pacific, *Global Biogeochem. Cycles*, 29, 1309–1332, doi:10.1002/2015GB005134.

Chapter 1:

Introduction

1 Introduction

1.1 Atmospheric carbon dioxide and global climate change

The natural processes of the global climate system are being affected by human activities, thus influencing present day climate (Karl and Trenberth, 2003). Evidence indicate that an important source of global climate change is human-induced changes on atmospheric composition, particularly carbon dioxide (CO_2) (Lacis et al., 2010). CO_2 concentrations in the atmosphere have dramatically increased since the industrial revolution, from less than 300 parts per million (ppm) (Joos and Spahni, 2008) to more than 400 ppm (NOAA, 2016, preliminary data). It is hypothesized that this increase is one of the main drivers of the rise in the mean global temperature (IPCC, 2007).

Although there are likely some negative feedbacks, compensating for the CO_2 increase in the atmosphere, such as an increase in primary productivity in the Arctic (Arrigo et al., 2008; Frey et al., 2014), the majority of the responses expected at decadal time scales are positive (IPCC, 2014), i.e., ocean acidification (Feely et al., 2004), decrease of albedo due to snow/ice melting (Comiso et al., 2008), or ocean stratification and a possible consequent weakening of the North Atlantic thermohaline circulation (Joos et al., 1999; Pérez et al., 2013). Therefore, it is essential to consider all possible feedbacks and quantify their impact on the carbon system in order to apply socioeconomic measures, as well as possible geoengineering strategies (Latham et al., 2014) to minimize (MacMartin et al., 2014; Rasch et al., 2008) and stabilize atmospheric CO_2 concentrations (Kumar et al., 2011; Smetacek and Naqvi, 2008) (see also Climate Intervention report by National Research Council, 2015).

1.2 Carbon dioxide sources and sinks

The anthropogenic CO_2 emissions are mainly grouped into those derived from fossil-fuel combustion and cement production or due to land-use and land-cover change (Le Quéré et al., 2014). Data provided by the Carbon Dioxide Information Analysis Center (Boden et al., 2016; Houghton, 2008) shows the increasing trends of both sources, especially fossil-fuel carbon emissions, over the past >150 years (Figure 1.1).

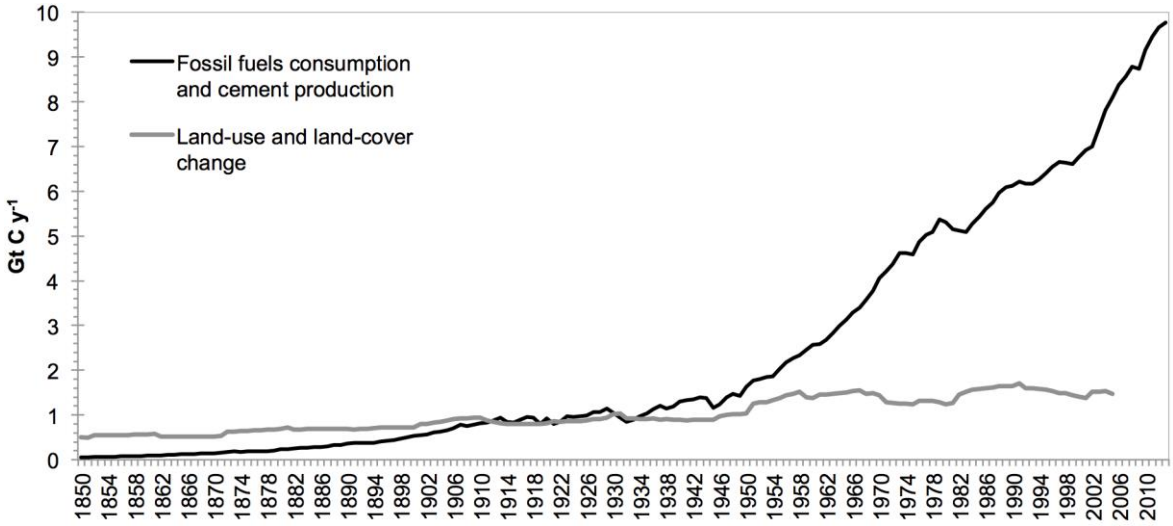

Figure 1.1: Annual global carbon emissions due to fossil-fuel consumption and cement production (data from (Boden et al., 2016) and land-use and land-cover change (data from Houghton, 2008) since 1850.

The changes in land-use and land-cover since 1980 represent an average global flux of 1.5 GtC^{1} y^{-1} (12.5% of anthropogenic carbon emissions from 1990 to 2010; Friedlingstein et al., 2010; Houghton et al., 2012) and 7.5 GtC y^{-1} for the fossil fuel combustion and cement production (from Boden et al. (2016) data from 1990 to 2013). When considering all of these inputs, one could expect atmospheric CO_2 levels significantly higher than what is currently measured. Indeed, the rise in atmospheric CO_2 is only about half of what is expected due to measured "CO_2 sinks" (IPCC, 2001; Parekh et al., 2006).

The oceans and the biosphere are natural carbon sinks, and the processes by which they remove CO_2 from the atmosphere are known as carbon sequestration, such as carbon uptake by physicochemical processes occurring in the oceans, or through the photosynthesis in the biosphere by photoautotrophic organisms in both terrestrial and marine systems. Global analyses show that the biosphere absorbs approximately 60% of anthropogenic CO_2 emissions, partitioned between absorption by the oceans and storage in terrestrial ecosystems (Khatiwala et al., 2009). The strength of these sinks, however, is temporally and spatially variable, as well as sensitive to climate change. Therefore, it is necessary to understand the natural mechanisms of CO_2 uptake if we are to predict future changes in atmospheric CO_2 concentrations and its subsequent impact on the biosphere.

[1] 1 GtC corresponds to 3.667 $GtCO_2$

1.3 The ocean as a CO_2 sink

The ocean plays a crucial role in the climate system through thermohaline circulation, which transfers warm waters from the tropics to the polar regions releasing heat to the atmosphere (Figure 1.2). The strength of this circulation, however, is sensitive to the changes in atmospheric CO_2 concentrations: the resulting increase in atmospheric temperatures, leading to weaker meridional temperature gradients and weaker zonal winds, directly affects sea surface temperatures and freshwater inputs and therefore increases ocean stratification and reduces deep convection (Pérez et al., 2013; Schmittner et al., 2007, 2005).

Due to its high heat capacity (i.e., the heat capacity of the upper 3.5 m layer of the ocean is equivalent to the heat capacity of the global atmosphere; Trenberth and Stepaniak, 2004), the ocean stores heat, ameliorating atmosphere temperature changes. Indeed, according to the last Intergovernmental Panel on Climate Change (IPCC, 2014), between 1971 and 2010 more than 60% of the net energy increase in the climate system has been stored in the upper ocean (0-700 m), and ~30% stored in the deeper ocean. In addition, oceans are not only storing heat, but they are also a significant sink for anthropogenic CO_2, taking up more than a fourth of the emissions arising from fossil-fuel use and land-use and land-cover change, representing the largest CO_2 reservoir (Sabine et al., 2004).

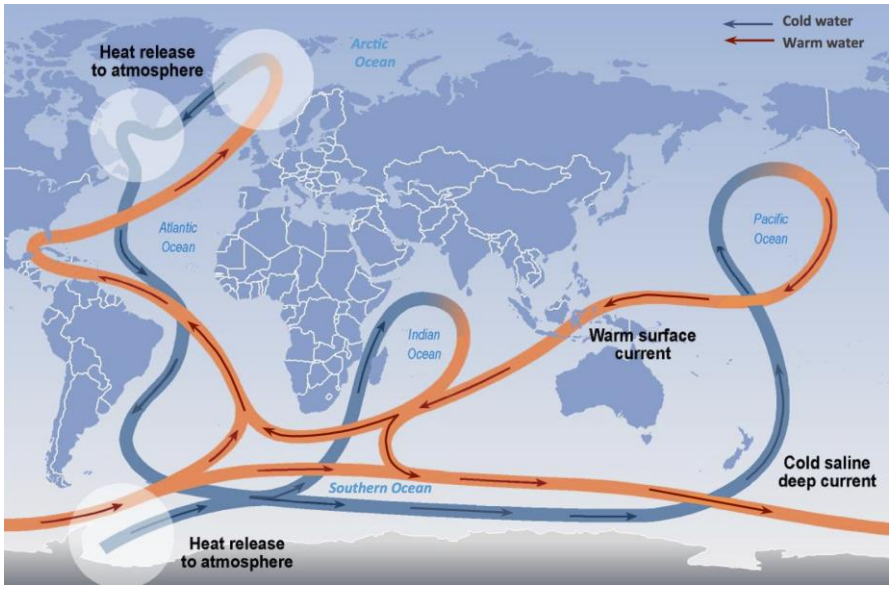

Figure 1.2: Thermohaline circulation. Adapted from IPCC 2001.

1.3.1 The Solubility Pump

Gas exchange between the surface layers of the ocean and the atmosphere allows the diffusion of CO_2 into the oceans. Most of this CO_2 reacts with seawater to form carbonic acid (H_2CO_3) and its dissociation products, bicarbonate (HCO_3^-) and carbonate (CO_3^{2-}) ions (Figure 1.3). The direction and magnitude of the sea-air CO_2 transfer flux are primarily driven by the partial pressure of CO_2 (pCO_2) in surface waters, which is mainly controlled by seawater temperature and biological utilization of CO_2.

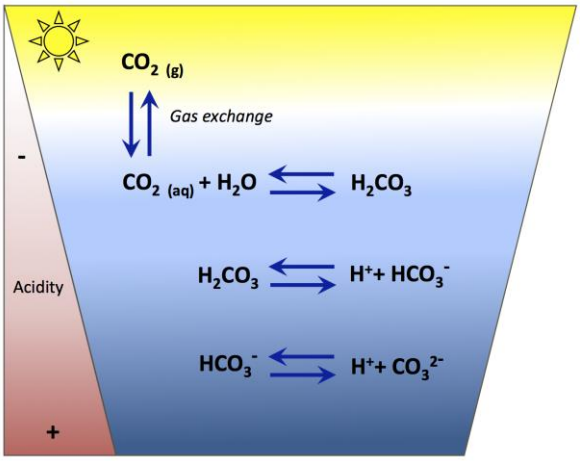

Figure 1.3: Carbonate system equilibrium equations.

With low sea surface temperatures, the solubility of CO_2 increases. CO_2 is therefore removed more efficiently from the atmosphere at high latitudes, and is sequestered when those cold (and CO_2-rich) surface waters subduct and form North Atlantic Deep Water or Antarctic Intermediate and Deep Waters (Figure 1.4). Thermohaline circulation therefore favors the uptake of atmospheric CO_2 and sequestration from the atmosphere for up to ~1000 years, until the deep ocean waters regain contact with the surface. These physicochemical processes that transport CO_2 from the ocean's surface to its interior are commonly known as the "solubility pump", which accounts for 30-40% of the dissolved inorganic carbon gradient from surface to depth (Toggweiler et al., 2003).

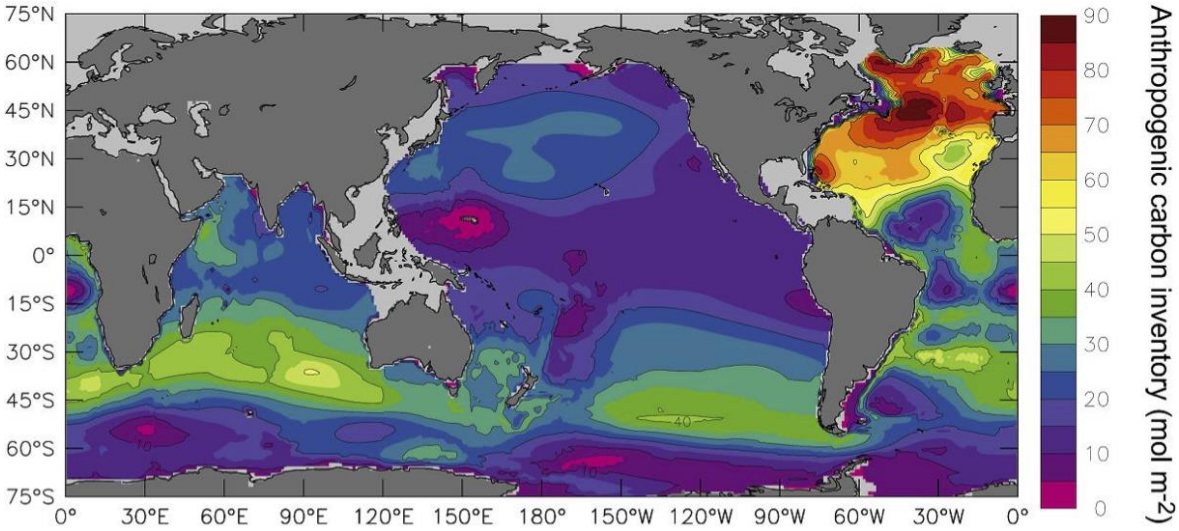

Figure 1.4: Column inventory of anthropogenic carbon (mol m^{-2}) as of 1994 from Sabine et al. (2004). The global inventory of anthropogenic carbon uptake by the ocean between 1750 and 1994 is estimated to be 118 ± 19 Gt C (IPCC, 2007).

1.3.2 The Biological Carbon Pump

Another major mechanism by which the ocean is able to remove CO_2 from the atmosphere and keep it isolated for long periods of time is through biologically mediated processes. Phytoplankton convert CO_2 into fixed carbon, e.g. carbohydrates or calcium carbonate, and produces oxygen through photosynthesis (primary production; PP). This fixed carbon is then used by heterotrophic organisms for energy production. Part of the CO_2 fixed in photosynthesis is transferred to the interior of the ocean, mainly by gravitational settling of particulate organic carbon (POC) (Boyd and Trull, 2007). Diffusion, advection and vertical mixing of dissolved organic carbon (DOC) (Hansell, 2013; Hansell et al., 2012), and active biotransport of organic and inorganic carbon (i.e., $CaCO_3$) by diel vertical migrating zooplankton (Steinberg et al., 2008) are other carbon removal pathways. These biologically mediated processes that remove CO_2 from the atmosphere constitute the "biological carbon pump" (BCP) (Figure 1.5), which is a key component of the marine and global carbon cycle (Ducklow et al., 2001; Volk and Hoffert, 1985).

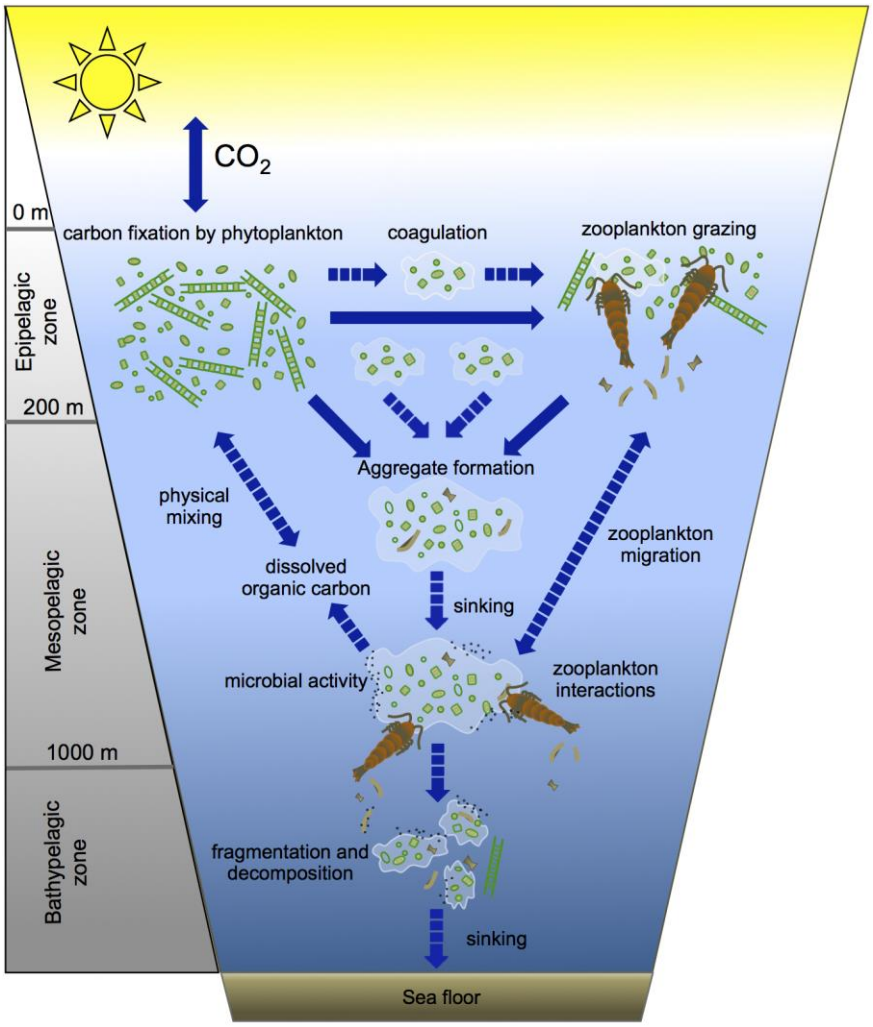

Figure 1.5: Simplified diagram of the principal components of the biological carbon pump, with production of organic matter in the upper layers, aggregation and sinking of particulate organic matter and remineralization or decomposition along the water column down to the sea floor.

1.4 Factors influencing the strength of the Biological Carbon Pump

The amount of carbon fixed and its subsequent export flux to depth is related to the abundance and composition of the planktonic community, and the interactions of the organisms within the pelagic food web structure. Thus food webs play a major role on controlling how much of the fixed carbon is efficiently transferred to greater depths (Boyd and Newton, 1995, 1999). Due to remineralization and heterotrophic consumption, the particulate flux of organic matter is attenuated with depth (Buesseler et al., 2007b; Martin et al., 1987) and it is estimated that only about 1-3% of the POC that escapes the euphotic zone reaches abyssal depths (Antia et al., 2001; Honjo, 1996; Honjo et al., 2008). The rate at which this sinking matter is decomposed depends on a variety of factors such as particle formation and aggregation, sinking speeds, and degradation rates. Although from a global perspective the BCP should be inefficient at transporting fixed carbon to depth, the

magnitude of exported C is comparable to the annual increase in CO_2 in the atmosphere driven by anthropogenic remobilisation of fossil fuel reserves (IPCC, 2013). The BCP accounts for 60-70% of the surface to depth dissolved inorganic carbon gradient (Schmittner et al., 2007) and it has been estimated that without it the atmospheric CO_2 levels would be 200 ppm higher than modern day levels (Parekh et al., 2006). Changes in the efficiency of the BCP therefore influence the ocean-atmosphere partitioning of CO_2.

There is substantial spatial and temporal variability regarding the amount of net primary production exported below the euphotic zone, mainly as a consequence of different biological communities and ecosystem structures (Buesseler, 1998; Francois et al., 2002). Additionally, ballasting (adsorption onto the surface of higher density materials) associated with biogenic (e.g. $CaCO_3$ or SiO_2) or lithogenic minerals from eolian or riverine inputs can lead to more efficient export by enhancing the sinking velocity of the particles and/or protecting them from microbial degradation (Armstrong et al., 2002; Klaas and Archer, 2002; Sanders et al., 2010). Therefore, the efficiency of the BCP, understood as the fraction of primary production that is exported below the euphotic zone (export flux), and the fraction that reaches the seabed (sequestration flux), is driven by a multitude of processes, often interrelated and most of which not quantitatively understood (see review by Turner, 2015). As a consequence, recent estimates of global BCP strength are variable, ranging from ~5 GtC y^{-1} to 13 GtC y^{-1} (Boyd and Trull, 2007; Henson et al., 2011; Laws et al., 2011).

In addition, the production of particulate organic matter in surface waters and its export flux from the euphotic zone influences the biogeochemical cycles of other major nutrients (e.g., N, P or Si) (Honjo et al., 2008) and micronutrients (e.g., Fe, Co), and also affects the distribution of scavenged-type trace metals (e.g., Al) (Bruland and Lohan, 2003) and other potentially harmful compounds (e.g., polychlorinated biphenyl) (Gustafsson et al., 1997a). The vertical sinking of particles connects the ocean surface with deep waters, affecting the distribution of nutrients and biominerals (e.g., opal belt in the Southern Ocean), and represents an important food source for pelagic and benthic organisms (Smith et al., 2008). Therefore, the study of the particle cycling is of broad interest not only for constraining the carbon cycle, but also for estimating elemental budgets. This research therefore complements a variety of research fields such as those including pelagic and benthic biological studies.

An early approach attempting to linking particle flux with primary production was done by Dugdale and Goering (1967). They stated that "*the rate of export of organic nitrogen from the production system cannot exceed the rate at which new nitrogen becomes available to replace it if the phytoplankton is to maintain itself*". They used ^{15}N-labeled compounds to measure the nutrient uptake rate and proposed the terms "new production", to refer to all primary production associated with the supply of allochthonous nitrogen entering the euphotic zone, mainly by vertical mixing and upwelled waters or via nitrogen fixation, and "regenerated production" when the source is recycled nitrogen (ammonia or dissolved organic nitrogen). About a decade later, Eppley and Peterson (1979) used a similar approach and coined the terms *f*- and *e*-ratios, to refer to the ratio between new and total production (*f*-ratio) and the fraction of primary production being exported (*e*-ratio). These early studies provided key concepts regarding the quantification of the relationship between *f*- and *e*-ratios that have proved useful for the development of global carbon export models (e.g., Dunne et al., 2007; Laws et al., 2000, 2011). However, uncertainties regarding the estimates of new production have raised since the generation of nitrate by nitrification, as well as the magnitude of nitrogen fixation, are often either underestimated or disregarded (Wafar et al., 1995; Yool et al., 2007). Additionally, this type of model is usually not able to describe the biological pump mechanistically, e.g., as a complex network between several component processes that are altered by physicochemical and biological forcing.

Frost (1984) proposed one of the first steady-state food web models that showed how food web structure determined the amount and fraction of exported production. Since then, the linkages between food web structure and export, as well as export efficiency, have become a central question among particle flux studies (Kriest and Evans, 1999; Kriest and Oschlies, 2011; Stemmann et al., 2004). These models, however, require detailed biological and geochemical information, which limits their applicability to specific regions of the ocean (Boyd et al., 2008; Michaels and Silver, 1988; Richardson and Jackson, 2007). Results are therefore questionable when applied to basin or global scale simulations (Doney, 1999), due to the lack of observations of contributing processes that influence the final export flux (Boyd and Trull, 2007). As a consequence, the magnitude and variability of the particle flux over temporal and spatial scales remains poorly understood (Burd et al., 2010).

Additionally, global climate change, with all of its possible feedbacks, increases the inherent complexity of the BCP. It has been hypothesized that increases in global ocean temperatures will increase upper ocean stratification thereby influencing marine food web dynamics (Beaugrand et al., 2008; Doney, 2006; Hays et al., 2005; Richardson and Schoeman, 2004). Indeed, it has been

suggested that in a warmer, more stratified ocean, environmental selection will favor smaller phytoplankton (Morán et al., 2010; Taylor et al., 2012) and, likely, nitrogen-fixing organisms (Karl et al., 2002). This may alter both particle flux and composition, with profound implications for marine biogeochemistry (Bopp et al., 2005). Increasing stratification has also been hypothesized to play a role in the significant expansion in the area and volume of oxygen minimum zones (Keeling et al., 2010), which could further influence the remineralization of particles as they sink through the water column. On the other hand, the increase of greenhouse gase concentrations may favour the intensification of coastal upwelling systems, however, the ecological responses of such intensification are still uncertain (Sydeman et al., 2014). In general, the magnitude of the BCP is predicted to decline due to global climate change, resulting in reduced ocean carbon storage and hence increased atmospheric CO_2 levels (Manizza et al., 2010; Matsumoto et al., 2010). Being able to quantify accurately the strength of the global BCP is essential to understand the Earth's carbon cycle and, consequently, the impact of the anthropogenic perturbations on the atmospheric CO_2 levels.

1.5 Particle export measurements

There are several methods to measure new or export production. Eppley (1989) outlined four major methodologies: i) nutrient uptake, ii) geochemical budgets, iii) sediment traps, and iv) naturally occurring particle-reactive radionuclides. However, thanks to technological advances, other approaches have been developed, such as the use of in situ digital imaging to quantify particle size distribution (Boss et al., 2014; Guidi et al., 2008). Additionally, a growing body of literature uses satellite-based models to obtain surface export fluxes. However, satellite-based estimates require the former approaches to obtain the relationships between *f*- and *e*-ratios or the export fluxes that, when combined with satellite derived data (i.e., sea surface temperature or surface chlorophyll), can be extrapolated from specific (in space and time) measurements to annual and basin scale estimates (Campbell and Aarup, 1992; Dunne et al., 2007, 2005; Henson et al., 2011; Laws et al., 2011, 2000; Siegel et al., 2014). As a result, although satellite-based models are the only approach that can provide a basin wide synoptic view of the strength of the BCP, they are limited by a paucity of observations, both in space and time (Boyd and Trull, 2007).

The measurement of nutrient uptake rates using ^{15}N-labeled compounds in bottle incubation experiments allows for an estimate of new production through the *f*-ratio concept, first proposed by Dugdale and Goering (1967) and Eppley and Peterson (1979). Although this technique has been extensively used (see review by Brandes et al., 2007), its methodological and theoretical grounds

have been recently questioned as a consequence of measurements that indicate that nitrification near the surface play a more important role than previously considered, accounting for about half of the nitrate consumed by growing phytoplankton (Yool et al., 2007).

The geochemical budgets rely on the fact that, under steady-state conditions, the nutrients supplied to the euphotic zone should balance the downward export of organic material (Eppley and Peterson, 1979). Therefore, geochemical budgets of nutrients or oxygen can also be used to examine the net fluxes into or out of the surface ocean integrating all forms of carbon transport (i.e., particle settling, zooplankton migration and physical mixing of POC and DOC) (Jenkins and Wallace, 1992; Sanders et al., 2005).

Upper-ocean sediment traps are a direct method to measure the flux of sinking particles. These devices have been widely used for export production measurements (Antia et al., 2001; Honjo et al., 1982; Martin et al., 1987) and valuable insights into the link between surface processes and mesopelagic and benthic fluxes have emerged from trap studies, contributing to our understanding of ocean biogeochemical cycles. Although the basic premise is simple, there are several issues related to their design and methodology, such as hydrodynamics and contamination by swimmers via death and solubilization of particulate material. These processes ultimately affect the trapping efficiency, both qualitatively and quantitatively. Several studies have discussed these issues in detail (i.e., Buesseler et al., 2007a, 2000; Gardner, 2000; Gustafsson et al., 2004), and many improvements have been made to overcome them ranging from free-drifting neutrally buoyant trap designed to address hydrodynamic-derived biases (see Valdes and Price, 2000; Lampitt et al., 2008 or Owens et al., 2013) or to the minimization of swimmers and solubilization (Lee et al., 1992; Antia, 2005). Despite uncertainties in the efficiency with which traps collect the true settling flux of particles, they are still the most direct approach of sampling sinking material and the only means by which time-series sampling of sinking particles is conducted in the mid waters of the ocean. Additionally, in contrast to chemical approaches, they can provide samples of sinking particles for biochemical analyses, although their spatial coverage is relatively reduced.

Optical imaging systems are another direct method for examining sinking particles. This method has been used since the 80s to study *in situ* concentrations of particles larger than tens of micron (Honjo et al., 1984). Since then, the digital imaging acquisition systems have evolved allowing fast *in situ* measurements of particle size distribution and abundance profiles with high spatial resolution (Boss et al., 2014). Optical techniques that allow the remote characterization of particulate flux provide a great advantage since they do not require particle sampling and

manipulation (i.e., filtration). However, the use of optical proxies for POC has been proven complicated by the highly variable relationships reported in the literature for POC *vs* particulate beam attenuation and particulate backscattering (Cetinić et al., 2012), hence imaging techniques have been used in combination with sediment traps to obtain POC export fluxes (i.e., Guidi et al., 2008). Nevertheless, optical techniques have great potential in this field and advances have already been made to determine chemical characteristics of their optical properties (Estapa et al., 2012; Guay and Bishop, 2002).

Of specific interest to the present work is the fourth method outlined by Eppley (1989), which consists of using naturally occurring particle-reactive, short-lived radionuclides as tracers of particulate matter (Bacon et al., 1976; Bhat et al., 1969; Buesseler et al., 1992; Coale and Bruland, 1985). This method takes advantage of the contrasting properties in seawater and differences in half-lives of a radioisotope pair to measure export occurring on the time scales of days to months (Benitez-Nelson and Moore, 2006; Cochran and Masqué, 2003). The radiotracer pair ^{238}U:^{234}Th is the most commonly and extensively used to study particle export and determine the strength of the BCP in the upper ocean (Coale and Bruland, 1985; Le Moigne et al., 2013b). There are other pairs that have also been used to quantify particle removal from the surface layers, such as the ^{210}Pb:^{210}Po, ^{228}Ra:^{228}Th and ^{90}Sr:^{90}Y pairs, although to date they have been used in a more limited number of studies (Cai et al., 2002; Cochran and Masqué, 2003; Orlandini et al., 2003).

1.6 ^{238}U:^{234}Th disequilibrium to examine particle dynamics

In marine systems, naturally occurring radionuclides from the decay chains of ^{238}U, ^{235}U and ^{232}Th (Figure 1.6) have been used to trace a variety of oceanic processes (Cochran and Masqué, 2003). Their biogeochemical behavior (e.g., particle-reactive *vs* conservative) and their half-lives are key characteristics to determine their applicability. Radioisotopes that tend to remain in solution can be useful to quantify advection and diffusion processes (e.g., Moore, 2000) whereas those used to examine particle dynamics should have high particle affinity (Coale and Bruland, 1985). Moreover, the half-life of the radioisotope must be adequate to make it sensitive to the timescale of the change to be evaluated: short half-lives (<days) might not show appreciable disequilibrium with respect to their precursors, whereas half-lives of >years will integrate changes over long time scales and dilute possible deviations of the equilibrium over a seasonal scale.

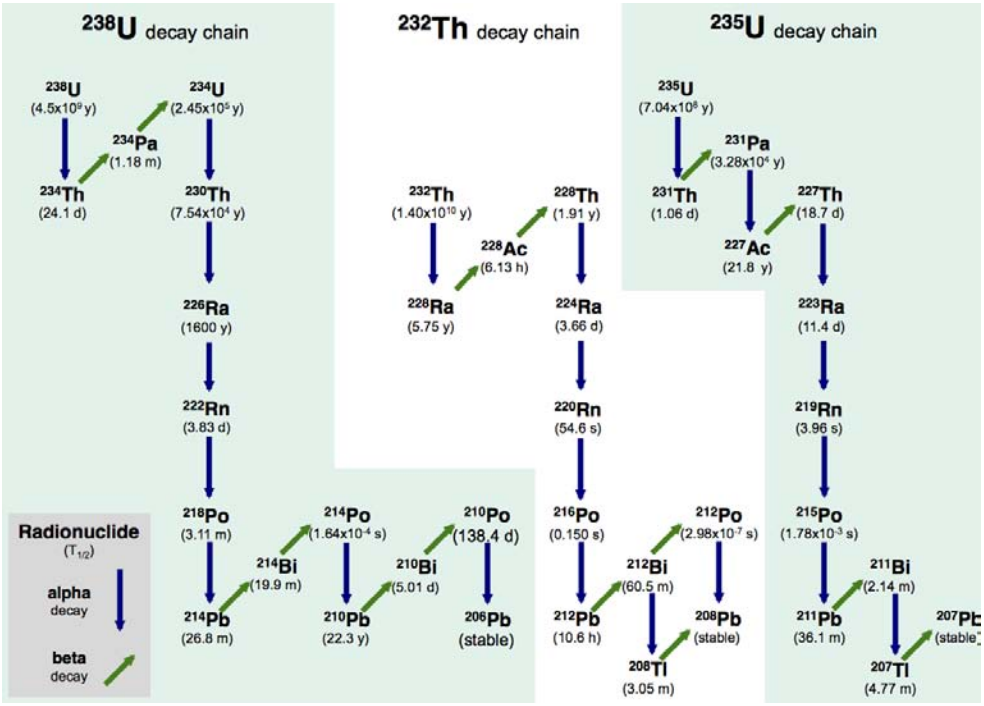

Figure 1.6: ^{238}U, ^{232}Th and ^{235}U decay chains. The half-life of each radioisotope is shown between brackets. Vertical blue arrows indicate alpha decay whereas diagonal green arrows are displayed for beta decay (adapted from Rodellas, 2014).

The study of particle fluxes using radioactive tracers utilizes the contrasting behavior and the difference in half-lives of a parent-daughter radionuclide pair (Bhat et al., 1969; Coale and Bruland, 1985). In general terms, this means that the daughter is often characterized by a high affinity for particles, whereas the parent is relatively unreactive or characterized by conservative behavior. Additionally, the parent has a longer half-life than its progeny thus, in absence of external processes, parent and daughter should be in secular equilibrium, i.e., the activities should be the same. Deviations from secular equilibrium can therefore be used to quantify the magnitude of the process responsible for the disequilibrium (e.g., particle export) and since these radionuclides are produced and decay at known rates, they can be used as 'biogeochemical clocks', integrating changes in processes over different time scales depending on the tracer used.

Thorium-234 has been widely used as a tracer to estimate the magnitude of downward particle fluxes (Waples et al., 2006) and, to a lesser extent, remineralization in the upper ocean (Maiti et al., 2010; Savoye et al., 2004). This short lived, highly particle reactive (K_d ~10^6-10^7; IAEA, 1985) radionuclide is produced continuously in seawater through alpha decay of its longer lived soluble parent, Uranium-238 ($T_{1/2}$ = 4.5 · 10^9 y) (Bacon and Anderson, 1982; Moore and Hunter, 1985) in oxic seawater, uranium is conservative and occurs and remains dissolved as a stable carbonate ion complex $UO_2(CO_3)_3^{4-}$ (Djogic et al., 1986). Thus, as Th is removed by settling particles from the upper ocean layers, ^{234}Th is depleted relative to ^{238}U in the surface ocean. An increase in ^{234}Th

activity is observed with increasing depth, as particle concentrations decrease, and secular equilibrium reoccurs (Figure 1.7). Hence, the disequilibrium between ^{234}Th and ^{238}U found in surface waters reflects net particle export on timescales ranging from several days to months (Coale and Bruland, 1985).

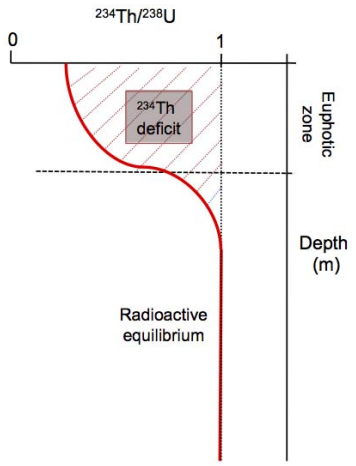

Figure 1.7: Idealized ^{234}Th:^{238}U profile, with deficit of ^{234}Th in surface water and radioactive equilibrium at depth.

Assuming steady-state conditions, the ^{234}Th flux can be calculated by integrating the deficit of ^{234}Th with respect to ^{238}U and by multiplying it by the decay constant of ^{234}Th ($\lambda = 0.0288$ d^{-1}) (see section 1.6.1). By multiplying this flux by the ratio of the element or chemical species of interest to ^{234}Th measured on sinking particles, the particle fluxes of a specific element can be derived (see section 1.6.2). Indeed, the main application of ^{234}Th as a particle flux proxy since its first reported measurements in the ocean by Bhat et al. (1969) has been to estimate POC fluxes, since ^{234}Th half-life makes it a suitable tracer to examine biologically mediated seasonal changes in POC production and export (Buesseler et al., 1992; Coale and Bruland, 1985). However, the processes related with POC export and remineralization can affect other elements, such as nutrient-type trace metals, essential for phytoplankton growth and its biological functioning (e.g., Fe, Cd or Co) or particle reactive elements and compounds, like aluminum or polychlorinated biphenyls, which are scavenged from the surface layers adsorbed onto settling particles (Dulaquais et al., 2014; Gustafsson et al., 1997a, 1997b; Weinstein and Moran, 2005). The use of ^{234}Th as a particle tracer thus provides essential information for constraining the processes affecting the particle dynamics and also trace elements cycling and distribution in the ocean (Cochran et al., 2006; Moran and Buesseler, 1993; Savoye et al., 2006).

1.6.1 Export fluxes and ^{234}Th deficits

^{234}Th export fluxes can be described and quantified by a suite of models of varying complexity (see review by Savoye et al., 2006; Figure 1.8). One of the simplest, the one-box irreversible steady state scavenging model, does not differentiate between particulate and dissolved thorium, thus it is used when total activities of ^{234}Th in the water column are measured, and does not provide any information about sorption/desorption kinetics or changes in the system with time. The model can be refined if ^{234}Th is measured in particulate and dissolve phases (two-box model), or if different particulate size classes are measured (three-box model), etc. More complexity can also be included by considering a reversible model with sorption/desorption and aggregation/disaggregation rates. The more complex the model is, the better it may describe the ocean's complexity in a realistic manner. However, as the model complexity increases the number of unknowns increases too (Doney et al., 2004; Turner, 2015). Uncertainties in the parameters used but also regarding which processes should be included and which ones not are a limitation for highly complex models (Cochran and Masqué, 2003; Savoye et al., 2006).

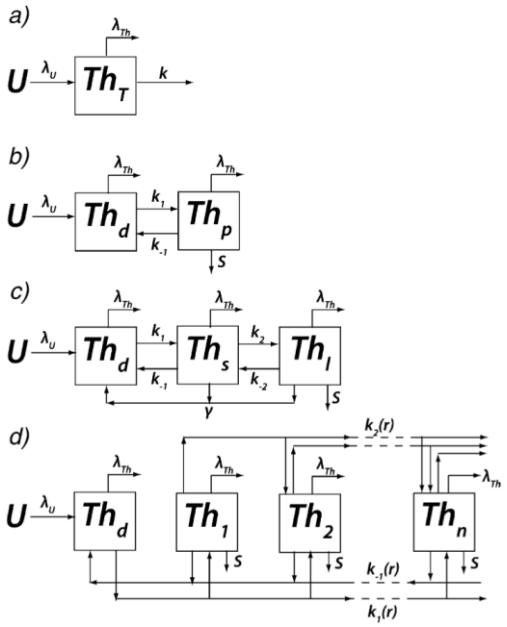

Figure 1.8: Schematic diagrams of the major classes of thorium scavenging model, with increasing complexity. For all the models, U represents the uranium activity with λ_U and λ_{Th} being the decay constants for the uranium and thorium isotopes, respectively and S represents the settling rate of particulate material. a) One-box model with the total thorium (Th_T) being the sum of dissolved and particulate and with the uptake onto particles and particle sinking represented by the total scavenging rate constant k. b) Two-box model with thorium activity divided between the dissolved (Th_d) and the particulate (Th_p) phases. The rate constants k_1 and k_{-1} represent adsorption and desorption of thorium (no differentiation between different desorption processes is done). c) Three-box model that considers size fractionation, with the particulate phase divided into small (non-settling) particles and large (settling) particles (Th_s and Th_l, respectively). The rate constants k_2 and k_{-2} represent aggregation and disaggregation rates between these compartments and γ the remineralization rate of particulate material back to the dissolved phase. d) This model contains an explicit representation of the particle size distribution. It includes n+1 boxes and represents dissolved thorium and n particle size class. Particles in each size class have a settling rate. Thorium can be adsorbed and desorbed from each particle size classes and be transferred between size classes by particle aggregation. (From Savoye et al., 2006).

Despite its limitations, the simplicity and ease of application of the one-box irreversible scavenging model has made it, by far, the most extensively used model to determine ^{234}Th fluxes (Savoye et al., 2006). It is also the primary formulation used in this work.

Briefly, the one-box model represents the change of total ^{234}Th activity with time as the balance between continuous production of ^{234}Th from ^{238}U, radioactive decay of ^{234}Th, removal of ^{234}Th by particle scavenging and input or output of ^{234}Th by physical transport:

$$\frac{\partial A_{Th}}{\partial t} = \lambda(A_u - A_{Th}) - P + V \tag{1.1}$$

Where:

A_U and A_{Th} are the ^{238}U and ^{234}Th total activities (expressed in dpm m^{-2}) respectively, λ the decay constant of ^{234}Th (λ = 0.0288 d^{-1}), P is the net removal flux of ^{234}Th (expressed in dpm m^{-2} d^{-1}), and V is the sum of the advective and diffusive fluxes.

In studies conducted in dynamic regimes, such as upwelling areas or eddy fields, the physical transport term, V, should be developed into a more detailed formulation by considering both, advection and diffusive transport in both the horizontal and vertical directions (see Savoye et al., 2006 for further detail). However, in most open ocean areas advection and diffusion are minimal and this term is considered negligible compared with the downward flux of ^{234}Th (Buesseler et al., 1998).

If non steady-state conditions ($\partial A_{Th}/\partial t \neq 0$) are to be considered, the same study site needs to be reoccupied over time, preferably between 1–2 weeks and one ^{234}Th half-life period (24 days), since for longer time intervals (>48 d) non steady-state and steady-state approaches are almost never significantly different. Moreover, intervals <1 week lead to high uncertainties because the non steady-state approach is very sensitive to changes in ^{234}Th activity (Savoye et al., 2006).

By neglecting V, assuming that the same water mass is sampled, and that P is also constant over the time period between both samplings, equation 1.1 can be solved as:

$$P = \lambda \left[\frac{A_U\left(1 - e^{-\lambda \Delta t}\right) + A_{Th1} e^{-\lambda \Delta t} - A_{Th2}}{1 - e^{-\lambda \Delta t}} \right] \tag{1.2}$$

Where;

Δt is the interval of time between two occupations of a single station, A_{Th1} and A_{Th2} are the ^{234}Th activities for the first and second sampling date of the same station, respectively.

Logistics during most open ocean cruises do not permit stations to be reoccupied. Therefore, for open ocean stations with minimal physical transport and only occupied once, steady state conditions are assumed and applied ($\partial A_{Th}/\partial t = 0$), and the net export flux of ^{234}Th (P) between two different depths, z_1 (m) and z_2 (m) is simplified to:

$$P = \int_{z_1}^{z_2} (A_U - A_{Th})\, \lambda\, dz \tag{1.3}$$

The integrated deficits of ^{234}Th relative to ^{238}U used in equation 1.3 are obtained using a trapezoidal integration approach, described in detail by Buesseler et al. (1992). In essence, from the activity profiles of both radionuclides, the deficit area is partitioned into a set of boxes spanning the distance between two consecutive mid points z (m), located at the mean distance between two consecutive sampling depths.

$$z = z_i + \frac{z_{i+1} - z_i}{2} \tag{1.4}$$

The deficit of each box, obtained by subtracting the ^{234}Th activity (A_{Th}) from the ^{238}U activity (A_U), is multiplied by the width (w_i; m) of the corresponding box to calculate the integrated deficit I_i (dpm m^{-2}) of that box:

$$w_i = \left(z_i + \frac{z_{i+1} - z_i}{2}\right) - \left(z_{i-1} + \frac{z_i - z_{i-1}}{2}\right) \tag{1.5}$$

$$I_i = w_i \cdot (A_U - A_{Th})_i \tag{1.6}$$

Finally, the flux of ^{234}Th, P (dpm m^{-2} d^{-1}), is calculated by multiplying the integrated inventory of the deficit area, which is the sum of the inventories of each of the boxes, by the decay constant of ^{234}Th (equations 1.3 and 1.7 are considered equivalent):

$$P = \lambda \sum I_i \tag{1.7}$$

1.6.2 Particulate organic carbon flux estimates using ^{234}Th

Based upon early correlations observed between the ^{234}Th:^{238}U disequilibria and biological activity in the upper ocean reported by Coale and Bruland (1987, 1985), the use of the residence time of particulate ^{234}Th was first proposed as a mechanism to estimate the flux of POC by Eppley (1989). However, the preferential regeneration of organic carbon from particulate organic matter

and the recycling of POC in the euphotic layer, results in very different residence times of particulate ^{234}Th and POC. As such, this approach is no longer used (Murray et al., 1989).

A more direct method was applied by Tsunogai and Minagawa (1976) but was not formalized until Buesseler et al. (1992). These authors proposed that POC flux estimates could be obtained by using the deficiency in total ^{234}Th with respect to ^{238}U, by assuming that that deficit is due solely to the association of ^{234}Th with particles sinking from the euphotic zone. By multiplying the resulting flux with the POC:^{234}Th ratio on sinking particles, one could obtain the POC flux as follows:

$$P_{POC} = P_{Th} \cdot \left(\frac{POC}{^{234}Th}\right)_{Sinking\ \ particles} \tag{1.8}$$

Where;

P_{POC} is the POC flux and P_{Th} is the flux of ^{234}Th.

The ratio of POC to ^{234}Th ratio shown in equation 1.8 (hereafter C/^{234}Th) is usually obtained from particles collected below the photic zone, as they are considered more representative of particles that actually sink to depth (Buesseler and Boyd, 2009). Indeed, the C/^{234}Th ratio on sinking particles is considered one of the principal uncertainties of the ^{234}Th flux approach. There exists extensive discussions examining differences in C/^{234}Th ratios and relating ratio variability to the different particle collection devices used (i.e., sediment traps, *in situ* pumps or bottles), as well as regional and seasonal differences, and changes with depth (see review by Buesseler et al., 2006). Despite more than two decades using C/^{234}Th ratios together with the surface ^{234}Th deficiencies to determine export fluxes of POC, the question of how particulate C/^{234}Th ratios vary with time, depth, particle type, size, or sinking velocity cannot be resolved by considering a single process or model. Nonetheless, several recommendations have been proposed to reduce the derived uncertainties of the ^{234}Th flux approach in estimating POC fluxes and facilitate comparisons between different studies (see Buesseler et al., 2006 and references therein), such as measuring the ratio below the mixed layer at the depth where export is to be quantified or to analyze POC and ^{234}Th on the same particle sample. Additionally, the collection of size-fractionation data and the use of independent sampling technics for comparison are also encouraged.

1.7 Objectives

The general objective of the present work is to explore the application of the ^{238}U:^{234}Th pair in a variety of locations with contrasting oceanographic characteristics and with different spatial scales to allow a better comprehension of the processes affecting the particulate flux in each one of the areas and to provide new insights into the variability of the POC export at a regional and basin-wide scale. The study areas and the specific aims addressed in each location are:

1) *North Western Atlantic Ocean*: A basin-wide export distribution study was along a transect extending from 64ºN to the equator was conducted to evaluate carbon export estimates under a broad variety of biogeochemical regions. A suit of satellite-derived carbon export models were compared to the estimates obtained with the ^{234}Th method in order to assess their agreement and to investigate possible latitudinal trends, which could contribute to improve the estimates of the global carbon budged from satellite-based plataforms.

2) *$10^{\circ}E$ meridian along the Antarctic Circumpolar Current:* In the Southern Ocean, carbon export out of the surface layer due to blooms of large diatoms is the main biological process for the sequestration of atmospheric CO_2 in the deep ocean. The processes governing the magnitude of particulate carbon export and associated nutrients remain key questions in the Southern Ocean. This study aimed to provide new estimates of late summer carbon export flux and attenuation, and to explore its links to the overlaying planktonic community and the frontal zones.

3) *The Gulf of California and Eastern Tropical North Pacific:* Seasonal stratification coupled with low oxygen mid waters suggests that this system facilitates an increasingly diazatroph-dominated food web. This study aimed to examine linkages between surface productivity and particulate export fluxes under oceanographic conditions similar to those expected in a future warmer ocean.

Chapter 2:

Analytical methods

2 Analytical methods

This section is dedicated to the sampling techniques and analytical procedures used to determine total and particulate ^{234}Th activities in seawater samples used in the research presented in the following chapters. Additional details on method for ancillary measurements are found in their respective chapters.

2.1 Seawater samples

Due to its relatively low concentrations, the determination of total ^{234}Th activities from seawater requires a pre-concentration step. Since ^{234}Th is highly particle reactive, a co-precipitation method is commonly applied. The method used here is the MnO_2 co-precipitation technique (Benitez-Nelson et al., 2001; Pike et al., 2005) which, contrary to iron hydroxides precipitates used in earlier days, preferentially scavenges ^{234}Th while ^{238}U remains in solution.

2.1.1 ^{238}U activities

Uranium-238 activities were inferred from salinity data. The relationships used in *Chapter 5* was established by Pates and Muir (2007) (equation 2.1). At the time of data processing this was the most adequate ^{238}U-S relationship available.

$$^{238}U = (0.0713 \pm 0.0012) \times S \ (dpm\ L^{-1}) \quad (2.1)$$

In *Chapters 3 and 4* the ^{238}U-S relationship used was determined by Owens et al. (2011) (equation 2.2) in a study that re-evaluated the ^{238}U-S relationship by including a broader variety of study regions, with a larger salinity range.

$$^{238}U\ (\pm 0.047) = 0.0786 \times S - 0.315 \ \ (dpm\ L^{-1}) \quad (2.2)$$

For a salinity of 35 the percent difference between ^{238}U activities calculated using both equations is 2.4%, although the values agree within error. In *Chapter 3* the ^{238}U activities derived from the ^{238}U-S relationship were also corroborated by the results obtained with the accelerator mass spectrometry measurements done in selected samples (Casacuberta et al., 2014).

2.1.2 Co-precipitation

Four-liter seawater samples were collected directly from the CTD-rosette bottles into calibrated bottles to determine total ^{234}Th activities. Samples were acidified to pH 1-2 using concentrated nitric acid (~5 mL HNO_3 65%) and a yield tracer, ^{230}Th, was added immediately after sample collection (<1 h) to account for possible losses of ^{234}Th during the co-precipitation procedure. Samples were shaken vigorously and allowed to equilibrate for ~8 h. After equilibration, the pH of the samples was raised up to ~8.5 using ammonia hydroxide (~6 mL NH_4OH 25%) and 50 µL of potassium permanganate ($KMnO_4$ with a concentration of 7.5 g L^{-1}) and 50 µL of manganese (II) chloride ($MnCl_2$ with a concentration of 30 g L^{-1}) were added to create a manganese dioxide (MnO_2) precipitate with which thorium co-precipitated. After each reagent addition, samples were vigorously shaken and allowed to stand for at least 6 h prior to filtration through 25 mm quartz filters (Whatman® QMA filters) (Figure 2.1). Start and end filtration times were noted in order to to correct for radioactive decay and to monitor any filtration issues (i.e., rapid filtration is often a sign of a broken filter).

Figure 2.1: Filtration system with 8 bottles connected to an Eyela aspirator vacuum pump (left image) and the resulting QMA filter with MnO_2 precipitate (right image).

2.1.3 Beta counting

After filtration, filters were dried in an oven at 50-60ºC and mounted on plastic RISØ cups under one layer of plastic film and two layers of standard aluminum foil (or one layer of thicker aluminum foil of 30 mg cm^{-2}) for beta counting in a low background RISØ proportional counter (Figure 2.2). Since ^{234}Th emits weak beta radiation (E_{max} 0.20 MeV) compared to its decay product, ^{234m}Pa ($T_{1/2}$ = 1.17 min), which is a high-energy beta emitter (E_{max} 2.29 MeV), the aluminum foil covers transmit about 80% of ^{234m}Pa but only 4% of ^{234}Th betas (Rutgers van der Loeff and Moore,

1999). Samples were counted in 60 min cycles until the uncertainty of the counting was <3%. Samples were re-counted after >6 months to determine the background activity of other longer-lived beta emitters, with <3% uncertainty. The average background activity was ~0.40 cpm, including a background detector of ~0.2 cpm. Typical samples had net counts of 1.5 to 2.5 cpm.

Figure 2.2: RISØ beta counter covered by a shield of old lead, with an anticoincidence module on top and the green filter support outside the detector (left image). On the right, empty plastic RISØ cups (top) and samples mounted on plastic RISØ cups ready to be measured (bottom).

Calibration for the relative efficiency of the detectors was carried out using ^{238}U standards. Replicates of deep water samples (>1500 m), where ^{238}U and ^{234}Th are expected to be in secular equilibrium, were collected at selected stations to confirm the calibration. Uncertainties for the ^{234}Th activity were calculated by propagating errors associated with counting, calibration, background corrections and ^{238}U activities, and were always <10%. The data reported in *Chapters 3-5* were processed and analyzed at Universitat Autònoma de Barcelona (Spain), University of South Carolina (USA) and at the Alfred Wegener Inisitiute (Germany), all laboratories that participated in the intercomparision of ^{234}Th measurements in both water and particulate samples as part of the GEOTRACES inter-calibration program (Maiti et al., 2012).

2.1.4 ^{230}Th recoveries

The ^{230}Th yield was determined by inductively coupled plasma mass spectrometry (ICP-MS) after background beta counting was completed. This measurement required the digestion of the MnO_2 precipitate and further purification via ion-exchange column chemistry, adding a known amount of ^{229}Th as a second yield tracer (Pike et al., 2005).

Briefly, filters were spiked with ^{229}Th (gravimetrical addition) in order to determine the efficiency of ^{230}Th recovery in the samples by using the $^{230}Th/^{229}Th$ ratios (^{230}Th: $T_{1/2}$ = 75380 y and ^{229}Th: $T_{1/2}$ = 7340 y) measured by ICP-MS, and normalized to ^{229}Th atom concentration.

To digest the precipitate, 10 mL of 8M HNO_3/10% H_2O_2 was first added to the beaker containing the filter. The beaker was covered with parafilm, sonicated for 30 minutes and allowed to stand cover for 6 h. The solution was then transferred to a 2 mL bed-volume anion-exchange column filled with AG 1-X8, 100-200 mesh chloride for resin (Bio-Rad Laboratories) as described in Pike et al. (2005). The effluent collected at the end of the column steps was then evaporated to <0.5 mL and allowed to cool. Each sample was redissolved with 2 mL of 5% HNO_3 and 0.08% HF and filtered using an Acrodisc 0.2 μm HT Tuffryn membrane syringe filters (Gelman Laboratory) into 1-2mL screw cap vials. Exactly 120 μL was subsequentely transferred into an ICP-MS vial and 880 μL of 2.2% HNO_3 added, obtaining the final ICP-MS sample solution of 2.5% HNO_3/ 0.01% HF. This method was applied to analyze the samples presented in *Chapter 5*.

In order to reduce the time necessary for the purification procedure, a simplified adaptation of Pike et al. (2005) method (F. Dehairs, *pers comm*) was used for all of the samples presented in *Chapters 3 and 4*. This adaptation removes column purification, but follows the remaining procedure described in Pike et al. (2005). This adaptation of Pike et al. (2005) method was tested in 15 samples. The results obtained with the simplified method agreed well within error with those obtained using the ion-exchange columns (Figure 2.3). Recoveries obtained using both methods averaged 90 ± 10%.

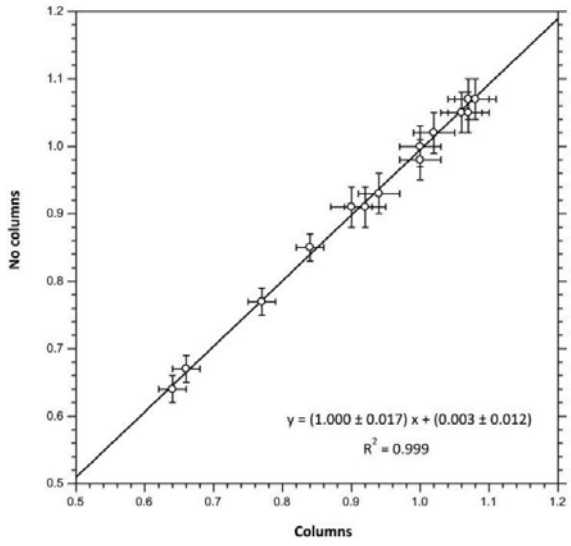

Figure 2.3: Comparison between the $^{229}Th/^{230}Th$ ratios obtained when following the classic method developed by Pike et al. (2005), which included the ion-exchange column step (Columns) vs the simplified procedure that avoids the column purification (No columns).

2.2 Particulate samples

In all of the studies presented here, battery-operated *in situ* pumps (*Challenger Oceanic* or *McLane*) were deployed to collect particulate material (Figure 2.4). The number of depths sampled varied depending on the study; however, 100 m was always sampled for easier comparison with previous works. The pumps were typically deployed for 1.5-2.5 h and filtered between 400 and 2200 L. In *Chapters 3* and *4* size fractionation was not possible and only the >53 µm fraction was sampled. The particulate material from the >53 µm screen was rinsed using 0.2 µm filtered seawater and an aliquot was filtered through pre-combusted QMA filters with positive pressure (<0.3 bar) for ^{234}Th, POC and PN analyses. Particulate ^{234}Th samples were counted following the same procedure as previously detailed for ^{234}Th seawater samples (see section 2.1.3). POC and PN concentrations were measured by high temperature combustion with mass spectrometer detection (Eurovector C/N Element analyzer) according to the JGOFS protocols (Knap et al., 1996), after being treated with 0.1 M HCl solution to remove carbonate. In *Chapter 5* size fractionated samples of 1–53 µm and >53 µm were collected by filtering through a 142 mm diameter acid-rinsed 53 µm mesh Nitex® screen, to sample the large particle fraction, as done in *Chapters 3 and 4*, followed by a 142 mm diameter, 1 µm pore-size pre-combusted QMA filter beneath to collect small particles (Figure 2.4). The particulate material from the 1-53 µm QMA filter was sub-sampled using a methanol cleaned metal punch. Ten punches of 21 mm diameter (26% of total filter area of the 142 mm diameter QMA) were compressed at 1 ton of pressure for 1 minute into plastic RISØ cups. Additional punches were sampled for POC and PN analysis.

Figure 2.4: *In situ* pump being deployed (left image). On the right, Nitex screens used to collect the fraction >53 µm (top), QMA filter used to collect the fraction 1-53 µm with few 21 mm punches removed from the main filter (middle) and the total 21 mm diameter punches obtained from QMA filters (bottom).

Surface-tethered sediment traps data were only collected in *Chapter 5*. Each VERTEX-style sediment trap (Buesseler et al., 2007a) was equipped with 12 tubes per depth (Figure 2.5), filled with an unpoisoned brine solution and deployed for 24 h. The material collected by the trap was filtered onto pre-combusted QMA filters. The filters were dried and prepared for beta counting, as done for the other samples previously described (see section 2.1.3). POC and PN were also analyzed in these samples to obtain POC(PN)/^{234}Th ratios.

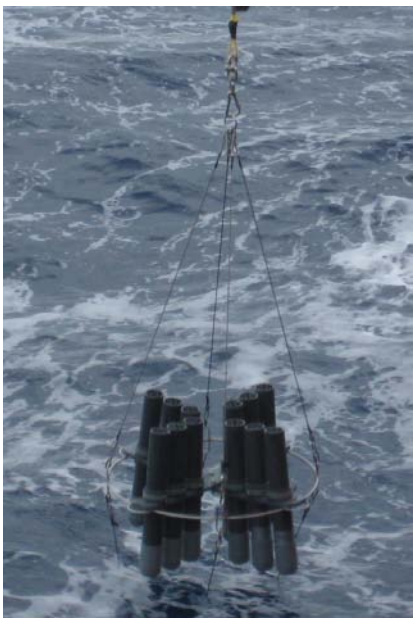

Figure 2.5: VERTEX-style surface-tethered sediment trap.

Chapter 3:

Latitudinal distribution of particulate carbon export across the North Western Atlantic Ocean

This chapter is based on:

Puigcorbé V., M. Roca-Martí, P. Masqué, C.R. Benitez-Nelson, M. Rutgers v.d. Loeff, A. Bracher and S. Moreau. Latitudinal distribution of particulate carbon export across the North Western Atlantic Ocean; Submitted to *Deep-Sea Research I*

3 Latitudinal transect across the North Western Atlantic Ocean

3.1 Objectives

Carbon export fluxes were measured in the North Western Atlantic Ocean under the GEOTRACES frame using the ^{234}Th approach to evaluate basin-scale export variability. Here the objective was to investigate the latitudinal distribution of carbon export, from the equator to 64°N (northern half of the GA02 transect), across a wide variety of biogeochemical domains, with high spatial resolution. ^{234}Th-derived carbon estimates were compared to three different satellite-based export models to evaluate the agreement between methodologies, since remote sensing technics allow for sampling at much greater spatial and temporal resolution. Thus, the large increase in export data in the Atlantic Ocean derived from the GEOTRACES Program, combined with satellite observations and modeling efforts could contribute to improve the estimates of carbon export in this ocean basin and therefore reduce the uncertainty in the global carbon budget.

3.2 Introduction

The biogeochemical cycling of carbon and major nutrients is strongly influenced by particle cycling and export (Honjo et al., 2008). Carbon dioxide fixation by phytoplankton and the subsequent downward particle flux of biogenic carbon, a process often referred to as the "biological pump" (Volk and Hoffert, 1985), is a key component in the global carbon cycle. Yet understanding the magnitude and variability of this flux over temporal and spatial scales remains limited (Britten and Primeau, 2016; Burd et al., 2010). As a consequence, global-scale models of the ocean carbon export are variable, ranging from ~5-6 GtC y^{-1} (Henson et al., 2011; Siegel et al., 2014) to 13 GtC y^{-1} (Laws et al., 2011). This uncertainty highlights the need for continuing *in situ* carbon export field sampling over large geographical provinces and across seasonal timescales (Britten and Primeau, 2016; Siegel et al., 2016).

Thorium-234 has been widely used as a tracer to estimate particle fluxes (e.g., Coale and Bruland, 1985; Cochran and Masqué, 2003) and, to a lesser extent, remineralization in the upper ocean (Maiti et al., 2010; Savoye et al., 2004), with the estimation of particulate organic carbon (POC) fluxes being the most significant application (see review by Waples et al., 2006). However, the processes related to POC export and remineralization also influences other elements, such as trace metals essential for phytoplankton growth and biological functioning (e.g., Fe, Cd or Co) or

particle reactive elements (e.g., Pb or Al) and compounds (e.g., PCBs) that are scavenged from the surface ocean and adsorbed onto settling particles (Dulaquais et al., 2014; Gustafsson et al., 1997a, 1997b; Weinstein and Moran, 2005). Thus, the use of ^{234}Th as a particle tracer provides essential information for constraining processes affecting particle dynamics and also trace element cycling and distribution in the ocean, which is the aim of the GEOTRACES program.

GEOTRACES is a perfect platform to examine particle flux across a large-scale latitudinal and longitudinal gradients. As part of the Dutch GEOTRACES program, the GA-02 section was sampled in 2010-2011. This section covered more than 17,000 km at high spatial resolution (usually <2º latitude, ~150 km) and spanned a diversity of biogeochemical regions, such as deep-water formation zones, subtropical gyres, oligotrophic seas, waters influenced by dust inputs, and areas influenced by riverine outflows. Here, we discuss ^{234}Th and ^{234}Th-derived carbon export fluxes obtained in the northern half of that section, from the Irminger Sea, southeast of Greenland, to the equator (Figure 3.1). The southern half of the transect was presented in Owens et al. (2015). We describe regional export variability in the Northern Western Atlantic Ocean and the results are discussed with regards to various regional processes. We also present a compilation of POC export estimates (hereafter C export) from previous open ocean studies using ^{234}Th:^{238}U disequilibria in the Atlantic Ocean, provide estimates of C export efficiencies, and compare our ^{234}Th-derived C export fluxes with different satellite-based export models.

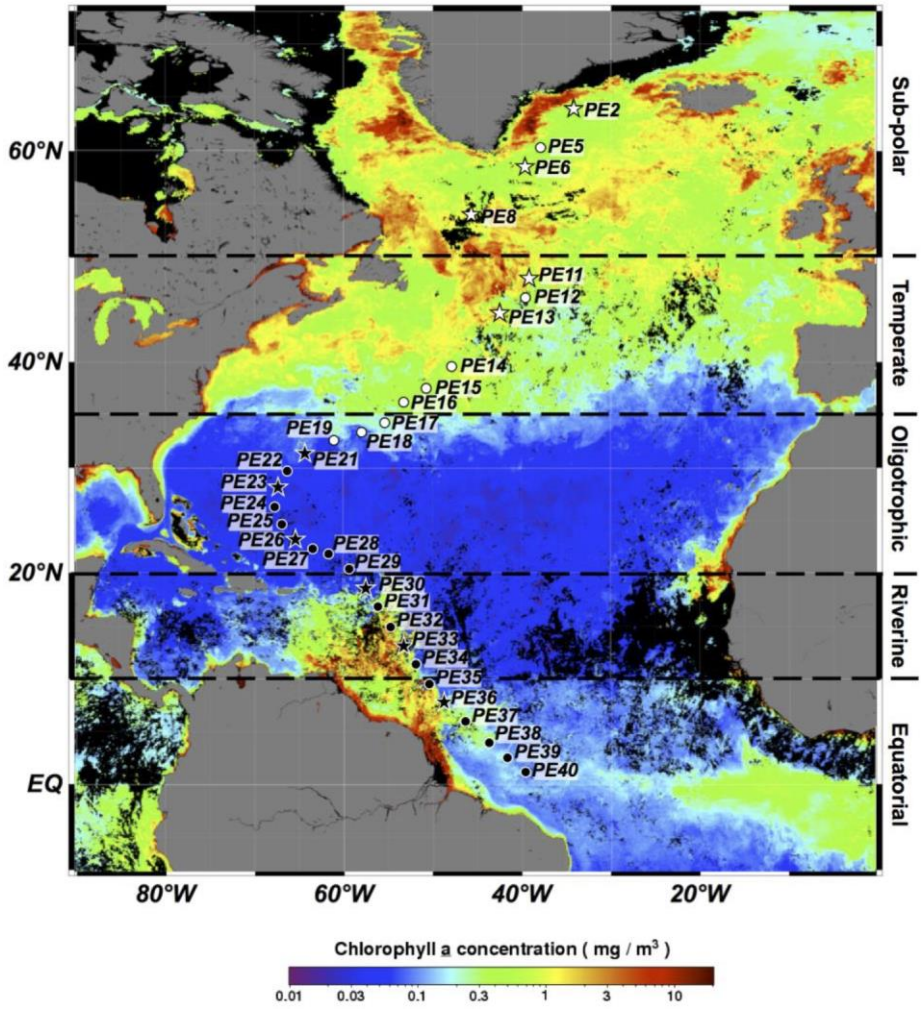

Figure 3.1: Stations locations along the northern GA02 transect, between May 2nd and July 4th 2010, overlain by mean chlorophyll-a concentration (mg m^{-3}) derived from MODIS AQUA remote sensing data (http://oceancolor.gsfc.nasa.gov) corresponding to sampling time (i.e., May for sub-polar and temperate domains, May-June for oligotrophic domain, June for riverine domain and June-July for equatorial domain). White symbols correspond to stations sampled during the 64PE319 cruise and black symbols during the 64PE321 cruise. Stars indicate those stations where particle samples were also collected. Black horizontal dashed lines indicate the different domains sampled.

3.3 Methods

3.3.1 Total ^{234}Th

A total of 33 stations were sampled (n = 344 samples) from 64ºN to the equator for total ^{234}Th activities (dpm L^{-1}). Samples were collected during two consecutive cruises: 64PE319 (28 April to 25 May) and 64PE321 (11 June to 8 July), on board R/V *Pelagia* in 2010 (Figure 3.1). Total ^{234}Th concentrations were measured from 4 L of seawater collected at a minimum of 12 depths over the upper 1000 m, processed as described in *Chapter 2*. The average recovery of ^{230}Th was 88 ± 13% (n = 335). Uranium-238 activities were inferred from salinity using the relationship established by

Owens et al. (2011) and were further confirmed by direct measurement of ^{238}U concentrations (Casacuberta et al., 2014) in samples collected during the same expeditions (n = 15) (see *Chapter 2*). Uncertainties for ^{234}Th activities averaged 5 ± 1% (n = 344) and were always ≤10%. ^{234}Th and ^{238}U concentrations along the GA02 transect are available online (British Oceanographic Data Centre, http://www.bodc.ac.uk/geotraces/data/idp2014/) and are part of the GEOTRACES Intermediate Data Product 2014 (Mawji et al., 2015).

3.3.2 Particulate ^{234}Th and C

Samples for particulate ^{234}Th and organic C were collected at 11 stations using *in situ McLane* and *Challenger* filtration pumps (ISP) deployed at 100 m (see Figure 3.1). Pumping times lasted about 2.5 h and the volume filtered ranged from 1800 to 2200 L. Particles were collected using a 53 µm mesh Nitex screen and was washed off the screen with 0.2 µm-filtered seawater and an aliquot equivalent to 100-900 L was taken to analyze ^{234}Th and POC concentrations as described in *Chapter 2*.

3.3.3 Satellite data and export models

3.3.3.1 Particle size distribution

Satellite-derived densities for pico-, nano- and microplankton reflecting the 0.5-2 µm, 2-20 µm and 20-50 µm size classes, respectively, were obtained from the GlobColour OSS2015 demonstration products (http://hermes.acri.fr/index.php?class=demonstration_products) as monthly mean values with 25-km resolution (the product is only available is these spatial and temporal resolutions for the timing of the sampling). This data product is based on the merging of MERIS, MODIS and SeaWiFS level-2 data with the GSM (Garver-Siegel-Maritorena) model (Maritorena et al., 2002) and the algorithm developed by Maritorena and Siegel (2005) over the whole globe with a resolution of 4.63 km.

As described in the GlobColour product user guide (GlobColour, 2015), the particle backscattering product (bbp) at wavelengths 443, 490, 510 and 555 nm were computed from the respective wavelength's GlobColour level-3 remote sensing reflectance products based on the non-spectral algorithm (neural-network approach) of Loisel et al. (2006). The wavelength specific bbp were then used to derive the spectral exponent (logarithmic slope) of the particulate backscattering coefficient (bbps-log) following Loisel et al. (2006) and the particle size distribution was determined using a semi-analytical formula using Mie-theory following Kostadinov et al. (2009).

The total particle volume in each size class was calculate following equation 6a in Kostadinov et al. (2009) and then used to calculate the fraction of each size class on the total particle volume.

3.3.3.2 Primary productivity and carbon export models

Three different approaches were used to obtain net primary productivity rates (NPP) from satellite data (Table A.1.1).

First, NPP rates (in g C m^{-2} day^{-1}) were determined from the GlobColour OSS2015 demonstration products as monthly mean values collocated to the sampled stations with 25-km resolution (the product is not available for the timing of the sampled stations at higher temporal or spatial resolution). As described in the GlobColour product user guide (GlobColour, 2015), NPP was calculated from the GlobColour level-3 chlorophyll-a (Chl-a) concentration, photosynthetic available radiation and sea surface temperature (SST) following the method of Antoine and Morel (1996) (A&M96).

NPP was also obtained from the Ocean Productivity website at Oregon State University (http://www.science.oregonstate.edu/ocean.productivity/) with a 9-km spatial resolution and 8 day temporal resolution data from MODIS and SeaWiFS satellites. We used both the Vertically Generalized Production Model (VGMP; Behrenfeld and Falkowski, 1997) and the Carbon-based Production Model (CbPM; Behrenfeld et al., 2005; Westberry et al., 2008). VGPM is a "chlorophyll-based" model: it estimates NPP from satellite Chl-a, available light and photosynthetic efficiency, which also depends on temperature. CbPM is a carbon-based model that uses remote sensing retrievals of particulate scattering coefficients to estimate phytoplankton carbon concentration. 9-km resolution SST and satellite-derived Chl-a were obtained from the Ocean Color Data website (http://oceandata.sci.gsfc.nasa.gov). Z_{eu} was calculated from Chl-a following Morel and Berthon (1989). Weekly NPP, SST and Z_{eu} at 9-km resolution were calculated for all the sampling stations by integrating ~4 weeks (32 days) prior the sampling in order to compare with the integration time of ^{234}Th (mean life ~35 days).

C export was then estimated from three different models using satellite-derived SST, NPP and Z_{eu}: i) Dunne et al. (2005) (D05); ii) Laws et al. (2011) (L11); and iii) Henson et al. (2011) (H11). The D05 model, which is an empirical model based on a compilation of export data obtained through a variety of methodologies, provides export estimates using SST and NPP as predictor variables, and is computed as:

$$\text{Export (D05)} = \text{NPP} \times [\, -0.0101 °C^{-1} \times \text{SST} + 0.0582 \times \ln(\text{NPP}/Z_{eu}) + 0.419]$$

The L11 model is a steady state food web model with a negative relationship between export and temperature and a curvilinear correlation between export and NPP:

$$\text{Export (L11)} = \text{NPP} \times 0.04756\ (0.78 - 0.43\ \text{SST} / 30)\ \text{NPP}^{0.307}$$

And the H11 model is based on an exponential relationship between ^{234}Th-derived export and SST and is computed as:

$$\text{Export (H11)} = \text{NPP} \times 0.23 \times \text{EXP}(-0.08 \times \text{SST})$$

3.3.4 Complementary data

Oceanographic data (temperature, salinity, attenuation coefficient, fluorescence and dissolved oxygen) were obtained from sensors attached to sampling rosette, which included a Seabird SBE9+ Underwater Unit with a SBE4 conductivity sensor (± 0.3 mS m^{-1}), a SBE3+ thermometer (± 0.001°C), a Chelsea Aquatracka MKIII fluorometer (± 0.2 µg L^{-1}), a Wetlabs C-Star transmissometer (± 0.02%FS $°C^{-1}$) and a SBE43 dissolved oxygen sensor (± 2%).

Nutrient concentrations were determined colorimetrically according to the methods described by Grasshoff et al. (1983). Analyses were performed on board using a Seal Analytical QuAAtro Autoanalyser as detailed in the cruise reports (64PE319: Gerringa, 2010; 64PE321: Rijkenberg, 2010).

3.4 Results

3.4.1 Hydrography

The northern GA-02 section covered the Atlantic Ocean from the Irminger Sea to the equator along the deep basins of the western Atlantic Ocean (Figure 3.1). A detailed hydrographical description of the complete GA-02 section can be found in van Aken (2011).

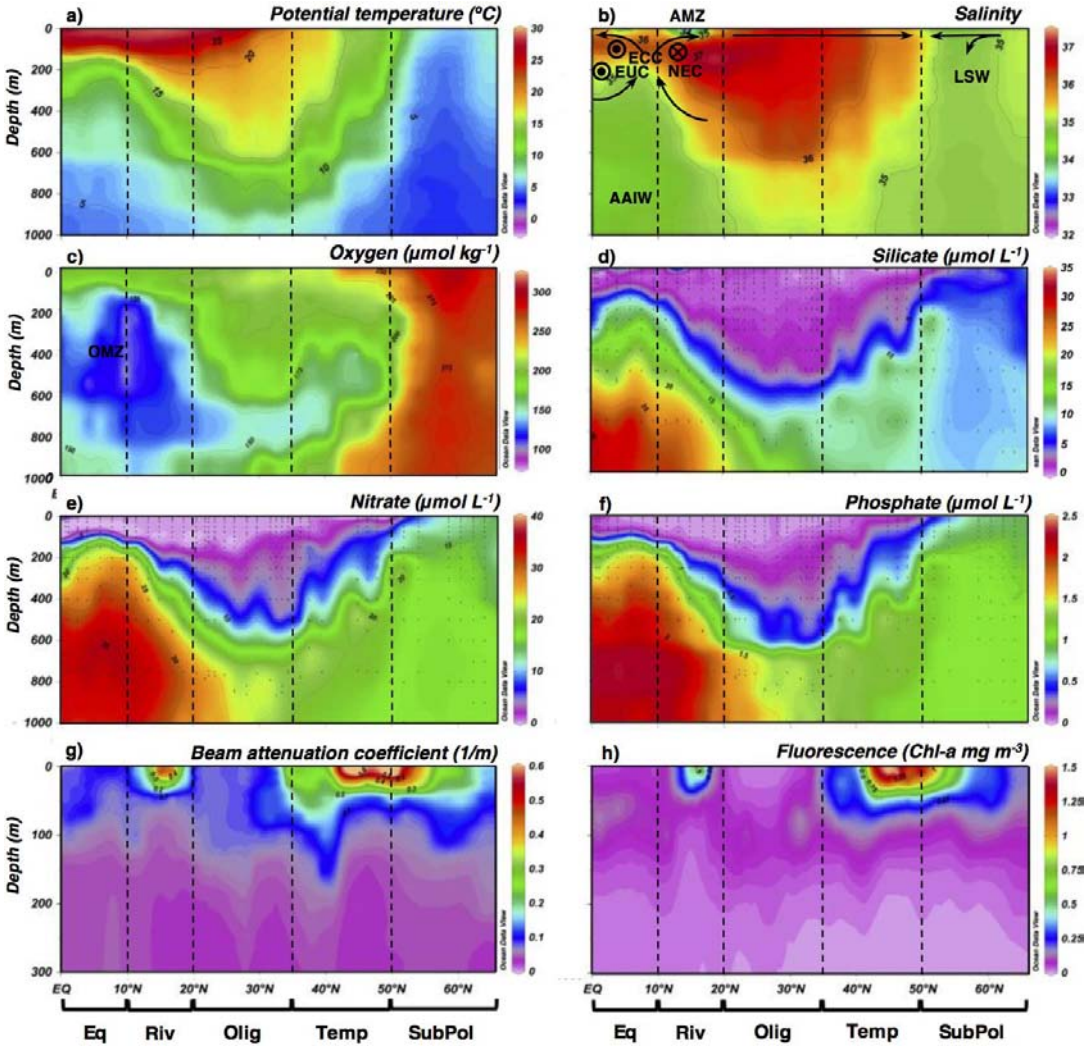

Figure 3.2: Section plots along of a) Potential temperature, b) Salinity c) Oxygen, d) Silicate e) Nitrate, f) Phosphate g) Beam attenuation coefficient and h) Fluorescence. Note the different depth range for plots g) and h). Dashed lines indicate the domains (see also Figure 3.1): Equatorial (Eq), Riverine (Riv), Oligotrophic (Olig), Temperate (Temp) and Sub-polar (SubPol). Approximate locations and current patterns (black arrows and symbols in b) of the equatorial current system are indicated (NEC: North Equatorial Current; ECC: Equatorial Counter Current; EUC: Equatorial Undercurrent), as well as the direction of the surface currents (cross = west, dot = east). In plot b) the area influenced by the Amazon Plume (AMZ) and the most distinct water masses (LSW: Labrador Sea Water and AAIW: Antarctic Intermediate Water) are also indicated and in plot c) the minimum oxygen zone (OMZ) is shown. See text for further details.

Main hydrographic parameters are presented in Figure 3.2 to illustrate the different oceanic regimes encountered along the transect. We divided the study area into 5 regions/domains: Sub-polar (>50ºN), temperate (35ºN-50ºN), oligotrophic (20ºN-35ºN), riverine (10ºN-20ºN) and equatorial (0º-10ºN) (Figure 3.1).

In general, ^{234}Th deficits were most apparent in the upper 100 m (Figure 3.3). Sub-polar and temperate latitude stations (>35ºN; PE2-PE16) tended to have deeper deficits that in some cases reached depths of 250 m. ^{234}Th activities in surface waters were typically <1.5 dpm L^{-1}, although profiles from stations PE2, PE8 and PE11 showed equilibrium/slight deficits throughout the upper 100 m. Stations sampled to the south had reduced ^{234}Th deficits, such that PE22, PE24 and PE26 located in the subtropical gyre between 20ºN and 30ºN had minimal deficits. ^{234}Th excesses were observable below ~200 m within these subtropical latitudes, being particularly apparent at station PE24 (~26ºN; up to 0.61 ± 0.15 dpm L^{-1} between 200 and 500 m).

In the riverine domain, moving towards the equator, ^{234}Th depletion became increasingly identifiable in the surface layers (<100 m), although it was less intense than in the northern latitudes (^{234}Th activities >2 dpm L^{-1}). The exception were stations PE31, PE32 and PE33 that had large deficits in the upper 50 – 100 m, with ^{234}Th activities of 1.5 dpm L^{-1} in the upper 25 m. These stations also had lower ^{238}U activities in the upper 30 m than the rest of the profiles (2.2-2.3 dpm L^{-1} compared to 2.5-2.6 dpm L^{-1}), due to low salinity in the surface layers. In the equatorial domain, the deficit of ^{234}Th was smaller and shallower (at 100 m or above) than the deficits observed in the temperate latitudes. Station PE38 presented excess between 100 and 200 m, which seemed to extend to greater depths (below 550 m), although the vertical resolution below 200 m was poor.

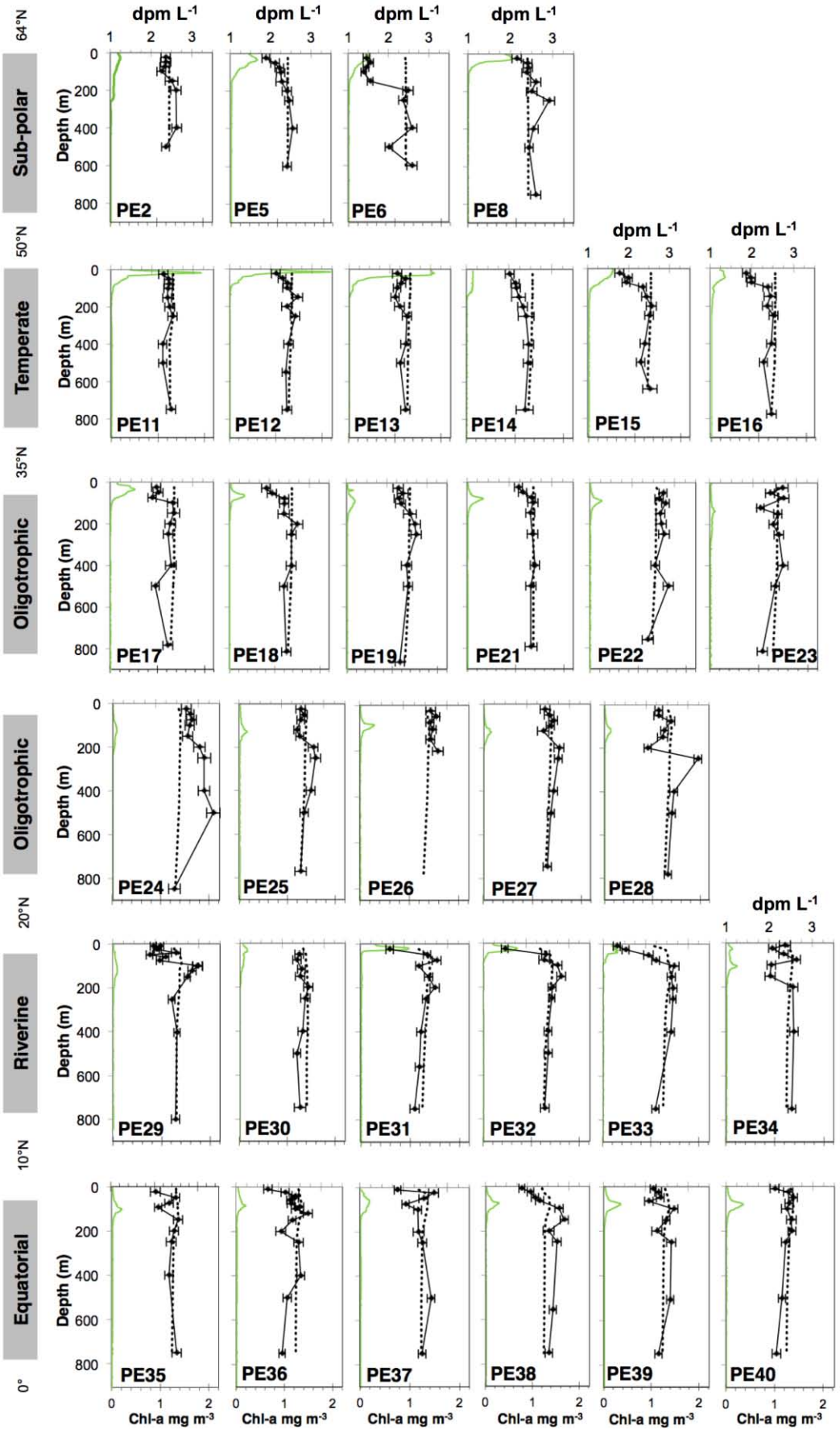

Figure 3.3: Concentration profiles for ^{234}Th (in dpm L^{-1}; black diamonds and solid line), ^{238}U (in dpm L^{-1}; dotted line) and fluorescence (in mg m^{-3}; green line) of each station (see Figure 3.1 and Table A.1.1 for station location).

Th-234 fluxes were calculated at three depths in order to compare with previous studies: i) at 100 m, since that is the depth where *in situ* pumps were deployed, following historical sampling protocols; ii) at the depth of the primary production zone (PPZ; defined as the depth where fluorescence is reduced to 10% of its maximum value, Owens et al., 2015), following a similar approach as the one proposed by Buesseler and Boyd (2009); and iii) at the deficit depth (the shallowest depth where ^{234}Th and ^{238}U are in equilibrium) (Figure 3.4, Table A.1.2). The three approaches were applied assuming a 1-dimensional steady state model. Advection and diffusion processes were considered to be negligible compared to the downward flux of ^{234}Th, as generally assumed in the open ocean (see review by Savoye et al., 2006) and confirmed in previous studies in the North Atlantic (Buesseler et al., 2008; Resplandy et al., 2012; Thomalla et al., 2006).

Fluxes of ^{234}Th measured at the PPZ and at the deficit depths were greater (by at least 10%) than ^{234}Th fluxes calculated at 100 m for the majority of the stations (18 stations, when using the PPZ, and at 20 stations when estimating the flux at the deficit depth). ^{234}Th fluxes at the PPZ and deficit depths were lower (>10%) than those measured at 100 m at 9 and 2 stations, respectively, due to shallow ^{234}Th excess (Figure 3.4, Table A.1.2). Note that 3 stations did not have any shallow ^{234}Th deficits (PE22, PE24 and PE26, located between 23ºN and 30ºN). In the following discussion, we focus on the ^{234}Th fluxes at 100 m for easier comparison with prior studies. However, it is important to note that recent studies (Buesseler and Boyd, 2009) question the use of a fixed depth and highlight the importance of using a biologically meaningful depth to estimate ^{234}Th (and consequently C-derived) fluxes. Therefore, we also report the ^{234}Th fluxes at the PPZ and at the deficit depth in Table A.1.2.

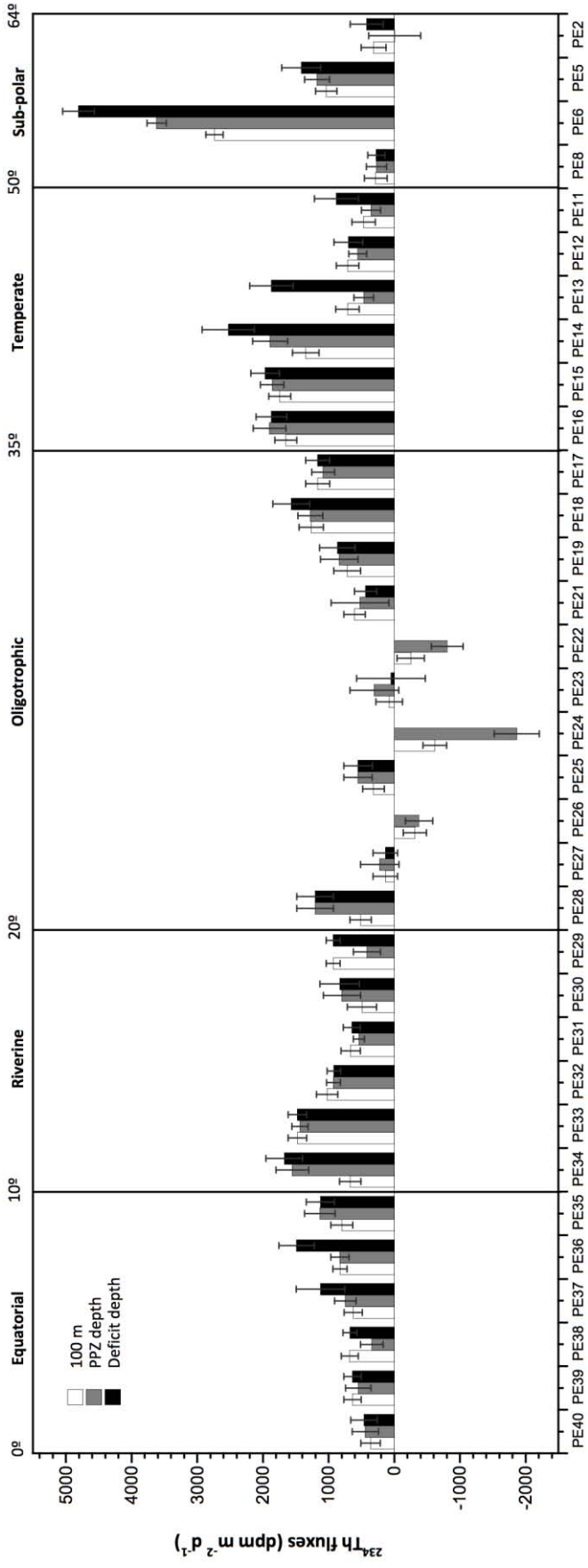

Figure 3.4: ^{234}Th fluxes determined at each station at 3 different depths: 100 m, PPZ depth and deficit depth.Vertical lines indicate the different domains and their latitudinal limits are indicated by the degrees (north) on top

Th-234 fluxes at 100 m ranged from -620 ± 180 dpm m^{-2} d^{-1} to 2740 ± 140 dpm m^{-2} d^{-1} (Table A.1.2, Figure 3.4). The magnitude of the fluxes are described according to a latitudinal distribution: higher fluxes were found in the southern half of the temperate domain, and at a single station, PE6, in the sub-polar waters. Lower fluxes were measured in the subtropical gyre, particularly between ~20ºN and 30ºN, with negligible or even negative fluxes at several stations (PE22, PE23, PE24, PE26 and PE27). The stations influenced by the Amazon River plume (PE32 and PE33) had higher fluxes compared to those in the same region where there was no evidence of riverine influence and are within the range observed in the southern part of the temperate domain (>1000 dpm m^{-2} d^{-1}). Finally, the equatorial domain is the region where fluxes were less variable between stations, averaging 660 ± 170 dpm m^{-2} d^{-1}.

3.4.2 C/^{234}Th ratios and derived C export fluxes

Measured C/^{234}Th ratios in large particles (>53 µm) ranged from 2.3 to 16 µmol C dpm^{-1} (7.9 ± 5.0 µmol C dpm^{-1}; n = 11; Table A.1.3). Due to time constrains, ISP deployments along the transect were limited. In order to calculate C export fluxes for the entire section we followed the approached of Owens et al. (2015), where C/^{234}Th ratios were derived from a power law regression (see Figure 8 from Owens et al., 2015). Here, this curve was adapted to: i) cover a larger depth range (from 30 to 270 m); ii) to use only those samples obtained from the northern hemisphere during the GEOTRACES sections GA02 (our study) and GA03 (longitudinal section across the North Atlantic; see Owens et al. (2015) for details; note that Owens et al. (2015) measured total C instead of POC, but the authors argue that inorganic C in those samples is likely often less than 10% of the total C or within the error of the ^{234}Th-derived C fluxes) (Figure 3.5); and iii) to account for the uncertainties of the averaged C/^{234}Th ratios. Samples were grouped into 20 m bins (30 to 190 m) and into 40 m bins (190 and 270 m, to account for fewer samples at deeper depths). Binned data were averaged and then used to derive the power law regression.

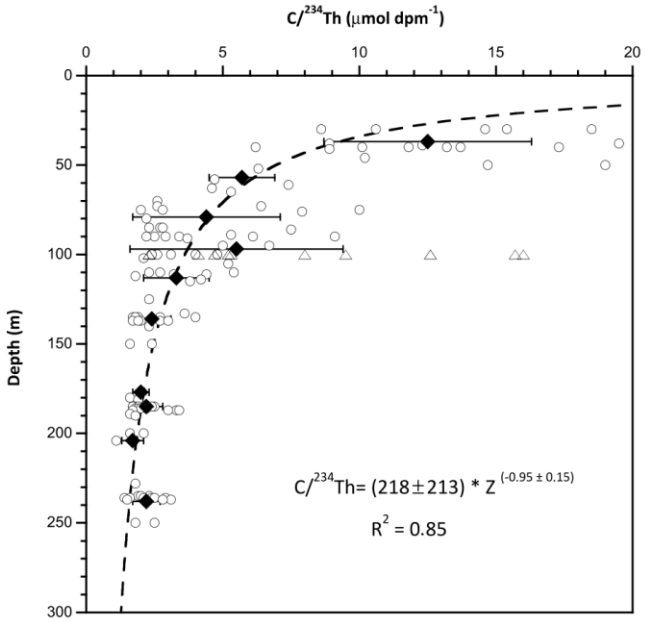

Figure 3.5: C/^{234}Th ratios profiles from large (>51 μm) particles from Owens et al. (2015) for the North Atlantic cruise GA03 (open circles), together with the C/^{234}Th ratios obtained during this study (northern section of the GA02 cruise; open triangles). A power law regression was derived within the depth ranges of the PPZ and the depth of the ^{234}Th deficits using 20-40 m-binned averages (black diamonds). This regression was obtained weighting the C/^{234}Th ratios uncertainties and it can be used to calculate C/^{234}Th ratios at the desired depth for each station.

This C/^{234}Th-depth relationship was used to calculate the C flux at each station at 100 m (Table A.1.3; Figure 3.6 open squares) and may also be used to obtain C fluxes at the PPZ depth and at the deficit depth. The uncertainties of the C fluxes were obtained by propagating those of the ^{234}Th fluxes and the fitting of the C/^{234}Th ratios with depth. One issue to consider is that Owens et al. (2015) obtained their samples in autumn/winter (October, November and December) and only south of 40ºN, whereas our cruises were conducted in spring/summer (May, June and July) when higher NPP occurs (Antoine et al., 1996). Therefore, this curve fit should be considered with caution since the differences between the ratios from both studies and the larger amount of data from Owens et al. (2015) (with C/^{234}Th ratios generally lower than the ratios from this study) might be leading to a biased curve. Hence, we also estimated the C fluxes at 100 m using the average C/^{234}Th ratio obtained for each domain considering: i) only the ratios from this study (Figure 3.6 filled circles); and ii) a compilation of the C/^{234}Th ratios found in the literature, together with the ratios from this study (Figure 3.6, gray triangles) (Table 3.1, Figure 3.6 and Table A.1.3).

Table 3.1: Listing of studies included in the compilation, sampling year, number of ^{234}Th and/or C fluxes, integration depth, C/^{234}Th size fraction in µm ("Traps" is indicated when C/^{234}Th ratio were measured in sediment traps and "rosette" is indicated when a rossette was used to collect the particulate samples),comments regarding the model used (SS = steady state; NSS = non-steady state) together with the use of averaged or estimated C/^{234}Th ratios to calculate the C fluxes and other specific comments. The location or transect ("GA#" refer to GEOTRACES sections) and the domains sampled (SP = sub-polar; T = temperate; O = oligotrophic; R = riverine; U = upwelling; E = equatorial; see text for further details).

Reference	Year	N	Integr. depth (m)	C/^{234}Th	Comments	Location Transect	Domain
This study	2010	33	100	>53	SS	Northern half of GA02	SP, T, O, R, E
Estapa et al. (2015)	2011/12	20	100	-	SS; No C data	Sargasso Sea	T, O
Owens et al. (2015)	2010/11	38	100	>51	SS; C/^{234}Th from power-law	GA03 and southern half of GA02	T, O, E, U
Le Moigne et al. (2013)	2009	10	150	>53	SS	Porcupine Abyssal Plain	SP
Le Moigne et al. (2012)	2010	20	150	>53	SS	Irminger and Island Sea	SP
Sander et al. (2010)	2007	10	100	>53	SS	Island Sea	SP
Brew et al. (2009)	2006/07	4	100	>53	SS; Avg C/^{234}Th	BATS	O
Buesseler et al. (2008)	2004/05	64	150	>51	SS; Eddies	BATS	O
Thomalla et al. (2006)	2004	5	100	>51	SS	Atlantic Meridional Transect	T, O, E, U
Moran et al. (2003)	1999	3	100	>53	SS	Labrador Sea	SP
Sweeney et al. (2003)	1993/95	20	150	-	SS; No C data	BATS	O
Charette and Moran (1999)	1996	3	100	>53 rosette	SS	Equatorial Atlantic	R, E
Buesseler et al. (1992)	1989	3	150	Traps	NSS; Phytoplankton bloom	Porcupine Abyssal Plain	T
M81-1 (*unpublished*)	2010	16	100	-	SS; No C data	GA11	O, U, E

Average C fluxes varied depending on the C/^{234}Th ratio used, ranging from 2.7 to 13 mmol C m^{-2} d^{-1} when applying the ratios from this study, from 1.2 to 12 mmol C m^{-2} d^{-1} when using the average ratios from the compilation of studies and from 0.9 to 3.0 mmol C m^{-2} d^{-1} when using the power-law fit (Table 3.2). While absolute fluxes varied considerably, trends across latitudes within a given set of ratios were observed, with lowest C fluxes found in the oligotrophic and equatorial domains (0.9-5.7 mmol C m^{-2} d^{-1}), followed by the temperate (3.0-7.3 mmol C m^{-2} d^{-1}), and riverine domains (2.4-30 mmol C m^{-2} d^{-1}) (Table 3.2). In the sub-polar latitudes, there was large variability in C export (with deviations from the means often >100%), reflecting the high variability observed in ^{234}Th fluxes.

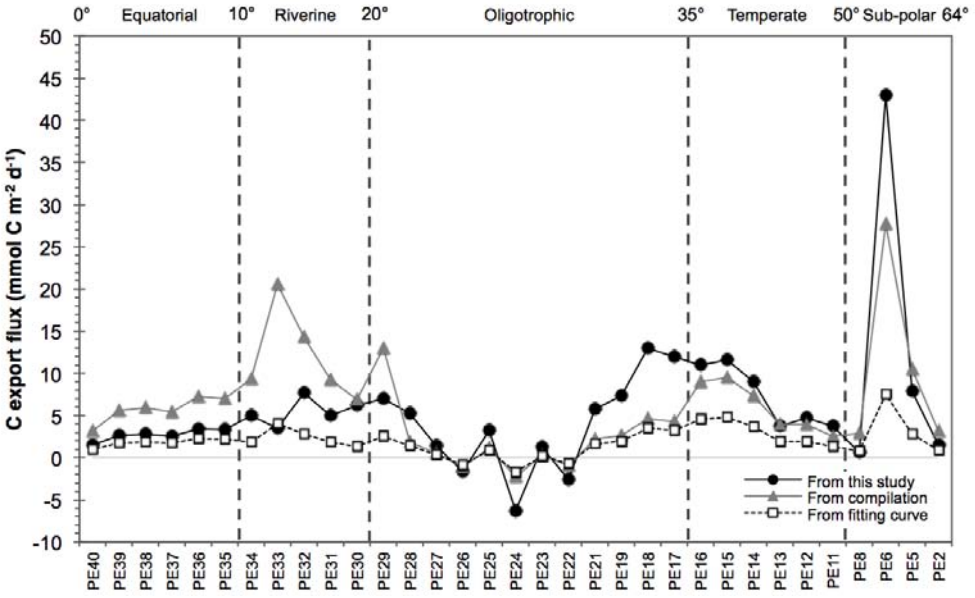

Figure 3.6: Carbon export fluxes at 100 m estimated using different C/^{234}Th ratios: using the domain averaged from ratios obtained during this study (black circles), using the domain averaged from a compilation of previous works together with data from this study (gray triangles, see Table 3.1 for a description of the studies used) and using the ratios derived from the power-law regression shown in Figure 3.5 (white squares). Latitudinal limits are indicated by the degrees (north) on top.

Table 3.2: Summary of C fluxes (in mmol C m^{-2} d^{-1}) in the North Atlantic. For this study, three different C flux estimates are reported depending on the C/^{234}Th ratio used.

Domain	Lat (ºN)	C flux at 100 m (this study) N	C/^{234}Th ratios from this study	C/^{234}Th ratios from compilation	C/^{234}Th from fitting curve	N	C flux at 100-150 m (other studies)
Sub-polar	50-65	5	13 ± 20	11 ± 12	3.0 ± 3.2	33[a, b, c]	17.5 ± 9.6
Temperate	35-50	6	7.3 ± 3.6	6.0 ± 3.0	3.0 ± 1.5	25[d,e,f,g]	8.3 ± 8.3
Oligotrophic	20-35	11	3.5 ± 5.9	1.2 ± 2.2	0.9 ± 1.6	87[d,e,h,i]	2.3 ± 1.6
Riverine	10-20	6	5.7 ± 1.5	12.2 ± 4.9	2.41 ± 0.97	2[j]	30 ± 12
Equatorial	0-10	6	2.69 ± 0.68	5.7 ± 1.5	1.80 ± 0.46	5[d,e,i]	4.9 ± 2.0

[a] Le Moigne et al. (2012); [b] Sanders et al. (2010); [c] Moran et al. (2003); [d] Owens et al. (2015); [e] Thomalla et al. (2006); [f] Le Moigne et al. (2013); [g] Buesseler et al. (1992); [h] Buesseler et al. (2008); [i] Brew et al. (2009); [j] Charette and Moran (1999). Note that two of the stations were considered riverine rather than equatorial because they were affected by the Amazon outflow.

3.4.3 Satellite-derived data: Particle Size Distribution and Net Primary Production

Particle size distribution derived from ocean color remote sensing data revealed spatial patterns that are consistent with the current understanding of oceanographic provinces (Figure 3.7), with the oligotrophic region being characterized by lower particle abundances (indicated by high transmission and fluorescence (Figure 3.2) and satellite Chl-a data, Figure 3.1and Figure 3.8) and larger quantities of picoplankton-sized particles, whereas microplankton-sized particles were more abundant in the temperate and sub-polar areas, as well as the riverine domain.

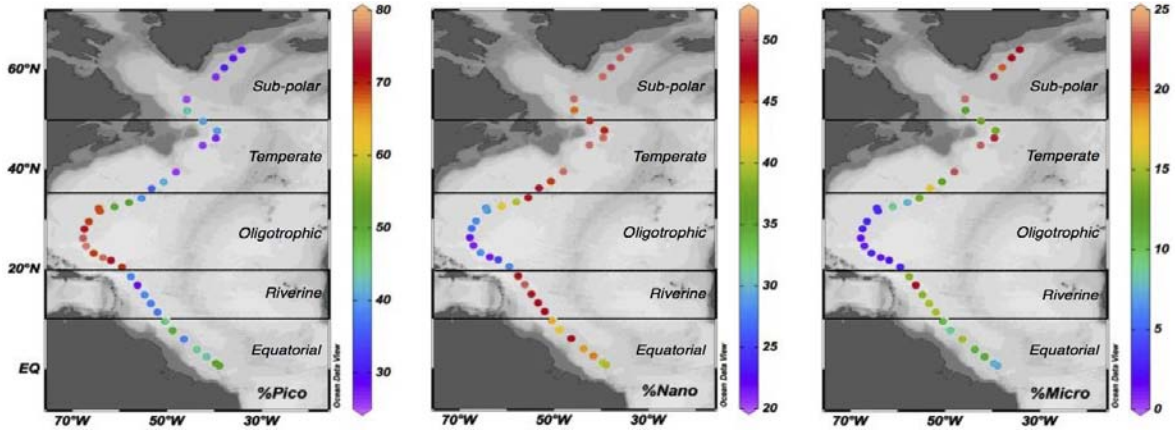

Figure 3.7: Percentage of picoplankton-sized particles (0.5–2 µm) (%Pico), nanoplankton-sized particles (2–20 µm) (%Nano), and microplankton-sized particles (20–50 µm) (%Micro) obtained from the GlobColour OSS2015 demonstration products as monthly mean values for May to July 2010 (see text for further details). Notice the different color scales.

Satellite-derived NPP ranged from 0 to 70, from 13 to 260 and from 25 to 330 mmol C m^{-2} d^{-1} for the CbPM, VGPM and A&M96 models, respectively (Table A.1.1; Figure 3.9). Highest values along the transect were obtained in the riverine and temperate domains for all models, although the increase was much more apparent using the A&M96 model in the riverine and equatorial areas, while the VGPM model produced the highest NPP values in the temperate domain. If we do not consider the sub-polar domain, for which the CbPM model provides a NPP of ~0 in three out of four stations, the lowest NPP was estimated in the oligotrophic domain, where the three models agree best. In the sub-polar domain the A&M96 and VGPM models produce similar amplitude of NPP values. In general, the A&M96 and VGPM models generate 2-4 times higher NPP than CbPM, except in the equatorial domain.

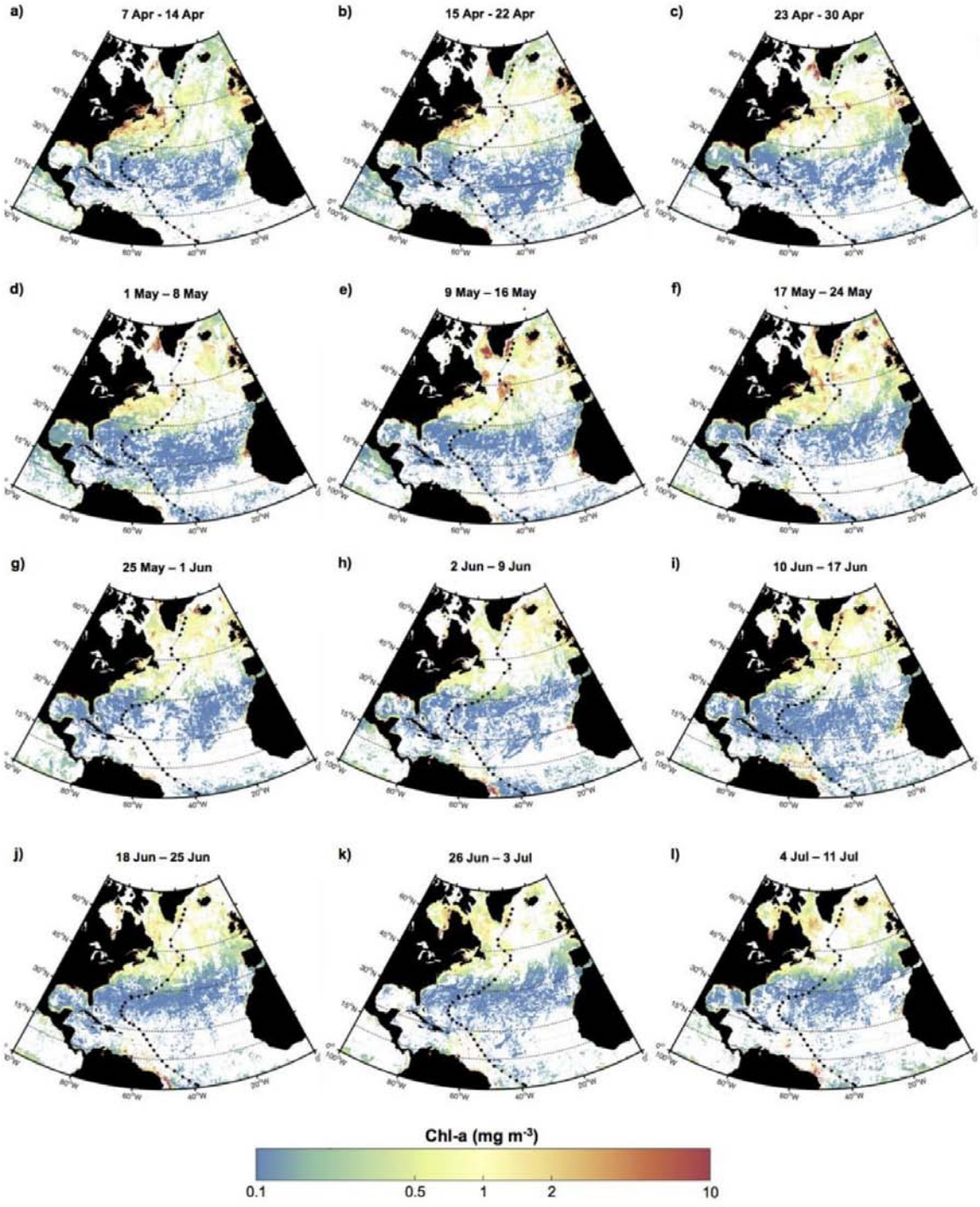

Figure 3.8: Station locations along the northern GA02 transect, between April 7th and July 11th 2010, overlain by mean 8-day chlorophyll-a concentration (mg m^{-3}) composite derived from MODIS AQUA remote sensing data. Dashed horizontal lines indicate the different domains sampled.

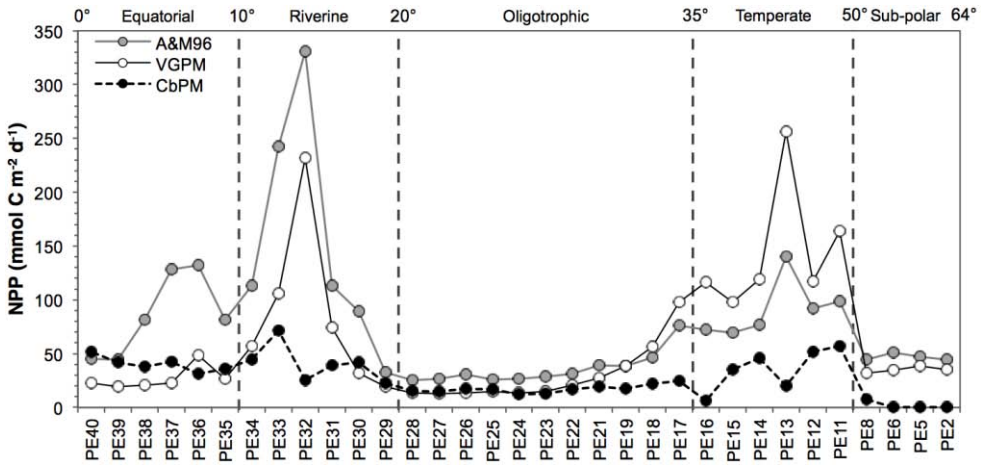

Figure 3.9: Latitudinal section (north) of satellite-derived net primary productivity (NPP) obtained using the Antoine and Morel (1996) (A&M96), the VGPM model and CbPM model results (see text for details). Latitudinal limits are indicated by the degrees (north) on top.

3.5 Discussion

Particle fluxes in the open ocean are strongly linked to surface productivity, plankton community structure and food web dynamics, which are in turn shaped by environmental conditions such as ocean physics and nutrient composition and supply (Ducklow et al., 2001). Given the observed regional differences in physical and ecological characteristics within the North Atlantic (Longhurst 1995, 2010) and the impact that distinct biome-specific scaling has on global carbon export predictions (Britten and Primeau, 2016), high spatial and time scales resolution has become essential to provide robust estimates of carbon export and to assess the links and sensitivity to global change (Galbraith et al., 2015; Honjo et al., 2014; Siegel et al., 2014). Here, we discuss estimates of ^{234}Th and C export fluxes considering the biogeochemical characteristics of the sampled areas (Figure 3.1) and present estimates of C export efficiencies along the entire transect. Regional results are then placed in context of the entire North Atlantic and compared with previous studies (see Table 3.1 for references of the studies included in the compilation) and satellite-derived export estimates.

3.5.1 ^{234}Th fluxes in the North Atlantic

Th-234 fluxes along the northern GA02 transect, together with a compilation from previous studies in open waters of the Atlantic Ocean between 10°S and 64°N, are presented in Figure 3.11 (see Figure 3.10 and Table 3.1 for locations and further details). This compilation is also used to compare the C export rates in each one of the domains (see section 3.5.2).

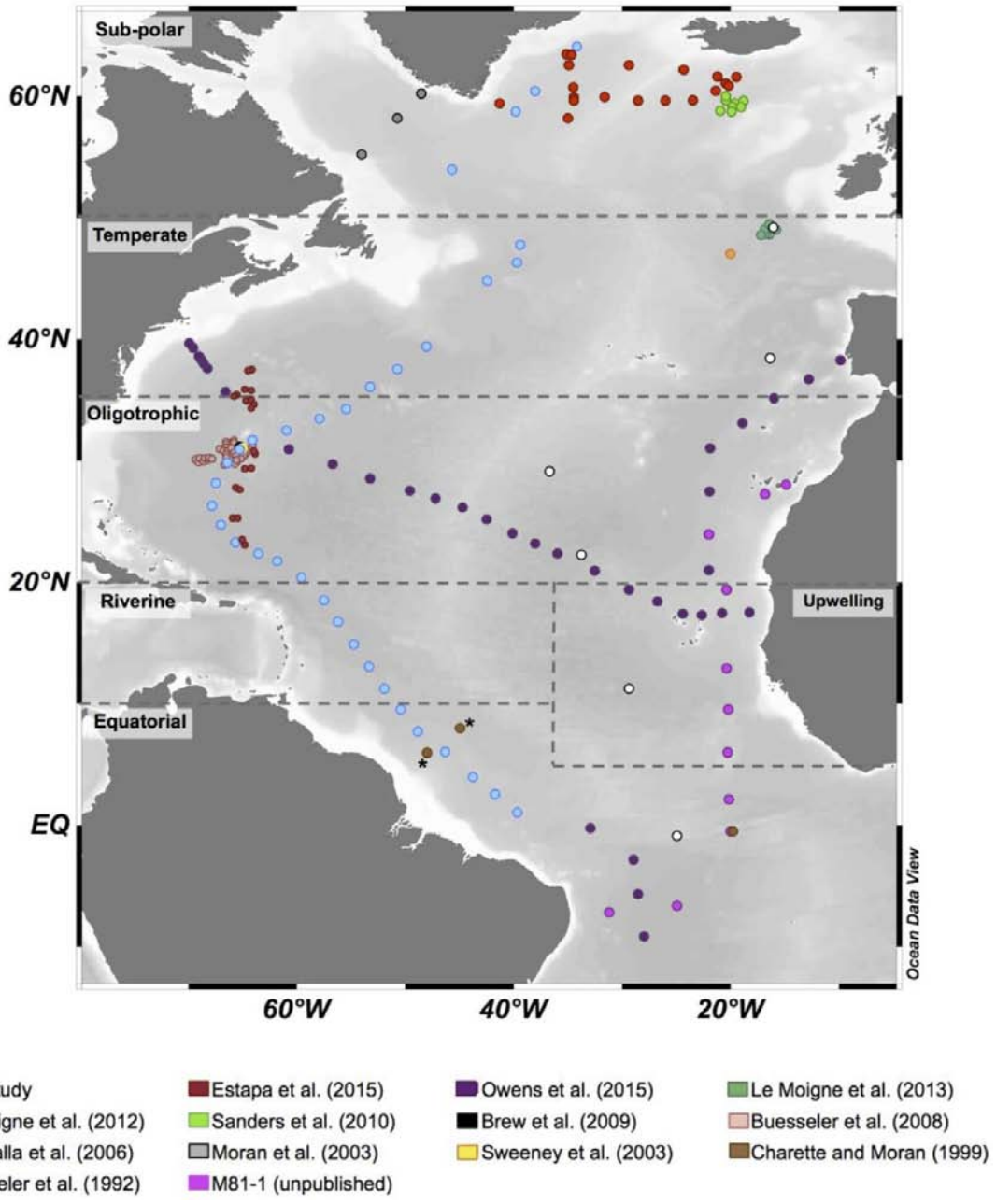

Figure 3.10: Map with the locations considered in the compilation for each study. Dashed lines indicate the limits of the domains. Two stations from Charette and Moran (1999) marked with * should be considered riverine rather than equatorial since they were affected by the Amazon outflow.

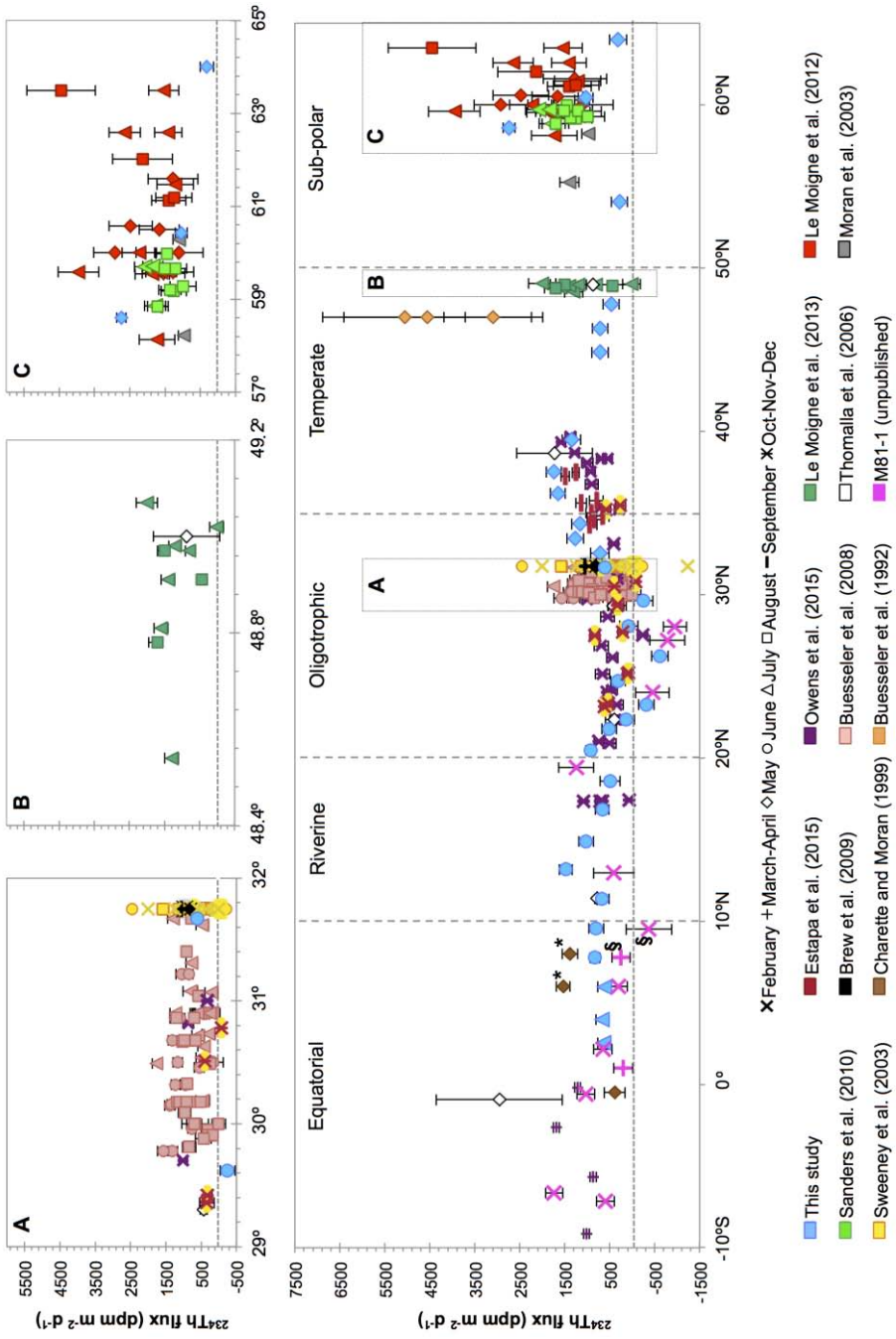

Figure 3.11: North Atlantic ^{234}Th fluxes at 100-150 m. The different colors are used to differentiate between studies whereas the different symbols are used to indicate the sampling time. Horizontal dashed lines indicate the 0 flux and vertical dashed lines are used to divide the stations into the different domains. Two stations from Charette and Moran (1999) marked with * should be considered riverine rather than equatorial because they were affected by the Amazon outflow. The stations from Owens et al. (2015), Thomalla et al. (2006) and M81-1(*unpublished*) located in the riverine domain belong to the upwelling domain since they were sampled in the eastern basin. Similarly, two stations from M81-1 (*unpublished*) marked with § located between 5°-10°N were also sampled in the eastern basin, therefore they belong to the upwelling domain rather than the equatorial.

Sub-polar (>50ºN)

Spring blooms may lead to substantial efficient and substantial particle export in this domain when irradiance periods are longer and mixed layer depths are shallower (e.g., Martin et al., 2011). The sampling of this domain took place at the beginning of May, when the water column began to stratify, as indicated by shallow mixed layer depths (<25 m; Table A.1.1), favoring the beginning of the spring bloom. Satellite images showed an increase in surface Chl-a concentrations by middle of April that continued during the sampling in this area (Figure 3.8). Silicate concentrations in the upper 50 m (Figure 3.2) were depleted, particularly at stations PE5 and PE6, suggesting that the bloom may have been dominated by siliceous phytoplankton, e.g., diatoms, consistent with the major phytoplankton group found in the region during the spring (Henson et al., 2006).

This is an area with high seasonality, where production can occur in local spring blooms and where weather conditions (i.e., North Atlantic storm track) might favor mixing of the water column and patchiness of phytoplankton blooms. In such a dynamic region the variability in the magnitude of ^{234}Th export fluxes is to 8be expected. Indeed, we measured the largest ^{234}Th flux at 100 m at station PE6 (2740 ± 140 dpm m^{-2} d^{-1} at 100 m), whereas the ^{234}Th flux at station PE8 was about an order of magnitude smaller (280 ± 190 dpm m^{-2} d^{-1}). Station PE8 was also characterized by ^{234}Th excess below 150 m, specially marked at 250 m, which could indicate episodic export events prior to sampling that were subsequently remineralized.

Our estimates of ^{234}Th fluxes at PE5 and PE6 agree well with those reported by Le Moigne et al. (2012), in the same area during the same time period (first week of May 2010), Moran et al. (2003) and Sanders et al. (2010), although Le Moigne et al. (2012) measured two very high flux estimates (3950 and 4450 dpm m^{-2} d^{-1}). However, larger variability in ^{234}Th fluxes was observed in both our study and in Le Moigne et al. (2012) compared to Sanders et al. (2010) and Moran et al. (2003). This could be related to the strong negative phase of the North Atlantic Oscillation (NAO) in the winter of 2009/2010: Henson et al. (2013) showed that the extreme NAO influenced the wind conditions, favoring an unusually large phytoplankton bloom in the Irminger Sea at that time.

Temperate (35ºN-50ºN)

Large phytoplankton blooms occur in the North Atlantic in spring, triggered by the increase in light and stratification of the water column (Henson et al., 2009; Sverdrup, 1953). As in the higher latitudes of this transect (>50ºN), predominance of large phytoplankton, especially diatoms, is observed during blooms (e.g., Taylor et al., 1993). Indeed, diatom blooms in these high latitudes of

the Atlantic Ocean can lead to significant particle export (Michaels and Silver, 1988), providing more than 50% of the annual biogenic particle mass flux in this region (Honjo and Manganini, 1993). Satellite images showed high Chl-a concentrations (>7 mg m^{-3}) in those latitudes during the sampling period (Figure 3.1), where particle size distributions derived from satellite data also indicate highest contribution of microplankton-sized particles (Figure 3.7). High fluorescence and beam attenuation coefficient values between 40ºN and 55ºN were also measured, with the highest values found at ~45ºN where stations PE12 and PE13 were sampled (Figure 3.2 and Figure 3.3). However, ^{234}Th fluxes at those stations were relatively low (~710 dpm m^{-2} d^{-1}), about 20% of the ^{234}Th fluxes previously measured during blooms in this area (e.g., Buesseler et al., 1992). This might indicate that we sampled the northern zone at an early stage of the bloom, when drawdown fluxes were still relatively low. Indeed, satellite images showed low Chl-a concentrations (<0.7 mg m^{-3}) at the beginning of May and then reached a maximum (~10 mg m^{-3}) between 11th and 15th of May (Figure 3.8), when stations PE11, PE12 and PE13 were sampled and characterized by higher fluorescence concentrations relative to the rest of the stations of this domain (~2 mg m^{-3} *vs* <0.5 mg m^{-3}; Figure 3.3). ^{234}Th fluxes at the southern stations (PE14, PE15 and PE16) were significantly higher (1350-1740 dpm m^{-2} d^{-1}), and we hypothesize that the bloom had already occurred by the time of sampling.

Oligotrophic (20ºN – 35ºN)

Phytoplankton are nutrient-limited in the oligotrophic North Atlantic (Graziano et al., 1996; Mills et al., 2004) and blooms occur when the mixed layer reaches depths deep enough to supply nutrients to surface waters (January-March) (Steinberg et al., 2001). At low nutrient concentrations picophytoplankton groups such as *Synechococcus* and *Prochlorococcus* dominate (Lomas and Moran, 2011; Sarmiento and Gruber, 2006, and references therein; Steinberg et al., 2001), as also seen in the particle size distribution data (Figure 3.7).

The sampling of this region took place during the end of May and the middle/end of June. The mixed layers at the majority of the stations were <20 m (Table A.1.1), isolating the surface waters from the nutrient rich deeper waters, and thus limiting the possibility of phytoplankton blooms. This is evidenced by the low satellite-derived Chl-a concentrations (Figure 3.1) and by the smaller (<0.5 mg m^{-3}) and deeper (down to 135 m) fluorescence maxima compared to other regions (Table A.1.1). Fluxes of ^{234}Th were low or negative from station PE21 (BATS; Bermuda Atlantic Time Series) to PE27, due to minor/negligible deficit of ^{234}Th or because of remineralization in the upper

100 m that compensated small ^{234}Th deficits. Previous works by Thomalla et al. (2006) and Owens et al. (2015) found similar results.

High surface concentrations of Fe, Mn and Al (Middag et al., 2015; Rijkenberg et al., 2014) suggested that a dust event from the Sahara Desert may have occurred between 20ºN and 30ºN. Although phytoplankton can respond to such events (e.g., Cassar et al., 2007, Southern Ocean; Izquierdo et al., 2012, Mediterranean Sea; Mills et al., 2004 and Moore et al., 2006, North Atlantic Ocean), such a response was not observed during our study in either beam attenuation coefficients or fluorescence values or significant ^{234}Th deficit (Figure 3.2 and Figure 3.3).

The ^{234}Th excess at depth at some stations, especially at station PE24, could be indicative of remineralization, suggesting that there might have been a phytoplankton response or particle export event in the past. Similar features were also reported by Sweeney et al. (2003) and Owens et al. (2015) (Figure 3.11). However, satellite images of Chl-a concentration (Figure 3.8) do not indicate the existence of a phytoplankton bloom prior to sampling nor do iron concentrations support remineralization (Rijkenberg et al., 2014). Therefore, the excesses of ^{234}Th at depth might be due to the advection of adjacent waters (i.e., Kim et al., 2003), although we have no indication of nearby large export fluxes and thus cannot provide with a plausible explanation.

Riverine (10ºN-20ºN)

Within this region, the distinctive feature that defines this domain is the influence of the Amazon River plume in the surface waters. Although the Amazon estuary is located further south, within the equatorial domain, the riverine outflow was encountered between 11ºN and 18ºN, as reflected by low salinity (<34) in the upper 30-40 m and silicate concentrations reaching as high as 8 μM at 10 m (Figure 3.2) (Reul et al., 2014; Rijkenberg et al., 2014). Fluorescence and beam attenuation also reflect the intrusion of the river plume as well as high Chl-a concentrations derived from satellite data (Figure 3.1). Indeed, a significant change in color (greenish) and transparency of the waters was also visually evident from onboard. Riverine outflows favor the stratification of surface waters due to significant salinity gradients which, together with nutrient inputs, enhance new primary production (Eppley and Peterson, 1979). DeMaster et al. (1986) showed that the high particle concentration within the Amazon River plume also scavenges particle-reactive species from open ocean waters. Stations in the core of the riverine input (i.e., PE32 and PE33) had larger ^{234}Th deficits, resulting in about two times higher ^{234}Th fluxes at 100 m than stations sampled outside the plume (average 1250 ± 320 vs 690 ± 220 dpm m^{-2} d^{-1}), and were comparable to ^{234}Th fluxes observed in the temperate latitudes and in the northern limit of the oligotrophic region.

Equatorial region (0º-10ºN)

The influence of the Amazon River plume was also observed in this domain in the upper 25 m, especially at ~4ºN, with low salinity (<34.5) and high silicate concentrations (~3.5 μM), although the signal was weaker compared to the riverine domain and was not as evident in either fluorescence or beam attenuation values. The high nutrient concentrations were coincident with a minimum oxygen concentrations and the entrance of the Antarctic Intermediate Water (AAIW) between 600 and 1200 m depth (van Aken, 2011).

Stations sampled within these latitudes had an average ^{234}Th flux at 100 m of 660 ± 170 dpm m^{-2} d^{-1}, similar to stations from the riverine domain, with the exception of those influenced by the Amazon River outflow. Previous studies in this region reported similar ^{234}Th flux estimates (Figure 3.11), except those in the eastern basin where episodic upwelling favors phytoplankton blooms and increase ^{234}Th export (Thomalla et al., 2006).

3.5.2 C export fluxes in the North Atlantic

There is a significant amount of data available of ^{234}Th-derived C fluxes in the North Atlantic. However, previous works has usually focused on the study of specific hydrographic or biological features (e.g., mesoscale eddies, phytoplankton blooms, etc.) that occur in relatively limited areas, or along transects with low spatial coverage. The GEOTRACES Program sections (Owens et al., 2015 and this study) contribute significantly to the existing data set, providing greater spatial coverage for constraining C export. Indeed, combining our work with that of Owens et al., (2015) accounts for more than a 50% increase in the number of estimates presented in the global database of Le Moigne et al. (2013) from this area. These sections provide information that can be applied not only to better understand the biogeochemical models for C but also other trace elements, such as cobalt (Dulaquais et al., 2014). We also compiled ten previous studies that, when coupled with our work, amounts to a total of about 200 estimates of C export fluxes at 100-150 m (see Table 3.1) using the ^{234}Th-method in the Atlantic open ocean waters (10ºS to 64ºN).

3.5.2.1 C/^{234}Th ratios compilation

A critical component of the ^{234}Th-derived C fluxes is the C/^{234}Th ratio measured in particulate samples. This is necessary for converting ^{234}Th fluxes into C fluxes. Basic questions such as how to accurately sample the particles that are responsible for that export remain enigmatic and controversial (i.e., Lampitt et al., 2008; Burd et al., 2010; Bishop et al., 2012). Besides the

technical difficulties in particle collection, the questions of how and why C/^{234}Th ratios vary in marine systems have been raised by several studies for more than a decade (see review by Buesseler et al., 2006), with still no clear agreement. Nonetheless, one of the most common methods is to use large particles (>50 μm) collected using *in situ* filtration pumps placed below the depth of the euphotic zone (usually standardized as 100-150 m), where C/^{234}Th variability has been found to be smaller (e.g., Jacquet et al., 2011; Owens et al., 2015; Puigcorbé et al., 2015). This method has also provided C/^{234}Th ratios that were in good agreement with those obtained from sediment traps (e.g., Planchon et al., 2015; Roca-Martí et al., 2015). The compilation presented here is based on this methodology, with the exception being the ratios obtained using sediment traps during the North Atlantic Bloom Experiment (NABE; Buesseler et al., 1992), and those from Charette and Moran (1999) that were measured in particles collected by filtering water (>53 μm) from a rosette (Table 3.1).

C/^{234}Th ratios obtained during this study ranged from 2.3 to 16 μmol C dpm^{-1} and were within the range observed from previous studies (1.9 – 25 μmol C dpm^{-1}; Figure 3.12), although relatively high ratios were measured in the oligotrophic domain (16 ± 2 μmol C dpm^{-1}) where, previous studies presented ratios usually reported ratios <5 μmol C dpm^{-1}. Data on C/^{234}Th ratios are not evenly distributed across domains (Figure 3.12). A large fraction of the data correspond to the oligotrophic domain (n = 38), with the majority (n = 23) reported by Buesseler et al. (2008) from a relatively small area (2º of latitude and ~5º of longitude) and focusing on mesoscale eddies.

The sub-polar domain is also highly sampled with regards to C/^{234}Th ratios (n = 36) compared to the temperate domain (n = 23) and the riverine and equatorial domains (n = 4 for each domain). Because of their proximity to the Mauritanian upwelling zone and their distance from the Amazon River outflow, stations between 5ºN and 20ºN in the eastern basin are considered as upwelling stations rather than riverine.

Ratios ranged from 1.7 to 25 μmol C dpm^{-1}, averaging 6 ± 5 μmol C dpm^{-1} (n = 174). Variability in the C/^{234}Th ratios, regardless of the domain, is larger in summer; May (2.3-25 μmol C dpm^{-1}), July (2.5-22 μmol C dpm^{-1}), and August (2-19 μmol C dpm^{-1}). In winter months (October to January), C/^{234}Th ratios range from 2.2 to 6.7 μmol C dpm^{-1}.

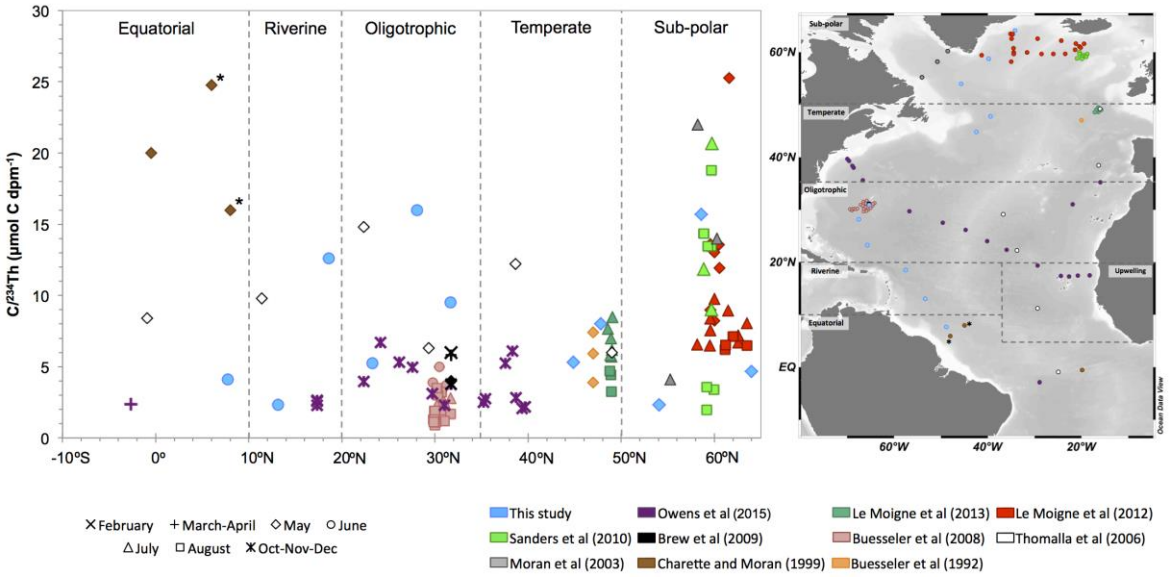

Figure 3.12: Compilation of C/^{234}Th ratios in particles >53 µm at 100-150 m. The map indicates the location of the stations. The different colors are used to differentiate between studies whereas the different symbols are used to indicate the sampling time. Dashed gray lines represent the latitudinal limits of the different domains. Two stations from Charette and Moran (1999) marked with * should be considered riverine rather than equatorial because they were affected by the Amazon outflow. Stations from Owens et al. (2015) and Thomalla et al. (2006) sampled between 10º-20ºN were located in the eastern basin, therefore they belong to the upwelling domain rather than the riverine.

3.5.2.2 C export fluxes compilation

Our dataset has a similar latitudinal trend in C export relative to previous studies (Figure 3.13). The emerging general picture is that highest C export fluxes (mmol C m^{-2} d^{-1}) are found in the sub-polar domain (17 ± 12; n = 37), followed by the riverine (12 ± 12; n = 8), the temperate (8 ± 7; n = 31), the equatorial (4 ± 2; n = 11) and the oligotrophic (2 ± 2; n = 98) regions. Table 3.2 is a summary of the average C export rates for each domain, differentiating between this study and prior studies included in the comparison. Relatively low estimates were obtained in our dataset when applying the C/^{234}Th ratio calculated using the power law regression from Figure 3.5, particularly in the riverine and the sub-polar domains (Table 3.2; Figure 3.13). This is likely due to the fact that these domains were not included in the dataset from Owens et al. (2015) used to obtain the C/^{234}Th fitting curve and also because ratios reported by Owens et al. (2015) were sampled during Oct-Dec, when C/^{234}Th ratios tend to be lower and less variable, whereas the ratios from this study and the compilation of previous studies are mainly obtained during spring/summer months. Additionally, considering the biogeochemical variability along the transect, it would probably be more appropriate to obtain a power-law fit for each domain. Unfortunately, this is not possible at this stage due to the lack of C/^{234}Th ratio profiles.

High latitudes were characterized by high C export fluxes (up to ~40 mmol C m^{-2} d^{-1}) but also large variability, probably due to the strong weather conditions (i.e., storms) and patchiness of phytoplankton blooms. The variability observed in the riverine region was also large, mainly due to the inclusion of stations clearly influenced by the Amazon outflow (stations PE32 and PE33 and also two stations from Charette and Moran, 1999), as well as stations located outside the river plume. Indeed, the stations from the western basin that were not affected by the riverine outflow had C export fluxes similar to those from the equatorial or oligotrophic domains, which had the lowest C flux estimates. The sole exception was one station reported by Thomalla et al. (2006) in the equatorial domain, for which a C export of 25 ± 12 mmol C m^{-2} d^{-1} was attributed to the occurrence of a short phytoplankton bloom triggered by the nutrient input from a local upwelling event. The equatorial station from Charette and Moran (1999) (at 0.5ºS) had also a relatively high C flux export compared to the rest of the stations from the domain, although with large uncertainties. This large export flux was mainly driven by a high C/^{234}Th ratio (20 µmol C dpm^{-1}; Figure 3.12), and the authors suggested that it was a consequence of dust inputs. However, the ratios from Charette and Moran (1999) where obtained from particles collected with a bottle rosette, which have been found to usually provide higher C/^{234}Th ratios than to *in situ* pumps (Liu et al., 2009).

With regards to the temporal distribution of C fluxes, July and August were the most sampled months (n = 45 and 43, respectively), followed by May and June (n = 33 and 32, respectively). There are only 5 estimates of C fluxes in early spring (March-April) and all are from the oligotrophic domain. The fall/winter (October to January) period had a total of 36 estimates, again with all of the measurements from the oligotrophic and equatorial domains, as well as the upwelling stations in the eastern basin. Hence, the sampling was not evenly spaced through the months, nor through the domains, so seasonal biases may exist in the compilation. Similarly, C/^{234}Th ratios derived from the power-law fit (Figure 3.5) might be underestimated due to the inclusion of data from Owens et al. (2015) obtained during the fall/winter months. Therefore, in the next two sections we discuss export efficiencies and satellite-derived export models in comparison to ^{234}Th-derived C export fluxes obtained using the average C/^{234}Th ratio of this study for each domain because, although variability exists in C/^{234}Th ratios even when sampled during the same period, this variability should be representative of the sampling period of this study.

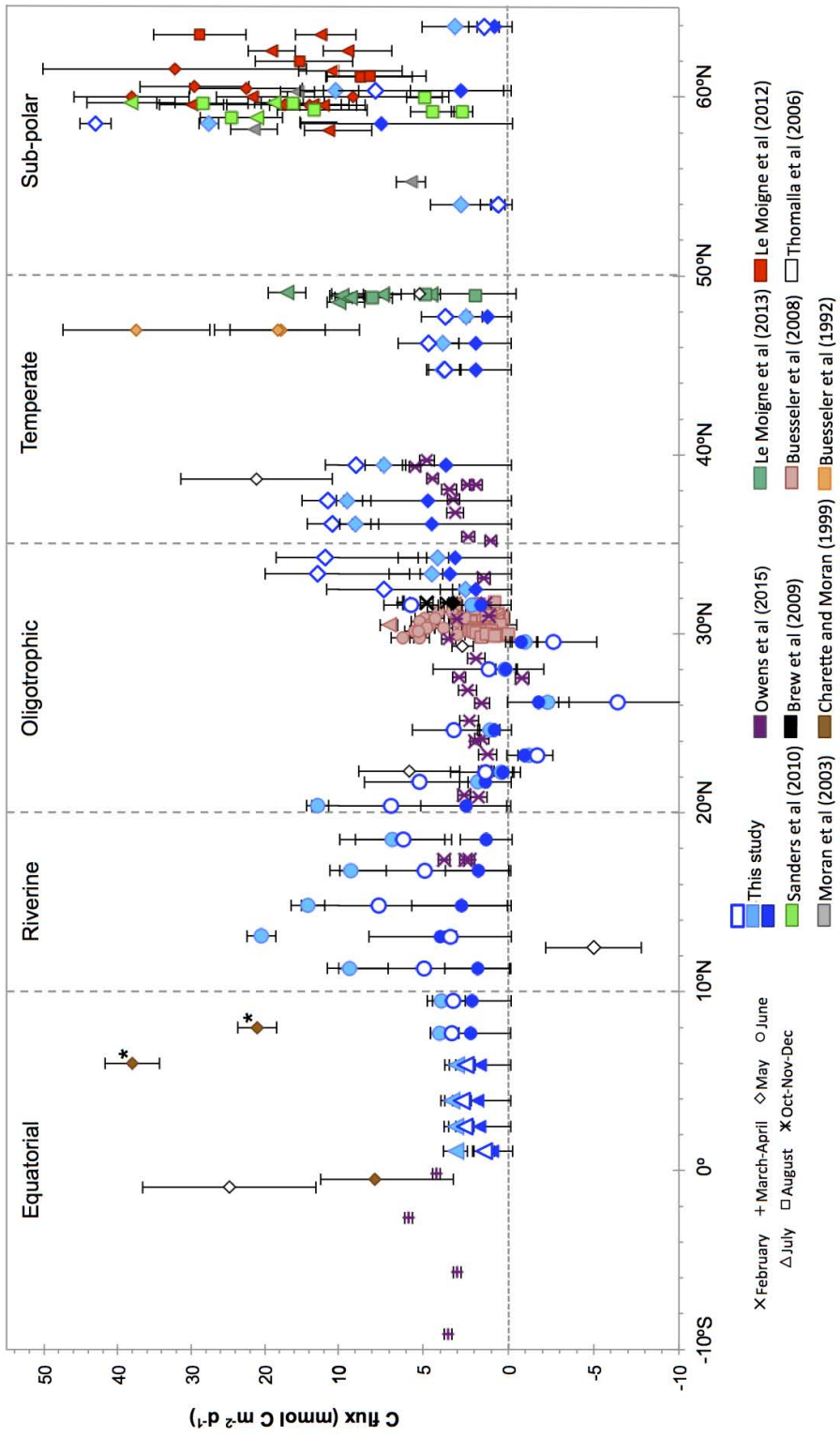

Figure 3.13: Carbon export fluxes at 100-150 m. The different colors are used to differentiate between studies whereas the different symbols are used to indicate the sampling time. The three blue color combinations refering to this study indicate the different $C/^{234}Th$ ratios used to calculate the C fluxes, with empty symbols framed by dark blue indicating the fluxes calculated using the $C/^{234}Th$ ratios from this study, in light blue for fluxes obtained using the averaged $C/^{234}Th$ ratio from the compilation of studies for each domain and dark blue indicating the use of the equation derived from the power law regression (Figure 3.5). Two stations from Charette and Moran (1999) marked with * should be considered riverine rather than equatorial because they were affected by the Amazon outflow. Stations from Owens et al. (2015) and Thomalla et al. (2006) located between 10°-20°N were sampled in the eastern basin, therefore they belong to the upwelling domain rather than the riverine. For station location see Figure 3.10.

3.5.3 Carbon export efficiencies

Carbon export efficiencies were determined using the three different satellite-derived models for NPP estimates. Large differences were found between the estimates of NPP, which were higher for most areas for A&M96 than for the other models, except for the temperate domain, while the VGPM model provided with consistently higher values than the CbPM model, except in the equatorial and the oligotrophic domains (Figure 3.9). In general, the best agreement between the 3 models was found for the oligothropic area. Maiti et al. (2016) found similar results in the Gulf of Mexico, where the VGPM model resulted in about 40% higher NPP than the CbPM model. According to Westberry et al. (2008), the CbPM deviates significantly in the distribution and timing of production because, contrarily to conventional "chlorophyll-based" models which assign all changes in Chl-a to a change in biomass, hence a change in NPP, the CbPM distinguishes between changes in Chl-a caused by photo-adaptation and changes due to growth (NPP).

Export efficiencies were generally below 25% across the entire transect when using the A&M96 and the VGPM models to derive NPP. When using the CbPM model, export efficiencies were significantly higher (up to 60%) in the transition stations between the oligotrophic and the temperate domains and at station PE32 (Figure 3.14). NPP from A&M96 lead to export efficiencies <10% at the majority of stations (20 out of 33) and agrees well with the global compilation of direct estimates by Buesseler (1998). Unrealistically high export efficiencies (>100%) were obtained at station PE6 when using NPP derived from the VGPM model and at station PE16 when using NPP derived from the CbPM model (this model estimates 3-fold to one order of magnitude lower NPP at PE16 relative to the surrounding stations). In the sub-polar domain, export efficiencies obtained from the CbPM model are not presented due to unrealistically low NPP estimates.

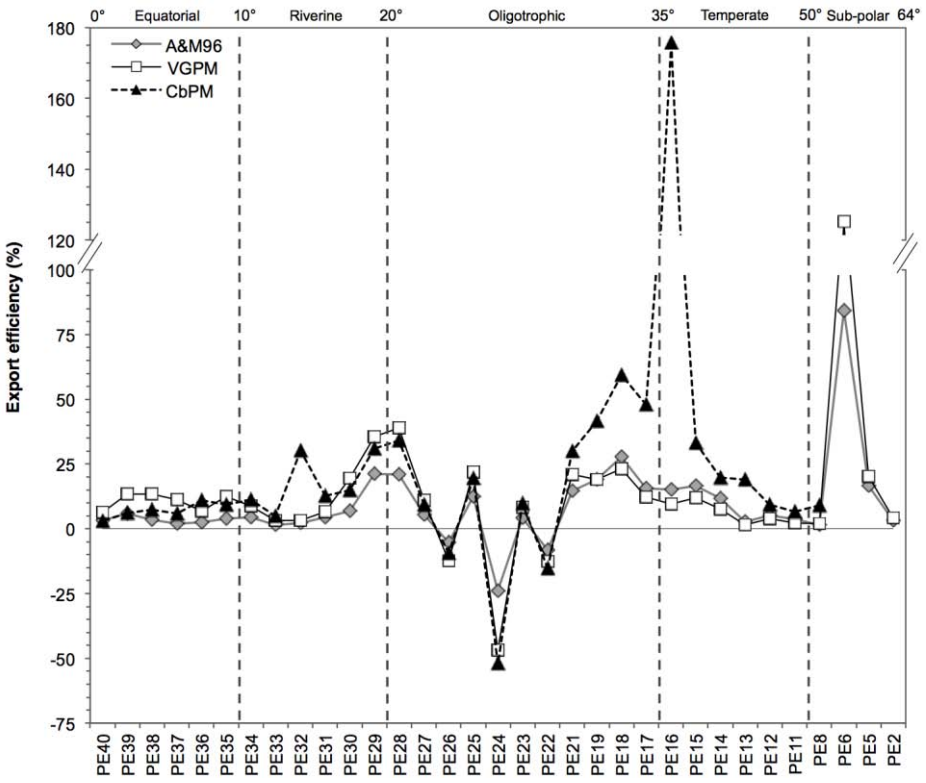

Figure 3.14: Export efficiencies obatined using three different NPP estimates (see Figure 3.9) and compared to carbon export fluxes at 100 m calculated using the C/^{234}Th ratios measured duting this study.). Latitudinal limits are indicated by the degrees (north) on top.

3.5.4 Comparison with satellite-based export models

Satellite-derived C export models have the potential to provide estimates of C export at regional to global scales year around. In addition, these models have a predictive power that can be used to forecast the impacts on the global carbon cycle from possible changes in environmental conditions (e.g., changes in temperature, stratification, etc.). Satellite-based models, however, also have a myriad of assumptions and limitations and recent studies have highlighted the necessity to develop sub-ecosystem-scale parameterization in order to provide more accurate results (Galbraith et al., 2015; Siegel et al., 2014).

The three satellite-based export models described in section 3.3.3.2 (D05, L11 and H11) were applied and compared to the ^{234}Th-derived C export estimates obtained along the northern section of the GA02 transect. In order to apply these models, we used the three different satellite-derived NPP estimates from A&M96, CbPM and VGPM models (Figure 3.15).

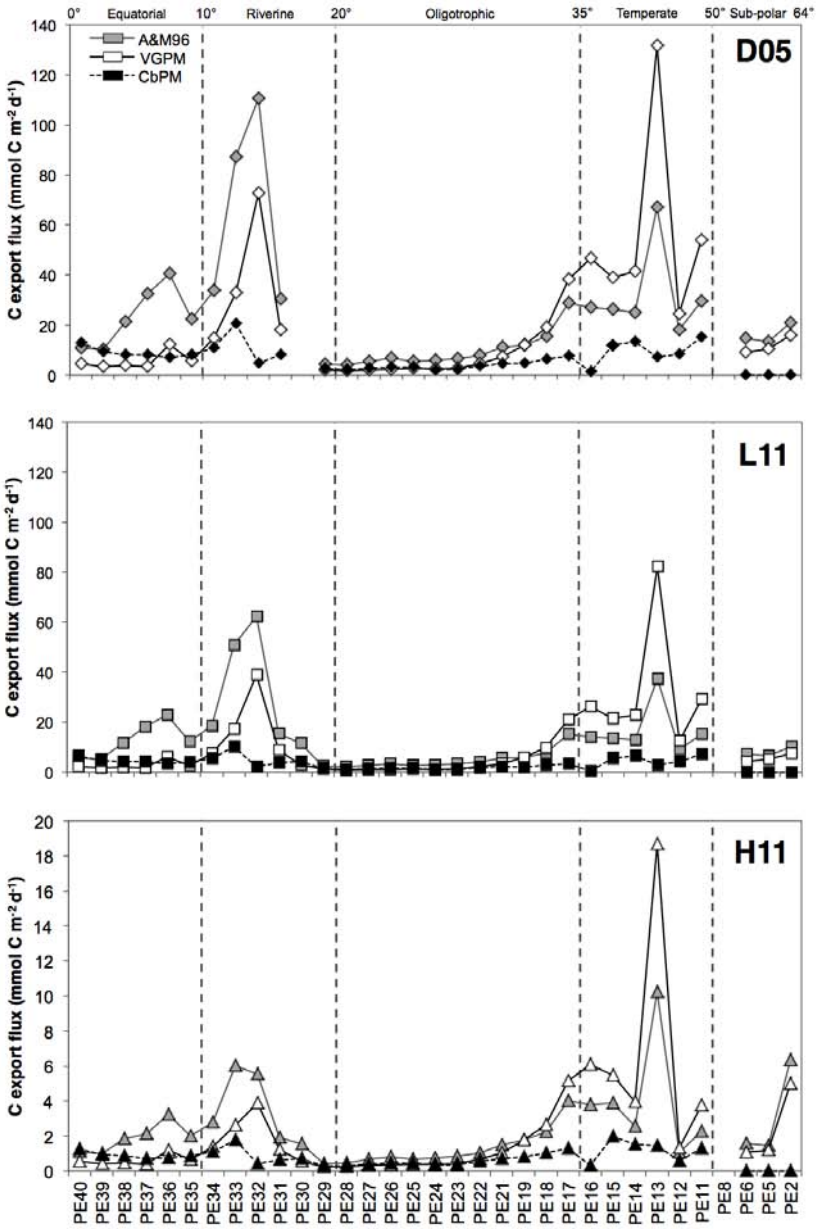

Figure 3.15: Latitudinal carbon export estimates obtained with the three different export models (D05, L11 and H11) and the three different NPP estimates (A&M96, VGPM and CbPM). Latitudinal limits are indicated by the degrees (north) on the top pannel.

The results of the export models were closer to our ^{234}Th-derived C export estimates when using the CbPM model (Figure 3.16), and thus we use it in the following discussion, except for the sub-polar region, where because of unrealistically low NPP values we used the average NPP obtained from the A&M96 and VGPM models.

Latitudinal C export fluxes derived from the three export models and ^{234}Th-derived C export using the domain averaged C/^{234}Th ratios of this study are shown in Figure 3.17. The magnitude of the fluxes differs significantly between models and with ^{234}Th-derived C export. For example, H11 significantly underestimates C export along the entire section relative to ^{234}Th-derived C export estimates, whereas L11 and D05, despite the high variability, provide estimates that are in better agreement (within a 3-fold margin) (Figure 3.17). The export determined using the H11 model depends more heavily on temperature, and thus leads to low export fluxes (<2 mmol C m^{-2} d^{-1}) throughout the entire section. Maiti et al. (2013) conducted a similar comparison between ^{234}Th- and satellite-derived C export in the Southern Ocean and observed a 2 to 4-fold overestimation of C export using the L11 and D05 models, with NPP obtained from the VGPM and the CbPM models. Stukel et al. (2015) found similar results in the eastern North Pacific Ocean. In the North Western Atlantic Ocean, we observe that D05 tends to significantly overestimate C export relative to *in situ* estimates in the equatorial domain, whereas L11 appears to underestimate C export, mainly in the northern half of the oligotrophic domain and at several riverine stations. Overall, the three models used here capture most of the geographical trends in C export, but not the absolute values. We therefore argue that parameterization of satellite-derived models should be revised and adapted to the specific oceanic regimes, taking into account factors beyond temperature and NPP, such as the trophic structure, grazing intensity or recycling efficiency (Maiti et al., 2013). In addition already the variation among NPP model results shows that further optimization of these is necessary, which is an on-going process also fostered by various inter-comparison and validation activities (e.g., Carr et al., 2006; Saba et al., 2011).

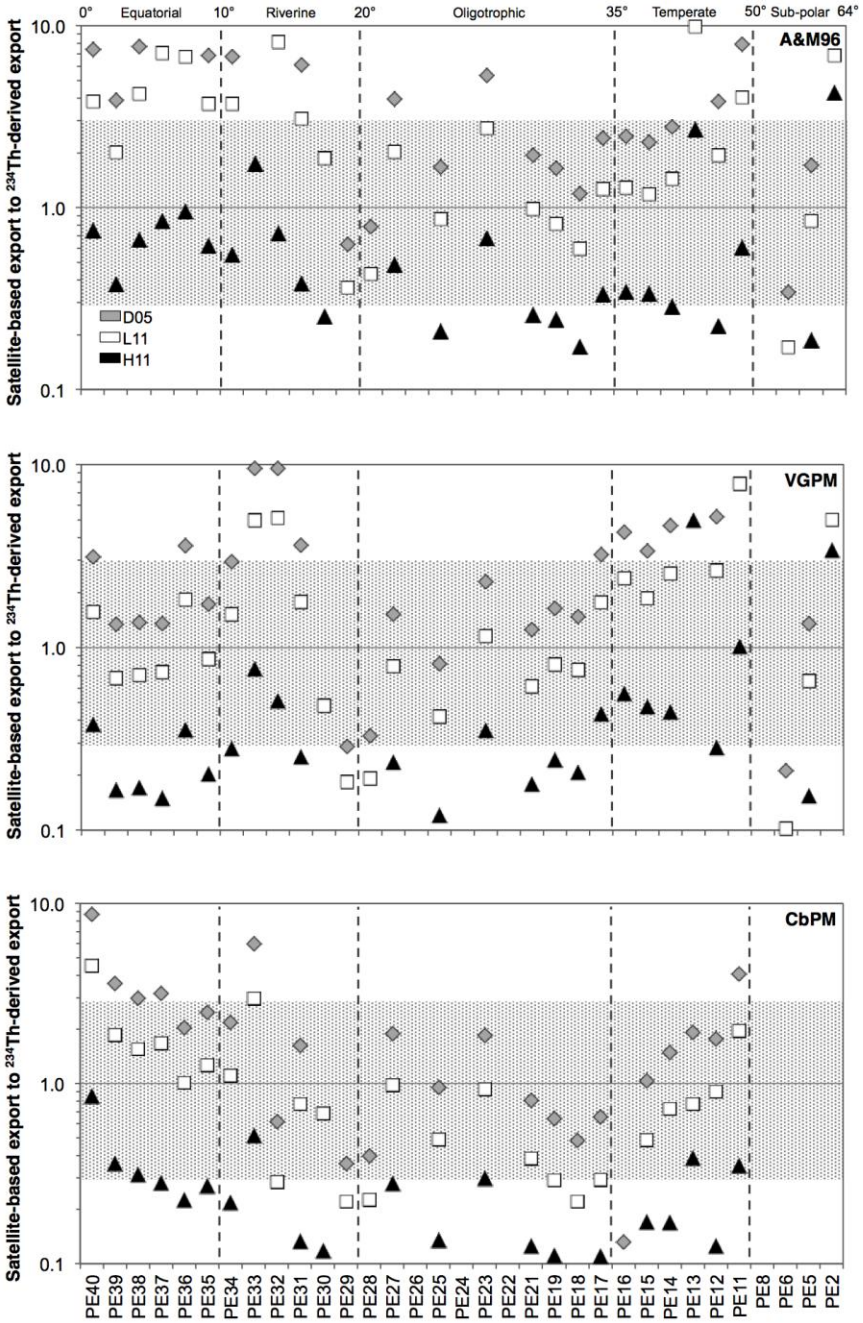

Figure 3.16: Comparison between carbon export estimates obtained with satellite-derived export models (D05, L11 and H11) vs ^{234}Th-derived estimates. The three panels are dedicated to the three different net primary productivity estimates (A&M96, VGPM and CbPM) used on the export models (see text for details). The shaded background indicates a 3-fold difference between ^{234}Th and model derived estimates). Latitudinal limits are indicated by the degrees (north) on top.

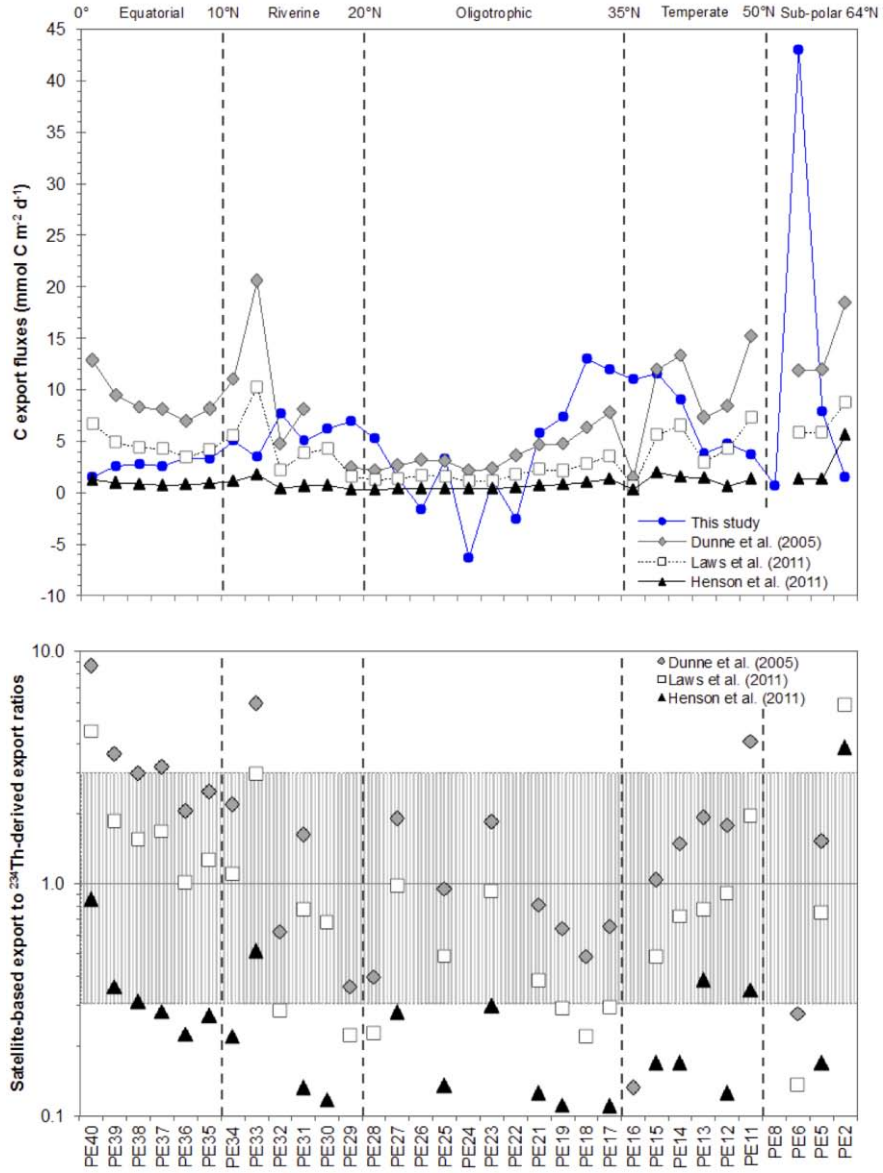

Figure 3.17: Upper panel: Satellite-derived export models comparison (using NPP estimated with the CbPM model, except for the sub-polar domain where the NPP values were averaged between A&M96 and the VGPM model; see text for details), together with ^{234}Th-derived C export fluxes obtained at 100 m using C/^{234}Th from this study averaged by domains. Lower panel: Ratios between the three satellite-based export models *vs* ^{234}Th-derived export fluxes. The shaded gray area represents a 3-fold difference between estimates). Latitudinal limits are indicated by the degrees (north) on top.

3.6 Conclusions

GEOTRACES is a global program whose objective is to "identify processes and quantify fluxes that control the distributions of key trace elements and isotopes in the ocean" (www.geotraces.org; Mawji et al., 2015). The spatial coverage of ^{234}Th-derived C export presented here, together with the sections presented in Owens et al. (2015) increased significantly the number of C export estimates for the North Atlantic Ocean (i.e., Le Moigne et al., 2013b).

Upper ocean ^{234}Th fluxes distribution agreed with previous studies, with high and variable export fluxes in the high latitudes and low to negligible in the oligotrophic region. ^{234}Th fluxes did not reflect the Sahara dust inputs between 20ºN and 30ºN identified by high concentrations of dissolved trace metals. On the other hand, the Amazon River outflow clearly impacted ^{234}Th inventories in the upper ocean, resulting in enhanced export to depth.

Carbon fluxes also compared well with previous studies, independently of the C/^{234}Th ratio estimate used, except for the riverine and sub-polar domains where fluxes were underestimated. Due to differences between satellite-derived NPP estimates, the export efficiencies varied widely, however, the majority of stations had export efficiencies <25% regardless of the NPP estimate used and were <10% when using the A&M96 NPP estimates, which is in agreement with the results presented by *Buesseler* [1998] that indicate that the majority of the global ocean has export efficiencies <10%.

When applying satellite-derived export models, similar latitudinal trends were observed between the three export models, although there were clear differences regarding the magnitude of the export. The Dunne et al. (2005) and Laws et al. (2011) models provided C export estimates closest to values obtained with the ^{234}Th approach (within a 3-fold difference), but with no clear tendency to over or underestimate the ^{234}Th-derived C export fluxes. The Henson et al. (2011) model, on the other hand, consistently provided lower export estimates probably due to the stronger dependency on temperature. In general, satellite-based export models are strongly influenced by SST and NPP, but lack biological parameters that influence C export. Tuning models and including biological parameters at a regional scale will help improve satellite-modeling efforts and provide export estimates in better agreement with *in situ* observations. Continued observing efforts are needed to resolve these open questions and thereby reduce uncertainty in the global carbon budget and improve carbon cycle monitoring from satellite-based platforms.

Chapter 4:

Particulate organic carbon export across the Antarctic Circumpolar Current at 10ºE: Differences between north and south of the Antarctic Polar Front

This chapter is based on:

Puigcorbé V., M. Roca-Martí, P. Masqué, C.R. Benitez-Nelson, M. Rutgers v.d. Loeff, L.M. Laglera, A. Bracher, W. Cheah, V.H. Strass, M. Hoppema, J. Santos-Echeandía, B.P.V. Hunt, E.A. Pakhomov and C. Klaas (2016), Particulate organic carbon export across the Antarctic Circumpolar Current at 10°E: Differences between north and south of the Antarctic Polar Front, *Deep-Sea Research II*. doi: 10.1016/j.dsr2.2016.05.016

4 Particulate carbon export across the Antarctic Circumpolar Current

4.1 Objectives

In this study, new estimates of late summer particulate organic carbon (POC) export flux for the Atlantic sector of the Southern Ocean, along the 10ºE meridian, across four different frontal zones are presented. The aim was to assess how the physical boundaries and zonal biology affect the magnitude and the efficiency of surface POC export and its transfer efficiency to depth. To do so, we analyzed water column distributions of ^{234}Th, combined with the measured ratio of POC/^{234}Th (hereafter C/^{234}Th) in order to obtain POC export fluxes and examine their variability as a function of physical oceanographic conditions, primary productivity and planktonic community stocks and composition.

4.2 Introduction

The Southern Ocean (SO) is a key component of Earth's climate due to its pivotal role in the regulation of atmospheric carbon dioxide (CO_2) and nutrient supply to other ocean basins (Gruber et al., 2009; Landschützer et al., 2015; Sarmiento et al., 2004; Takahashi et al., 2009). The SO consists of several hydrographic and biogeochemical regions delimited by zonal fronts, mostly characterized by strong horizontal temperature and salinity gradients (Orsi et al., 1995; Pollard et al., 2002b; Whitworth and Nowlin, 1987). The region between the southern limit of the Antarctic Polar Front (APF) and the southern boundary of the Antarctic Circumpolar Current (ACC) is characterized by upwelling of nutrient- and CO_2-rich deep waters (Hoppema et al., 2000; Nowlin and Klinck, 1986; Tomczak and Godfrey, 2001) and as a consequence, high macronutrients concentrations occur in the surface waters with persistent high concentrations of unused nitrate in a sufficiently lit and stratified euphotic zone.

Several *in situ* artificial iron fertilization experiments have shown that the low phytoplankton concentrations and productivity within the SO are due to iron limitation (Boyd et al., 2007; Coale et al., 2004; Smetacek et al., 2012). Changes in SO iron input and the resulting increase in particulate carbon export to greater depths (through the "biological pump") are hypothesized to be responsible for an approximately 30 ppm decrease in atmospheric CO_2 during glacial periods (Aumont and Bopp, 2006; Köhler et al., 2005). A better understanding of the relationship between primary productivity and the efficiency of the biological carbon pump is thus required in order to

determine past and present climate change impacts on the SO carbon cycle and atmospheric CO_2. Previous studies have shown that export of organic matter to the deep ocean is not necessarily proportional to primary production rates (e.g., Buesseler, 1998), and discrepancies exist between models and *in situ* measurements (Arrigo et al., 1998; Gruber et al., 2009; Maiti et al., 2013). Sediment traps have shown regional variations among the various circumpolar zones and zonal sectors in POC export to the deep sea (see Boyd and Trull, 2007 and references therein). However, scarce spatial coverage of sediment traps studies, and the possible biases associated with traps (mainly due to hydrodynamics and solubilization; Buesseler et al., 2007; Usbeck et al., 2003) warrant the use of other complementary approaches, such as the radionuclide pair $^{234}Th/^{238}U$, to quantify the spatial and temporal variability of the biological pump in the SO.

The fronts of the ACC have been found to coincide with boundaries between regions of similar phytoplankton biomass (Sokolov and Rintoul, 2007). Moreover, phytoplankton composition and distribution appear to be strongly linked to physical zonation within the SO (Laubscher et al., 1993; Read et al., 2002). Sediment records also reflect such boundaries, with large opal accumulation found south of the APF (Geibert et al., 2005; Tréguer and De La Rocha, 2013), as a consequence of spatial segregation of phytoplankton communities due to differences temperature and nutrient regimes (Falkowski et al., 1998). This in turn also affects zooplankton community composition and distribution (Hunt and Hosie, 2005; Pakhomov and McQuaid, 1996; Pollard et al., 2002a) and their grazing dynamics. Thus, physical controls on biogeochemical zonation are expected to influence the pelagic community structure, which will affect the composition of the sinking particles, and hence the downward flux of organic matter (Korb et al., 2012; Quéguiner, 2013).

4.3 Methods

Samples were collected along a meridional transect at 10ºE, between 44ºS to 53ºS, from the 11th to the 22nd of January, 2012 (Figure 4.1 and Figure 4.2) within the framework of the Eddy-Pump survey during the R/V *Polarstern* cruise ANT-XXVIII/3 (Wolf-Gladrow, 2013).

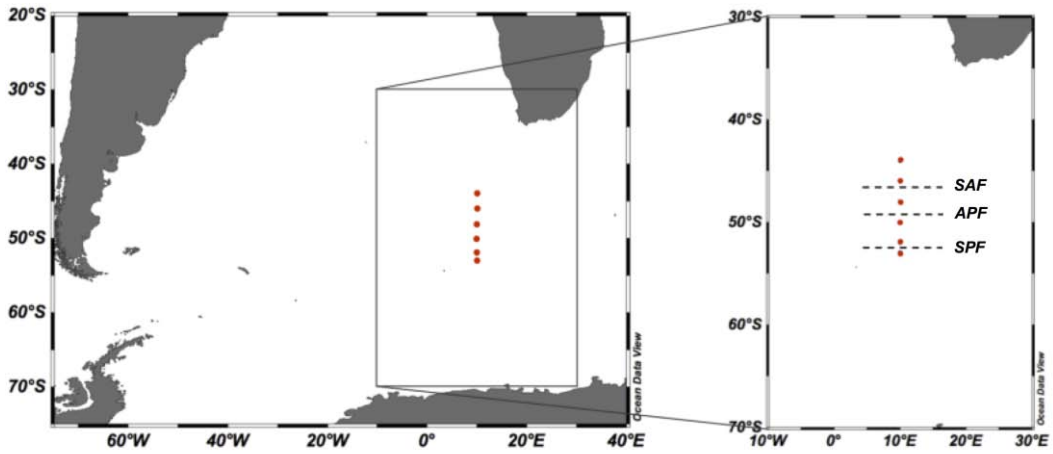

Figure 4.1: Maps of the sampled transect. Red dots indicate the location of the 6 stations where ^{234}Th profiles were analyzed. Dashed horizontal lines indicate the position of the fronts**.**

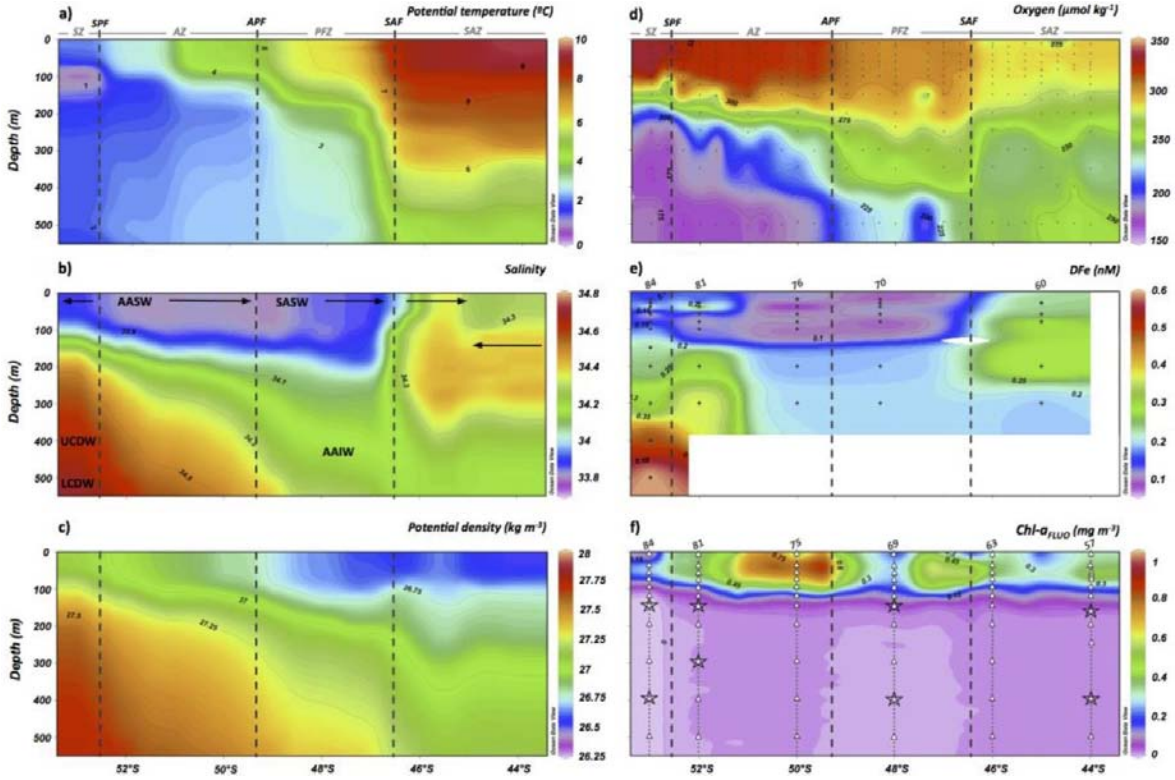

Figure 4.2: Potential temperature (a), salinity (b), potential density (c), dissolved oxygen (d), dissolved iron (e) and chlorophyll-a estimated from fluorescence (f) section plots for the upper 500 m along 10ºE. Water masses are shown in the salinity section plot: Antarctic Surface Waters (AASW), Antarctic Intermediate Water (AAIW), Sub-Antarctic Surface Water (SASW), Upper Circumpolar Deep Water (UCDW) and Lower Circumpolar Deep Water (LCDW). Horizontal black arrows in panel b) denote the direction of the main water flow. Vertical dashed black lines indicate the position of the fronts: Sub-Antarctic Front (SAF), Antarctic Polar Front (APF) and Southern Polar Front (SPF) based on Strass et al. (this issue). The frontal zones are indicated on panels a) and d) in gray: Sub-Antarctic Zone (SAZ), Polar Frontal Zone (PFZ), Antarctic Zone (AZ) and Southern Zone (SZ). Numbers in italic in panels e) and f) indicate the station number where samples were collected to analyze dissolved iron (black dots indicate sampled depths) and ^{234}Th concentrations (white triangles indicate sampled depths; stars indicate those depths where particulate samples were also collected).

4.3.1 Th-234

Six stations (St. 57, 63, 69, 75, 81 and 84) were sampled for total ^{234}Th using a CTD-rosette equipped with 12 L Niskin bottles (Figure 4.2f; Table 4.1). Seawater samples (4 L each) were collected at 12 discrete depths in the upper 500 m of the water column and processed as described in *Chapter 2*.

Table 4.1: Latitude, station number, sampling date, position relative to the location of the fronts (i.e., -SAF for stations located north of the SAF; SPF- for stations located south of the SPF), primary production zone (PPZ) depth and the equilibrium depth (Eq. depth) for the stations sampled for ^{234}Th analysis.

Lat. (ºS)	**St.** #	**Date** (2012)	**Fronts location**	**PPZ** (m)	**Eq. depth** (m)
44	57	11-Jan	-SAF	144	200
46	63	13-Jan	-SAF	122	150
48	69	15-Jan	SAF-APF	160	200
50	75	17-Jan	APF-SPF	124	200
52	81	19-Jan	APF-SPF	105	120
53	84	22-Jan	SPF-	96	100

Th-230 recoveries were measured following the adaptation of the method described in Pike et al. (2005) described in *Chapter 2*. Average recoveries of 95 ± 5% were obtained (n = 68). ^{238}U activities (in units of dpm L^{-1}) were determined from salinity data using the relationship from Owens et al. (2011) (see *Chapter 2* for details). Replicate deep water samples (2500 m) were collected at selected stations to confirm the calibration, with a resulting ^{234}Th/^{238}U activity ratio of 1.05 ± 0.09 (n = 7), consistent with that expected for secular equilibrium.

4.3.2 Particulate samples

Samples for analysis of particulate matter composition and particle associated ^{234}Th were collected at 100 and 300 or 400 m depth using *in situ* pumps (ISP; *Challenger Oceanic*) equipped with 142 mm diameter filter holders. Samples were taken at the same stations as seawater ^{234}Th profiles, except those at 46ºS and 50ºS (Table 4.2). Between 840 and 1500 L seawater was filtered through 53 µm pore-size Nitex screens. The particulate material was rinsed from the screen using filtered seawater, collected in an acid-cleaned plastic beaker and stirred to homogenize the sample. A volumetric fraction of the rinse solution, representing ~30% of the total volume, was filtered onto pre-combusted 25 mm quartz filters (QMA, Millipore) for ^{234}Th analysis. Another aliquot of a similar volume was also filtered through a pre-combusted QMA filter for POC and particulate

organic nitrogen (PON) analyses (see section 4.3.5). Filters were dried overnight at 50ºC. ^{234}Th particulate samples were counted at sea and recounted for background activities 5-7 months later, as was done for the water samples, with associated uncertainties <10%.

Table 4.2: Particulate ^{234}Th, POC and PON concentrations, C/N ratios and C(N)/^{234}Th ratios at 100 and 400 m on >53µm particles. C(N)/^{234}Th ratios at equilibrium depth are presented in italic grey font, indicative of estimated values obtained by interpolation (see text for details).

Lat.	C/N (µmol/µmol)		C/^{234}Th (µmol C dpm^{-1})			N/^{234}Th (µmol N dpm^{-1})		
(ºS)	100 m	400 m	100 m	Eq. depth#	400 m	100 m	Eq. depth#	400 m
44	5.5	9.3	16 ± 1	*14 ± 2*	4.6 ± 0.4	2.8 ± 0.2	*2.6 ± 0.3*	0.49 ± 0.04
48	10	6.7	11 ± 1	*11 ± 2*	7.8 ± 0.6	1.06 ± 0.12	*1.1 ± 0.2*	1.16 ± 0.09
52*	5.4	5.2	16 ± 1	*16 ± 1*	25 ± 2	2.9 ± 0.2	*3.0 ± 0.3*	4.9 ± 0.4
53	6.1	6.0	20 ± 2	*20 ± 2*	21 ± 2	3.3 ± 0.3	*3.3 ± 0.4*	3.6 ± 0.4

(Table 4.2 continued)

Lat.	^{234}Th (dpm L^{-1})		POC (µmol C L^{-1})		PON (µmol N L^{-1})	
(ºS)	100 m	400 m	100 m	400 m	100 m	400 m
44	0.048 ± 0.004	0.0160 ± 0.0013	0.75	0.073	0.14	0.0079
48	0.151 ± 0.018	0.0176 ± 0.0014	1.6	0.14	0.16	0.020
52*	0.166 ± 0.013	0.0132 ± 0.0011	2.6	0.33	0.49	0.065
53	0.023 ± 0.002	0.0043 ± 0.0004	0.46	0.091	0.075	0.015

* Particulate material at 52ºS was obtained at 300 m instead of 400 m
# Equilibrium depths are provided in Table 4.1

4.3.3 Dissolved iron

Five stations (St. 60, 70, 76, 81 and 84) were sampled for dissolved iron profiles (DFe) using metal-free GO-FLO bottles attached to a Kevlar line, at 5-7 discrete depths between 20 and 300 m (Figure 4.2e). The GO-FLO bottles were transferred to a clean plastic "bubble" where the atmosphere was kept clean by over pressurization with filtered air. DFe samples (~ 60 mL) were collected in 60 mL LDPE bottles directly from the GO-FLO bottles using pressurized nitrogen and inline 0.2 µm pore-size sterile capsules (Sartobran 300).

Seawater DFe concentrations were determined on board according to the voltammetric method which is based on the electroactivity of iron complexed to DHN (Laglera et al., 2013). Briefly, immediately after filtration, samples were spiked with 12 µL HCl (30%; Merk, Trace Select) per 10 mL seawater for a pH of 2.0 (NBS scale) and 30 µM of DHN (2,3-dihydroxynaphthalene). After

allowing equilibration for 24 h at room temperature, samples were spiked with 500 µL of a BrO_3^-/POPSO solution, and adjusted to pH ~8.7 with NH_4OH (15%, UltraTrace, Sigma). Analytical sensitivity was determined for each sample using two standard additions of 0.3 nM iron. The settings of the voltammetric analysis and other additional information can be found in Laglera et al. (2013).

4.3.4 Nutrients and dissolved oxygen

Macronutrients were analyzed colorimetrically on board using a Technicon TRAACS 800 auto-analyzer (Seal Analytical), according to Grasshoff et al. (1983) (for nitrate), Murphy and Riley (1962) (for phosphate) and Strickland and Parsons (1968) (for silicate). Details regarding the complete procedure are given in Hoppe et al. (2016).

Vertical profiles of dissolved oxygen through the entire water column (at about 20 discrete depths) were determined at all stations along the section (Figure 4.2d). Oxygen concentrations were measured using a standard automated Winkler technique with photometric endpoint detection. The precision as determined by the mean difference of duplicates was 0.7 µmol kg^{-1}, or better than 0.3% coefficient of variation.

4.3.5 POC and PON

POC and PON concentrations in the upper water column were measured on 1-2 L seawater samples collected directly from the Niskin bottles attached to the CTD-rosette at 7-8 discrete depths (between 10 and 200 m depth). Samples were filtered onto pre-combusted 25 mm diameter GFF filters and stored in pre-combusted glass petri dishes. After filtration, filters were dried overnight at 50°C and stored at -20°C for further analysis on land. Before analysis, samples were thawed at room temperature and a few drops of 0.1 M HCl were added to the filters to dissolve the particulate inorganic carbon. Filters were then dried overnight at 50°C. POC and PON concentrations on the ^{234}Th filters were also analyzed after beta counting (see *Chapter 2*) for comparison with filters from the ISP measured directly for POC and PON, thus comparing two aliquots of the >53 µm size fraction, in order to assess within station variability. Samples were corrected for C and N blanks (1.37 ± 0.03 µmol C and 0.20 ± 0.02 µmol N), and averaged <10% of each signal. Measurement variability based on reference standard measurements was 3.6% (N) and 1.9% (C) for the upper water column samples.

4.3.6 Chlorophyll a

4.3.6.1 Satellite data

In order to capture regional synoptic variability in surface biological processes, merged chlorophyll-*a* (Chl-a) data (ESACCI-OC-L3S product, ~4 km, version 2.0, http://www.oceancolour.org from the daily Ocean Colour Climate Change Initiative OC-CCI, 2015) was averaged over the time period of interest. The OC-CCI data product provides high quality ocean color products combining the Medium Resolution Imaging Spectrometer (MERIS) on Envisat, the Moderate resolution Imaging Spectrometer (MODIS) on the Aqua satellite and the Sea-viewing Wide Field-of-view Sensor (SeaWiFS) on Orb-View-2 sensors. For the time frame of this study only MERIS and MODIS data were available. Current data processing improves limitations of ocean color remote sensing in polar regions due to low solar elevation and frequent cloud cover. This is achieved by an improved atmospheric correction applied to MERIS data with the Polymer algorithm (Steinmetz et al., 2011), and to MODIS data following the algorithm of Gordon and Wang (1994) with several subsequent modifications and improvements according to IOCCG (2010).

4.3.6.2 In situ Chl-a

Water samples for Chl-a determination by means of fluorometry (Chl-a_{FLUO}) were collected at 8 depths between 10 and 200 m. Samples were filtered onto 25 mm GFF filters and treated following the method described in Hoppe et al. (2016). Chl-a content was measured in a Turner 10-AU fluorometer. Calibration of the fluorometer was carried out at the beginning and at the end of the cruise, with results diverging by 2%. Chl-a content was calculated using the equation given in Knap et al. (1996) using average parameter values from the two calibrations.

Chl-a concentrations were also determined by high performance liquid chromatography (HPLC; Chl-a_{HPLC}). Water samples were filtered and shock-frozen in liquid nitrogen and stored at -80°C until analysis in the home laboratory following the method of Barlow et al. (1997), as described in detail in Cheah et al. (2016). Chl-a_{HPLC} was calculated as the sum of concentrations of monovinyl *a* and chlorophyllide *a* (divinyl chlorophyll *a* was below detection in all samples). Chl-a inventories were determined to a depth of 100 m according to the method described by Morel and Maritorena (2001).

As shown by Hoppe et al., (2016), both Chl-a data sets (Chl-a_{HPLC} and Chl-a_{FLUO}) were very similar ($r^2 = 0.97$, $p < 0.001$, n = 104, Chl-a_{FLUO} = 0.990 * Chl-a_{HPLC} + 0.0837). Chl-a_{HPLC} data was used to derive primary production rates (see section 4.4.6).

4.3.7 Phytoplankton size classes

Three pigment-based phytoplankton size classes (micro-, nano-, and picophytoplankton) were estimated following the procedure as in Uitz et al. (2009), using defined marker pigment concentrations in relation to Chl-a_{HPLC}, which has been tested for the SO waters (e.g., Uitz et al., 2009). Microphytoplankton corresponds to phytoplankton with size >20 μm, nanophytoplankton between 2-20 μm, and picophytoplankton between 0.2-2 μm. Detailed description of the calculation is presented in Cheah et al. (2016).

4.3.8 Zooplankton

Zooplankton samples were collected from the upper 250 m of the water column during double oblique tows using a Rectangular Midwater Trawl (RMT 1+8) equipped with 1 m^2 (0.33 mm mesh size) and 8 m^2 (4.5 mm mesh size) nets. RMT8 samples were representative of the macrozooplankton and RMT1 samples were representative of the mesozooplankton (Atkinson and Peck, 1990; Ward, 1989). A flowmeter (Hydro Bios, Kiel) was mounted in the mouth of the RMT8 to measure the water volume filtered. Net tows were conducted at a speed of 2 to 2.5 kn. RMT8 samples were preserved in a 4% formaldehyde and seawater solution. Specimens were identified to the species level, counted and measured. Dry weight biomass was calculated using known length-weight relationships (Mizdalski, 1988; E.A. Pakhomov, *unpublished data*). RMT1 samples were split and one half preserved in a 4% formaldehyde and seawater solution formalin, and the other half sieved, dried at 50^{o}C for 48 hours, and weighed for sample dry weight.

4.4 Results

4.4.1 Hydrography: Fronts and water masses

Vertical meridional potential temperature (θ), salinity, potential density, oxygen, DFe and Chl-a_{FLUO} over the upper 500 m are shown in Figure 4.2. A detailed description of the hydrographic characteristics encountered along the 10°E transect is given in Strass et al. (2016). The Sub-Antarctic Front (SAF), located at 46.5ºS, was identified by an abrupt southward decrease in surface temperature and salinity. The Antarctic Polar Front (APF), apparent at 49.3ºS based on density profiles, was also associated with the northernmost extent of the temperature minimum layer. Finally, at 52.5ºS, the Southern Polar Front (SPF) was defined by a strong increase in salinity and steep decrease in surface temperatures.

Also indicated in Figure 4.2b are the water masses sampled along the 10ºE transect (Strass et al., this issue). Antarctic Surface Waters (AASW) and Sub-Antarctic Surface Waters (SASW) occupied the upper ~100 m south of the SAF. Below the pycnocline, Antarctic Intermediate Water (AAIW), with its salinity minimum of 34.2, extended northward of the SAF below depths of 300 to 400 m, whereas Upper Circumpolar Deep Water (UCDW) (salinity = 34.75 and θ = 2ºC) was only found south of the SPF. North of the SAF, a subsurface salinity maximum was evident between 100 and 300 m. This feature likely originated farther north where it was subsequently displaced southward as an anticyclonic eddy Strass et al. (2016). Previous observations of such subsurface lobes of saltier water indicate that this is a common feature of the Subtropical Frontal Zone, located farther north of this transect (Heath, 1976; Smythe-Wright et al., 1998). Poleward compensation of Ekman convergence has been suggested as the origin of these features (Heath, 1976), which were occasionally found as far south as 50ºS (Deacon, 1945).

4.4.2 Dissolved iron

DFe concentrations were generally low along the meridional transect, ranging from 0.08 to 0.33 nM in the upper 100 m and varied with the major gradients of other ancillary parameters (Figure 4.2e). Highest concentrations were measured in the upper 25 m of the SAZ (44ºS-46ºS) decreasing southwards, with almost full depletion at southwards, with almost full depletion at ~50ºS. This corresponds to the area where the highest Chl-a_{FLUO} values were also found (Figure 4.2f). Indeed, Chl-a_{FLUO} and DFe concentrations were significantly inversely correlated (Spearman correlation coefficient, $\rho = -0.83$, $p < 0.0001$, $n = 21$).

A subsurface increase of DFe was observed at 40 m at the two southernmost stations (81 and 84) as well as a layer (60-80 m) of depleted DFe (0.07-0.13 nM), that matched a deep Chl-a_{FLUO} maximum (~0.6 mg m^{-3}) (Figure 4.2e,f). At these same stations below 100 m, higher concentrations of DFe occurred, which were positively correlated with salinity and negatively correlated with oxygen (Pearson correlation coefficient, r = 0.82 and ρ = -0.85, respectively, p <0.01, n = 9). Furthermore, these high DFe concentrations were associated with the highest concentrations of nitrate and phosphate measured along this section (>35 μM for nitrate and >2.4 μM for phosphate; data not shown). A subsurface maximum of DFe (80-200 m) was also observed in the SAZ, coinciding with a subsurface salinity maximum (Figure 4.2b,e).

4.4.3 ^{234}Th deficits and fluxes

Significant deficits of ^{234}Th relative to ^{238}U (up to ~45%) were found in the upper 100-200 m of the water column at all the stations (Figure 4.3), with lowest deficiencies (~25%) observed at the two southernmost stations (52ºS and 53ºS). Deficits were consistent with the primary production zone (PPZ), here defined as the depth where fluorescence is reduced to 10% of its maximum value (Owens et al., 2015; Table 4.1). No significant ^{234}Th excess was observed. At 300-350 m, an additional small depletion of ^{234}Th was measured at the two southernmost stations. This depletion was not considered when estimating fluxes at depth due to poor vertical resolution below 200 m.

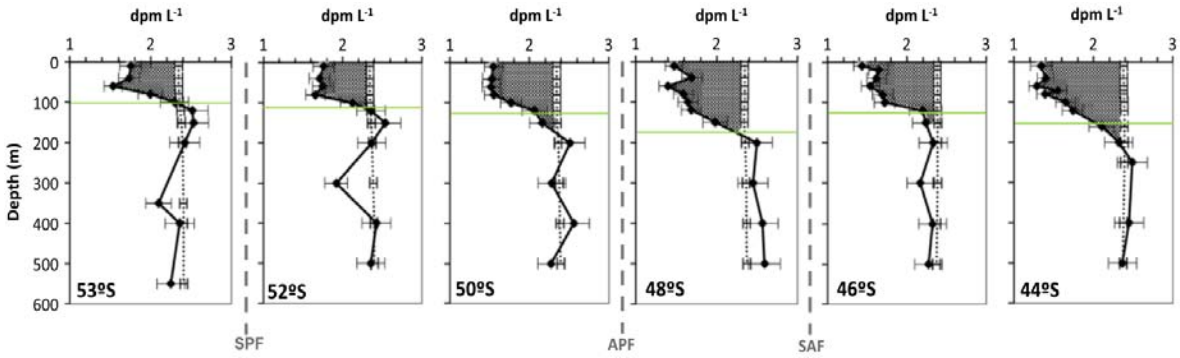

Figure 4.3: Profiles of total ^{234}Th (black diamonds) and ^{238}U (dashed line) activities at selected stations along the 10ºE transect. Areas highlighted in grey indicate ^{234}Th surface deficits. Horizontal green lines indicate the PPZ depth (see text for details). Vertical gray dashed lines between the panels indicate the location of the fronts.

Steady state water column ^{234}Th fluxes, derived from the integrated ^{234}Th deficits with respect to ^{238}U activities, were determined at three depths at each station (Table 4.3; Figure 4.4): i) the equilibrium depth (Eq. depth; i.e., first depth where there is no significant difference between ^{238}U and ^{234}Th activities within error; Table 4.1); ii) 100 m, for better comparison with literature values

and to match the shallow ISP deployment depth, and iii) 400 m to match the deep ISP deployment depth and to examine flux attenuation with depth.

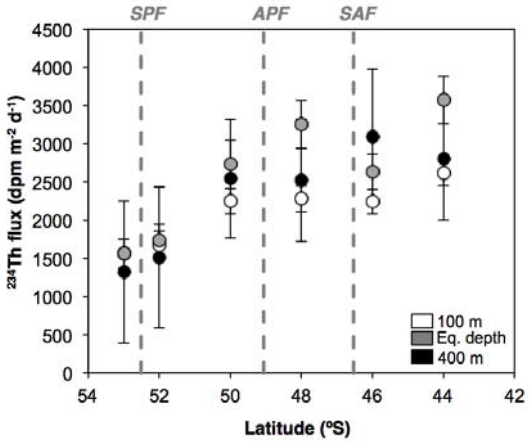

Figure 4.4: Export fluxes of ^{234}Th estimated at 100 m (white symbols), equilibrium depth (grey symbols) and at 400 m (black symbols) along the transect. Vertical grey dashed lines indicate the position of the fronts.

Table 4.3: Export fluxes of ^{234}Th, POC and PON along the transect, together with estimated primary production rates (PPRes), export efficiencies (ThE) and transfer efficiencies (Trans. Eff.). POC and PON fluxes in italic gray font are indicative of estimated values using C(N)/^{234}Th that were not obtained at those stations (i.e., at 46ºS and 50ºS the ratios used were sampled at 44ºS and at 52ºS, respectively; see text for details).

Lat.	Th fluxes (dpm m^{-2} d^{-1})			POC fluxes (mmol C m^{-2} d^{-1})		
(ºS)	100 m	Eq. depth[#]	400 m	100 m	Eq. depth[#]	400 m
44	2610 ± 160	3570 ± 310	2800 ± 800	41 ± 4	50 ± 7	13 ± 4
46	2240 ± 160	2630 ± 230	3090 ± 890	*35 ± 4*	*37 ± 5*	*14 ± 4*
48	2280 ± 170	3250 ± 310	2520 ± 800	25 ± 4	34 ± 7	20 ± 6
50	2250 ± 170	2730 ± 320	2540 ± 780	*35 ± 4*	*43 ± 6*	*64 ± 20*
52	1670 ± 190	1730 ± 210	1510 ± 920	26 ± 4	27 ± 4	*38 ± 24
53	1560 ± 190	1560 ± 190	1320 ± 930	32 ± 5	32 ± 5	28 ± 20

(Table 4.3 continued)

Lat.	PON fluxes (mmol N m^{-2} d^{-1})			PPRes (mmol C m^{-2} d^{-1})	ThE (%)	Trans. Eff. (%)
(ºS)	100 m	Eq. depth [#]	400 m	100 m	100 m	Eq. depth to 400 m
44	7 ± 1	9 ± 1	1.4 ± 0.4	59 ± 12	69 ± 15	26 ± 9
46	*6.3 ± 0.7*	*7 ± 1*	*1.5 ± 0.5*	54 ± 11	55 ± 18	38 ± 13
48	2.4 ± 0.3	3.5 ± 0.7	3 ± 1	54 ± 11	46 ± 11	58 ± 22
50	*5 ± 3*	*8 ± 1*	*13 ± 4*	86 ± 17	35 ± 12	148 ± 52
52	4.9 ± 0.7	5.1 ± 0.8	*8 ± 9	74 ± 15	36 ± 9	**141 ± 90
53	5.2 ± 0.8	5.2 ± 0.8	5 ± 3	73 ± 15	44 ± 11	89 ± 64

[#] Equilibrium depths are provided in Table 4.1
*C(N)/^{234}Th ratios were sampled at 300 m
** Transfer efficiency between Eq. depth and 300 m

Fluxes were calculated using a 1-D steady state model (Coale and Bruland, 1985) and neglecting advective and diffusive fluxes. An estimate of the magnitude of these fluxes is provided further below (see section 4.5.1). The fluxes at 100 m ranged from 1560 to 2610 dpm m^{-2} d^{-1} (average 2100 ± 400 dpm m^{-2} d^{-1}). The equilibrium depth was generally found at 150-200 m (except at 52ºS and 53ºS). These deeper ^{234}Th deficits represented a 20 - 40% increase in the ^{234}Th flux estimates, compared to those at 100 m. Thus, ^{234}Th flux estimates at the equilibrium depth ranged from 1560 to 3570 dpm m^{-2} d^{-1}, with an average flux of 2600 ± 800 dpm m^{-2} d^{-1}. Similar fluxes were also obtained at 400 m, ranging from 1320 to 3090 dpm m^{-2} d^{-1} (average 2300 ± 720 dpm m^{-2} d^{-1}) (Table 4.3). ^{234}Th fluxes estimated at the three depth horizons decreased with latitude (r^2 = 0.92, p = 0.010; r^2 = 0.89, p = 0.015 and r^2 = 0.89, p = 0.017; for fluxes at 100 m, at equilibrium depth and at 400 m, respectively).

4.4.4 Particulate samples: ^{234}Th, POC and PON concentrations and ratios

Particulate (>53 μm particle size) ^{234}Th activities were 1 - 17% of the total ^{234}Th measured at 100 m, and were between 3-13 times higher than those measured at 400 m (<1% of total ^{234}Th) (Table 4.2). POC and PON concentrations were measured in two different filter sets, one where particulate ^{234}Th was also analyzed (C_{Th} and N_{Th}) and the other for POC and PON analyses only (C_{CN} and N_{CN}), to check for heterogeneity in sampling. The POC and PON concentrations measured on both filter sets were similar, validating our measurements on the ^{234}Th filters used to obtain the C/^{234}Th (C_{Th}) and N/^{234}Th (N_{Th}) ratios (C_{Th} = 0.91 * C_{CN} + 0.24 and N_{Th} = 0.90 * N_{CN} + 0.01; r = 0.99, p <0.001 and n = 14 for both data sets).

POC and PON concentrations (from particles >53 μm) decreased with depth at all the stations (Table 4.2). C/N ratios remained nearly constant with depth at the two southernmost stations (change <4%), while they varied by a factor of about 2 north of the APF (Table 4.2). C/^{234}Th ratios at 100 m ranged from 11 to 20 μmol C dpm^{-1} and from 4.6 to 25 μmol C dpm^{-1} at 400 m. North of the APF, C/^{234}Th ratios at 100 m were higher than the ratios at 400 m. At the southernmost station, at 53°S, the ratio was found to be similar at both depths, and increasing with depth at 52ºS (Table 4.2). N/^{234}Th ratios ranged from 1.1 to 3.3 μmol N dpm^{-1} at 100 m and from 0.49 to 4.9 μmol N dpm^{-1} at 400 m. Due to time constrains, ISP could not be deployed at all stations (Figure 4.2f). Therefore, in order to calculate POC and PON export fluxes at 46ºS and 50ºS (see section 4.4.5) we used C/^{234}Th and N/^{234}Th ratios measured at stations at 44ºS and 52ºS, which belonged to the same biogeochemical provinces, respectively (44ºS and 46ºS: SAZ 50ºS and 52ºS AZ; Figure 4.2).

4.4.5 POC and PON fluxes

POC and PON export fluxes were obtained by multiplying the ^{234}Th fluxes by the C(N)/^{234}Th ratios of the particles collected with the ISP (Table 4.3). These export estimates are therefore based on the assumption that the C(N)/^{234}Th ratios of particles >53 μm are representative of sinking matter. The rationale for using this conversion factor is that in the SO, large particles, such as diatoms and fecal pellets, are considered to be main drivers of the particulate export flux (Cavan et al., 2015; Honjo et al., 2008; Laurenceau-Cornec et al., 2015; Rutgers van der Loeff et al., 2002). Thus, one would expect particles >53 μm to be representative of the sinking material, rather than smaller particle sizes. POC fluxes at 100 m ranged from 25 to 41 mmol C m^{-2} d^{-1}, with no clear latitudinal variation (Figure 4.5). However, POC export flux estimates at 400 m, indicated enhanced export in the southern half of the transect, whereas at the two northernmost stations significant attenuation of the flux with depth was observed (Table 4.3; Figure 4.5). PON fluxes at 100 and 400 m ranged from 2.4 to 7 mmol N m^{-2} d^{-1} and from 1.4 to 13 mmol N m^{-2} d^{-1}, respectively, showing similar patterns to the POC fluxes (Table 4.3). From 44ºS to 48ºS, POC and PON fluxes at the equilibrium depth tended to be higher than at 100 m, ranging from 34 to 50 mmol C m^{-2} d^{-1} and from 3.5 to 9 mmol N m^{-2} d^{-1}, respectively, whereas in the southern half of the transect no significant differences were observed between both depths (Table 4.3).

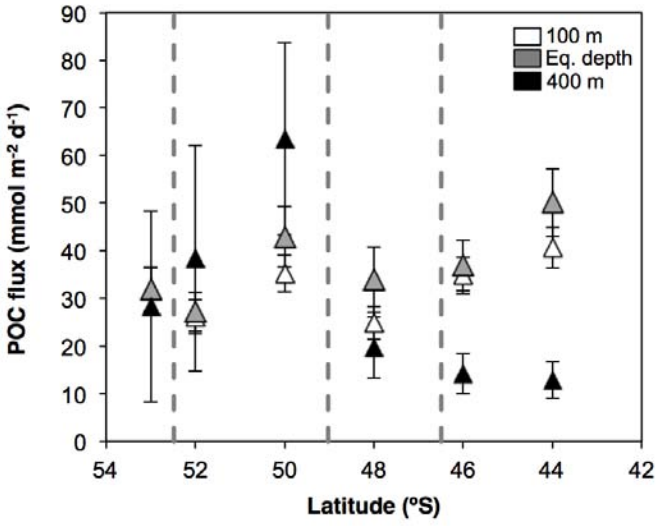

Figure 4.5: Export fluxes of POC estimated at 100 m (white triangles), equilibrium depth (grey triangles) and at 400 m (black triangles) along the transect. Vertical grey dashed lines indicate the position of the fronts.

4.4.6 Derived primary production

Measurements of *in situ* daily primary production using ^{14}C uptake (PP; see Hoppe et al., 2016 for details) coincided with ^{234}Th sampling at only two stations (81 and 84). Therefore, we used estimated primary production rates (PPRes). PPRes were derived from the relationship between Chl-a_{HPLC} standing stock measurements in the upper 100 m of the water column (Chl-a_{HPLC}_100m) and PP at 100 m from the stations sampled at ~12ºW (from 29 Jan to 17 Feb 2012; data from Hoppe et al., this issue) and at stations 81 and 84 (C.J.M Hoppe, *unpublished data*): PP = 232 + 13 * Chl-a_{HPLC}_100m (with PP expressed in mg C m^{-2} d^{-1}; $r^2 = 0.82$, $p < 0.001$, n = 11). Using this equation, PPRes estimated for all stations had a mean relative deviation of -3% and a standard deviation of 20% when compared to directly measured PP (n = 11). The derived PPRes ranged from 54 to 86 mmol C m^{-2} d^{-1} (Table 4.3). The stations north of the APF showed significantly lower PPRes than in the southern half of the transect (56 ± 3 mmol C m^{-2} d^{-1} *vs* 78 ± 7 mmol C m^{-2} d^{-1}).

4.4.7 Phytoplankton and zooplankton distribution

Along the transect, a clear shift in phytoplankton communities was observed north and south of the APF (Figure 4.6, see also Cheah et al., 2016). Nanophytoplankton dominated north of the APF, with microphytoplankton abundances <40%. South of the APF the phytoplankton community was dominated by microphytoplankton (>60%). Picophytoplankton represented <10% along the entire transect.

Total mesozooplankton biomass was an average of 45% higher than macrozooplankton biomass across the transect (Figure 4.7). An exception was at 52ºS where the macrozooplankton biomass was inflated by a large ctenophore catch. Mesozooplankton biomass was elevated in the vicinity of the APF, but no clear difference was observed between the areas to the north and south of this front. Macrozooplanton biomass tended to be higher south of the APF, but stations with comparable biomass were recorded north of the APF. Overall, the macroplankton community north of the APF was dominated (in order of numerical importance) by chaetognaths (54%), while south of the APF salps (tunicata) accounted for up to 91% of the numerical abundance (Figure 4.7).

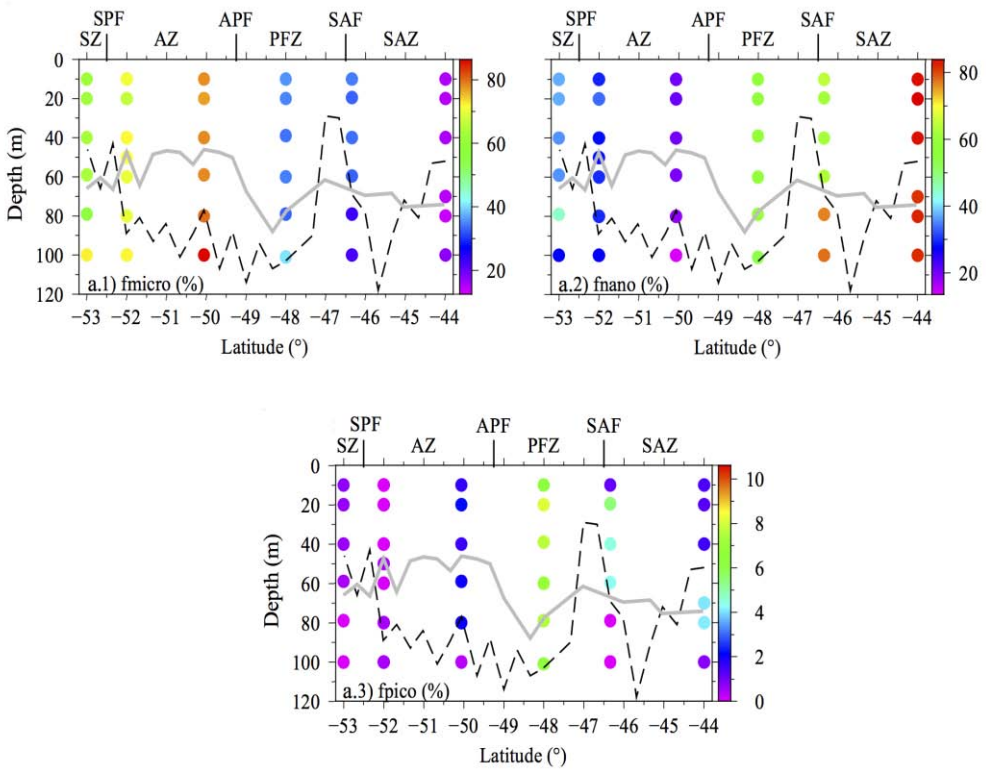

Figure 4.6: Relative contribution (%) of integrated phytoplankton size classes in the upper 100 m: micro- (a.1), nano- (a.2) and picophytoplankton (a.3) derived from pigment analysis. The zonation delimited by the fronts is indicated in panels a): Sub-Antarctic Zone (SAZ), Polar Frontal Zone (PFZ), Antarctic Zone (AZ) and Southern Zone (SZ). The location of the fronts is shown above the acronyms of the zones: Sub-Antarctic Front (SAF), Antarctic Polar Front (APF) and Southern Polar Front (SPF). Notice the different scale used in panel a.3 (% of pico). Dashed black lines indicate mixed layer depths (criteria: 0.02 kg m^{-3} greater than the density at the surface; Cisewski et al., 2008). Grey lines indicate the euphotic zone depths (criteria: for stations with PAR measurements, 1% of surface PAR at 0 m; for stations without PAR measurements, Z_{eu} was derived from CTD fluorometer Chl-a profiles; Morel and Maritorena, 2001) (see Cheah et al., 2016 for further details).

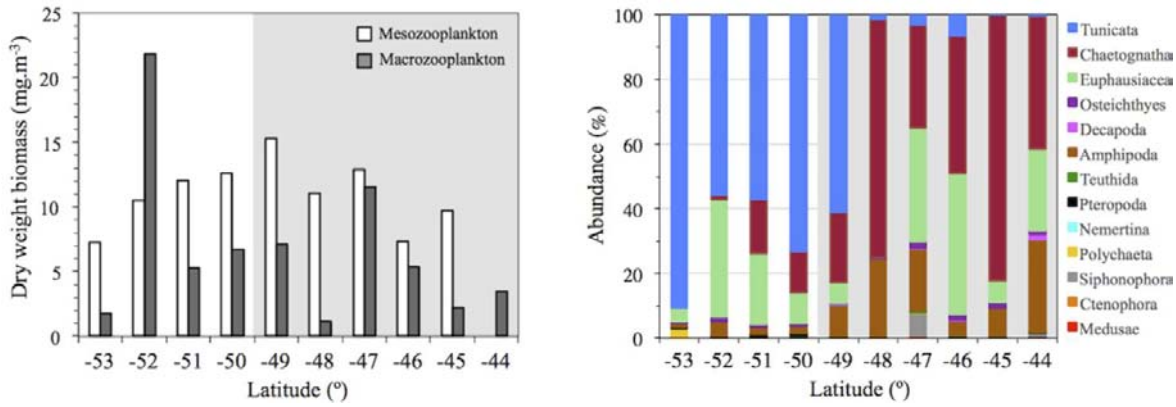

Figure 4.7: Dry weight mesozooplankton and macrozooplankton biomas along the transect (left panel); Relative contribution (%) of abundance of the different macrozooplankton taxa (right panel). Grey-white background is used to delimit north (grey) and south (white) of the APF.

4.5 Discussion

The SO has been previously described as "one of the ocean's most efficient biological pumps" (Buesseler et al., 2001), although it has recently been suggested that on a global scale, its carbon export potential might be lower than previously thought (Maiti et al., 2013). High POC export fluxes (>20 mmol C m^{-2} d^{-1}) occurring in late austral spring/summer following phytoplankton blooms have been observed repeatedly (Buesseler et al., 2003; Friedrich and Rutgers van der Loeff, 2002; Savoye et al., 2008).

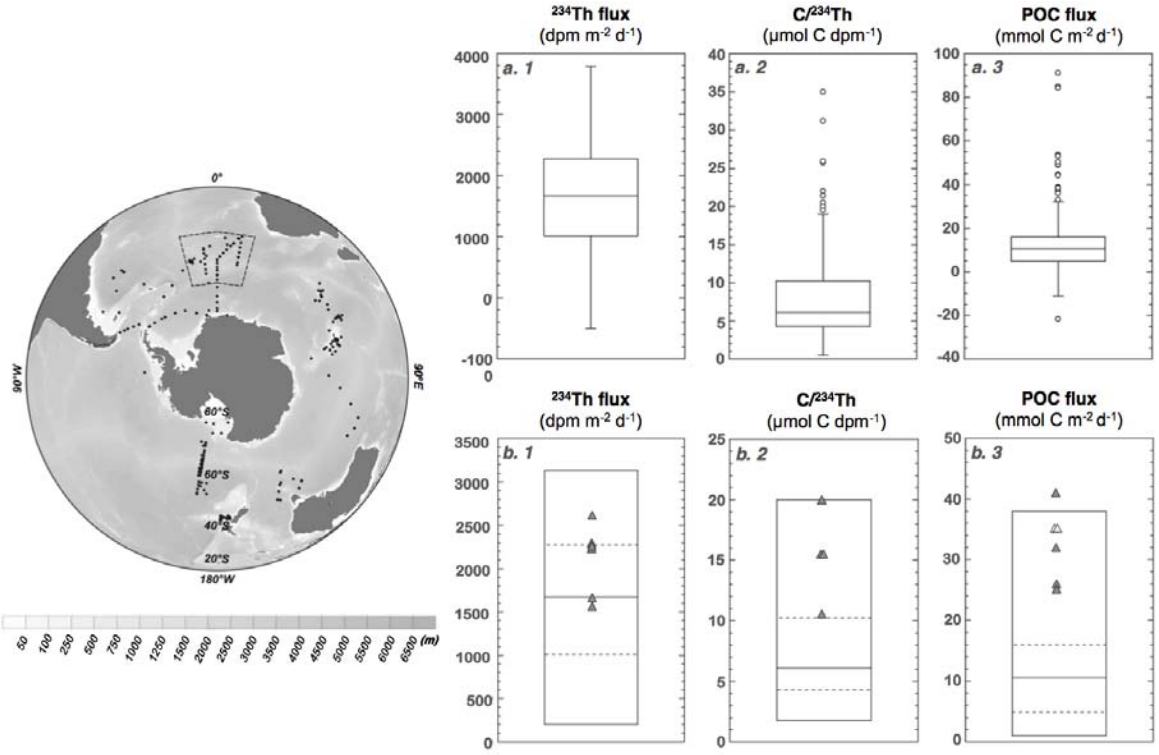

Figure 4.8: Top row: Box plots for ^{234}Th fluxes (*a.1*), C/^{234}Th ratios (*a.2*) and POC fluxes (*a.3*), with outliers displayed as individual points (empty circles). Bottom row: Percentile plots for ^{234}Th fluxes (*b.1*), C/^{234}Th ratios (*b.2*) and POC fluxes (*b.3*). Each box encloses 90% of the data, with the bottom and top of each box representing 5% and 95% of the data. Solid line represents 50% of the data and dashed lines represent 25%, and 75% percentiles. Data included here refer to 100 ± 10 m depth and are derived from this study together with, the data included in the dataset compilation by Le Moigne et al. (2013) for the SO (>40ºS), Planchon et al., 2015, Rosengard et al., 2015, Savoye et al., 2008 and Roca-Martí et al., (2016); ^{234}Th fluxes n = 201; C/^{234}Th n = 160; POC fluxes n = 273. Grey triangles in percentile plots have been included for visual information to indicate the values obtained in this study. The white triangles that appear on the POC flux percentile plot indicate derived values for those stations where no in situ pumps were deployed (see text for details). Map inset shows the location of the plotted data, with color-bar indicating bathymetry. The dashed black line delimits the stations considered to be geographically comparable to this study (see section 4.5.5).

Our estimates of ^{234}Th fluxes at 100 m (1560 to 2610 dpm m^{-2} $d^{-1)}$ are within the mid to upper range of previously reported estimates (from negligible to 3800 dpm m^{-2} d^{-1}; on average 1660 ± 920 dpm m^{-2} d^{-1}, n = 201; Figure 4.8). Our Th-derived POC fluxes estimated along the 10ºE transect (25 to 41 mmol C m^{-2} d^{-1}) are, however, among the highest fluxes reported to date within the SO (from negligible to 91 mmol C m^{-2} d^{-1}; on average 13 ± 13 mmol C m^{-2} d^{-1}; n = 273; Figure 4.8; also see compilations by Maiti et al., 2013 and Le Moigne et al., 2013), and close to values found in areas with natural and artificially high iron inputs (e.g., Morris et al., 2007; Smetacek et al., 2012). This is surprising given that our measurements were conducted in open ocean areas of the ACC. In the following sections, the effects of physical processes are investigated in order to validate the 1-D steady state approach applied (section 4.5.1). The distribution of DFe is discussed relative to previous studies and with ^{234}Th activity profiles. Biological uptake and possible inputs linked to water masses are also explored (section 4.5.2). Variability in export along the transect is also examined in light of planktonic community structure in order to provide insight into the main drivers of POC export fluxes throughout the region (section 4.5.3), and how differences in food webs may affect POC export and transfer efficiencies to depth (section 4.5.4). Finally, a comparison with previous studies is also presented to highlight the large variability within the SO, mainly linked to the timing and magnitude of the phytoplankton blooms (section 4.5.5).

4.5.1 Physical transport processes: effect on ^{234}Th export fluxes

Steady state conditions were assumed to calculate ^{234}Th export fluxes as none of the stations were revisited during the expedition. Previous studies have shown export fluxes to be relatively constant over time in the study area during the austral summer, with no significant differences between results obtained when applying steady and non-steady state conditions (Rutgers van der Loeff et al., 2011, 2002). In general, in the open ocean, diffusion and advection are considered to be negligible compared to the vertical downward flux of ^{234}Th on sinking particles (see review by Savoye et al., 2006) except in strong upwelling areas (Buesseler et al., 1998). However, the study area is located in a dynamic region characterized by three fronts where advective and diffusive processes could be significant (Strass et al., 2016). For instance, Strass et al. (2002b) reported mesoscale frontal dynamics that influenced chlorophyll distribution patterns, which were highly correlated with other biological parameters, such as primary production (Strass et al., 2002a) and zooplankton abundances (Pollard et al., 2002a). Therefore, we assessed the assumption of negligible physical processes on our ^{234}Th flux calculations (see details in Appendix A.2). Our estimates indicate that, overall, the combination of advective and diffusive fluxes would represent

7-17% of the ^{234}Th export fluxes at 100 m, comparable to their associated uncertainties (6-12%). Therefore, by taking into account physical transport mechanisms, the uncertainty of ^{234}Th export fluxes would increase to 10-21%, in agreement with previous results presented by Resplandy et al. (2012), where errors due to the dynamic transport of ^{234}Th related to small-scale structures were found to be <20%.

4.5.2 Dissolved iron distributions

The distribution of Chl-a in the SO is mainly regulated by inputs of new iron to the system (Sokolov and Rintoul, 2007). DFe concentrations in the Atlantic sector of the ACC progressively decrease eastwards as the ACC moves from the main iron source (the Antarctic Peninsula and South Georgia, de Jong et al., 2012). Despite the high spatial variability shown here, our DFe data are in excellent agreement with the few prior sampling efforts carried out in this sector of the SO (Figure 4.9) (Chever et al., 2010; Klunder et al., 2011) suggesting that major features in DFe distributions are persistent during the austral summer.

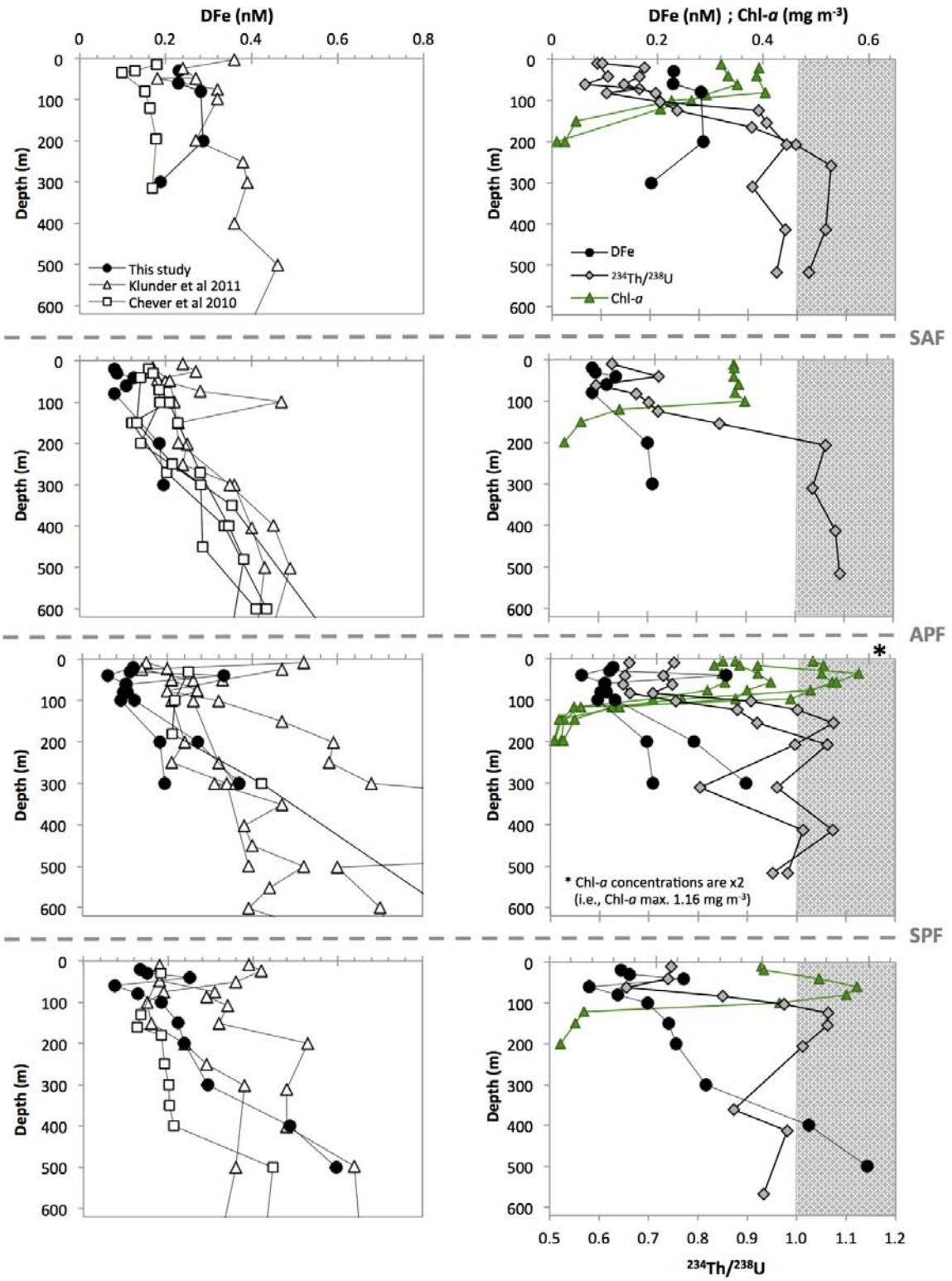

Figure 4.9: Dissolved iron profiles from this study (black dots) compared to Klunder et al. (2011) (white triangles) and Chever et al. (2010) (white squares) (left panels), and to $^{234}Th/^{238}U$ ratios (grey diamonds) and Chl-a concentrations (green triangles) (right panels). Profiles are grouped according to the location of the fronts, indicated by grey dashed lines. See Figure 1 for the station number of each DFe and ^{234}Th profile. Station numbers for Chl-a profiles: St. 60 and 63 (north of SAF), St. 69 (between SAF and APF), St. 75, 76 and 81 (between APF and SPF) and St. 84 (south of the SPF). The shaded areas, on the right panels, indicate ^{234}Th concentrations above equilibrium (i.e., $^{234}Th/^{238}U$ ratios >1). Note that Chl-a concentrations for stations located between APF and SPF are the double of those indicated by the axis (i.e., max. Chl-a =1.16 mg m^{-3}, instead of 0.58 mg m^{-3}).

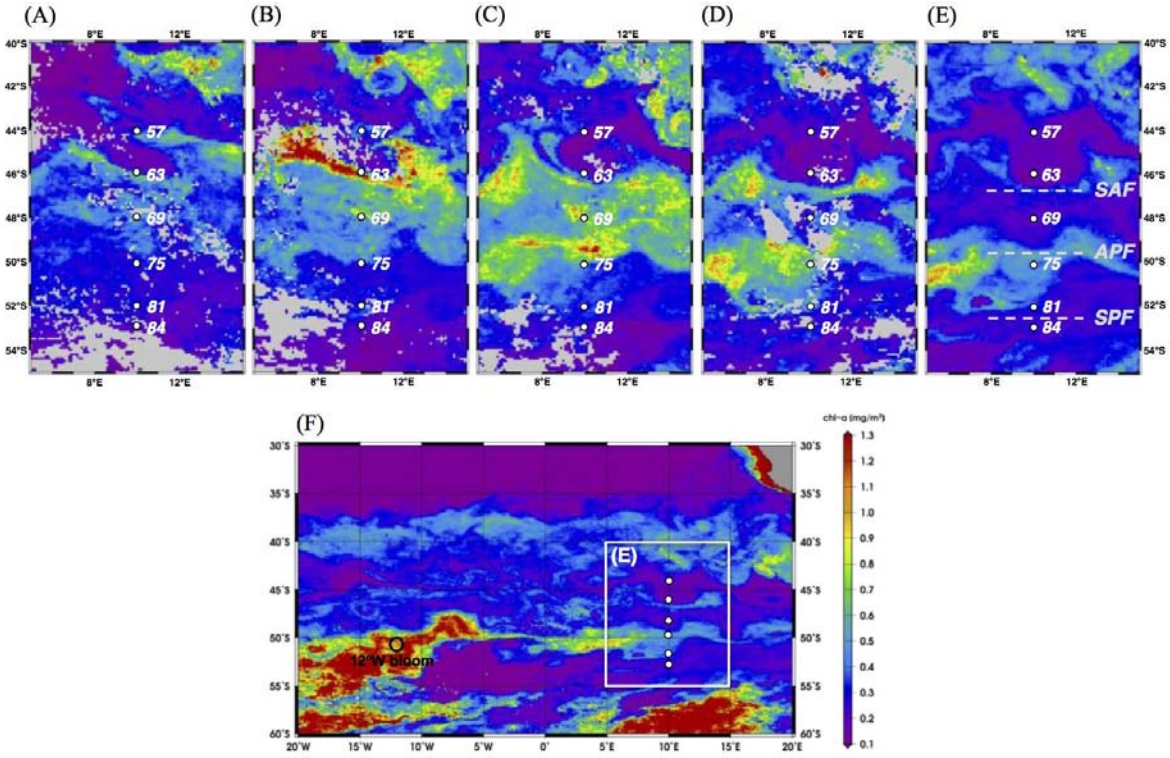

Figure 4.10: 12-day mean of satellite Chl-a concentration from the OC-CCI Chl-a product version 2.0 for the study area with the station positions (black dots) and the fronts (dashed white lines) plotted in panel E. Satellite images prior to the cruise: A) 19 Nov - 1 Dec 2011; B) 2-13 Dec 2011; C) 14 - 27 Dec 2011; D) 28 Dec 2011-10 Jan 2012; During the cruise: E) 11-22 Jan 2012; F) 11-22 Jan 2012, with larger spatial coverage to include the bloom area located at 12ºW (black circle) and the transect area (black rectangle indicated as E) with black dots to show the location of the stations.

Satellite images show high Chl-a concentrations (up to 1.3 mg m^{-3}) north of the APF about a month prior to the cruise (Figure 4.10). However, DFe concentrations in that area were not as depleted as in the central region of the transect during the cruise (Figure 4.2e). The biological uptake of DFe north of the APF might havebeen limited by silicate availability since silicate concentrations were in the range of limiting concentratrions, namely ≤1 µM (Figure 4.11) (Le Moigne et al., 2013a, Cheah et al., 2016). Additionally, the high salinity intrusion at 100-300 m supports a lateral advection of DFe (Figure 4.2b,e). During the cruise, the highest Chl-a concentrations (up to 1.2 mg m^{-3}; Figure 4.9) were measured between 49ºS and 52ºS (Figure 4.10e), leading to strong depletion of DFe in the upper 100 m. The low DFe values were probably caused by recent biological uptake and the subsequent removal through sinking particles. Biological uptake of DFe would explain its inverse correlation with Chl-a_{FLUO} (ρ = -0.83, p <0.0001, n = 21). In general, DFe and $^{234}Th/^{238}U$ profiles followed a similar trend with depth, and are inverse to Chl-a_{FLUO} profiles, with DFe depletion matching the increase of ^{234}Th deficits (Figure 4.9). This suggests that the process causing the reduction of DFe concentrations also

affected the ^{234}Th deficits at a similar depth range. However, it should be noted that the gradient in ^{234}Th deficits are steeper than gradients in DFe (between ~60 - 200 m), probably due to a more rapid turnover of Fe than that of ^{234}Th, a finding also reported by Klunder et al. (2011).

The highest DFe concentrations were found in the southern part of the transect (St. 81 and 84), below ~300 m associated with UCDW waters, where oxygen concentrations were (<200 μmol kg^{-1}) (Figure 4.2d). Indeed, DFe concentrations below 100 m were strongly correlated with salinity and negatively correlated with oxygen at those two stations ($r = 0.82$ for salinity and $\rho = -0.85$ for oxygen, with $p < 0.01$ and $n = 9$ for both correlations). Higher DFe concentrations have been found previously in UCDW waters (Klunder et al., 2011) and are typical of reduced oxygen concentrations due to an increase of iron solubilization during POC remineralization and stabilization of highly soluble Fe(II) (Millero et al., 1987). Low Chl-a_{FLUO} values despite high concentrations of all major nutrients at the southern end of the transect (Figure 4.11) indicate, however, that little of the DFe in UCDW waters reached the photic layer.

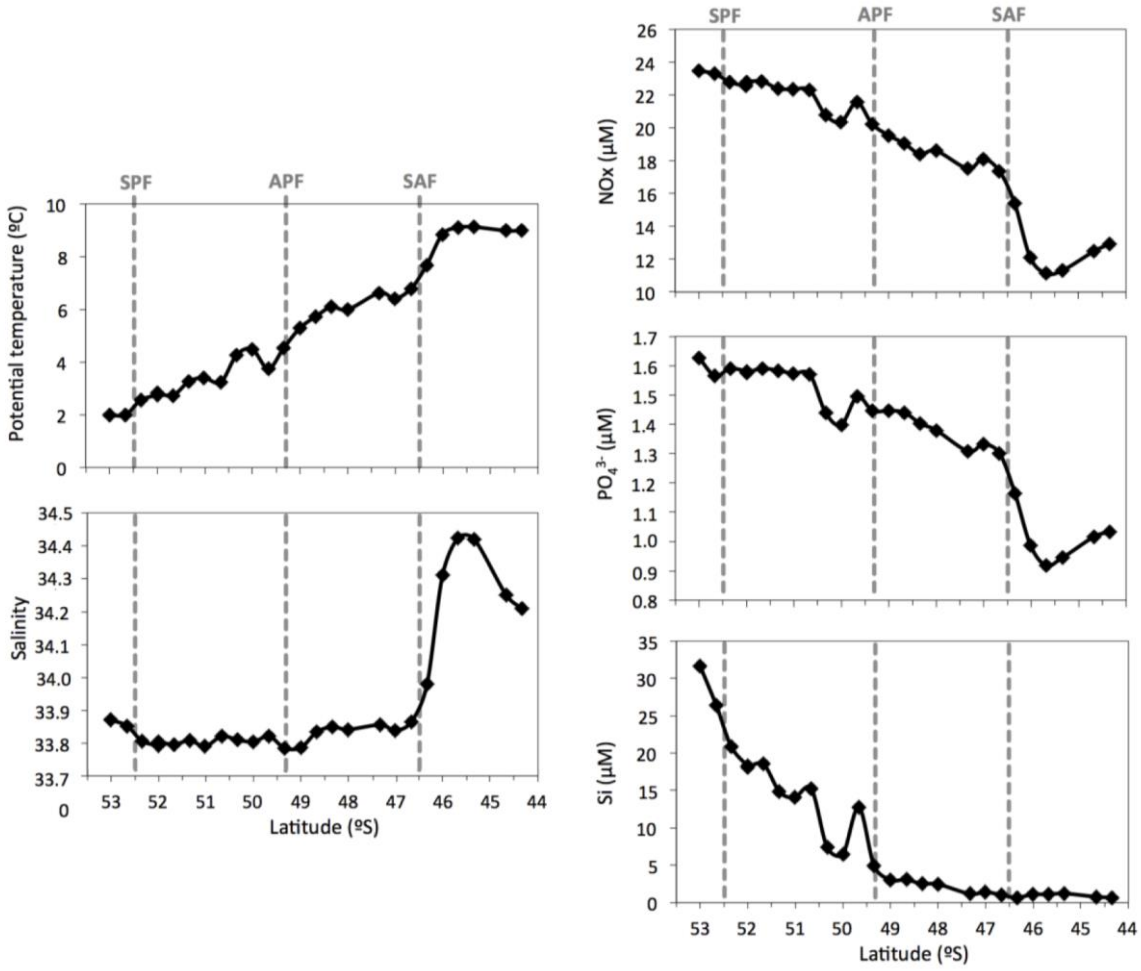

Figure 4.11: Subsurface (~20 m) distribution of potential temperature, salinity, nitrate+nitrite (NOx), phosphate and silicate along the transect. Vertical grey dashed lines indicate the location of the fronts.

4.5.3 Differences in planktonic community N-S of the APF: effects on POC export and attenuation

SO fronts are physical boundaries that delimit zones of distinct physical, chemical, and biological properties (e.g., Read et al., 2002; Strass et al., 2002b) that in turn could regulate the particle export flux. In this study we did not observe a clear zonation related to the fronts regarding ^{234}Th export fluxes, although enhanced export was measured in areas where, as indicated by satellite imagery (Figure 4.10), phytoplankton blooms occurred and peaked about a month prior to our sampling (north of the APF). Since the ^{234}Th method integrates over time scales of several weeks, we could expect a decoupling between ^{234}Th deficiencies in the upper water column as compared to the biological parameters measured during the cruise (e.g., Chl-a concentrations or primary production) (Buesseler, 1998).

POC export fluxes at 100 m were in the higher end of the range of previous reported estimates, mainly driven by high C/^{234}Th ratios (Figure 4.8). Further, contrary to ^{234}Th fluxes, POC fluxes were not correlated with latitude ($r^2 = 0.27$; $p = 0.29$; similar for PON fluxes: $r^2 = 0.08$; $p = 0.59$) (Figure 4.5). Differences between stations north and south of the APF were found when comparing changes in POC export fluxes at 100 and 400 m. Due to changes in C/^{234}Th ratios with depth, POC fluxes between 100 and 400 m depth showed higher attenuation north of the APF than southern stations, which showed little to no attenuation (Figure 4.5; Table 4.3). C content in particles varies due to particle volume and composition, whereas ^{234}Th is quickly adsorbed onto the particles' surface sites (Santschi et al., 2006). As a consequence, first order dynamics predicts an increase in C/^{234}Th ratio in large particles due to high volume:surface area ratios (Buesseler et al., 2006). However, additional aspects of the biological community (e.g., dominant phytoplankton group, bacterial activity, grazing, nutrient limitation) may also affect C content and C/^{234}Th ratios in particles and their variation with depth (Buesseler et al., 2006; Jacquet et al., 2011; Puigcorbé et al., 2015), leading to the large variability observed (Figure 4.8; Buesseler et al., 2006).

Below we discuss the differences encountered between north and south of the APF and their impact on the POC export flux and attenuation (Table 4.4 summarizes the comparison between stations north and south of the APF).

Table 4.4: Comparison between the results observed north and south of the APF summarizing the main parameters examined.

Parameter	N of APF	S of APF
Satellite data	Bloom before cruise	Bloom during cruise
Nutrient concentration (NOx, PO^{3-}_4, Si)	Low	High
dFe concentration	Subsurface maximum	Depleted in bloom and subsurface minimum
Primary production rates (PPRes, mmol C m^{-2} d^{-1})	54-59	73-86
Phytoplankton community	Haptophytes	Diatoms
Grazers	Chaetognaths, euphasiids	Salps and euphausiids
^{234}Th export	High-Moderate	Moderate
POC flux 100 m	High	High
Export efficiency (POC flux 100 m/PPRes)	High (up to 69%)	Moderate (up to 44%)
POC-attenuation	Moderate	Negligible
Transfer efficiency (POC flux 400/Eq. depth)	Moderate (<60%)	High (up to >100%)

4.5.3.1 North of the APF: small phytoplankton and higher particle attenuation

In accordance with nutrient distribution (low Si north of the APF and low nitrate and phosphate north of the SAF; Figure 4.11) planktonic communities north of the APF were dominated by nanophytoplankton (mainly haptophytes; Cheah et al., 2016 and Figure 4.6) and had higher abundances of carnivorous zooplankton (B.P.V. Hunt *pers. comm*. and Figure 4.7). The higher POC:Chl-a ratios found north of the APF also reflect communities in a later stage of development with a larger fraction of heterotrophs or detritus (Figure 4.12). Indeed, in this half of the transect, a bloom took place a month prior to the sampling period (Figure 4.10; Figure 4.13).

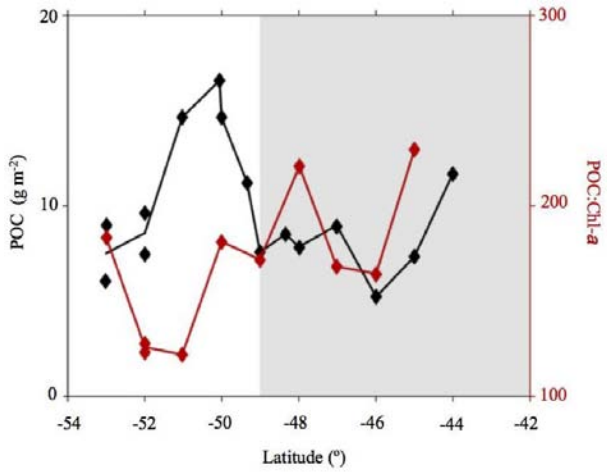

Figure 4.12: POC stocks in the upper 100 m (black) and POC:Chl-a ratios (red). Gray-white background is used to delimit north (gray) and south (white) of the APF.

Since the ^{234}Th approach integrates over a period of time of a few weeks, the important ^{234}Th deficits observed at the northern stations were most probably a consequence of that bloom, which might have been dominated by larger phytoplankton groups, such as diatoms. However, during the sampling time (post-bloom conditions), the small size of the dominant phytoplankton group (<20 μm), combined with the lack of dense frustules and skeletons associated with diatoms, probably led to the formation of a sinking particulate pool also dominated by small and more slowly sinking particles. Both processes would allow more remineralization, which might explain the larger attenuation of POC and ^{234}Th fluxes and C/^{234}Th ratios with depth in the northern half of the transect. The differences observed in C/N ratios with depth at both stations also suggest alteration of the particle composition with depth (Table 4.2). Overall, POC flux attenuation was observed north of the APF, with up to a 74% decrease in flux between equilibrium depth and 400 m, although it should be noted that vertical resolution below 200 m was poor.

4.5.3.2 South of the APF: large phytoplankton and low particle attenuation

In the southern half of the transect, south of the APF, higher nitrate and silicate concentrations (Figure 4.11) favored larger phytoplankton, in particular diatoms (Figure 4.6; Cheah et al., 2016). The higher POC standing stocks combined with lower POC:Chl-a ratios (Figure 4.12) indicate that communities south of the APF had a higher proportion of phytoplankton relative to that observed towards the north, where the bloom had occurred a month prior to our expedition (Figure 4.10). The southern region was also likely subject to more intense grazing pressure due to higher abundances of herbivorous zooplankton, mostly salps (tunicata) (Figure 4.7). Pigment analyses also suggest that grazing took place at those latitudes (Cheah et al., 2016). The structure of the diatom dominated planktonic community in this area (including thickly silicified species characteristic of iron deficient open ocean areas of the SO; Assmy et al., 2013) and abundance of salps, might have led to both retention of POC at the surface (Assmy et al., 2013; Iversen et al., 2016) as well as production of a sinking particle pool constituted by large fast sinking particles that were rapidly able to reach 400 m and only be minimally affected by remineralization (Rutgers van der Loeff et al., 2002). Salps were 2-3 orders of magnitude more abundant at the southern stations compared to northern stations (B.P.V. Hunt, *pers. comm.*). These large grazers can produce fast sinking fecal pellets (200-2700 m d^{-1}, Bruland and Silver, 1981; Iversen et al., this issue; Madin, 1982; Phillips et al., 2009; Turner, 2002) and have rapid defecation rates (Madin, 1982), making them potentially important contributors to POC export (Ebersbach and Trull, 2008; Perissinotto and Pakhomov, 1998; Phillips et al., 2009; Smith et al., 2013). The additional ballasting due to the inclusion of thickly silicified diatoms, such as *Fragilariopsis kerguelensis* which dominated assemblages at

station 84 (53ºS; C. Klaas, *pers. comm.*), may also increase the sinking velocities of fecal pellets and aggregates (Francois et al., 2002; Klaas and Archer, 2002), reducing their residence time in the upper ocean. This could help explain the small variation of the C/N ratios and low/negligible POC flux attenuation with depth at the southernmost stations (Table 4.2 and Table 4.3).

Additional information regarding POC export south of the APF is derived from surface tethered sediment traps deployed at 53ºS, at 100 and 400 m (Iversen *et al., unpublished data*). Differences between both techniques (from water column ^{234}Th deficits versus POC export measured directly from the sediment traps) are typically found in the literature to be within a factor of 2 to 4, partly due to their time scale of collection (several weeks *vs* ~24 h), as well as methodological issues between techniques (Buesseler, 1991). As such, both methods can be used to complement one another. The particulate C/^{234}Th ratios collected using sediment traps were about a factor of 3 lower than those collected using ISP, although similar to ISP, the ratio did not change with increasing depth (6.5 ± 0.5 and 6.9 ± 0.6 μmol C dpm^{-1}, at 100 and 400 m, respectively). Sediment trap particles also contained a large presence of fecal pellets (M.H. Iversen, *pers. comm.*). While the lack of a change in C/^{234}Th ratios confirms the results obtained for ISP particles (>53 μm), the differences in magnitude of the C/^{234}Th ratios suggest that the POC fluxes estimated using ISP particles represent an upper limit, at least at 53ºS. POC fluxes measured by sediment traps at 53ºS (M.H. Iversen *pers. comm*.) also show small flux attenuation with depth (36% and 11%, for sediment traps and the ^{234}Th method, respectively), again confirming the results obtained with the ^{234}Th approach.

4.5.4 Export and transfer efficiencies

Numerous studies have reported significant carbon export from the upper water column in the SO based on a variety of methodological approaches (e.g., oxygen or nutrient mass balance, short-lived radionuclides, sediment traps) and across different frontal regions (Buesseler et al., 2001; Cochran et al., 2000; Friedrich and Rutgers van der Loeff, 2002; Hoppema et al., 2002; Rutgers van der Loeff et al., 1997; Savoye et al., 2008; Schlitzer, 2002; Usbeck et al., 2003) and productivity systems (Cavan et al., 2015; Ebersbach et al., 2011; Manno et al., 2015; Rembauville et al., 2015a, 2015b; Salter et al., 2012). The overall emerging picture from these studies suggests that in areas with high productivity downward transport of organic carbon is mainly driven by blooms of diatoms (leading to the export of 30-50% of SO net primary production), with zooplankton fecal material as a major pathway for exporting carbon to the deep ocean after the major sedimentation

pulse (diatom dominated spring bloom) in areas with low productivity (Cavan et al., 2015; Laurenceau-Cornec et al., 2015; Manno et al., 2015; Rembauville et al., 2015a).

In this study, export efficiencies were calculated by dividing the Th-derived POC fluxes at 100 m by the PPRes. Higher export efficiencies were coincident with lower PPRes, i.e., north of the APF (Table 4.3), similar to the results previously reported by Lam and Bishop (2007), Maiti et al. (2013) and Laurenceau-Cornec et al. (2015). Using the equation of Maiti et al. (2013) to obtain the export efficiencies based on the PP (Export efficiency = -0.3482 * log(PP) + 1.2239; Figure 3a in Maiti et al., 2013) we found good agreement with our data at stations 44ºS and 46ºS (ratios between measured and derived export efficiency of 1.1 and 1.0, respectively), whereas for the other stations, lower export efficiencies than predicted by the model of Maiti et al. (2013) were obtained (average ratio between both estimates 0.71 ± 0.07; n = 4). The decoupling between the peak of the productive period (before the cruise) and the timing of export (declining of productive period; during the cruise) could be responsible for the higher export efficiencies (average 60%, range 46-69%) measured north of the APF. Rutgers van der Loeff et al. (1997) found similar results during an austral spring bloom where there was also a delay between the increase in phytoplankton standing stocks and ^{234}Th depletion, similar to Buesseler et al. (2003), who reported a delay between onset of production and export of up to 1 month. Export efficiencies south of the APF were lower (max. 44%). A relatively small export efficiency (27%) was also confirmed south of the APF using sediment trap results obtained at 53ºS (M.H. Iversen, *pers. comm.*).

Stations located south of the APF, however, had the highest transfer efficiencies (i.e., the percentage of POC flux at the equilibrium depth that reaches 400 m), ranging between 89% and 148% (Table 4.3). As discussed previously, these high transfer efficiencies can be explained by fast-sinking and weakly attenuated sinking material, combined with the effect of diel vertical migration of zooplankton (Cavan et al., 2015). Alternatively, these high transfer efficiency might be due to an overestimate of our C/^{234}Th ratios based on particles >53 μm (not necessarily sinking particles). Differences in attenuation are, however, primarily due to the fact that, in strong contrast to stations north of the APF, C/^{234}Th ratios south of the APF do not change with depth. C/^{234}Th ratios in sediment trap material (measured only at 53ºS), although lower than the ratios obtained from ISP, also present no decrease with depth. A comparison of C/^{234}Th ratios from several trap deployments south of the APF during the same cruise (Roca-Martí et al., 2016) did not show a systematic bias for C/^{234}Th ratios for ISP collected material compared to trap collected material.

Further, no large differences were observed in C/^{234}Th ratios between 100 and 300 m, similar to our results. In Roca-Martí et al. (2016), Chl-a and fucoxanthin were found to be efficiently transferred between 100 and 300 m indicating that these pigments were exported to 300 m with little to no breakdown. Results from Cedhagen et al. (2014), obtained during the same expedition, also corroborate these findings as large concentrations of algal pigments were observed in the cytoplasm of foraminifera collected at depths >4000 m. Moreover, at station 81 (52ºS; ~3500 m depth), Ruff et al. (2014) observed a large number of diatom frustules and intact fecal pellets in the top layers of the sediments, even down to 5 cm depth. Combined these studies suggest rapid transport of material to sediments using a variety of pathways.

4.5.5 Comparison with previous studies

A global compilation of ^{234}Th-derived POC export estimates by Le Moigne et al. (2013), available in http://doi.pangaea.de/10.1594/PANGAEA.809717, contains a number of studies located in the SO (iron fertilization experiments not included). Considering all these studies together with the results from our expedition, presented here and in (Roca-Martí et al., 2016), as well as Planchon et al. (2015), Rosengard et al. (2015) and Savoye et al. (2008), we observed wide ranges in ^{234}Th export fluxes and C/^{234}Th ratios, with subsequent variability in the derived POC fluxes at 100 ± 10 m depth (Figure 4.8). This compilation, however, includes a variety of areas that are difficult to compare with our open ocean stations due to the large differences in phytoplankton assemblage and growth and biogeochemical aspects linked to their geographical location (e.g., ice coverage or Fe inputs from continental shelves). Therefore, here we only discuss our results together with studies conducted in the Atlantic sector of the open ACC (between 40ºS-60ºS and 15ºE-15ºW; see map inset in Figure 4.8) namely Rutgers van der Loeff et al. (1997, 2002, 2011), Planchon et al. (2013), Roca-Martí et al. (2016) and Smetacek et al. (2012), outside the iron fertilization patch.

Except for the SO-JGOFS expedition (Rutgers van der Loeff et al., 1997), which was conducted during the austral spring (Oct-Nov 1992; 6ºE), all the studies discussed here were conducted during the austral summer (Dec-Jan) or late austral summer (Feb-Mar). During the austral spring, short but intense bloom events seem to contribute significantly to the annual C export. Data in Rutgers van der Loeff et al. (1997) support this observation with a maximum ^{234}Th export flux of 3250 dpm m^{-2} d^{-1} at 100 m during a productive period of only 22 days and POC fluxes ranging from 19 to 38 mmol C m^{-2} d^{-1}, similar to the results observed during our study. Rutgers van der Loeff et al. (2002) reported constant export fluxes during a two-week period of the austral summer

three years later (1995/1996). ^{234}Th and POC export fluxes at 100 m were 865 dpm m^{-2} d^{-1} and 8.8 mmol C m^{-2} d^{-1}, respectively. The magnitude of the fluxes presented by Rutgers van der Loeff et al. (2002) is similar to those reported by Planchon et al. (2013) during the Bonus GoodHope (BGH) expedition (Feb-Mar 2008), ranging from 870 to 1200 dpm m^{-2} d^{-1} and from 2.3 to 5.1 mmol C m^{-2} d^{-1} for the section of their transect between 44ºS and 53ºS. This is almost 3 times lower ^{234}Th fluxes and about an order of magnitude smaller POC export fluxes than the estimates calculated in our study. Rutgers van der Loeff et al. (2011) reported ^{234}Th fluxes along the prime meridian (Feb 2008) that also decreased with increasing latitude, and were up to 1.6 times lower than the export fluxes from the current study at similar locations with respect to the frontal systems. The maximum POC export fluxes estimated by Rutgers van der Loeff et al. (2011) were 11 mmol C m^{-2} d^{-1} using the bulk of particles to obtain C/^{234}Th ratios, although this value decreases by a factor of 2 when using >50 μm particles (5.4 mmol C m^{-2} d^{-1}). The differences between both estimates highlight the importance that the particle composition has on C/^{234}Th ratios and the necessity of properly sampling the particles that are contributing to the export flux, which is still an open topic of discussion (Bishop et al., 2012; Durkin et al., 2015; Puigcorbé et al., 2015). Smetacek et al. (2012) examined ^{234}Th and Th-derived POC fluxes outside an iron fertilized patch (Feb-Mar 2004), reporting estimates of ~1600-2500 dpm m^{-2} d^{-1} and ~32-41 mmol C m^{-2} d^{-1}, respectively, close to the values reported here. Finally, Roca-Martí et al., (2016) provide results from a bloom at ~12ºW and ~51ºS during our expedition, where average ^{234}Th and Th-derived POC export fluxes at 100 m were 2390 ± 340 dpm m^{-2} d^{-1} (n = 14) and 36 ± 15 mmol C m^{-2} d^{-1} (n = 9), respectively.

The results from the 2012 Eddy-Pump survey presented here and in Roca-Martí et al. (2016) are comparable to the spring bloom export presented in Rutgers van der Loeff et al. (1997) and also with the summer fluxes estimated by Smetacek et al. (2012) outside of the iron fertilized patch. The main factor driving the differences between POC flux estimates are the C/^{234}Th ratios, which were much lower during the 2008 expeditions (ranging from 1.7 to 4.8 μmol C dpm^{-1}) (Planchon et al., 2013 and Rutgers van der Loeff et al., 2011) than the ratios measured during this study (16 ± 4 μmol C dpm^{-1}), in Roca-Martí et al. (2016) (14 ± 3 μmol C dpm^{-1}) and in Smetacek et al. (2012) (17 ± 3 μmol C dpm^{-1}).

As previously discussed, the planktonic community structure will affect the type and composition of the particles generated in surface layers. Thus, the sampling time related to a bloom event (i.e., sampling prior, during or after a bloom) can lead to differences in the C/^{234}Th ratios measured. High Chl-a concentrations (>1 mg m^{-3}) covering large areas can be observed from satellite images during the sampling period of this expedition (Jan-Feb 2012; see also Figure 1 in Hoppe et al.,

2016) and in Smetacek et al. (2012), prior to iron fertilization. These features were minimal and mainly located farther west in Jan-Feb 2008 (see Figure 7 in Rutgers van der Loeff et al., 2011). As suggested by Planchon et al. (2013) and Rutgers van der Loeff et al. (2011), the low fluxes obtained during the 2008 expeditions were probably due to a post-bloom situation, where the intensive export had already occurred and remineralization led to reduced POC export fluxes. Our study was carried on earlier in the summer, probably during the late export phase where remineralization is not able to compensate the ^{234}Th deficits created by the still present particle export. Additionally, comparison between summers 2007/2008 and 2011/2012 using satellite images (Figure 4.13) suggests that the higher export fluxes measured during 2012 were probably not only a consequence of the sampling time but also due to the larger magnitude of the bloom of that year. Thus, not only the timing of sampling relative to the bloom, but also its magnitude, can result in clearly different estimates of POC export fluxes, mainly due to the variability in the C/^{234}Th ratios, even during the austral summer.

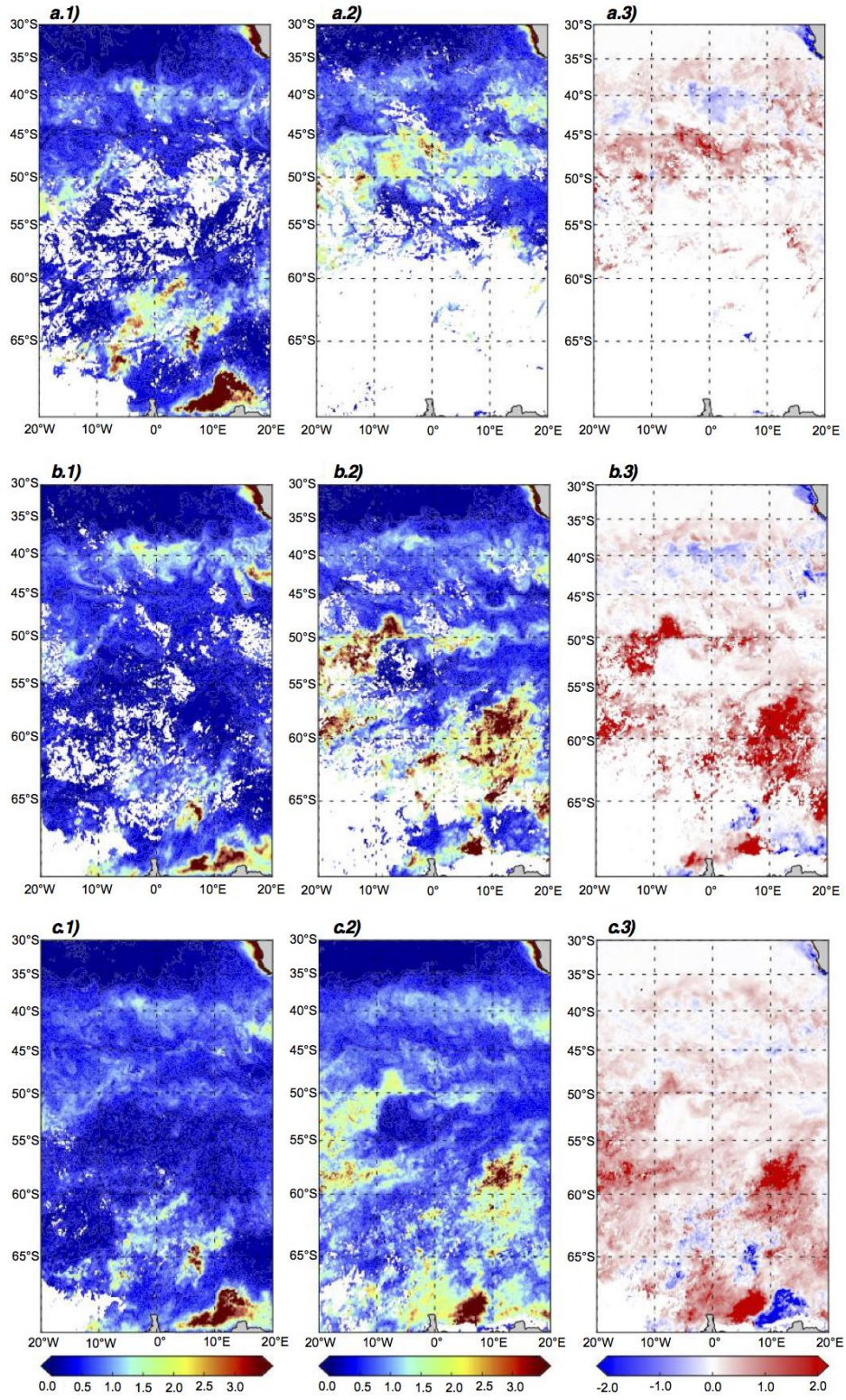

Figure 4.13: Sea surface Chl-a concentrations (in mg m^{-3}) (from MODIS-Aqua obtained using the algorithm of Johnson et al., 2013) for the austral summers of 2007/2008 (Rutgers van der Loeff et al., 2011 and Planchon et al., 2013; panels *a.1*, *b.1* and *c.1*) and 2011/2012 (i.e., this study; panels *a.2*, *b.2* and *c.2*). The 2011/2012 - 2007/2008 differences are shown in panels *a.3*, *b.3* and *c.3*. Subplots *a.1* and *a.2* present the sea surface Chl-a prior to the sampling periods, i.e, January and February 2008 (*a.1*) and December 2011 (*a.2*). Subplots *b.1* and *b.2* present the sea surface Chl-a during the sampling periods, i.e., February and March 2008 (*b.1*) and January 2012 (*b.2*). Subplots *c.1* and *c.2* present the sea surface Chl-a for the entire summer (December, January, February and March) of 2007/2008 (*c.1*) and 2011/2012 (*c.2*).

4.6 Conclusions

We used ^{234}Th as a tracer to estimate downward particle fluxes across the ACC in order to examine the effect of hydrographic conditions, separated by fronts, on POC export, export efficiencies and transfer efficiencies. ^{234}Th fluxes were higher in the northern part of the transect, due to a bloom that occurred about a month before our arrival, as revealed by satellite images. POC fluxes at 100 m were relatively high (25-41 mmol C m^{-2} d^{-1}) and did not show significant differences linked to the frontal zones. However, a major N-S shift in planktonic community was reflected in the variation of the C/^{234}Th ratios with depth. Small phytoplankton with low Chl-a concentrations dominated north of the APF, whereas south of the APF diatoms were more abundant, Chl-a was higher, and salps dominated the macrozooplankton community. This probably resulted in sinking particle pools that differed in their composition: aggregates of small particles in the north versus fast-sinking large particles in the south. Export efficiencies were generally high (35-69%), partly due to a temporal decoupling between production and export, with slightly higher values in the northern section, where derived primary production rates were lower and small phytoplankton dominated. On the other hand, due to the absence of attenuation of the C/^{234}Th ratios with depth at the southern stations, POC fluxes at 400 m were similar or even higher than at 100 m, which translates to high transfer efficiencies in the region where diatoms and salps were more abundant.

Comparison with previous studies highlights the dynamic biological character of the study area, with phytoplanktonic blooms of different magnitude that, together with the time elapsed between the climax of the bloom and the sampling period, probably led to the differences observed between studies in which large variability regarding C/^{234}Th ratios was observed. This supports the use of combined techniques, such as sediment traps and the ^{234}Th-method, to estimate the magnitude and composition of particle fluxes. Further efforts are needed to link the planktonic community to variability of C/^{234}Th ratios, both below the euphotic zone and at greater depths, and to constrain the strength and efficiency of the biological pump in this region.

Chapter 5:

Small phytoplankton drive high summertime carbon and nutrient export in the Gulf of California and Eastern Tropical North Pacific

This chapter is based on:

Puigcorbé, V., C.R. Benitez-Nelson, P. Masqué, E. Verdeny, A.E. White, B.N. Popp, F.G. Prahl, and P.J. Lam (2015), Small phytoplankton drive high summertime carbon and nutrient export in the Gulf of California and Eastern Tropical North Pacific *Global Biogeochem. Cycles*, 29, 1309–1332, doi:10.1002/2015GB005134

5 Carbon and nutrient export in the Gulf of California and Eastern Tropical North Pacific

5.1 Objectives

The goal of this study is to better understand the processes influencing particulate organic carbon, nitrogen and biogenic silica export in the Gulf of California and the Eastern Tropical North Pacific during the stratified summer period when smaller phytoplankton and nitrogen-fixing organisms likely dominate this area. We used free floating sediment traps and ^{234}Th: ^{238}U: disequilibrium to quantify export fluxes. We further examined how element/^{234}Th ratios collected at high resolution throughout the upper water column influence ^{234}Th derived particle export results and provide insight into the composition and source of particles contributing to the sinking flux.

5.2 Introduction

Oceanic particle cycling and export play major roles in the biogeochemical cycling of carbon and associated nutrients (Honjo et al., 2008). Yet understanding their magnitude and variability over temporal and spatial scales remains limited (Burd et al., 2010). Such knowledge is particularly needed as large scale changes in climate are already influencing the marine system, as documented in ocean acidity, upper ocean circulation patterns, and the rate of particle export (Doney et al., 2012; Feely et al., 2004; Taylor et al., 2012). It has been hypothesized that future increases in global ocean temperatures will increase upper ocean stratification thereby influencing a marine food web structure (Beaugrand et al., 2008; Doney, 2006; Hays et al., 2005; Richardson and Schoeman, 2004) that favors smaller phytoplankton (Morán et al., 2010; Taylor et al., 2012) and, likely, nitrogen-fixing organisms (Hutchins et al., 2007; Karl et al., 2002). This shift in phytoplankton ecology may alter both particle flux and composition, with profound implications for marine biogeochemistry (Bopp et al., 2005). Increasing stratification has also been hypothesized to play a role in the significant areal and volumetric expansion of oxygen minimum zones (Keeling et al., 2010), which further influences the remineralization of particles as they sink through the water column (DeVries and Deutsch, 2014). Thus, understanding the biogeochemistry of warm, stratified regions underlain by a strong oxygen minimum zone is of immediate and broad interest.

One such region is the Eastern Tropical North Pacific (ETNP), where more than 35% of global water column denitrification takes place (Cline and Richards, 1972; Codispoti and Richards, 1976). The persistent oxygen minimum zone extends from the equator to 25ºN and westward from the coast to 140ºW (Paulmier and Ruiz-Pino, 2009). ETNP suboxia, and thus denitrification, are maintained by a combination of remineralized particulate organic material (Van Mooy et al., 2002) and both horizontal and vertical circulation/ventilation patterns (Duteil and Oschlies, 2011; Gnanadesikan et al., 2012). The Gulf of California (GC) is a subtropical semi-enclosed sea located along the southwest coast of North America (Figure 5.1). Suboxic and partly denitrified waters from the ETNP (i.e., N:P < 16:1), enter into the central GC between 500 and 1000 m depth via the California Undercurrent, which also transports the denitrified waters to the north along the continental slope of North America (Bray and Robles, 1991; Castro et al., 2001; Liu and Kaplan, 1989; Roden, 1958). In winter, the GC is characterized by strong northwestern winds that induce upwelling. This physical oceanographic change results in high rates of nitrate-driven primary production (White et al., 2007) and a biological community dominated by diatoms and silicoflagellates, which increase opal fluxes to depth (Santamaría- del- Angel et al., 1994; Thunell et al., 1996). In summer, weaker winds blow from the southeast, allowing ETNP surface waters to penetrate into the GC and water column stratification to reoccur (Badan-Dangon et al., 1991; Roden, 1958). Summertime nutrient limitation leads to lower biological production and a plankton community structure characterized by coccolithophores and foraminifera, which contribute to enhanced carbonate fluxes (Brand, 1994; Thunell et al., 1996; Ziveri and Thunell, 2000). In contrast to seasonal changes in the biomineral fluxes, vertical fluxes of particulate organic carbon and nitrogen remain invariant (Lyons et al., 2011; Thunell, 1998; White et al., 2013) and do not correlate with overlying surface productivity, suggesting that export production may be more efficient in the summer than during the winter. One hypothesis for this summertime increase in export efficiency is based on that the GC biological food web undergoes a fundamental change seasonally.

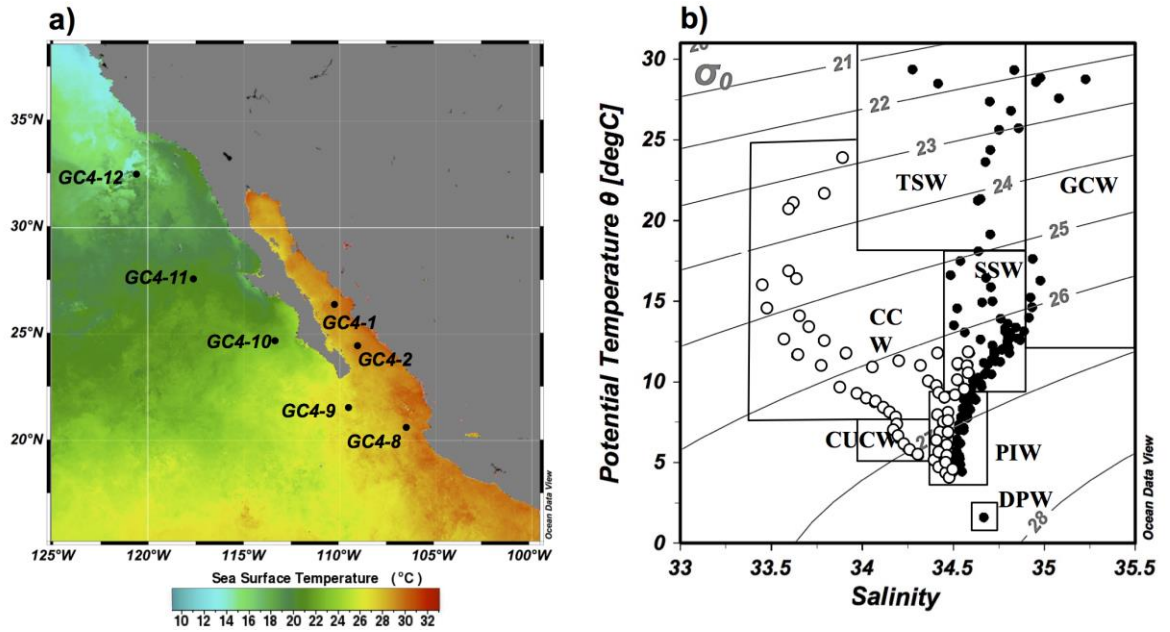

Figure 5.1: Hydrographic characteristics and location of the sampled stations. Panel a) indicates the location of the stations along the Gulf of California and the eastern tropical North Pacific transect, overlain on the mean surface temperature for July 2008 derived from MODIS AQUA remote sensing data (http://oceancolor.gsfc.nasa.gov). Panel b) corresponds to the T-S diagram of the upper 1000 m of the seven stations. At station GC4-8, sampling occurred down to 3000 m depth. Contour lines represent isopycnal surfaces (σ_θ). Open circles represent ETNP stations (GC4-10, GC4-11, and GC4-12). Filled circles represent Transition zone (GC4-8 and GC4-9) and GC (GC4-1 and GC4-2) stations. The rectangles represent different water masses: California Current Water (CCW), California Undercurrent Water (CUCW), Subtropical Subsurface Water (SSW), Pacific Intermediate Waters (PIW), Tropical Surface Waters (TSW), Gulf of California Waters (GCW), and Deep Pacific Water (DPW).

Upon summer stratification, the ensuing intensification of nitrate limitation and presence of residual phosphate as a consequence of the upwelling of waters with low N/P ratios is consistent with conditions that have been hypothesized to favor the growth of nitrogen-fixing organisms (Karl, 2002). High rates of N_2 fixation, as well as episodic decreases in the $\delta^{15}N$ value of sinking particulate nitrogen captured in deep sediment traps located in the central GC basins (e.g., Carmen and Guaymas Basin), suggest that diazotrophy may also significantly contribute to the sinking particulate matter flux during the summer period (Altabet et al., 1999; Thunell, 1998; White et al., 2007, 2013). This variability in food web structure caused by seasonal stratification combined with low oxygen in mid-waters of the GC and adjacent ETNP, therefore provide an excellent opportunity to study the linkages between surface productivity and particulate export fluxes under oceanographic conditions similar to those expected in a future warmer ocean.

5.3 Methods

5.3.1 Seawater samples

Samples were collected at 7 stations within the GC and ETNP adjacent waters, with one station (GC4-2) resampled after approximately 6 days (GC4-2b), during July-August 2008 aboard the R/V *New Horizon* (Figure 5.1). At each station, seawater samples were collected throughout the water column using Niskin bottles. Total ^{234}Th was measured from 4 L of seawater collected at 24 discrete depths over the upper 1000 m. Samples were processed following the procedure described in *Chapter 2*. The average chemical recovery of ^{230}Th was 91 ± 7% (n = 171). ^{238}U activities were calculated from salinity data using the relationship from Pates and Muir (2007) (see *Chapter 2*). Water column ^{234}Th fluxes (WC fluxes) at various depths were derived from the integrated ^{234}Th deficits with respect to ^{238}U concentrations (see *Chapter 2*).

5.3.2 Particulate samples

Sinking particles were collected using VERTEX-style sediment traps (ST) deployed for 24 h at each station. Each ST was equipped with 12 tubes per depth (100 and 105 m), filled with an unpoisoned NaCl brine solution. Three tubes from each depth were used to determine particulate ^{234}Th. The content of each tube was filtered at sea separately onto 25 mm diameter acid-rinsed and pre-combusted quartz microfiber filters (Whatman, QMA) and treated for ^{234}Th, particulate carbon (PC) and particulate nitrogen (PN) analyses as described in *Chapter 2*. Swimmers were identified via visual inspection and removed from the filtered sample. Particulate inorganic carbon was also determined on those filters. The filter were collected without aeration in 20 mL glass serum vials and preserved by addition of $HgCl_2$ and stored under dark and room temperature conditions. The CO_2 produced was quantified with an infrared detector (Li-Cor 6252) (detailed description of the methods is presented in Benitez-Nelson et al., 2007). Particle stable isotopic composition (δ^{15}N and δ^{13}C values) was determined by high temperature combustion with mass spectrometri detection as described in Prahl et al. (2005).

Particulate samples were also collected at each station from 9 to 13 depths over the upper 500 m using *in situ* pumps (ISP). Between 400 to 700 L of water were filtered and size fractionated as described in *Chapter 2*, between two particle sizes: small particles (SP; 1-53 μm) and large particles (LP; >53 μm). SP were sampled using a 1 μm pore-size acid rinsed and combusted QMA, as described in *Chapter 2*. LP were collected using a 53 μm nitex screen that was rinsed into an

acid clean plastic beaker using 0.2 μm filtered seawater and mixed with a stirring plate to homogenize the sample. From the rinse, a ¼ aliquot was filtered onto pre-combusted 25 mm QMA for direct analysis of ^{234}Th, while the remaining solution was filtered onto precombusted GF/F for analysis of PC, PN and the stable isotopic composition of both elements (δ^{13}C, δ^{15}N) following the same procedures used for ST samples. Biogenic silica (bSi) was only analyzed from the >53 μm size fraction via wet alkaline digestion following as described in DeMaster (1991).

5.3.3 Particle size distribution and phytoplankton community data

The magnitude of the particle beam attenuation coefficient at 660 nm is to a first order proportional to the concentration of suspended particles (Gardner et al., 2006), whereas its spectral slope is related to the slope of the particle size distributions (PSD) under certain assumptions (Kostadinov et al., 2012). In section 5.4.3.1 the PSD analysis are described.

Profiles of the total beam attenuation coefficient, c(λ), and the total absorption coefficient, a(λ), were collected at each sampling station with a WetLabs AC-s at 82 wavelengths (400.5 – 752.7 nm; mean binwidth = 4.3 nm). The absorption spectra of colored dissolved organic matter (CDOM, $a_g(\lambda)$) was measured in parallel with a WetLabs AC-9 (412, 440, 488, 510, 555, 630, 650, 676, and 715 nm) with 0.2 μm cartridge filters attached to the instrument inflow. CDOM spectra were interpolated to ac-s wavelengths. All data were filtered to remove outliers (generally due to bubbles at shallow depths), binned to 1 m and corrected for in situ temperature and salinity dependent variations in absorption and attenuation as per Twardowski et al. (1999). Pure water calibrations were performed every 2 d to ensure there was no instrument drift.

Complementary phytoplankton community structure was obtained by microscopy and pigment analysis using high-performance liquid chromatography (HPLC). Primary production and N_2 fixation rates were also measured using *in situ* incubations with ^{13}C-labelled bicarbonate and ^{15}N-labelled nitrogen gas additions, respectively. Detailed information regarding these procedures is given in White et al. (2013).

5.4 Results

5.4.1 Hydrography

Sampled stations were grouped into three subregions based on their hydrographic properties: the ETNP (GC4-10, GC4-11, and GC4-12), the transitional zone (GC4-8 and GC4-9) and the GC (GC4-1 and GC4-2). At the time of sampling, ETNP stations were characterized by cooler (17-24ºC) and fresher (salinity ~33.7) surface waters and fresher subsurface waters (to 300 m) associated with California Current Water (CCW) (Figure 1). Deeper waters were comprised of California Undercurrent Water (CUCW, GC4-12) and Subtropical Subsurface Water (SSW, GC4-10 and GC4-11), with Pacific Intermediate Waters (PIW) found at depths greater than 500 m (Lynn and Simpson, 1987).

Within the GC, stations GC4-1 and GC4-2 were located within two narrow sub-basins: the del Carmen (26º20'N, 110º40'W) and Pescadero Basins (24º00'N, 108º50'W), respectively. Surface waters (0-100 m) were characterized by salty (salinity >34.9) Gulf of California Waters (GCW). Colder deeper SSW waters occurred down to 500 m with even colder waters below the SSW, classified as PIW (Castro et al., 2006) (Figure 5.1). The transitional zone (GC4-8 and GC4-9) was characterized by a mixture of physical regimes, with upper waters dominated by Tropical Surface Waters (TSW). Deep Pacific Waters (DPW) were only observed at the deepest sampled depth (3000 m) at station GC4-8.

The study area was characterized by oligotrophic conditions, with surface layers (upper 20 m) containing N-poor and P-replete concentrations (0.03-0.09 μmol L^{-1} for nitrate + nitrite and 0.3-0.8 μmol L^{-1} for phosphate; White et al., 2013). Warm and salty surface waters cooled and freshened as they moved out of the GC and northward along the ETNP transect. Mixed layer depths also deepened along with the depth of the euphotic zone (Ez), defined here as the depth of 0.1% light penetration (as in Buesseler and Boyd, 2009) and determined using profile data from a photosynthetically active radiation (PAR) sensor on the CTD rosette (Table 5.1). This depth is where ^{234}Th was found to be in equilibrium with ^{238}U at the majority of stations sampled (see section 5.4.2 and Figure 5.2).

5.4.2 ^{234}Th and ^{238}U profiles and ^{234}Th fluxes

Total ^{234}Th activities ranged from 0.8 to 2.8 dpm L^{-1} (Figure 5.2), with particulate ^{234}Th activities (Table A.3.1) in the small particles (1-53 μm) accounting for 4 to 33% of the total activity measured (average 14 ± 6%). ^{234}Th activities in large particle (>53 μm) accounted for a smaller fraction of the total ^{234}Th activity, averaging 5 ± 4% with a range of 0.4 to 17%.

A deficit of ^{234}Th with respect to ^{238}U over the upper 100 m was observed at all stations (Figure 5.2). The magnitude of this deficit, however, was greater within the GC, where ^{234}Th disequilibrium was found to depths of 700 and 300 m at stations GC4-1 and GC4-2, respectively. Excess ^{234}Th activity was only measured between 80 and 250 m (average 0.25 ± 0.05 dpm L^{-1}) in the most northern station of the ETNP sampling region (GC4-12), representing almost 60% of the ^{234}Th deficit measured in the upper 100 m.

Table 5.1: Euphotic zone depth, net primary production, ^{234}Th fluxes and elemental/^{234}Th ratios

Station	Ez	NPP	^{234}Th fluxes		ST ratios		SP ratios		LP ratios		
	(m)	(mmol C m^{-2} d^{-1})	(dpm m^{-2} d^{-1})		PC/^{234}Th µmol/dpm	PN/^{234}Th µmol/dpm	PC/^{234}Th µmol/dpm	PN/^{234}Th µmol/dpm	PC/^{234}Th µmol/dpm	PN/^{234}Th µmol/dpm	bSi/^{234}Th µmol/dpm
			Sediment trap	Water column							
GC4-1	75	67 ± 10	6300 ± 1030	2600 ± 200	5 ± 1	0.7 ± 0.1	2.4 ± 0.3	0.38 ± 0.04	1.59 ± 0.04	0.182 ± 0.005	0.27 ± 0.01
GC4-2	90	34 ± 3	4900 ± 570	3400 ± 140	5.5 ± 0.7	0.7 ± 0.1	3.1 ± 0.3	0.50 ± 0.05	1.4 ± 0.1	0.14 ± 0.01	0.039 ± 0.004
GC4-2b	75	32 ± 3	2600 ± 340	NA	9 ± 2	1.2 ± 0.3	5.1 ± 0.6	0.84 ± 0.09	2.3 ± 0.2	0.26 ± 0.02	0.16 ± 0.01
GC4-8	110	31 ± 3	3500 ± 340	1400 ± 170	16 ± 5	2.2 ± 0.6	3.9 ± 0.4	0.78 ± 0.08	1.9 ± 0.2	0.23 ± 0.02	0.064 ± 0.006
GC4-9	80	27 ± 5	2000 ± 330	1100 ± 210	6 ± 1	0.7 ± 0.2	1.3 ± 0.1	0.22 ± 0.02	1.0 ± 0.1	0.11 ± 0.01	0.011 ± 0.001
GC4-10	95	47 ± 4	3100 ± 450	900 ± 220	5.6 ± 0.7	0.8 ± 0.1	2.3 ± 0.3	0.30 ± 0.03	1.8 ± 0.2	0.16 ± 0.02	0.11 ± 0.01
GC4-11	100	30 ± 4	1400 ± 170	1700 ± 190	11 ± 1	1.1 ± 0.1	2.7 ± 0.2	0.44 ± 0.03	1.6 ± 0.1	0.12 ± 0.01	0.12 ± 0.01
GC4-12	90	117 ± 8	1700 ± 170	1900 ± 150	13 ± 2	1.6 ± 0.3	2.4 ± 0.2	0.35 ± 0.03	1.79 ± 0.09	0.18 ± 0.01	0.47 ± 0.02

Euphotic zone depth (Ez) defined as 0.1% light level. Net primary production (NPP) was integrated in the upper 60 m. ^{234}Th fluxes were calculated at 100 m. Elemental/^{234}Th ratios from the different particulate material collected at 100 m (ST = sediment trap; SP = ISP small particles, LP = ISP large particles, see text for details). NA is noted when samples were not available.

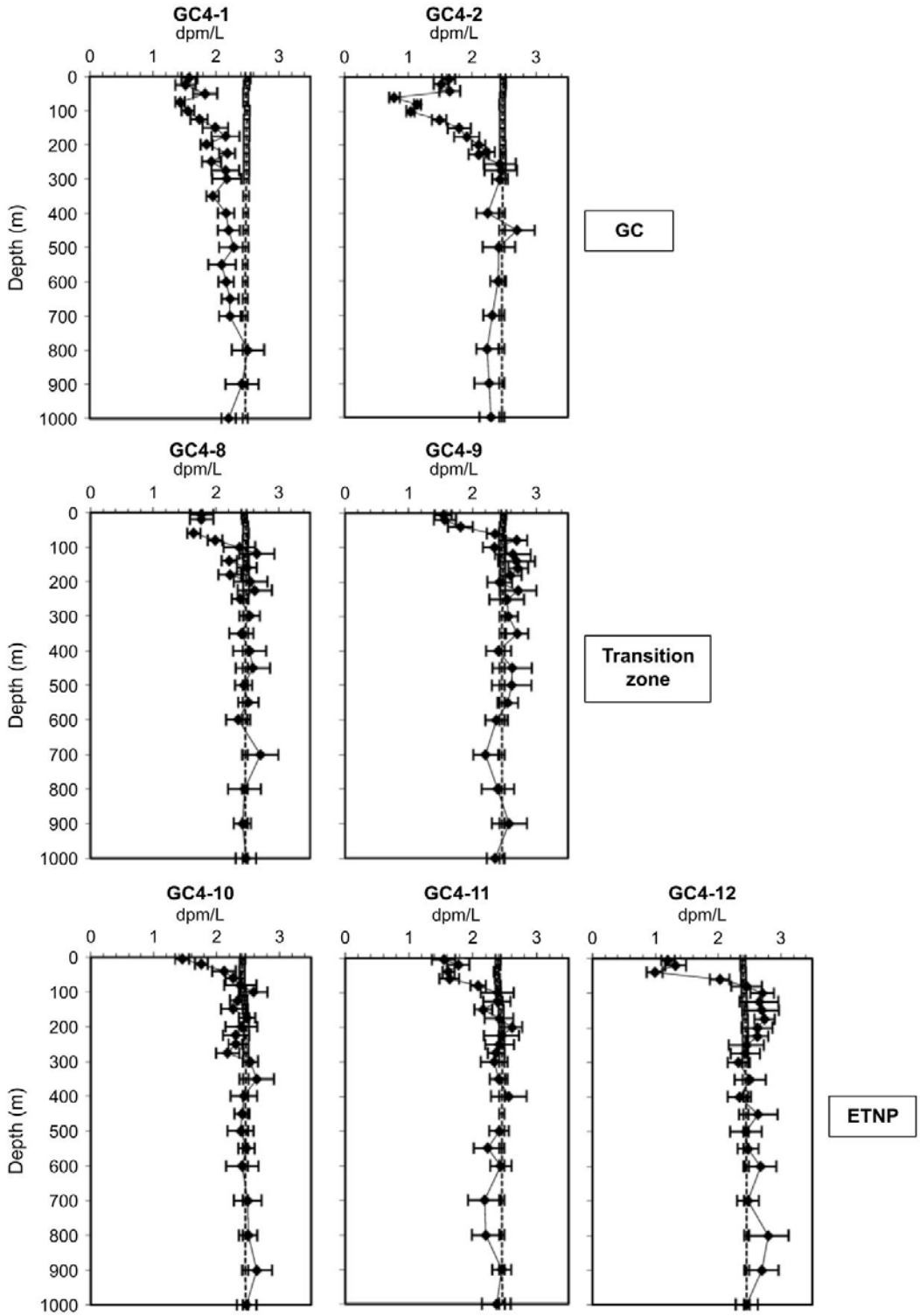

Figure 5.2: ^{234}Th (black diamonds) and ^{238}U (dashed line) activity profiles (in dpm/L) down to 1000 m obtained at each station. The profiles are presented in the three groups corresponding to GC stations (GC4-1 and GC4-2), Transition zone stations (GC4-8 and GC4-9), and ETNP stations (GC4-10, GC4-11, and GC4-12).

^{234}Th fluxes obtained from ST at 100 and 105 m were in excellent agreement (average factor 1.04 ± 0.13). We therefore focus on ST results collected at 100 m, which is a commonly used depth, to estimate particle fluxes found in the literature. The WC derived ^{234}Th fluxes were obtained by integrating the ^{234}Th deficit over the upper 100 m using a steady-state one-dimensional model. Both the ST and the WC derived ^{234}Th fluxes are presented in Table 5.1 and Figure 5.3. WC fluxes at 100 m, which ranged from 890 ± 220 to 3400 ± 140 dpm m^{-2} d^{-1}, were in excellent agreement with those obtained directly from the ST (ratios between both estimates averaged 0.9 ± 0.1) at the most northern stations of the ETNP (GC4-11 and GC4-12). At the remaining stations, ST fluxes at 100 m ranged from 1400 ± 170 to 6300 ± 1000 dpm m^{-2} d^{-1}, and are thus 1.4 to 3.5 times higher (average 2.3 ± 0.8) than those derived from the WC. Both methods yielded larger fluxes within the interior of the GC. At the reoccupation of station GC4-2 (GC4-2b), 6 days after the first sampling, ST ^{234}Th flux decreased by almost 50%, from 4900 ± 570 to 2600 ± 340 dpm m^{-2} d^{-1}, which highlights the short timescale of ST measurements compared to WC ^{234}Th deficits.

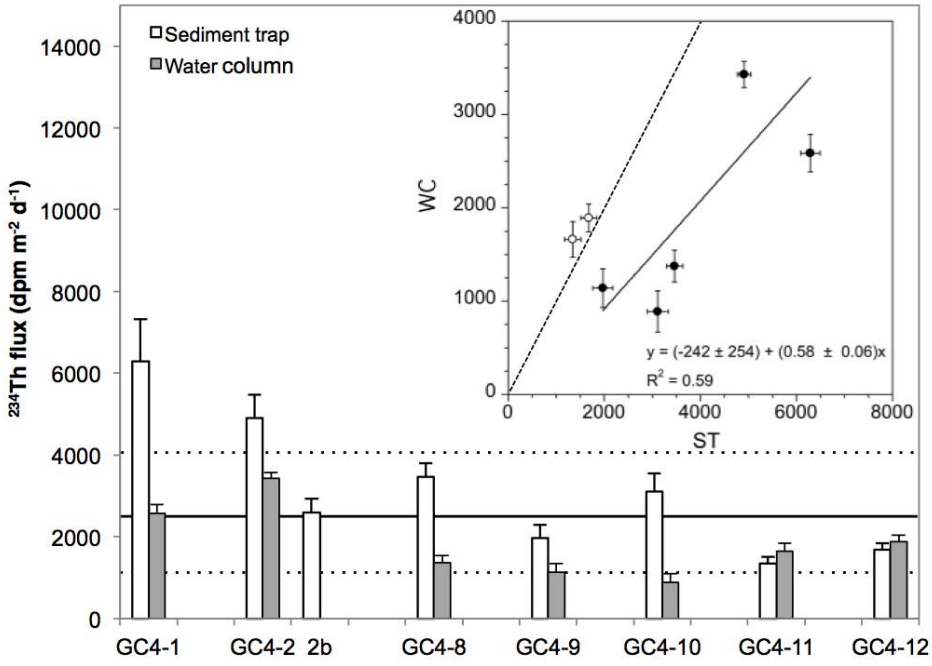

Figure 5.3: Sediment trap (ST) (open bars) and water column (WC) (grey bars) derived ^{234}Th fluxes at 100 m. Solid line indicates average fluxes, considering direct fluxes from the ST and WC-derived fluxes. Dashed lines indicate the standard deviation. The inset figure represents WC-derived ^{234}Th fluxes (dpm m^{-2} d^{-1}; y axis) vs ST fluxes (dpm m^{-2} d^{-1}; x axis). Open circles correspond to stations GC4-11 and GC4-12, and closed circles correspond to the remaining stations. The solid line and equation indicate the linear regression for the closed circles. The dashed line indicates the ideal 1:1 relationship between the ST and WC-derived fluxes.

5.4.3 Particle distribution and composition

5.4.3.1 Particle size distribution analysis

The particulate beam attenuation coefficient, $c_p(\lambda)$, was calculated by subtraction of CDOM absorption, $a_g(\lambda)$, from $c(\lambda)$. The general shape of the spectra of beam attenuation $c_p(\lambda)$ is well-approximated by a power-law as follows (Bricaud et al., 1998) (equation 5.1):

$$c_p(\lambda) = c_p(\lambda_0)(\lambda/\lambda_0)^{-\gamma_{cp}} \quad (5.1)$$

As previously mentioned, the magnitude of the particle beam attenuation coefficient at 660 nm, $c_p(660)$, is to a first order proportional to the concentration of suspended particles (Gardner et al., 2006), whereas its spectral slope, γ_{cp}, is related to the slope of the PSD under certain assumptions by $\xi = \gamma_{cp} + 3$ (Kostadinov et al., 2012). γ_{cp} was calculated using ordinary least squares regression on the log-transformed data within 440–676 nm. Larger values of ξ, i.e. steeper slopes, indicate higher abundance of small particles. The percent contribution of picoplankton (0.5-2.0 μm), nanoplankton (2.0-20 μm), and microplankton (20-50 μm) to total particle volume was then calculated according to Equation 2 in Kostadinov et al. (2010). It is important to highlight that the examination of the slope of the beam attenuation profile to obtain particle size classes is based on the scattering of particles without discriminating live particles from detritus.

PSD profiles (Figure 5.4) clearly reflect a decline in the relative contribution of small particles as we transited out of the GC into the transition zone and into the ETNP. To link these changes to the size structure of the phytoplankton community structure we refer to the HPLC data presented in White et al. (2013). HPLC-based estimates of cell size use the relative proportion of diagnostic pigments to estimate the contributions of picophytoplankton (<2 μm), nanophytoplankton (2-20 μm), and microphytoplankton (20-200 μm) and makes simplifying assumptions about the size classes associated with each pigment considered. Therefore, both approaches provide independent estimates of particle size distributions. While the absolute size distributions differ between techniques and is to some extent expected given that these methods are fundamentally measuring different properties (e.g., the slope of scattering spectra and pigment ratios), they both show a measurable shift in particle size from smaller particles to larger particles across the transition zone from the GC into the ETNP.

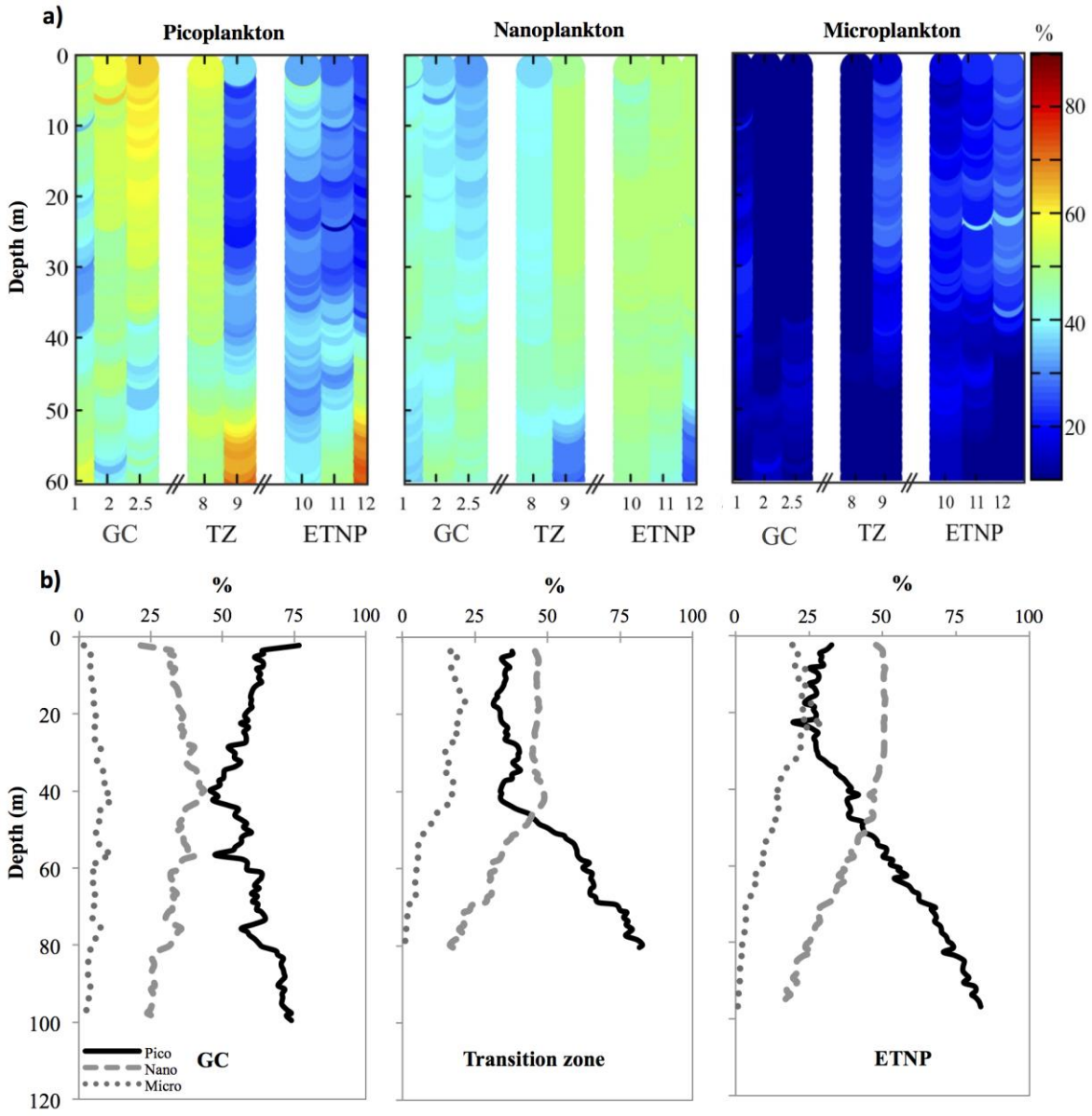

Figure 5.4: Particle size distribution profiles for pico-, nano-, and microplankton abundances obtained at each station (a) and averaged particle size distribution profiles grouped by regions (b): GC, Transition zone, and ETNP. Profiles on panels a) are cropped to a depth of 60 m for simpler comparison to HPLC data from Figure 6 in White et al., 2013.

5.4.3.2 Elemental composition

The PC and PN concentrations in particles collected with the ISP ranged from 0.2 to 3.4 µmol C L^{-1} and 0.03 to 0.55 µmol N L^{-1} for small particles (1-53 µm) and 0.03 to 2.6 µmol C L^{-1} and 0.002 to 0.34 µmol N L^{-1} for large particles (>53 µm) (Table A.3.1). Small particles accounted for the bulk of the PC and PN, averaging 85 ± 9% and 89 ± 11% of the total particulate pool, respectively. Depth patterns were similar between the two size classes at all stations. Maximum PC and PN concentrations were typically located between 20 and 50 m, and

decreased by as much as a factor of 10 down to a depth of 500 m. The PC/PN ratios showed little change with depth, averaging 7 ± 1 in small particles, while the average PC/PN ratio in large particles was significantly higher (10 ± 2) (p <0.0001; n = 165). Inorganic carbon was minimal in both size fractions, with no significant differences between PC and POC (average factor difference 1.1 ± 0.1, n = 20, for small particles and 1.0 ± 0.2, n = 16, for large particles). Carbon content within the ST material was also dominated by POC (average factor difference between PC and POC 1.3 ± 0.3, n = 8), with an average PC/PN ratio of 8 ± 1 (n = 8).

5.4.3.3 Stable isotopic composition

$\delta^{15}N$ and $\delta^{13}C$ values were measured on particles collected at each station (Table A.3.1). Profiles of $\delta^{15}N$ values were relatively constant over the upper 100 m with no significant difference between the ISP small and large particles (p >0.1; n = 100; $\delta^{15}N$ = 9.6 ± 1.8 ‰). In contrast, the $\delta^{13}C$ values of small and large ISP particles were significantly different throughout the water column, with smaller particles averaging -22.0 ± 1.2 ‰ and large particles averaging -20.1 ± 0.8 ‰ over the upper 100 m (p <0.0001 in both cases; n = 102 for samples above 100 m and n = 66 for deeper samples). There were no significant differences between the $\delta^{15}N$ of ST and ISP samples from the upper 100 m (p >0.5 for both size classes). However, significant differences were apparent between the $\delta^{13}C$ of ST (-21.8 ± 1.3 ‰; n = 8) and large ISP particles (p <0.0001; n = 60), whereas no differences were observed between the $\delta^{13}C$ values of ST and small ISP particles.

5.4.3.4 Elemental/^{234}Th ratios

Elemental ratios of PC and PN to ^{234}Th collected using the ISP were higher in the small versus large size classes over the upper 100 m, but converged with increasing depth at 200–500 m (Figure 5.5). The PC/^{234}Th ratios of small and large particles measured at 100 m were on average lower than the ratios obtained from the ST by a factor of 3.2 ± 1.4 and 5.8 ± 2.8, respectively (Table 5.1). The magnitude of this difference varied both regionally and with particle size, with station GC4-8 and the northernmost stations of the ETNP showing the largest contrast. PN/^{234}Th ratios followed a similar trend (Table 5.1). Close examination of the data shows that the elemental to ^{234}Th ratios measured in ST samples at 100 m are much more comparable to those measured in both ISP-collected size classes at the surface (Figure 5.5). The bSi/^{234}Th ratios measured in the large size fraction of particulate material collected with the ISP ranged from 0.12 to 0.45 μmol dpm^{-1}, with the highest values measured at stations GC4-1 and GC4-12 (Table 5.1).

5.4.3.5 *Attenuation analysis*

The high resolution of the ISP sampling along the water column allows us to estimate a net attenuation term, *b*, which indicates how rapidly PC and PN are attenuated relative to ^{234}Th, e.g., larger absolute *b* values imply higher attenuation rates. Similar to the commonly used Martin curve, applied to evaluate the particle flux attenuation with depth (Martin et al., 1987), the *b* term was obtained from a power regression of PC and PN to ^{234}Th ratios versus depth throughout the water column at each station (equation 5.2; Figure 5.5), such that:

$$PC/^{234}Th = PC/^{234}Th_o \cdot (Z/Z_o)^{-b} \quad (5.2)$$

where $PC/^{234}Th_o$ is the term obtained from the fitting using least-squares regression that represents the $PC/^{234}Th$ ratio at the base of the euphotic zone (μmol dpm^{-1}), and Z is the depth at which we calculate the $PC/^{234}Th$ ratio and Z_o is the depth of the euphotic zone. The same equation can be applied to $PN/^{234}Th$ ratios.

Element to ^{234}Th ratios measured in large and small ISP particles were plotted separately to examine possible size-dependant differences in attenuation profiles (Figure 5.5). The results indicate that PC and PN in small particles are attenuated at a significantly faster rate relative to ^{234}Th with depth, with *b* terms for small particles being 0.66 and 0.76 for PC and PN, respectively compared to 0.39 and 0.65 for large particles (Kolmogorov-Smirnov test p <0.0001; n = 88 for both data sets, PC and PN).

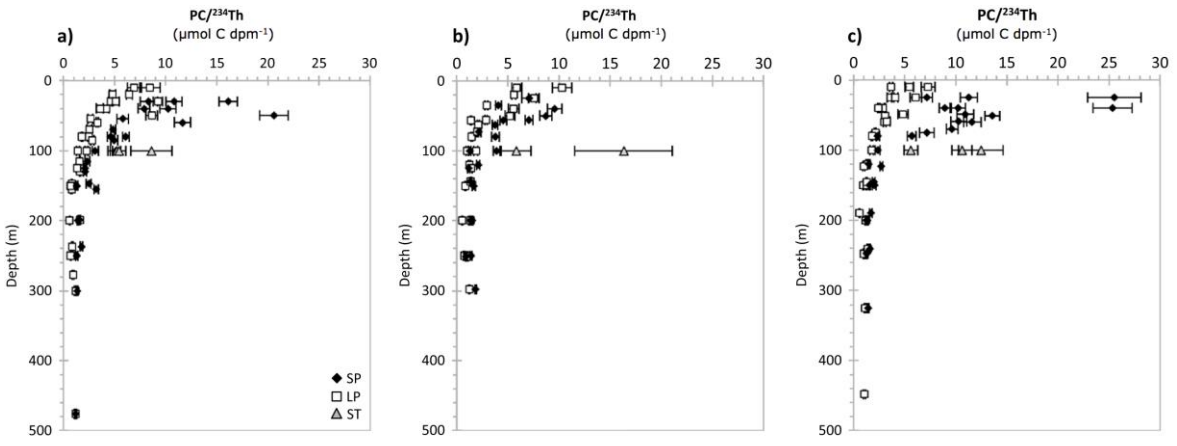

Figure 5.5: Particulate $PC/^{234}Th$ ratio profiles at (a) the GC stations (GC4-1, GC4-2, and GC4-2b), (b) the Transition zone stations (GC4-8 and GC4-9), and (c) the ETNP stations (GC4-10, GC4-11, and GC4-12), obtained with the in situ pumps from small particles (SP) (black diamonds) and large particles (LP) (open squares). Ratios measured in the sediment traps (ST) are presented as grey triangles. Small particles were only plotted below 20 m due to subsurface maxima located at that depth.

5.4.4 PC, PN and bSi fluxes

The absolute magnitude of PC and PN fluxes at 100 m (Figure 5.6 and Table 5.2) was determined directly using ST and indirectly from the WC derived ^{234}Th fluxes using station-specific ST and ISP element/^{234}Th ratios presented in Table 5.1. The magnitude of the derived elemental fluxes was strongly driven by the elemental/^{234}Th ratio used (i.e., ST ratio > small particle ratio > large particle ratio). Although fluxes obtained from ST varied considerably (~50% decrease) over relatively short time periods (<7 d) at station GC4-2 regarding ^{234}Th fluxes, such changes were not clearly reflected in the PC and PN fluxes due to the PC(PN)/^{234}Th variation (~50% increase).

Elemental fluxes obtained directly with the ST and by means of WC ^{234}Th deficits using the elemental ratios obtained from ST were in relatively good agreement. ST fluxes were higher by an average factor of 1.5 ± 0.9 for PC fluxes and 1.6 ± 0.9 for PN fluxes at all stations, except at GC4-2b and at the northernmost ETNP station (GC4-12). As mentioned previously, values for elemental/^{234}Th ratios tended to be higher in small versus large particles, but converged with increasing depth. As a result, PC and PN fluxes at 100 m derived using WC ^{234}Th deficits and ratios measured on small and large particles, agreed within a factor of 1.8 ± 0.6 for PC and 2.7 ± 0.8 for PN. In contrast, when fluxes estimated using ST elemental/^{234}Th ratios are compared with those estimated using ISP data, we find that the former were always higher, ranging from a factor of 1.7 to 10 for PC (average 3.2 ± 1.4 and 5.8 ± 2.8 for small and large particles respectively) and from a factor of 1.3 to 10 for PN (average 2.5 ± 1.0 and 6.5 ± 2.4 for small and large particles respectively). Fluxes estimated using PC and PN to ^{234}Th ratios for the combined small and large ISP particles were in agreement with ST fluxes within a factor of 2 - 4. These particle flux estimates highlight the large variability that occurs as a consequence of the different element/^{234}Th ratios used.

Fluxes of bSi estimated from WC ^{234}Th deficits and values for bSi/^{234}Th ratios measured in ISP large particles were only significant where microscopy and pigment composition indicated a diatom-dominated community structure (White et al., 2013): at stations GC4-12 (0.91 ± 0.11 mmol bSi m^{-2} d^{-1}) and GC4-1, below the nitracline (30 m), (0.69 ± 0.07 mmol bSi m^{-2} d^{-1}). At all other locations, where a picocyanobacterial-dominated community structure was observed (Figure 5.4; White et al., 2013), bSi fluxes were 0.01 - 0.20 mmol bSi m^{-2} d^{-1}.

Table 5.2: Summary of particulate C, N and bSi fluxes.

Station	PC fluxes (mmol C m^{-2} d^{-1})				PN fluxes (mmol N m^{-2} d^{-1})				bSi fluxes (mmolSi $m^{-2}d^{-1}$)
	ST	ST ratio	SP ratio	LP ratio	ST	ST ratio	SP ratio	LP ratio	LP ratio
GC4-1	18	14 ± 3	6.1 ± 0.8	4.1 ± 0.3	2.3	1.8 ± 0.4	1.0 ± 0.1	0.47 ± 0.04	0.70 ± 0.06
GC4-2	27	19 ± 3	11 ± 1	4.9 ± 0.5	3.4	2.4 ± 0.3	1.7 ± 0.2	0.50 ± 0.05	0.13 ± 0.01
GC4-2b[a]	22	30 ± 7	18 ± 2	7.7 ± 0.6	3.0	4.0 ± 1.0	2.9 ± 0.3	0.90 ± 0.07	NA
GC4-8	28	22.3 ± 0.8	5.4 ± 0.8	2.6 ± 0.4	4.9	3.0 ± 0.4	1.1 ± 0.2	0.31 ± 0.05	0.09 ± 0.01
GC4-9	12	7 ± 2	1.5 ± 0.3	1.2 ± 0.2	1.4	0.8 ± 0.3	0.3 ± 0.1	0.12 ± 0.03	0.012 ± 0.002
GC4-10	17	5 ± 1	2.1 ± 0.6	1.6 ± 0.4	2.5	0.7 ± 0.2	0.3 ± 0.1	0.14 ± 0.04	0.09 ± 0.03
GC4-11	15	18 ± 3	4.5 ± 0.6	2.6 ± 0.3	1.5	1.8 ± 0.3	0.7 ± 0.1	0.27 ± 0.04	0.19 ± 0.03
GC4-12	21	24 ± 4	4.5 ± 0.5	3.4 ± 0.3	2.7	3.0 ± 0.6	0.7 ± 0.1	0.34 ± 0.03	0.89 ± 0.08

Fluxes obtained directly from the sediment traps (ST) or derived from the water column ^{234}Th deficits at 100 m using sediment trap ratios (ST ratio), *in situ* pump small particles (SP ratio) or large particles (LP ratio) (see text for details).
[a]GC4-2b derived fluxes were calculated using the water column ^{234}Th flux form GC4-2 and element to ^{234}Th ratios from GC4-2b.

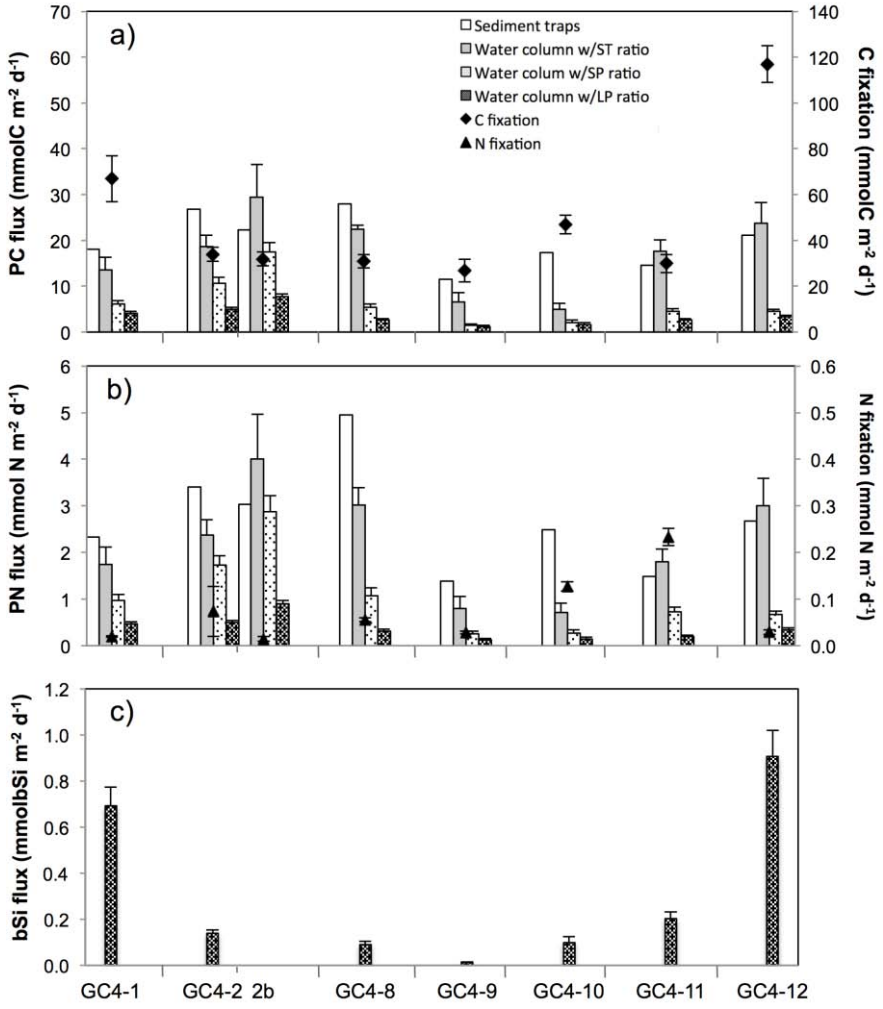

Figure 5.6: ^{234}Th-derived fluxes and direct measurements by ST at 100 m. The legend depicted in plot a) is the same for all plots. a) PC fluxes (bars) together with C fixation rates integrated over the upper 60 m (black diamonds); b) PN fluxes (bars) together with N fixation rates integrated over the upper 60 m (black triangles). Note the different scales when comparing PC flux and C fixation and PN flux and N fixation. c) bSi fluxes. C and N fixation data obtained from White et al. (2013). GC4-2b-derived fluxes were calculated using the WC-^{234}Th flux from GC4-2 and the element to ^{234}Th ratios from GC4-2b.

5.5 Discussion

A major goal of this study was to examine particle export within the ETNP and GC in response to overlying water column productivity and community composition and to use these results as an analog for understanding other stratified tropical ecosystems. Previous work in the GC found that PC and PN fluxes to depth remain fairly constant (winter (Nov-Feb) and summer (Jun-Sep) averages export fluxes at ~500 m were not significantly different; 19 ± 4 versus 21 ± 3 mg C m^{-2} d^{-1}, p >0.5), even though primary productivity rates are significantly higher during the winter months (~2 mg m^{-3} versus <0.5 mg m^{-3}) (Lyons et al., 2011; Thunell, 1998; White et al., 2013). This observation suggests that the export efficiency in summer is greater than in winter. Several studies have suggested that N_2 fixation may enhance PC and PN export fluxes in the North Pacific subtropical gyre (Dore et al., 2002; Scharek et al., 1999) and recent work in the GC region indicates that N_2 fixation may be significant during the stratified summer period when nutrients have been depleted (White et al., 2007). Such trends remain enigmatic, however, as the temporal and spatial variability in N_2 fixation in this area (from 14 to 795 μmol N m^{-2} d^{-1}; White et al., 2013) appears to be too large to explain the relatively uniform PC export observed throughout the year.

We have used ^{234}Th as a tracer to estimate particle fluxes within the ETNP and GC during the summer of 2008. This approach has been widely employed to examine episodic events that may be missed using ST due to temporal constraints and potential methodological issues (e.g., Buesseler et al., 2007a, 1992). The application of the ^{234}Th method, however, also requires a number of assumptions, including the determination of the element/^{234}Th ratio necessary to convert ^{234}Th fluxes into the elemental flux of interest. Therefore, we also examine the approaches used in the collection and application of element/^{234}Th ratios and discuss these results in light of regional variability in particle flux and the efficiency of the biological pump in the GC region and the ETNP adjacent waters.

Our overall assessment concludes that small particles are significant contributors to particle flux throughout the GC and ETNP in summer and that export efficiencies in stations dominated by picoplankton containing diazotrophs are higher than in those stations where diatoms were more abundant, confirming the inference from moored sediment traps from Thunell (1998), and agreeing with previous work from Dunne et al. (1999) who found that non-diatom production was responsible for the majority of the export. When examined on a global perspective, our results further suggests that the phenomenon is not unique to our study region, but may apply broadly to ecosystems dominated by smaller taxa, agreeing with previous work from oligotrophic regions

(e.g., Richardson and Jackson, 2007; Durkin et al., 2015). While others have shown that choosing a single particle fraction to estimate vertical export my be misleading (Dunne et al., 1997; Burd et al., 2007; Stewart et al., 2011), sampling uniquely large particles (>50 μm) is still the dominant approach used to estimate elemental fluxes derived from the ^{234}Th-method. Our data again supports this discussion, providing results that indicate the importance of the ecosystem and biological state of the region under interest.

5.5.1 ^{234}Th deficits and fluxes

In this study, ^{234}Th deficits mainly occurred over the upper 100 m, with little evidence of excess ^{234}Th at depth that would imply extensive particle remineralization (Bacon et al., 1996; Buesseler et al., 2008; Maiti et al., 2010). Our high-resolution sampling suggests that either the remineralization rates were too low to show a clear ^{234}Th excess peak or, if such a peak existed, it was not resolvable within the sampling depth intervals chosen at our stations (e.g., Maiti et al., 2010). Within the GC, ^{234}Th deficits reached depths of 700 m (GC4-1) and 300 m (GC4-2). Water column derived ^{234}Th fluxes at 100 m at those stations (>2500 dpm m^{-2} d^{-1}) are comparable to other productive coastal regions or to those found during the North Atlantic Bloom Experiment (e.g., Coale and Bruland, 1985; Buesseler et al., 1992). Indeed, the fluxes of ^{234}Th obtained from the GC ST at 100 m (≥5000 dpm m^{-2} d^{-1}) are among the highest measured of all previous WC ^{234}Th flux assessments globally (i.e., the maximum flux reported previously was of 5500 dpm m^{-2} d^{-1} for the mid and late SW Monsoon in the Arabian Sea by Buesseler et al., 1998. See summary by Le Moigne et al., 2013). Although this comparison should be taken cautiously due to the use of different methods (i.e., ST *versus* WC fluxes), it helps to highlight the high ^{234}Th fluxes observed at the stations located within the GC. We hypothesize that those stations are influenced by the lateral advection of water and particles from the nearshore due to their location within two narrow basins (Figure 5.1), as suggested by other studies using longer lived radionuclides (Smoak et al., 1999) and transmissometry profiles (data not shown). Since the total ^{234}Th activity is dominated by the dissolved phase, water from the margins would be expected to have low total ^{234}Th activity from high particle scavenging. Any laterally advected particles would further promote ^{234}Th scavenging, explaining the deep deficits in total ^{234}Th, and they would also increase the particulate ^{234}Th collected by the ST.

Differences between the methodologies used to determine ^{234}Th fluxes (directly from the ST or integrating the WC ^{234}Th deficits) were within a factor of 2 to 4 (average difference of 2.3 ± 0.8), consistent with that typically found in the literature when comparing these collection techniques.

These differences may be explained, in part, by the time scale of collection as well as methodological issues: deficits of ^{234}Th in the water column over the upper 100 m integrate over several weeks, thereby diluting episodic events of higher (or lower) particle fluxes that may have been observable using more short term deployments, such as the VERTEX style traps used here (Buesseler, 1991). ST, on the other hand, can be affected by large-scale turbulence and horizontal currents that potentially produce both under and over collection biases (Gardner, 2000), although the VERTEX-style traps used in this study were designed to minimize this issue (Gardner, 1980; Hargrave and Burns, 1979).

5.5.2 Elemental/^{234}Th ratios

One of the key issues in determining elemental fluxes from ^{234}Th disequilibria is measuring the element to ^{234}Th ratio of sinking particles. These ratios change spatially and temporally depending of the structure of the plankton community and food web dynamics, but also on the particle collection device used, such as ST and ISPs (Buesseler et al., 2006). Here, we explored differences in the element/^{234}Th ratios obtained using these two techniques, considering methodological issues, sinking velocity, and particle size and composition.

5.5.2.1 Methodological issues

The disagreement in PC/^{234}Th ratios between ST and large (>53 μm) ISP particles has been observed in several studies (see review by Buesseler et al., 2006) and is usually within a factor of 2 to 4 (e.g., North Atlantic Bloom Experiment, JGOFS, Buesseler et al., 1992; Equatorial Pacific, Buesseler et al., 1995, Bacon et al., 1996, and Murray et al., 1996; North Pacific Subtropical Gyre, Benitez-Nelson et al., 2001; Mediterranean Sea, Stewart et al., 2007; Mediterranean Sea and Northwest Atlantic, Lepore et al., 2009), but may differ by over an order of magnitude, as reported by Lalande et al. (2008) for the Barents Sea. Evidence suggests that ISP and ST sample different types of particles depending on their settling velocity. ST tend to under-collect slower sinking particles due to hydrodynamic discrimination (Gustafsson et al., 2004), while fast sinking particles are more likely missed by ISP (Lepore et al., 2009). Another issue is that size is not necessarily related to density, and ISP sampling may include communities dominated by large, C-rich neutrally-buoyant phytoplankton (i.e., non sinking, but with high PC/^{234}Th ratios) (Lalande et al., 2008).

Although the two sampling devices collect fundamentally different particle pools (ST particles represent an average particle size class with respect to flux, whereas ISPs collect particles that represent an average with respect to concentration), sampling biases such as swimmers in ST or the rupture of aggregates by ISPs may further exacerbate these differences. Swimmers have been previously reported as an important source of bias in the PC/^{234}Th ratio of ST if they are improperly removed, since they have a relatively high PC content relative to ^{234}Th (Buesseler et al., 1994; Coale, 1990). In this study, obvious swimmers were removed from particulate samples in both types of samples, ST and ISP. However, they may have altered the particle composition during the 24 h ST deployment period via feeding and cell lysis. Indeed, PC and PN fluxes obtained from ST at 100 and 105 m were in good agreement, but were more variable (ratios of fluxes at 100 and 105 m were 0.9 ± 0.4 for PC and 1.1 ± 0.3 for PN) than ^{234}Th fluxes (1.0 ± 0.1).

Another possible methodological issue may be related to the rupture of aggregates using ISP. Gardner et al. (2003) suggested that lower POC/^{234}Th ratios in ISP samples can result from the rupture of fragile high C concentration particles (e.g., transparent exopolymer particles (TEP) and bacteria) due to the high cross-filter pressure differentials created within an ISP. This would preferentially reduce PC retention. To our knowledge, however, there is no information regarding high TEP concentrations in the study area, nor an anomalous abundance of bacteria, although microscopy of the ST material showed the presence of marine snow (White et al., 2013). The loss of large C-rich particles could also occur due to washout when using ISP. Bishop et al. (2012) reported preferential loss of biogenic elements from the >51 μm size fraction when sampling with the most commonly used 142 mm filters holders for ISP. In that study, the values for the ratio of POC to ^{234}Th were not systematically compared between filter holder types, but a few ad hoc comparisons suggest that the loss of biogenic material was mirrored by an equivalent loss of particulate ^{234}Th activity (K. Maiti *pers. communication*). Therefore, the observed differences in the PC/^{234}Th ratios between large ISP particles and ST in this study do not seem related to the type of filter holder used.

5.5.2.2 Particle size, composition and attenuation

Several studies have documented a trend of increasing PC/^{234}Th ratios with increasing particle size as a function of the volume to surface area ratio, since ^{234}Th is mostly surface bound whereas C is distributed evenly throughout the particle (see review by Buesseler et al., 2006). However, the relation between PC/^{234}Th ratio and particle size is not straight forward and the magnitude of this change further depends on whether or not larger particles are comprised of aggregated smaller particles and whether or not that aggregation occurred via physical or biologically mediated

processes (i.e., grazing and fecal pellet production). In fact, in our study, smaller particles have consistently higher PC/^{234}Th ratios than larger particles, by an average factor of 2.0 ± 0.9 (p <0.0001; n = 80). Relatively higher PC/^{234}Th ratios in small particles have been reported previously by other studies in other regions (Buesseler et al., 1995 and Bacon et al., 1996, Equatorial Pacific; Santschi et al., 2003 and Hung et al., 2004, 2010, Gulf of Mexico; Cai et al., 2006 and Hung and Gong, 2007, China Sea and Kuroshio Current; Jacquet et al., 2011 and Planchon et al., 2013, Southern Ocean). As shown earlier, PC/^{234}Th ratios from both, small and large particles, measured in ISP particles significantly decrease with depth, a trend consistent with a number of prior studies, likely due to: 1) a reduction in biological production with increasing depth, 2) preferential loss of C (and N) relative to ^{234}Th, 3) potential changes in surface binding ligands with depth, and/or 4) increasing particulate ^{234}Th activities due to scavenging (Buesseler et al., 2006; Rutgers van der Loeff et al., 2002).

Settling speeds may reduce the PC/^{234}Th ratios measured in particles that reach deeper waters since faster sinking particles may be less influenced by biotic and abiotic processes due to their shorter residence times in the water column. Sinking velocities at 100 m were estimated by dividing the ^{234}Th flux at 100 m by the ^{234}Th concentration of the sinking particles collected at that same depth (Bacon et al., 1996). Since ^{234}Th activities were measured in both the small and large ISP particles, we estimated sinking velocities by assuming that the ^{234}Th removal was due to a combination of both small and large particles, or due to large particles alone, thus providing a range of sinking velocities. The average settling velocity determined using integrated WC fluxes and both size classes combined was 5 ± 2 m d^{-1}, while that for the large particles was 23 ± 7 m d^{-1}. When using ^{234}Th fluxes determined directly from ST samples, average sinking velocities increased by a factor of 2 (9 ± 5 m d^{-1} for combined size classes and 47 ± 24 m d^{-1} for large particles).

Based on Stokes' Law, a particle has to be either large or dense enough to overcome the friction force associated with the viscosity of the fluid in order to sink through the water column. One would therefore expect, for the same particle density, that the larger the particle, the faster it would sink, thereby reducing the time period the particle was subjected to breakdown within the water column. Hence, if residence time plays a role in setting the PC/^{234}Th ratio, one would expect a more rapid decrease in PC/^{234}Th ratios in smaller particles with depth (faster attenuation rates) than in larger particles, as a first approximation and assuming no subsurface production of small particles. In order to investigate this prospect further, we calculated an attenuation rate of the PC(PN)/^{234}Th ratio using a power law function in analogy to the classic Martin et al. (1987) formulation for carbon flux to depth, where the size of the b term indicates the rate of PC/^{234}Th

attenuation (equation 5.2). In this formulation, the general rate of change in the element/^{234}Th ratio is a combination of the net change in ^{234}Th particle activities due to adsorption, desorption, and remineralization, and a decrease in the PC and PN content due to remineralization (Figure 5.5). In this dataset, PC and PN concentrations decreased rapidly with depth relative to the small and inconsistent observed increases in specific particulate ^{234}Th activities. Therefore, attenuation of PC and PN is the dominant influence on the *b* term (Table A.3.1). The higher *b* exponents for PN compared to PC are consistent with the more labile nature of N (Gordon, 1971). Additionally, results suggest that PC and PN (relative to ^{234}Th) are attenuated at a similar or faster rate in small versus large ISP particles (Figure 5.5). Hence, these results support the hypothesis that residence time plays a role in setting the PC and PN to ^{234}Th ratio recorded in small and large particles with depth and helps to explain the convergence of these ratios deeper in the water column.

Higher elemental/^{234}Th ratios observed in the ST samples imply preferential collection of more rapidly sinking particles with shorter water column residence times. Rutgers van der Loeff et al. (2002) proposed that higher PC/^{234}Th ratios in ST material might be due to the collection of fresh aggregates, with particle ratios derived from a surface layer that were minimally altered en route to deeper ST. This explanation is consistent with the similarity observed between the elemental/^{234}Th ratios collected with the ISP from the surface waters and those measured in ST deployed at 100 m in this study. The existence of extra-large particles, with high sinking rates, could also be responsible for the higher PC/^{234}Th ratios obtained in the ST, since these particles are likely generated at the surface and do not appear to be comprised of smaller particles given their high PC/^{234}Th (over two orders of magnitude higher than particle aggregates) (e.g., Luo, 2013). However, we have no evidence to validate the existence of such particles in this system.

The more rapid attenuation of PC in small particles *vs* large particles was also confirmed by examining absolute PC changes with depth (Table A.3.1), using the approach of Lam et al. (2011) (equation 5.3):

$$[C] = [C_o] \cdot (Z/Z_o)^{-b} \qquad (5.3)$$

where $[C_o]$ is the carbon concentration (μmol L^{-1}) at the euphotic zone obtained from the curve fitting, Z is the depth at which we calculate the carbon concentration [C] and Z_o is the depth of the euphotic zone (Lam and Bishop, 2007).

A faster attenuation of large particles would be expected if large particles are comprised of labile compounds that are consumed and disaggregated as they sink, adding more refractory particles to the small size fraction along the water column. Conversely, a faster attenuation of small particles would be expected if the small particles were more labile. Using organic biomarkers of particles in different size fractions, Wakeham and Canuel (1988) found more labile material in the small size fraction, which they proposed was derived from the disaggregation of marine snow aggregates of fresh and delicate algal material that was not collected in the large size fraction or in sediment traps. They hypothesized that the marine snow contributed disproportionately to disaggregation in their system. Marine snow was qualitatively observed in our ST samples as well (see Figure 6 in White et al., 2013) . Therefore, differences between small and large particles may also be due to differences in their composition (i.e., source). The fact that PC/PN ratios in larger particles were on average higher than in small particles by a factor of 1.5 ± 0.2, further supports this hypothesis. Larger PC/PN ratios in smaller particles due to preferential remineralization of PN are expected given their longer residence times in the water column. However in this study, large particles are likely detritus comprised of degraded organic matter (lower PC/^{234}Th and PN/^{234}Th ratios than the small particles) poor in nutrients. Indeed, higher δ^{13}C values of large ISP particles suggest that significant degradation of large particles has occurred, presumably through zooplankton grazing and repacking (Fischer, 1991; Fry and Sherr, 1984). Similar observations were reported by Alldredge (1998), who found that large aggregates were older and more refractory than smaller ones, and by Alonso-González et al. (2010), whose organic biomarkers analyses revealed that slow sinking particles had the same degradation state, or were fresher than rapidly sinking particles. Mayor et al. (2014) recently argued that detritivorous metazoans fragment large particles in order to stimulate "microbial gardening" as a pathway to obtain small particles with labile compounds and nutritious microbial biomass. Therefore, higher PN content in small particles, coupled with the differences observed in δ^{13}C values, suggest that other processes, e.g., particle aggregation and microbial colonization, play a role in the observed differences in the particle size composition observed here.

5.5.2.3 b terms and phytoplankton groups

A global compilation of particle attenuation rates by Lam et al., (2011) found that the majority of study areas analyzed (~80 %; n = 55) were characterized by faster attenuation rates (larger *b* term) for the >53 μm particles relative to the 1-53 μm size class. Is it possible that the Gulf of California and the ETNP are uniquely different than most other studied regions of the global ocean? We compiled PC/^{234}Th data presented in previous studies, including the Equatorial Pacific,

Sargasso Sea, China Sea, Gulf of Mexico, Mediterranean Sea, Baltic Sea and Nord Sea fjords and also the Southern Ocean, and found that PC/^{234}Th ratios do not increase with increasing particle size when pico- and nanoplankton (usually *Synechococcus* and *Prochlorococcus*) dominate the planktonic community. Rather, they either have the opposite trend (PC/^{234}Th ratios decrease with increasing particle size) (Buesseler et al., 1995; Cai et al., 2006; Guo et al., 2002; Hung and Gong, 2007; Hung et al., 2010, 2004; Jacquet et al., 2011; Planchon et al., 2013; Santschi et al., 2003) or there is no clear pattern between particle size and PC/^{234}Th ratio (Brew et al., 2009; Hung and Gong, 2010; Lepore et al., 2009; Speicher et al., 2006; Stewart et al., 2010). Furthermore, when particles were collected according to their settling velocities in regions dominated by small cells, higher PC/^{234}Th ratios were found in slow sinking compared to fast sinking particles (Gustafsson et al., 2006) or there was no clear trend (Szlosek et al., 2009). Using published data from the studies mentioned above, we calculated *b* terms (when possible) for small and large particles and compared them with the global compilation of data presented in Lam et al. (2011) (Figure 5.7). We then took the ratio of the *b* term for large and small particles (LP/SP *b* ratio) such that a ratio of 1 indicates similar attenuation rates, a ratio higher than 1 suggests faster attenuation of large particles, and a ratio less than 1 suggests faster attenuation of small particles. Although the data are variable, LP/SP *b* ratios are ≤1 in 60% of the stations dominated by picoplankton, compared to 50% and 30% for nano- and microplankton dominated stations. This finding suggests that globally, small particles are attenuated at a similar or faster rate than large particles in regions with pico- and nanoplankton dominance. There were several stations were data is available that appear to be in the midst of transitioning from food webs dominated by small phytoplankton to those dominated by larger taxa, particularly diatoms. When all data are combined, comparisons between the same stations sampled during different seasons show that, regardless of the dominant group, when the importance of diatoms increases, values for the LP/SP *b* ratio become higher, mainly due to the increase in the *b* term of the large particles. These results indicate the importance of phytoplankton community in the attenuation rates of sinking particles and continue to support arguments against using “global” or “ocean basin” *b* terms in modeling efforts to estimate C export to the deep sea.

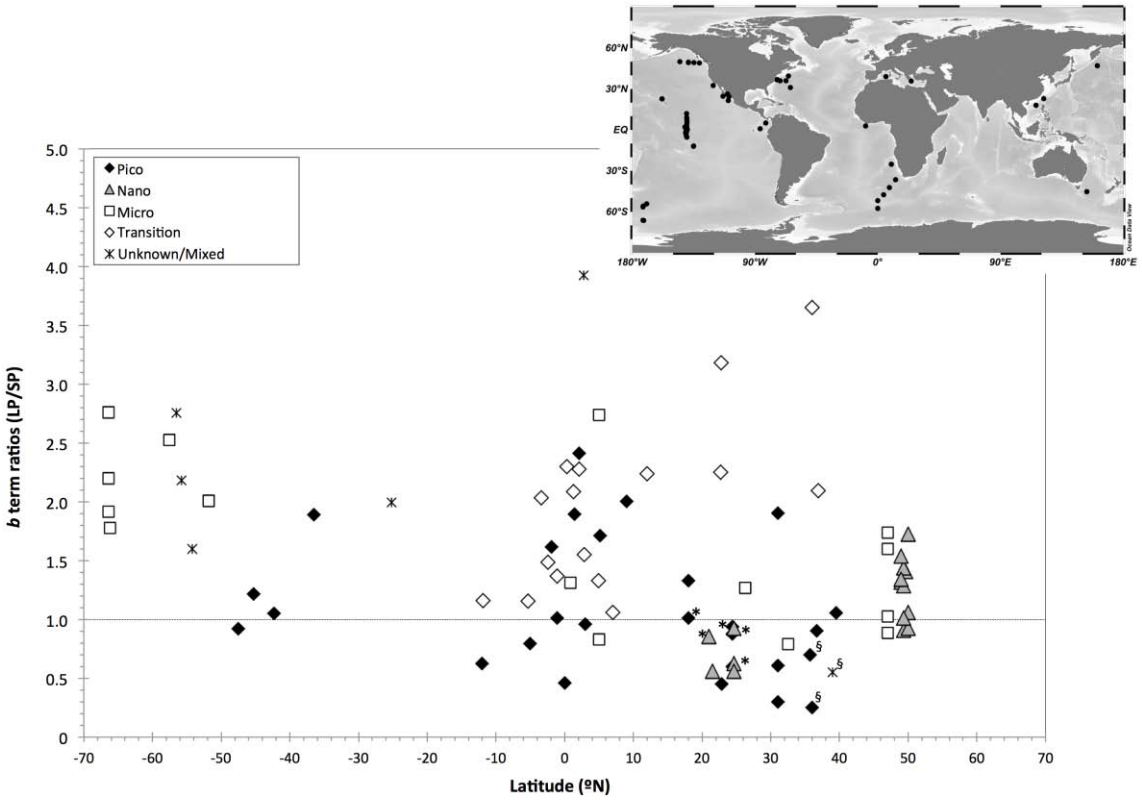

Figure 5.7: Global compilation of attenuation rate (*b* terms) ratios of large particles (>53 µm) versus small particles (1–53 µm) collected with ISPs including this study. The *b* terms have been obtained applying the power law fit from equation 5.3 to PC except for those stations marked with *, which have been obtained using the fit to PC/^{234}Th following equation 5.2. The *b* terms used at those stations marked with § were also obtained using fits to PC/^{234}Th following equation 5.2, but the small particle fraction only considered particles between 10–20 µm. The horizontal grey line indicates the 1:1 relationship between the *b* terms of large and small particles. Different symbols indicate the dominant particle size at the study site reported by the authors or derived from other studies conducted in the same region during the same season. Due to lack of detail regarding particle size abundances and distribution, when referring to "small particles" and "large particles", the data have been grouped as "pico" and "micro", respectively. The stations dominated by "nano" were clearly defined as such in the original studies. For the majority of studies, however, pico- and nano-dominated stations were usually not differentiated. Therefore, stations considered as pico-dominated might include areas where nanoplankton was also important. The "transition" stations are those that appeared to be transitioning from food webs dominated by small phytoplankton to those dominated by larger taxa, regardless of the dominant group at the sampling time. Map inset shows the locations of data from Cai et al. (2006), Hung and Gong (2007), Lepore et al. (2009), Stewart et al. (2010), Jacquet et al. (2011), Planchon et al. (2013), and the studies included in Lam et al. (2011): Bishop et al. (1977, 1978, 1980, 1986, 1999), Bishop and Fleisher (1987), Bishop (1992, 1999), Lam and Bishop (2007), and Bishop and Wood (2008).

5.5.2.4 Small particles and export fluxes

The discussion above demonstrates how the element/^{234}Th ratio may change with both depth and region depending on the sampling method, particle size, and food web structure. Historically, larger particles have been assumed to dominate particle export (Michaels and Silver, 1988), such that the larger size fraction of ISP (>53 µm) and ST particles are used to convert ^{234}Th fluxes into elemental export (Buesseler et al., 2006). More recent studies have challenged this view. Richardson and

Jackson (2007) used inverse modeling approaches to argue that pico- and nanoplankton can contribute to carbon export at rates proportional to their production, particularly in oligotrophic regions. Although this approach has been questioned by Landry et al. (2011), field studies by Brew et al. (2009), Lomas and Moran (2011) and Alonso-González et al. (2010) in the oligotrophic subtropics using organic biomarkers and degradation pigments estimate that smaller particles contribute as much as 50% of the measured POC export fluxes. Dunne et al. (1997) argued that in the Equatorial Pacific, the >53 μm ISP particles did not represent the sinking material that reached the ST. Grob et al. (2007) and Hung and Gong (2010) also suggested that the contribution of particles <50 μm to the settling flux could be larger than previously thought and, more recently, Hung et al. (2012) reported scanning electron microscopy images showing that the bulk of sinking particles contained mostly particles of such size. DNA analysis from trap material have further shown that small-sized eukaryotic taxa and cyanobacteria can contribute to the sinking particle flux below the euphotic zone (Amacher et al., 2013). Using gel traps Durkin et al. (2015) have also provided evidence of the importance of small particle sizes to carbon export flux in the upper mesopelagic waters. Signs of small particles sinking were also reported by Xu et al. (2011) who found the best agreement of POC/^{234}Th ratios with those in ST for intermediate-sized (10-50 μm) rather than larger (>50 μm) particles, suggesting that these smaller particles dominated the export flux. In that same study, the dominance of nanoplankton and pico-prymnesiophytes was proposed as the source of disagreement between POC/^{234}Th in large (>50 μm) ISP particles and ST particles.

Our results are consistent with the new paradigm that small particles play a significant role in particle settling fluxes, especially in oligotrophic regions. Based on HPLC analyses, the phytoplankton community was dominated by picophytoplankton, especially in the GC interior and entrance zone (GC4-1, in the upper 30 m, GC4-2, GC4-8 and GC4-9) (White et al., 2013), with picophytoplankton abundances decreasing and nanophytoplankton abundances increasing when exiting the gulf towards the northern stations. Higher abundances of microphytoplankton were found at all the stations between 30-50 m, especially at GC4-1 and GC4-12, where diatoms dominated (White et al., 2013). Particle size distribution (PSD) analysis (living and detrital particles) confirms these trends (Figure 5.4): PSD profiles showed a clear shift from small particles towards larger particles while moving out of GC and north along the ETNP transect.

A better agreement was found between measured fluxes derived using ST and ISP small particles ratios (Figure 5.6), due to their more similar elemental/^{234}Th ratios. To further explore the composition of the particulate samples, C and N isotopic composition (Table A.3.1) was examined. This data provides insight into particle sources and remineralization. For example, the δ^{13}C values

of particles can indicate terrestrial (>-24‰) versus marine sources (-22 to -10‰) (Peterson and Fry, 1987), when combined with particulate C/N ratios (marine ~ 6-7; terrestrial >20; Hedges et al., 1986). We found a significant difference between the $\delta^{13}C$ values of large ISP particles and ST particles (p <0.0001; n = 58), while there was no difference between $\delta^{13}C$ values in small ISP particles versus ST particles (p >0.5; n = 58). Lower PN concentrations and higher $\delta^{13}C$ values of larger ISP particles are consistent with enhanced degradation as well as zooplankton grazing and repackaging (Fry and Sherr, 1984) (e.g., fecal pellets). The reduced degradation signal observed in the smaller size class suggests that such particles settle through the water column and in to the ST in the form of large aggregates (Lomas and Moran, 2011).

Aggregation is enhanced by transparent exopolymers (TEP) which forms the mucus matrix of most marine snow (Engel et al., 2004; Passow, 2002; Verdugo et al., 2004). Guo et al. (2002) argued that small particles (<10 μm) may coagulate into the larger particle size class (10–53 μm) on time scales of <1 day. This rapid aggregation, and subsequent faster sinking, would also explain how small relatively undegraded particles reached the ST, leading to an increase in export flux efficiency in this region during the summer months. While marine snow aggregation dynamics remain enigmatic (Boyd and Trull, 2007), qualitative observations of the ST material suggests that, in our study area, small particle sinking is driven by aggregation into marine snow and through zooplankton-mediated packaging of small particles in fecal pellets, which are rarely captured by large particle ISP measurements using certain types of filter holders that are not designed specifically to retain these particles (Bishop et al., 2012; Gardner et al., 2003; Trent et al., 1978).

Data obtained at station GC4-2, which was sampled twice, 6 days apart, for particles also support our assertion that small particles are settling into the ST. During its second occupation, there was an increase in the PC/^{234}Th ratio in ST particles (5.5 to 8.6) and the maximum for PC/^{234}Th ratios of small ISP particles moved deeper in the water column, while the distribution of PC/^{234}Th ratio for large ISP particles remained unchanged. The PC/^{234}Th ratio from the ST material collected during the reoccupation (8.6) matched the ratio of the small particles collected with the ISP at 20 m during the first occupation (8.9). The settling speed for small particles derived using this observation is ~13 m d^{-1} (e.g., 80 m in 6 days), in agreement with the lower range of sinking velocities estimated earlier (see section 5.5.2.2). This "delay" was not observed in the PC/^{234}Th ratios of large particles: They were 6.4 and 8.6 at 20 m for GC4-2 and GC4-2b, respectively, agreeing with the ST ratios measured at each time point, and suggesting a much faster settling speed (in the upper range of the speeds estimated in section 5.5.2.2) for this particle size.

5.5.3 Particle fluxes and export efficiency

Within the GC, previous studies have shown that seasonal changes in phytoplankton community structure influence bSi and carbonate fluxes to depth, whereas PC and PN remain constant throughout the year (Lyons et al., 2011; Thunell, 1998). Typically, high bSi fluxes occur from late fall to early spring in response to upwelling-driven diatom blooms. Increasing stratification during the summer decreases primary production and carbonate becomes the main source of the biomineral sediment flux (Lyons et al., 2011; Thunell, 1998). Our results showed minimal PIC concentrations in the particulate samples collected (either by ISP or ST), likely due to the timing of our sampling. In agreement with Thunell (1998), we did not observe significant fluxes of bSi (Figure 5.6; Table 5.2), except at stations GC4-1 and GC4-12, the ones with highest NPP (Table 5.1) and where pigment analysis and microscopy observations provided evidence of a diatom-dominant phytoplankton community structure below 30 m and within the upper 60 m, respectively. In general, higher PC and PN fluxes occurred where picophytoplankton and diazotrophs were more abundant (GC4-2, GC4-8 and GC4-11) or where a diatom-dominated phytoplankton community was observed (GC4-1 and GC4-12).

To estimate the efficiency of export, we calculated *ThE* ratios by dividing the ^{234}Th-derived PC export fluxes at 100 m by NPP rates, as defined by Buesseler (1998) (Table 5.3). In those regions with efficient recycling (i.e., low PC flux below the depth of interest), *ThE* ratios should be relatively low (<10%). On the other hand, *ThE* ratios in excess of 10-50% are typically found not only during high production events, but when production and export are decoupled, such as in high-latitudes (Baumann et al., 2013; Buesseler, 1998; Buesseler et al., 2001; Schmidt et al., 2002; Thomalla et al., 2006). We further determined export efficiencies following that of Buesseler and Boyd (2009), where export efficiencies are calculated by normalizing PC fluxes to the depth of the Ez and at a reference depth 100 m below Ez (~200 m in this area) to allow for a comparison across regions with significantly different light penetration depths, where the major production of particles (that scavenge ^{234}Th) takes place. Thus, the normalized export efficiencies obtained are a combination of two terms: i) the export flux down to the base of the Ez relative to NPP and ii) the flux attenuation down to an "attenuation depth", 100 m below the Ez. The terms T_{100} and Ez-ratio presented in Table 5.3 refer to the PC flux at the attenuation depth divided by the PC flux at the Ez and the PC flux at the Ez divided by NPP, respectively. Therefore, T_{100} and Ez-ratio provide information regarding the importance of both processes responsible for the calculated export efficiencies, e.g. high export efficiencies could be due to efficient export down to the bottom of the

Ez (= high Ez-ratio values) or due to weak attenuation (= low T_{100} values or low "b" terms from equations 5.2 and 5.3) (Table 5.3).

All the estimates of *ThE* ratios, based on ST and WC fluxes, are presented in Table 5.3 and Figure 5.8, where similar trends between the different approaches can be observed. PC normalized export efficiencies are also presented in Table 5.3, to be consistent with the literature.

Table 5.3: Summary of export efficiencies.

Station	***ThE* ratios**				**Exp Eff 100 m below Ez**					
		100 m			SP			LP		
	ST	ST ratio	SP ratio	LP ratio	Ez-ratio[a]	T_{100}[b]	Eff[c]	Ez-ratio[a]	T_{100}[b]	Eff[c]
GC4-1	27%	20%	9%	6%	0.14	0.80	11%	0.07	1.34[d]	9%
GC4-2	79%	55%	31%	14%	0.49	0.54	27%	0.24	0.53	12%
GC4-2b	70%	92%	55%	24%	0.62	0.37	23%	0.11	0.55	11%
GC4-8	90%	72%	17%	8%	0.14	0.55	7%	0.07	0.40	3%
GC4-9	43%	25%	6%	4%	0.10	0.41	4%	0.09	0.45	4%
GC4-10	37%	11%	4%	3%	0.05	0.77	3%	0.03	0.63	2%
GC4-11	49%	59%	15%	9%	0.27	0.29	8%	0.09	0.84	7%
GC4-12	18%	20%	4%	3%	0.04	0.51	2%	0.03	0.23	1%

ThE ratios were calculated using the four approaches to estimate PC fluxes at 100 m (see Table 5.2). Export efficiencies 100 m below the Ez are also presented, together with Ez-ratio and T_{100} values.

[a] Ez-ratio = PC flux at Ez : NPP

[b] T_{100} = PC flux 100 m below Ez : POC flux at Ez

[c] Eff = Ez-ratio * T_{100}

[d] $T_{100} > 1$ due to high PC flux at attenuation depth as a consequence of an important ^{234}Th deficit below Ez and low PC/^{234}Th ratio at the attenuation depth.

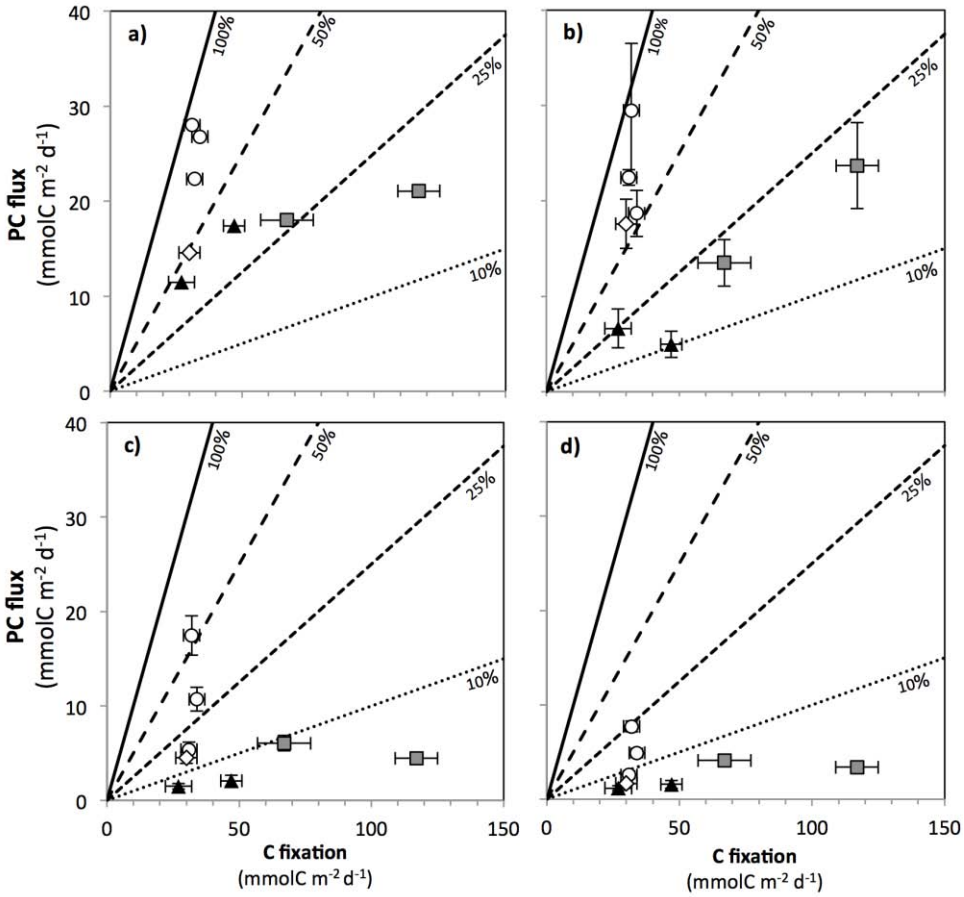

Figure 5.8: *ThE* ratios resulting from the various methods used to estimate PC fluxes. Symbols indicate high relative abundance of large diazotroph (open circles), small diazotroph (white diamonds), and diatoms (grey squares). Black triangles are stations were neither diatoms nor diazotrophs were abundant. Diagonal lines represent 10%, 25%, 50%, and 100% *ThE*. a) PC flux is directly obtained from ST, b) PC flux is derived from water column ^{234}Th fluxes and ST ratios, c) WC-derived ^{234}Th fluxes and small particle ratios, and d) WC-derived ^{234}Th fluxes and large particle ratios.

The results indicate that, at stations GC4-1 and GC4-12, where diatoms were the dominant phytoplankton and C fixation rates were highest, PC export efficiencies at 100 m were among the lowest measured, regardless of the approach used for derivation (less than 10% using ISP ratios and 18-27% when using ST ratios and fluxes; Table 5.3), similar to the results reported by Maiti et al. (2013) and Lam and Bishop (2007) in the Southern Ocean. In contrast, highest *ThE* ratios occurred at stations with higher abundances of picophytoplankton, GC4-2 and GC4-8, and where qPCR assays also revealed the highest specific planktonic nitrogenase gene (*nifH*) copies and gene expression recorded for large diazotrophs (*Trichodesmium* and *Richelia* symbioses) (White et al., 2013). *ThE* along the ETNP transect, where nanoplankton increased in relative abundance, were moderate to low (<40%, using ST material, and <5% using ISP ratios, excluding GC4-11). Station GC4-11 had higher *ThE* ratios (~50-60% using ST material, and 9-15% using ISP ratios) than GC4-10 and GC412, and was also the station with the highest abundance of *nifH* transcription by

unicellular diazotrophic cyanobacteria of the group A (UCYN-A) and where highest N_2 fixation rates were also observed (White et al., 2013).

White et al. (2013) reported absolute C fixation rates measured in the euphotic zone and the PC export efficiency recorded by ST in the study area during summer and winter months of 2005. Despite the differences in C fixation, export efficiencies in summer were equivalent or higher than winter records (average export efficiency of 34% and 18%, for summer and winter, respectively). The results presented here also show evidence of a high PC export efficiency during the summer of 2008. Therefore, our results support the hypothesis of more efficient particle export during the summer as a major reason for the lack of seasonality observed in carbon and nutrient fluxes in deep moored ST in the GC (Lyons et al., 2011; Thunell, 1998). The fact that most stations, with the exception of GC4-1 and GC4-12, were dominated by small phytoplankton further supports the supposition that pico- and nanophytoplankton and associated aggregation processes play an important role in driving PC fluxes in oligotrophic regions globally.

5.6 Conclusions

We used ^{234}Th as a tracer to estimate particle fluxes in a region where previous studies have suggested that particle export is more efficient during lower productivity summer months as a result of a change in food web dynamics, e.g. from larger to smaller plankton. PC and PN data were obtained from free-drifting surface-tethered sediment traps and large-volume *in situ* pumps in order to compare methodologies and to provide with more detailed profiles of elemental/^{234}Th ratios over the upper 500 m in two different particle size classes (1-53 μm and >53 μm). Large variability in values of PC and PN to ^{234}Th ratios was observed in the surface layer, with ratios for both size classes decreasing with depth. Although small particles had higher elemental to ^{234}Th ratios at the surface, attenuation rates were significantly higher for the smaller size class allowing both size class ratios to converge to 1 - 5 μmol·dpm^{-1} by 100 m. Elemental/^{234}Th ratios measured in sediment trap materials collected at 100 m tended to be higher than those measured at the same depth using *in situ* pumps, but agreed with *in situ* pumps ratios obtained from surface waters. This implies that sediment traps may have been more efficient in collecting rapidly sinking aggregated particles from surface waters that were less affected by decomposition processes. Elemental/^{234}Th ratios in small particles collected at 100 m were in better agreement with sediment trap ratios than those of large particles, suggesting a significant contribution of small particles to the export flux, even though small particle attenuation rates exceeded those of the larger size class. Particle size distribution measurements confirmed high abundances of small particles in the study area,

especially within the GC. Supporting elemental data includes the strong agreement between higher PN concentrations and lower $\delta^{13}C$ values in small particles with sediment trap material.

PC and PN fluxes were variable, but higher export fluxes did not always correspond to higher export efficiencies, reflecting the variability of the phytoplankton community structure observed across the region. Stations dominated by diatoms and with the highest C fixation measurements were among the lowest in export efficiency. In contrast, stations dominated by picophytoplankon had the highest export efficiencies. The presence of diazotrophs also favored enhanced export efficiency, although since observed N_2 fixation rates were highly variable, diazotrophic activity alone cannot explain the observed patterns of C export efficiency (White et al., 2013).

Combined, we argue that small phytoplankton are important contributors to particle export during the summer (oligotrophic period) in the GC and ETNP region. Comparison of our results with previous work suggests that faster attenuation rates in small particles with depth is a ubiquitous feature of the world's oligotrophic oceans when smaller phytoplankton taxa dominate the food web. In this study, despite the observed higher attenuation rates of small particles, stations dominated by small phytoplankton are characterized by more efficient export. As a result, export efficiencies are higher where smaller particles dominate the flux and may help to explain the apparent lack in correlation between PC export rates with NPP in oligotrophic regions (Burd et al., 2010).

Our results argue for the multiple particle size class sampling when using the ^{234}Th:^{238}U disequilibrium technique to determine export rates and the continued use of multiple methods to quantify PC export to depth. Such knowledge is critical for better predicting biological responses to large scale changes in climate that are already influencing the marine system. It will require a regional and ecosystem specific approach, with special attention paid to small plankton, which historically have been neglected as an efficient pathway for carbon export. Further work to understand the characteristics of material collected with sediment traps and *in situ* pumps over seasonal time-scales will provide much needed information regarding the mechanisms, origin and abundances of the particles that reach deeper layers, enhancing our understanding of particle dynamics in this region and other oligotrophic systems.

Chapter 6:

Conclusions and open questions

6 Conclusions and open questions

6.1 Conclusions

Oceanic particle cycling and export play major roles in the biogeochemical cycling of carbon and associated nutrients, as well as other chemical species. Particle fluxes in the open ocean are strongly linked to surface productivity, plankton community structure and food web dynamics, which are in turn shaped by environmental conditions such as ocean physics and other ecologically relevant parameters such as nutrient composition and supply. Understanding the magnitude and variability of this flux over temporal and spatial scales remains poorly understood (Britten and Primeau, 2016; Burd et al., 2010). As a consequence, estimates of the global biological pump strength are variable, ranging from ~ 5 GtC yr^{-1} (Henson et al., 2011) to 13 GtC yr^{-1} (Laws et al., 2011). The uncertainty in global-scale satellite-based models highlights the need for continuing *in situ* carbon export field sampling (Britten and Primeau, 2016; Siegel et al., 2016).

The main objective of this thesis was the application of ^{234}Th as a tracer for particle export in a variety of ocean regions in order to improve our understanding of the ocean's biological pump. The study areas encompass a wide variety of biogeochemical regimes and can be used to improve modeling efforts at larger scales.

The contributions of the three studies presented in this thesis (*Chapters 3-5*) are summarized below and future work and recommendations for improving the carbon export estimates are also discussed.

Chapter 3: **North Western Atlantic Ocean**

This study was part of the GEOTRACES program. This section allowed us to obtain information on particle export with high spatial coverage across a wide variety of biogeochemical regions. Higher export rates occurred in high latitude areas and negligible fluxes in the subtropical gyre, with the exception of those stations affected by the Amazon River plume and consistent with expectations and with previous studies. Interestingly, excess of ^{234}Th relative to ^{238}U was observed at depth at several stations in the oligotrophic domain, a feature also observed in previous studies for which there is no clear explanation yet (Owens et al., 2015; Thomalla et al., 2006).

In order to provide estimates of carbon export, the C/^{234}Th ratios in particles were extrapolated using a compilation of C/^{234}Th ratios from the North Atlantic. We also produced a power-law

regression curve that can be used to obtain carbon export fluxes at depth varying between 30 and 270 m. Our results were compared to previous studies as well as to satellite-based export models. While relatively good agreement was obtained in terms of patterns, large variability (up to >one order of magnitude) does exist in the magnitude of the export.

Our study, together with the study by Owens et al. (2015), contribute with a significant number of new measurements (more than a 50% increase compared to the North Altantic database compiled by Le Moigne et al., 2013) to the existing data set of C export in the Atlantic Ocean, and can be used not only to constrain carbon export estimations at an oceanic scale, but also to approach questions regarding export and remineralization rates related to trace elements in the North Atlantic Ocean. Additional data regarding community structure and particle composition would be highly valuable to determine the dominant species that drove the export.

Chapter 4: **Atlantic sector of the Southern Ocean**

Phytoplankton composition and distribution appear to be strongly linked to physical zonation within the Sourthern Ocean (Laubscher et al., 1993; Read et al., 2002), which in turn also affects zooplankton community composition, abundance, (Hunt and Hosie, 2005; Pakhomov and McQuaid, 1996; Pollard et al., 2002a) and grazing dynamics. In *Chapter 4* the influence of physical controls on biogeochemical zonation and, by extension, on downward flux of particulate organic carbon, was examined.

The sampled transect, from 44°S to 53°S, crossed three different fronts, the Sub-Antarctic Front (SAF), the Antarctic Polar Front (APF) and the Southern Polar Front (SPF) but export fluxes did not show similar zonation patterns. Rather, a clear N-S shift in planktonic community was observed and linked to the APF, with nanophytoplankton dominating the northern half of the transect, where primary production rates were lower and chaetognaths and euphasiids were the main grazers, and diatoms dominating south of the APF, with higher primary production rates and with high abundances of salps. These differences in planktonic community appear to have an impact on the depth variation of the C/^{234}Th ratios in sinking particles, leading to larger attenuation of particulate organic carbon and ^{234}Th fluxes and C/^{234}Th ratios with depth in the northern half of the transect, whereas low/negligible attenuation was observed at the southernmost stations As a consequence, although export efficiencies were relatively higher in the northern stations, the amount of exported carbon that reached depths of 400 m was higher in the southern stations.

These results, together with the high variability regarding C/^{234}Th ratios observed from a compilation of previous ^{234}Th studies conduted in the Southern Ocean, point to the need of a much careful examination of the links between plankton community and C/^{234}Th ratios, not just below the euphotic zone but also at greater depths, in order to constrain the strength and efficiency of the biological pump in this region. This information should also be included when applying satellite-based export models, some of which are strongly influenced by sea surface temperatures and satellite derived chlorophyll-a concentrations.

Chapter 5: **Gulf of California and Eastern Tropical North Pacific**

Seasonal stratification coupled with low oxygen in mid-waters of the Gulf of California and the adjacent Eastern Tropical North Pacific support an ecosystem that is is hypothesized to favor the growth of diazatroph organisms (Karl et al., 2002). Therefore, this region provided an excellent opportunity to study linkages between surface productivity and particulate export fluxes under oceanographic conditions similar to those expected in a future warmer ocean. In addition, since one of the critical assumptions behind using the ^{234}Th approach is the reliance on an element to ^{234}Th ratio needed to convert ^{234}Th fluxes into particulate elemental fluxes of interest, this chapter focused on understanding how and why the C/^{234}Th ratios obtained using sediment traps and *in situ* pumps differ and how the C/^{234}Th ratios vary with increasing water column depth and particle size. ^{234}Th-derived carbon export rates were further linked to the overlying food web and the physical regime.

The results suggest that sediment traps may have been more efficient collecting fast sinking particles that were relatively fresh and that small particles were important contributors to particle export during the summer (oligotrophic period). We also observed that higher export efficiencies occurred in picoplankton dominated surface waters, where relative concentrations of diazotrophs were also elevated. As a result, export efficiencies were found to be higher where smaller particles dominated the flux, which may help explain the apparent lack in correlation between particulate carbon export rates with net primary production in oligotrophic regions (Burd et al., 2010). This work adds to the increasing body of literature that suggests that particulate export in food webs dominated by larger phytoplankton may not be as efficient as in picoplankton and diazotroph dominated phytoplankton communities in oligotrophic areas.

This chapter further underscored the necessity of using multiple techniques to quantify particle flux given the intricacies and assumptions required in each technique. Additionally, multiple particle size class sampling when using the ^{234}Th:^{238}U disequilibrium technique is highly

recommended. The global compilation of remineralization rates linked to the plankton dominance presented in this study highlights the necessity of parameterizing particle attenuation when considering the major food webs rather than applying a unique global attenuation term in export models. A regional and ecosystem specific approach is critical for better predicting biological responses to large-scale changes in climate that are already influencing the marine system.

6.2 Open questions

Substantial effort has been devoted during the past few decades to improving our understanding, quantification and forecast capabilities in assessing the magnitude of changes observed in the Earth's climate system. A key component to evaluate these aspects is the global carbon cycle, in which the ocean's ecosystems play a critical role. Substantial improvements have been achieved on the quantification of the amount of particulate organic carbon being exported from the upper layers of the ocean to mesopelagic depths. Nevertheless, there are several pathways depending on ecological, biogeochemical and physical conditions, leading to different export efficiencies, and uncertainties still remain when trying to provide predictive understanding of how the ocean carbon cycle can be affected by a changing climate and the feedbacks between these various processes. Some of the open questions regarding the vertical export of particulate carbon in the ocean are summarized bellow, together with recommendations and potential lines of research involving the use of ^{234}Th as particlie tracer.

- *Links between the overlaying plankton community and the sinking particles:*

The structure of the plantonic community can lead to significant changes in the magnitude and composition of carbon export to depth. It is thus highly valuable to have biological information regarding the dominant groups of phytoplankton and the main grazers in the study area. Information about the particle composition, biominerals and lithogenic content is also necessary to better understand other mechanisms, such as the ballast effect, by which the particles may be exported to depth. Sampling different particle sizes to understand the role that each particle size is also critical as recent work argues that particulate export may be dominated by previously ignored small particles (<50 μm) or colloids (Dall'Olmo and Mork, 2014; Durkin et al., 2015; Puigcorbé et al., 2015; Richardson and Jackson, 2007).

- *Combined use of in situ pumps and sediment traps:*

The combined used of *in situ* pumps with sediment traps is highly recommended to counteract some of the limitations of both techniques. *In situ* pumps can be deployed at a higher temporal resolution, provide particle size fractionated samples, and multiple depth vertical profiles. On the other hand, sediment traps, and more specifically, the use of gel sediment traps, provide a technique for capturing particles that have actually sunk through the water column.

Similarly, the use of imaging technologies also presents a series of advantages, such as the capacity to observe the sinking particles (e.g., aggregates, single cells, fecal pellets) *in situ* and accurately estimate sinking velocities. There are still important limitations, especially in clear ocean waters, but effort is devoted to enable robust determination of optical properties (Boss et al., 2014) and, in future work, the use of this technology should be increasingly considered when evaluating the particulate export.

- *Particle flux attenuation:*

The Martin curve (Martin et al., 1987) has been commonly used to account for the attenuation of the particle flux with depth. Unfortunately, the number of studies providing with detailed vertical profiles to quantify such attenuation is scarce. As a consequence, biogeochemical models include such parameter in a generalized way, thus drawing unrealistical simple relationships between euphotic zone characteristics and the export reaching certain depths. Detailed examination of the variation of the export along the water column, linked to the characteristics of the overlaying plankton community, as well as the bacterial populations, in a wider variety of biogeochemical areas is necessary to incorporate this parameter into the biogeochemical models in a more realistic form.

Related to the attenuation of the particulate flux, the combined use of ^{234}Th and other tracers, such as barium, can provide additional information to constrain the estimates of remineralization (Planchon et al., 2013). Similarly, high vertical resolution of ^{234}Th shall allow a better resolution of deviations from equilibrium caused by remineralization processes, but also deviations from the equilibrium found at intermediate depths in several studies for which there is no clear explanation yet (Owens et al., 2015; Thomalla et al., 2006; *Chapter 3*).

- *Time-series:*

The seasonal and interannual variability of particle export can be substantial, but it is usually not systematically examined, neither spatially nor temporally. There is also variability related to episodic events that are not necessarily related to seasonality (i.e., dust events or eddies). The period time elapsed between biogeochemical changes and the effects on particle export also requires more attention to be locally accurate. Time-series studies can provide with essential information to understand the temporal variability of the particle flux, which is especially important under the current context of anthropogenic forcing of rapid climate change.

- *Th-234 as tracer for other elements and chemical species:*

The main application of the use of ^{234}Th as particle tracer has been the estimate of particulate organic carbon export fluxes. Nevertheless, this technique could be applied to derived the export fluxes of other elements (e.g., Fe, Cd or Co) that play a great an important role in phytoplankton growth and biological functioning, or particle reactive elements that can be used, for example, as tracers of eaolian inputs to the ocean (e.g., Al or Pb), or other chemical compounds, such as PCBs, that could have unintended impacts on human and environmental health (Dulaquais et al., 2014; Gustafsson et al., 1997a; Waples et al., 2006; Weinstein and Moran, 2005). The number of studies is still limited but plataforms such as GEOTRACES provide the perfect conditions to extend the use of this tracer beyond the evaluation of carbon export

- *Th-234 combined with other particle reactive radioisotopes:*

Although ^{234}Th is by large the most commonly used radioisotopes to evaluate particle export in the ocean, other tracers such as ^{210}Pb/^{210}Po, ^{228}Ra/^{228}Th and ^{90}Sr/^{90}Y have also been used to quantify particle removal from the surface layers (Cai et al., 2002; Cochran and Masqué, 2003; Orlandini et al., 2003). Combined, these tracers cover a large integration time scale, spanning from days to few years. There are still uncertainties related to these tracers that need to be assessed, since their use has not been that extensive. Nevertheless, some studies highlight the potential they present when used in combination, particularly the ^{234}Th:^{238}U and ^{210}Po:^{210}Pb pairs (Roca-Martí et al., 2016; Stewart et al., 2007; Verdeny et al., 2009), mainly due to their different integration time, thus increasing the scope of opportunities where ^{234}Th can be used.

References

References

Alldredge, A., 1998. The carbon, nitrogen and mass content of marine snow as a function of aggregate size. Deep Sea Res. Part I Oceanogr. Res. Pap. 45, 529–541. doi: 10.1016/S0967-0637(97)00048-4.

Alonso-González, I.J., Arístegui, J., Lee, C., Sanchez-Vidal, A., Calafat, A., Fabrés, J., Sangrá, P., Masqué, P., Hernández-Guerra, A., Benítez-Barrios, V., 2010. Role of slowly settling particles in the ocean carbon cycle. Geophys. Res. Lett. 37, L13608. doi:10.1029/2010GL043827.

Altabet, M.A., Pilskaln, C., Thunell, R., Pride, C., Sigman, D., Chavez, F., Francois, R., 1999. The nitrogen isotope biogeochemistry of sinking particles from the margin of the Eastern North Pacific. Deep Sea Res. I-Oceanographic Res. Pap. 46, 655–679. doi:10.1016/S0967-0637(98)00084-3.

Amacher, J., Neuer, S., Lomas, M., 2013. DNA-based molecular fingerprinting of eukaryotic protists and cyanobacteria contributing to sinking particle flux at the Bermuda Atlantic time-series study. Deep Sea Res. Part II Top. Stud. Oceanogr. 93, 71–83. doi:10.1016/j.dsr2.2013.01.001.

Antia, A., Koeve, W., Fischer, G., Blanz, T., Schulz-Bull, D., Scholten, J., Peinert, R., Neuer, S., Kremling, K., Kuss, J., 2001. Basin-wide particulate carbon flux in the Atlantic Ocean: Regional export patterns and potential for atmospheric CO_2 sequestration. Global Biogeochem. Cycles 15, 845–862. doi:10.1029/2000GB001376.

Antia, A.N., 2005. Solubilization of particles in sediment traps: revising the stoichiometry of mixed layer export. Biogeosciences 2, 189–204. doi:10.5194/bg-2-189-2005.

Antoine, D., André, J.-M., Morel, A., 1996. Oceanic primary production: 2. Estimation at global scale from satellite (Coastal Zone Color Scanner) chlorophyll. Global Biogeochem. Cycles 10, 57–69. doi:10.1029/95GB02832.

Antoine, D., Morel, A., 1996. Oceanic primary production: 1. Adaptation of a spectral light-photosynthesis model in view of application to satellite chlorophyll observations. Global Biogeochem. Cycles 10, 43–55. doi:10.1029/95GB02831.

Armstrong, R.A., Lee, C., Hedges, J.I., Honjo, S., Wakeham, S.G., 2002. A new, mechanistic model for organic carbon fluxes in the ocean based on the quantitative association of POC with ballast minerals. Deep Sea Res. Part II Top. Stud. Oceanogr. 49, 219–236. doi:10.1016/S0967-0645(01)00101-1.

Arrigo, K.R., van Dijken, G., Pabi, S., 2008. Impact of a shrinking Arctic ice cover on marine primary production. Geophys. Res. Lett. 35, L19603. doi:10.1029/2008GL035028.

Arrigo, K.R., Worthen, D., Schnell, A., Lizotte, M.P., 1998. Primary production in Southern Ocean waters. J. Geophys. Res. 103, 600,15515–15587.

Assmy, P., Smetacek, V., Montresor, M., Klaas, C., Henjes, J., Strass, V.H., Arrieta, J.M., Bathmann, U., Berg, G.M., Breitbarth, E., Cisewski, B., Friedrichs, L., Fuchs, N., Schüller, S.E., Steigenberger, S., Webb, A., Wolf-Gladrow, D., 2013. Thick-shelled, grazer-protected diatoms decouple ocean carbon and silicon cycles in the iron-limited Antarctic Circumpolar Current. Proc. Natl. Acad. Sci. 110, 20633–20638. doi:10.1073/pnas.1309345110.

Atkinson, A., Peck, J.M., 1990. The distribution of zooplankton in relation to the South Georgia shelf in summer and winter, in: Antarctic Ecosystems. Springer, pp. 159–165. doi:10.1029/JC087iC03p02045.

Aumont, O., Bopp, L., 2006. Globalizing results from ocean in situ iron fertilization studies. Global Biogeochem. Cycles 20, GB2017. doi:10.1029/2005GB002591.

Bacon, M.P., Anderson, R.F., 1982. Distribution of thorium isotopes between dissolved and particulate forms in the deep sea. J. Geophys. Res. 87, 2045–2056. doi:10.1029/JC087iC03p02045.

Bacon, M.P., Cochran, J.K., Hirschberg, D., Hammar, T.R., Fleer, A.P., 1996. Export flux of carbon at the equator during the EqPac time-series cruises estimated from ^{234}Th measurements. Deep Sea Res. Part II Top. Stud. Oceanogr. 43, 1133–1153. doi:10.1016/0967-0645(96)00016-1.

Bacon, M.P., Spencer, D.W., Brewer, P.G., 1976. ^{210}Pb/^{226}Ra and ^{210}Po/^{210}Pb disequilibria in seawater and suspended particulate matter. Earth Planet. Sci. Lett. 32, 277–296. doi: 10.1016/0012-821X(76)90068-6.

Badan-Dangon, A., Dorman, C.E., Merrifield, M.A., Winant, C.D., 1991. The lower atmosphere over the Gulf of California. J. Geophys. Res. Ocean. 96, 16877–16896. doi: 10.1029/91JC01433.

Barlow, R.G., Cummings, D.G., Gibb, S.W., 1997. Improved resolution of mono- and divinyl chlorophylls a and b and zeaxanthin and lutein in phytoplankton extracts using reverse phase C-8 HPLC. Mar. Ecol. Prog. Ser. 161, 303–307.

Baumann, M.S., Moran, S.B., Lomas, M.W., Kelly, R.P., Bell, D.W., 2013. Seasonal decoupling of particulate organic carbon export and net primary production in relation to sea- ice at the shelf break of the eastern Bering Sea: Implications for off- shelf carbon export. J. Geophys. Res. Ocean. 118, 1–19.

Beaugrand, G., Edwards, M., Brander, K., Luczak, C., Ibanez, F., 2008. Causes and projections of abrupt climate-driven ecosystem shifts in the North Atlantic. Ecol. Lett. 11, 1157–1168.

Behrenfeld, M.J., Boss, E., Siegel, D.A., Shea, D.M., 2005. Carbon-based ocean productivity and phytoplankton physiology from space. Global Biogeochem. Cycles 19, doi:10.1029/2004GB002299.

Behrenfeld, M.J., Falkowski, P.G., 1997. Photosynthetic rates derived from satellite-based chlorophyll concentration. Limnol. Oceanogr. 1–20.

Benitez-Nelson, C., Buesseler, K.O., Karl, D.M., Andrews, J., 2001a. A time-series study of particulate matter export in the North Pacific Subtropical Gyre based on 234Th: 238U disequilibrium. Deep Sea Res. Part I Oceanogr. Res. Pap. 48, 2595–2611.

Benitez-Nelson, C., Buesseler, K.O., Rutgers van der Loeff, M., Andrews, J., Ball, L., Crossin, G., Charette, M.A., 2001b. Testing a new small-volume technique for determining 234 Th in seawater. J. Radioanal. Nucl. Chem. 248, 795–799.

Benitez-Nelson, C.R., Bidigare, R.R., Dickey, T.D., Landry, M.R., Leonard, C.L., Brown, S.L., Nencioli, F., Rii, Y.M., Maiti, K., Becker, J.W., 2007. Mesoscale eddies drive increased silica export in the subtropical Pacific Ocean. Science. 316, 1017–1021.

Benitez-Nelson, C.R., Moore, W.S., 2006. Future applications of 234Th in aquatic ecosystems. Mar. Chem. 100, 163–165.

Bhat, S.G., Krishnaswamy, S., Lal, D., Moore, W.S., 1969. 234Th/238U ratios in the ocean. Earth Planet. Sci. Lett. 5, 483–491.

Bishop, J.K., 1992. POC from MULVFS casts, 25 September 2002 [WWW Document]. JGOFS Data Server, U.S. JGOFS Data Manag. Off. WHOI, Woods Hole, Mass. URL http://usjgofs.whoi.edu/jg/serv/jgofs/eqpac/ tt007/mulvfs_POC.html0 (accessed 2.6.15).

Bishop, J.K.B., 1999. Transmissometer measurement of POC. Deep Sea Res. Part I Oceanogr. Res. Pap. 46, 353–369.

Bishop, J.K.B., Calvert, S.E., Soon, M.Y.S., 1999. Spatial and temporal variability of {POC} in the northeast Subarctic Pacific. Deep Sea Res. Part II Top. Stud. Oceanogr. 46, 2699–2733. doi:10.1016/S0967-0645(99)00081-8.

Bishop, J.K.B., Collier, R.W., Kettens, D.R., Edmond, J.M., 1980. The chemistry, biology, and vertical flux of particulate matter from the upper 1500 m of the Panama Basin. Deep Sea Res. Part A. Oceanogr. Res. Pap. 27, 615–640. doi: 10.1016/0198-0149(80)90077-1.

Bishop, J.K.B., Edmond, J.M., Ketten, D.R., Bacon, M.P., Silker, W.B., 1977. The chemistry, biology, and vertical flux of particulate matter from the upper 400 m of the equatorial Atlantic Ocean. Deep Sea Res. 24, 511–548.

Bishop, J.K.B., Fleisher, M.Q., 1987. Particulate manganese dynamics in Gulf Stream warm-core rings and surrounding waters of the N.W. Atlantic. Geochim. Cosmochim. Acta 51, 2807–2825. doi: 10.1016/0016-7037(87)90160-8.

Bishop, J.K.B., Ketten, D.R., Edmond, J.M., 1978. The chemistry, biology and vertical flux of particulate matter from the upper 400 m of the Cape Basin in the southeast Atlantic Ocean. Deep Sea Res. 25, 1121–1161.

Bishop, J.K.B., Lam, P.J., Wood, T.J., 2012. Getting good particles: Accurate sampling of particles by large volume in-situ filtration. Limnol. Oceanogr. Methods 10, 681–710. doi:/10.4319/lom.2012.10.681.

Bishop, J.K.B., Stepien, J.C., Wiebe, P.H., 1986. Particulate matter distributions, chemistry and flux in the Panama Basin: response to environment forcing. Prog. Oceanogr. 17, 1–59. doi:http://dx.doi.org/10.1016/0079-6611(86)90024-8.

Bishop, J.K.B., Wood, T.J., 2008. Particulate matter chemistry and dynamics in the twilight zone at VERTIGO, ALOHA and K2 sites. Deep Sea Res. Part I Oceanogr. Res. Pap. 55, 1684–1706. doi:http://dx.doi.org/10.1016/j.dsr.2008.07.012.

Boden, T., Andres, B., Marland, G., 2016. Global CO_2 emissions from fossil-fuel burning, cement manufacture and gas flaring: 1751-2013. Carbon Dioxide Inf. Anal. Cent. http://cdiac.ornl.gov/trends/emis/tre_glob_2011.html.

Bopp, L., Aumont, O., Cadule, P., Alvain, S., Gehlen, M., 2005. Response of diatoms distribution to global warming and potential implications: A global model study. Geophys. Res. Lett. 32. doi:10.1029/2005GL023653.

Boss, E., Guidi, L., Richardson, M.J., Stemmann, L., Gardner, W., Bishop, J.K.B.B., Anderson, R.F., Sherrell, R.M., 2014. Optical techniques for remote and in-situ characterization of particles pertinent to GEOTRACES. Prog. Oceanogr. 133, 43–54. doi:10.1016/j.pocean.2014.09.007.

Boyd, P., Newton, P., 1995. Evidence of the potential influence of planktonic community structure on the interannual variability of particulate organic carbon flux. Deep Sea Res. Part I Oceanogr. Res. Pap. 42, 619–639. doi: 10.1016/0967-0637(95)00017-Z.

Boyd, P.W., Gall, M.P., Silver, M.W., Coale, S.L., Bidigare, R.R., Bishop, J.L.K.B., 2008. Quantifying the surface–subsurface biogeochemical coupling during the VERTIGO ALOHA and K2 studies. Deep Sea Res. Part II Top. Stud. Oceanogr. 55, 1578–1593. doi:10.1016/j.dsr2.2008.04.010.

Boyd, P.W., Jickells, T., Law, C.S., Blain, S., Boyle, E.A., Buesseler, K.O., Coale, K.H., Cullen, J.J., de Baar, H.J.W., Follows, M., et al., 2007. Mesoscale Iron Enrichment Experiments 1993-2005: Synthesis and Future Directions. Science, 315, 612–617. doi:10.1126/science.1131669.

Boyd, P.W., Newton, P.P., 1999. Does planktonic community structure determine downward particulate organic carbon flux in different oceanic provinces? Deep. Res. Part I 46, 63–91, doi: 10.1016/S0967-0637(98)00066-1.

Boyd, P.W., Trull, T.W., 2007. Understanding the export of biogenic particles in oceanic waters: Is there consensus? Prog. Oceanogr. 72, 276–312. doi:10.1016/j.pocean.2006.10.007

Brand, L.E., 1994. Physiological ecology of marine coccolithophores. Coccolithophores.Cambridge Univ. Press. Cambridge 39–49.

Brandes, J.A., Devol, A.H., Deutsch, C., 2007. New Developments in the Marine Nitrogen Cycle. Chem. Rev. 107, 577–589. doi:10.1021/cr050377t.

Bray, N.A., Robles, J.M., 1991. Physical oceanography of the Gulf of California. Gulf Penins. Prov. California, JP Dauphin BRT Simoneit Am. Assoc. Pet. Geol. Tulsa, Oklahoma 31, 1122–1131.

Brew, H.S., Moran, S.B., Lomas, M.W., Burd, A.B., 2009. Plankton community composition, organic carbon and thorium-234 particle size distributions, and particle export in the Sargasso Sea. J. Mar. Res. 67, 845–868.

Bricaud, A., Morel, A., Babin, M., Allali, K., Claustre, H., 1998. Variations of light absorption by suspended particles with chlorophyll a concentration in oceanic (case 1) waters: Analysis and implications for bio-optical models. J. Geophys. Res. Ocean. 103, 31033–31044.

Britten, G.L., Primeau, F.W., 2016. Biome-specific scaling of ocean productivity, temperature, and carbon export efficiency. Geophys. Res. Lett. doi:10.1002/2016GL068778.

Bruland, K.W., Lohan, M.C., 2003. 6.02 - Controls of Trace Metals in Seawater, in: Turekian, H.D.H.K. (Ed.), Treatise on Geochemistry. Pergamon, Oxford, pp. 23–47. doi:10.1016/B0-08-043751-6/06105-3.

Bruland, K.W., Silver, M.W., 1981. Sinking rates of fecal pellets from gelatinous zooplankton (Salps, Pteropods, Doliolids). Mar. Biol. 63, 295–300. doi:10.1007/BF00395999

Bryden, H.L., 1979. Poleward heat flux and conversion of available potential energy in Drake Passage. J. Mar. Res. 37, 1–22.

Buesseler, K., Ball, L., Andrews, J., Benitez-Nelson, C., Belastock, R., Chai, F., Chao, Y., 1998. Upper ocean export of particulate organic carbon in the Arabian Sea derived from thorium-234. Deep. Res. Part II 45, 2461–2487; doi:10.1016/S0967-0645(98)80022-2.

Buesseler, K.O., 1998. The decoupling of production and particulate export in the surface ocean. Global Biogeochem. Cycles 12, 297–310, doi: 10.1029/97GB03366.

Buesseler, K.O., 1991. Do upper-ocean sediment traps provide an accurate record of particle flux? Nature 353, 420–423.

Buesseler, K.O., Andrews, J.A., Hartman, M.C., Belastock, R., Chai, F., 1995. Regional estimates of the export flux of particulate organic carbon derived from thorium-234 during the JGOFS EqPac program. Deep Sea Res. Part II Top. Stud. Oceanogr. 42, 777–791.

Buesseler, K.O., Antia, A.N., Chen, M., Fowler, S.W., Gardner, W.D., Gustafsson, O., Harada, K., Michaels, A.F., Rutgers van der Loeff, M., Sarin, M., 2007a. An assessment of the use of sediment traps for estimating upper ocean particle fuxes. J. Mar. Res. 65, 345–416.

Buesseler, K.O., Bacon, M.P., Kirk Cochran, J., Livingston, H.D., 1992. Carbon and nitrogen export during the JGOFS North Atlantic Bloom Experiment estimated from ^{234}Th: ^{238}U disequilibria. Deep Sea Res. Part A.Oceanographic Res. Pap. 39, 1115–1137.

Buesseler, K.O., Ball, L., Andrews, J., Cochran, J.K., Hirschberg, D.J., Bacon, M.P., Fleer, A., Brzezinski, M., 2001. Upper ocean export of particulate organic carbon and biogenic silica in the Southern Ocean along 170°W. Deep Sea Res. Part II Top. Stud. Oceanogr. 48, 4275–4297.

Buesseler, K.O., Barber, R.T., Dickson, M.-L., Hiscock, M.R., Moore, J.K., Sambrotto, R., 2003. The effect of marginal ice-edge dynamics on production and export in the Southern Ocean along 170°W. Deep Sea Res. Part II Top. Stud. Oceanogr. 50, 579–603. doi:http://dx.doi.org/10.1016/S0967-0645(02)00585-4.

Buesseler, K.O., Benitez-Nelson, C.R., Moran, S.B., Burd, A., Charette, M., Cochran, J.K., Coppola, L., Fisher, N.S., Fowler, S.W., Gardner, W.D., 2006. An assessment of particulate organic carbon to thorium-234 ratios in the ocean and their impact on the application of ^{234}Th as a POC flux proxy. Mar. Chem. 100, 213–233.

Buesseler, K.O., Boyd, P.., 2009. Shedding light on processes that control particle export and flux attenuation in the twilight zone of the open ocean. Limnol. Oceanogr. 54, 1210–1232.

Buesseler, K.O., Lamborg, C., Cai, P., Escoube, R., Johnson, R., Pike, S., Masque, P., McGillicuddy, D., Verdeny, E., 2008. Particle fluxes associated with mesoscale eddies in the Sargasso Sea. Deep Sea Res. Part II Top. Stud. Oceanogr. 55, 1426–1444.

Buesseler, K.O., Lamborg, C.H., Boyd, P.W., Lam, P.J., Trull, T.W., Bidigare, R.R., Bishop, J.K.B., Casciotti, K.L., Dehairs, F., Elskens, M., 2007b. Revisiting carbon flux through the ocean's twilight zone. Science. 316, 567–570.

Buesseler, K.O., Michaels, A.F., Siegel, D.A., Knap, A.H., 1994. A three dimensional time-dependent approach to calibrating sediment trap fluxes. Global Biogeochem. Cycles 8, 179–193.

Buesseler, K.O., Steinberg, D.K., Michaels, A.F., Johnson, R.J., Andrews, J.E., Valdes, J.R., Price, J.F., 2000. A comparison of the quantity and composition of material caught in a neutrally buoyant versus surface-tethered sediment trap. Deep Sea Res. Part I Oceanogr. Res. Pap. 47, 277–294.

Burd, A.B., Hansell, D. a., Steinberg, D.K., Anderson, T.R., Arístegui, J., Baltar, F., Beaupré, S.R., Buesseler, K.O., DeHairs, F., Jackson, G. a., et al., 2010. Assessing the apparent imbalance between geochemical and biochemical indicators of meso- and bathypelagic biological activity: What the @$♯! is wrong with present calculations of carbon budgets? Deep Sea Res. Part II Top. Stud. Oceanogr. 57, 1557–1571. doi:10.1016/j.dsr2.2010.02.022.

Burd, A.B., Jackson, G.A., Moran, S.B., 2007. The role of the particle size spectrum in estimating POC fluxes from disequilibrium. Deep Sea Res. Part I Oceanogr. Res. Pap. 54, 897–918.

Cai, P., Dai, M., Chen, W., Tang, T., Zhou, K., 2006. On the importance of the decay of ^{234}Th in determining size-fractionated C/^{234}Th ratio on marine particles. Geophys. Res. Lett. 33, L23602. doi:10.1029/2006GL027792.

Cai, P., Huang, Y., Chen, M., Guo, L., Liu, G., Qiu, Y., 2002. New production based on ^{228}Ra-derived nutrient budgets and thorium-estimated POC export at the intercalibration station in the South China Sea. Deep Sea Res. Part I Oceanogr. Res. Pap. 49, 53–66. doi:http://dx.doi.org/10.1016/S0967-0637(01)00040-1.

Campbell, J.W., Aarup, T., 1992. New production in the North Atlantic derived from seasonal patterns of surface chlorophyll. Deep Sea Res. Part A. Oceanogr. Res. Pap. 39, 1669–1694. doi:http://dx.doi.org/10.1016/0198-0149(92)90023-M.

Carr, M.-E., Friedrichs, M.A.M., Schmeltz, M., Aita, M.N., Antoine, D., Arrigo, K.R., Asanuma, I., Aumont, O., Barber, R., Behrenfeld, et al., 2006. A comparison of global estimates of marine primary production from ocean color. Deep Sea Res. Part II Top. Stud. Oceanogr. 53, 741–770. doi:http://dx.doi.org/10.1016/j.dsr2.2006.01.028.

Casacuberta, N., Christl, M., Lachner, J., van der Loeff, M., Masque, P., Synal, H.-A., 2014. A first transect of ^{236}U in the North Atlantic Ocean. Geochim. Cosmochim. Acta 133, 34–46.

Cassar, N., Bender, M.L., Barnett, B.A., Fan, S., Moxim, W.J., Levy, H., Tilbrook, B., 2007. The Southern Ocean biological response to aeolian iron deposition. Science. 317, 1067.

Castro, C.G., Chavez, F.P., Collins, C.A., 2001. Role of the California Undercurrent in the export of denitrified waters from the eastern tropical North Pacific. Global Biogeochem. Cycles 15, 819–830.

Castro, R., Durazo, R., Mascarenhas, A., Collins, C.A., Trasviña, A., 2006. Thermohaline variability and geostrophic circulation in the southern portion of the Gulf of California. Deep Sea Res. Part I Oceanogr. Res. Pap. 53, 188–200.

Cavan, E.L., Le Moigne, F.A.C., Poulton, A.J., Tarling, G.A., Ward, P., Daniels, C.J., Fragoso, G., Sanders, R.J., 2015. Attenuation of particulate organic carbon flux in the Scotia Sea, Southern Ocean, is controlled by zooplankton fecal pellets. Geophys. Res. Lett. 42, 821–830. doi:10.1002/2014GL062744.

Cedhagen, T., Cheah, W., Bracher, A., Lejzerowicz, F., 2014. Algal pigments in Southern Ocean abyssal foraminiferans indicate pelagobenthic coupling. Deep Sea Res. Part II Top. Stud. Oceanogr. 108, 27–32. doi: 10.1016/j.dsr2.2014.07.017.

Cetinić, I., Perry, M.J., Briggs, N.T., Kallin, E., D'Asaro, E.A., Lee, C.M., 2012. Particulate organic carbon and inherent optical properties during 2008 North Atlantic Bloom Experiment. J. Geophys. Res. Ocean. 117, C06028. doi:10.1029/2011JC007771.

Charette, M.A., Moran, S.B., 1999. Rates of particle scavenging and particulate organic carbon export estimated using ^{234}Th as a tracer in the subtropical and equatorial Atlantic Ocean. Deep. Res. Part II 46, 885–906.

Cheah, W., Soppa Altenburg, M., Wiegmann, S., Ossebaar, S., Laglera, L.M., Strass, V., Santos-Echeandia, J., Hoppema, M., Wolf-Gladrow, D., Bracher, A., 2016. Importance of deep mixing and silicic acid in regulating phytoplankton biomass and community in the iron-limited Antarctic Polar Front region in summer. Deep Sea Res. Part II Top. Stud. Oceanogr. doi: 10.1016/j.dsr2.2016.05.019.

Chever, F., Bucciarelli, E., Sarthou, G., Speich, S., Arhan, M., Penven, P., Tagliabue, A., 2010. Physical speciation of iron in the Atlantic sector of the Southern Ocean along a transect from the subtropical domain to the Weddell Sea Gyre. J. Geophys. Res. Ocean. 115, C10050. doi:10.1029/2009JC005880.

Cisewski, B., Strass, V.H., Losch, M., Prandke, H., 2008. Mixed layer analysis of a mesoscale eddy in the Antarctic Polar Front Zone. J. Geophys. Res. Ocean. 113, C05017. doi:10.1029/2007JC004372.

Cisewski, B., Strass, V.H., Prandke, H., 2005. Upper-ocean vertical mixing in the Antarctic Polar Front Zone. Deep Sea Res. Part II Top. Stud. Oceanogr. 52, 1087–1108. doi:http://dx.doi.org/10.1016/j.dsr2.2005.01.010.

Cline, J.D., Richards, F.A., 1972. Oxygen deficient conditions and nitrate reduction in the eastern tropical North Pacific Ocean. Limnol. Oceanogr. 17, 885–900.

Coale, K.H., 1990. Labyrinth of doom: A device to minimize the“ swimmer” component in sediment trap collections. Limnol. Oceanogr. 35, 1376–1381. doi: 10.4319/lo.1990.35.6.1376.

Coale, K.H., Bruland, K.W., 1987. Oceanic stratified euphotic zone as elucidated by ^{234}Th: ^{238}U disequilibria. Limnol. Oceanogr. 32, 189–200.

Coale, K.H., Bruland, K.W., 1985. ^{234}Th:^{238}U disequilibria within the California Current. Limnol. Oceanogr. 30, 22–33. doi: 10.4319/lo.1985.30.1.0022

Coale, K.H., Johnson, K.S., Chavez, F.P., Buesseler, K.O., Barber, R.T., Brzezinski, M.A., Cochlan, W.P., Millero, F.J., Falkowski, P.G., Bauer, J.E.,et al., 2004. Southern Ocean Iron Enrichment Experiment: Carbon Cycling in High- and Low-Si Waters. Science. 304, 408–414. doi:10.1126/science.1089778.

Cochran, J.K., Buesseler, K.O., Bacon, M.P., Wang, H.W., Hirschberg, D.J., Ball, L., Andrews, J., Crossin, G., Fleer, A., 2000. Short-lived thorium isotopes (^{234}Th, ^{228}Th) as indicators of POC export and particle cycling in the Ross Sea, Southern Ocean. Deep Sea Res. Part II Top. Stud. Oceanogr. 47, 3451–3490.

Cochran, J.K., Feng, H., Amiel, D., Beck, A., 2006. Natural radionuclides as tracers of coastal biogeochemical processes. J. Geochemical Explor. 88, 376–379. doi: 10.1016/j.gexplo.2005.08.079.

Cochran, J.K., Masqué, P., 2003. Short-lived U/Th series radionuclides in the ocean: tracers for scavenging rates, export fluxes and particle dynamics. Rev. Mineral. Geochemistry 52, 461–492. doi: 10.2113/0520461.

Codispoti, L.A., Richards, F.A., 1976. An analysis of the horizontal regime of denitrification in the eastern tropical North Pacific. Limnol.Oceanogr 21, 379–388.

Comiso, J.C., Parkinson, C.L., Gersten, R., Stock, L., 2008. Accelerated decline in the Arctic sea ice cover. Geophys. Res. Lett. 35, L01703. doi:10.1029/2007GL031972.

Dall’Olmo, G., Mork, K.A., 2014. Carbon export by small particles in the Norwegian Sea. Geophys. Res. Lett. n/a–n/a. doi:10.1002/2014GL059244.

de Jong, J., Schoemann, V., Lannuzel, D., Croot, P., de Baar, H., Tison, J.-L., 2012. Natural iron fertilization of the Atlantic sector of the Southern Ocean by continental shelf sources of the Antarctic Peninsula. J. Geophys. Res. 117, G01029. doi:http://dx.doi.org/10.1029/2011JG001679.

Deacon, G.E.R., 1945. Water circulation and surface boundaries in the oceans. Q. J. R. Meteorol. Soc. 71, 11–25.

DeMaster, D.J., 1991. Measuring biogenic silica in marine sediments and suspended matter. Geophys. Monogr. Ser. 63, 363–367.

DeMaster, D.J., Kuehl, S.A., Nittrouer, C.A., 1986. Effects of suspended sediments on geochemical processes near the mouth of the Amazon River: examination of biological silica uptake and the fate of particle-reactive elements. Cont. Shelf Res. 6, 107–125. doi:http://dx.doi.org/10.1016/0278-4343(86)90056-7.

DeVries, T., Deutsch, C., 2014. Large-scale variations in the stoichiometry of marine organic matter respiration. Nat. Geosci. 7, 890–894.

Djogic, R., Sipos, L., Branica, M., 1986. Characterization of uranium (VI) in seawater. Limnol. Oceanogr. 31, 1122–1131.

Doney, S.C., 2006. Plankton in a warmer world. Nature 444, 695–696.

Doney, S.C., 1999. Major challenges confronting marine biogeochemical modeling. Global Biogeochem. Cycles 13, 705–714. doi:10.1029/1999GB900039.

Doney, S.C., Lindsay, K., Caldeira, K., Campin, J.-M., Drange, H., Dutay, J.-C., Follows, M., Gao, Y., Gnanadesikan, A., Gruber, et al., 2004. Evaluating global ocean carbon models: The importance of realistic physics. Global Biogeochem. Cycles 18, GB3017. doi:10.1029/2003GB002150.

Doney, S.C., Ruckelshaus, M., Duffy, J.E., Barry, J.P., Chan, F., English, C.A., Galindo, H.M., Grebmeier, J.M., Hollowed, A.B., Knowlton, N., 2012. Climate change impacts on marine ecosystems. Mar. Sci. 4, 11–37.

Dore, J.E., Brum, J.R., Tupas, L.M., Karl, D.M., 2002. Seasonal and interannual variability in sources of nitrogen supporting export in the oligotrophic subtropical North Pacific Ocean. Limnol. Oceanogr. 47, 1595–1607.

Ducklow, H.W., Steinberg, D.K., Buesseler, K.O., 2001. Upper ocean carbon export and the biological pump. Oceanogr. DC-OCEANOGRAPHY Soc. 14, 50–58.

Dugdale, R.C., Goering, J.J., 1967. Uptake of new and regenerated forms of nitrogen in primary productivity. Limnol. Ocean. 12, 196–206.

Dulaquais, G., Boye, M., Middag, R., Owens, S., Puigcorbé, V., Buesseler, K., Masqué, P., de Baar, H., Carton, X., 2014. Contrasting biogeochemical cycles of cobalt in the surface Western Atlantic Ocean. Global Biogeochem. Cycles 2014GB004903. doi:10.1002/2014GB004903.

Dunne, J.P., Armstrong, R.A., Gnanadesikan, A., Sarmiento, J.L., 2005. Empirical and mechanistic models for the particle export ratio. Global Biogeochem. Cycles 19, GB4026. doi:10.1029/2004GB002390.

Dunne, J.P., Murray, J.W., Aufdenkampe, A.K., Blain, S., Rodier, M., 1999. Silicon-nitrogen coupling in the equatorial Pacific upwelling zone. Global Biogeochem. Cycles 13, 715–726. doi:10.1029/1999GB900031.

Dunne, J.P., Murray, J.W., Rodier, M., Hansell, D.A., 2000. Export flux in the western and central equatorial Pacific: zonal and temporal variability. Deep Sea Res. Part I Oceanogr. Res. Pap. 47, 901–936.

Dunne, J.P., Murray, J.W., Young, J., Balistrieri, L.S., Bishop, J., 1997. ^{234}Th and particle cycling in the central equatorial Pacific. Deep Sea Res. Part II Top. Stud. Oceanogr. 44, 2049–2083.

Dunne, J.P., Sarmiento, J.L., Gnanadesikan, A., 2007. A synthesis of global particle export from the surface ocean and cycling through the ocean interior and on the seafloor. Glob. Biogeochem.Cycles 21. doi:10.1029/2006GB002907.

Durkin, C.A., Estapa, M.L., Buesseler, K.O., 2015. Observations of carbon export by small sinking particles in the upper mesopelagic. Mar. Chem. 175, 72–81. doi:10.1016/j.marchem.2015.02.011.

Duteil, O., Oschlies, A., 2011. Sensitivity of simulated extent and future evolution of marine suboxia to mixing intensity. Geophys. Res. Lett. 38, L06607.

Ebersbach, F., Trull, T.W., 2008. Sinking particle properties from polyacrylamide gels during the KErguelen Ocean and Plateau compared Study (KEOPS): zooplankton control of carbon export in an area of persistent natural iron inputs in the Southern Ocean. Limnol. Oceanogr. 53, 212–224.

Ebersbach, F., Trull, T.W., Davies, D.M., Bray, S.G., 2011. Controls on mesopelagic particle fluxes in the Sub-Antarctic and Polar Frontal Zones in the Southern Ocean south of Australia in summer—Perspectives from free-drifting sediment traps. Deep Sea Res. Part II Top. Stud. Oceanogr. 58, 2260–2276. doi:http://dx.doi.org/10.1016/j.dsr2.2011.05.025.

Engel, A., Thoms, S., Riebesell, U., Rochelle-Newall, E., Zondervan, I., 2004. Polysaccharide aggregation as a potential sink of marine dissolved organic carbon. Nature 428, 929–932.

Eppley, R.W., 1989. New production: history, methods, and problems, in: Berger, W.H., Smetacek, V.S., Wefer, G. (Eds.), Productivity of the Ocean: Present and Past. John Wiley & Sons, New York, pp. 85–97.

Eppley, R.W., Peterson, B.J., 1979. Particulate organic matter flux and planktonic new production in the deep ocean. Nature 282, 677–680.

Estapa, M.L., Boss, E., Mayer, L.M., Roesler, C.S., 2012. Role of iron and organic carbon in mass-specific light absorption by particulate matter from Louisiana coastal waters. Limnol. Oceanogr. 57, 97–112. doi:10.4319/lo.2012.57.1.0097.

Falkowski, P.G., Barber, R.T., Smetacek, V., 1998. Biogeochemical controls and feedbacks on ocean primary production. Science. 281, 200–206.

Feely, R.A., Sabine, C.L., Lee, K., Berelson, W., Kleypas, J., Fabry, V.J., Millero, F.J., 2004. Impact of anthropogenic CO_2 on the $CaCO_3$ system in the oceans. Science. 305, 362–366.

Feely, R.A., Sabine, C.L., Takahashi, T., Wanninkhof, R., 2001. Uptake and storage of carbon dioxide in the ocean: the global CO_2 survey. Oceanography 14, 18–32. doi:10.5670/oceanog.2001.03.

Fischer, G., 1991. Stable carbon isotope ratios of plankton carbon and sinking organic matter from the Atlantic sector of the Southern Ocean. Mar. Chem. 35, 581–596. doi:http://dx.doi.org/10.1016/S0304-4203(09)90044-5.

Francois, R., Honjo, S., Krishfield, R., Manganini, S., 2002. Factors controlling the flux of organic carbon to the bathypelagic zone of the ocean. Global Biogeochem. Cycles 16, 1087. doi:10.1029/2001GB001722.

Frey, K.E., Comiso, J.C., Cooper, L.W., Gradinger, R.R., Grebmeier, J.M., Saitoh, S.-I., Tremblay, J.-É., 2014. Arctic Ocean Primary Productivity [in Arctic Report Card 2014], Arctic Report Card 2014.

Friedlingstein, P., Houghton, R.A., Marland, G., Hackler, J., Boden, T.A., Conway, T.J., Canadell, J.G., Raupach, M.R., Ciais, P., Le Quere, C., 2010. Update on CO_2 emissions. Nat. Geosci. 3, 811–812.

Friedrich, J., Rutgers van der Loeff, M., 2002. A two-tracer (^{210}Po-^{234}Th) approach to distinguish organic carbon and biogenic silica export flux in the Antarctic Circumpolar Current. Deep Sea Res. Part I Oceanogr. Res. Pap. 49, 101–120.

Frost, B.W., 1984. Utilization of phytoplankton production in the surface layer, in: Global Ocean Flux Study: Proceedings of a Workshop, September 10-14, 1984. National Academy Press, Washington, D.C., Woods Hole, Massachusetts, pp. 125–135.

Fry, B., Sherr, E.B., 1984. delta ^{13}C measurements as indicators of carbon flow in marine and freshwater ecosystems. Contrib. Mar. Sci. 27, 13–47.

Galbraith, E.D., Dunne, J.P., Gnanadesikan, A., Slater, R.D., Sarmiento, J.L., Dufour, C.O., Souza, G.F. de, Bianchi, D., Claret, M., Rodgers, K.B., Marvasti, S.S., 2015. Complex functionality with minimal computation: Promise and pitfalls of reduced- tracer ocean biogeochemistry models. J. Adv. Model. Earth Syst. 7, 2012–2028. doi:10.1002/2015MS000463.

Gardner, W.D., 2000. Sediment trap sampling in surface waters. Cambridge University Press, Cambridge.

Gardner, W.D., 1980. Sediment trap dynamics and calibration: a laboratory evaluation. J. Mar. Res. 38, 17–39.

Gardner, W.D., Mishonov, A. V, Richardson, M.J., 2006. Global POC concentrations from in-situ and satellite data. Deep Sea Res. Part II Top. Stud. Oceanogr. 53, 718–740.

Gardner, W.D., Richardson, M.J., Carlson, C.A., Hansell, D., Mishonov, A. V, 2003. Determining true particulate organic carbon: bottles, pumps and methodologies. Deep Sea Res. Part II Top. Stud. Oceanogr. 50, 655–674.

Geibert, W., Rutgers van der Loeff, M.M., Usbeck, R., Gersonde, R., Kuhn, G., Seeberg-Elverfeldt, J., 2005. Quantifying the opal belt in the Atlantic and southeast Pacific sector of the Southern Ocean by means of ^{230}Th normalization. Global Biogeochem. Cycles 19, GB4001. doi:10.1029/2005GB002465.

Gerringa, L.J.A., 2010. Geotraces West Atlantic leg 1. Cruise report 64PE319 on RV Pelagia.

GlobColour, 2015. GlobColour User Guide; REF GC-UM_ACR-PUG-01. Version 3.1 [WWW Document]. URL http://www.globcolour.info/CDR_Docs/GlobCOLOUR_PUG.pdf (accessed 2.13.15).

Gnanadesikan, A., Dunne, J.P., John, J., 2012. Understanding why the volume of suboxic waters does not increase over centuries of global warming in an Earth System Model. Biogeosciences 9, 1159–1172.

Gordon, A.L., 1971. Oceanography of Antarctic waters. Wiley Online Library.

Gordon, A.L., Taylor, H.W., Georgi, D.T., 1977. Antarctic oceanographic zonation, in: Proceedings of SCOR/SCAR Polar Oceans Conference. Arctic Institute of North America, Montreal, Canada.

Gordon, D.C., 1971. Distribution of particulate organic carbon and nitrogen at an oceanic station in the central Pacific, in: Deep Sea Research and Oceanographic Abstracts. pp. 1127–1134.

Gordon, H.R., Wang, M., 1994. Retrieval of water-leaving radiance and aerosol optical thickness over the oceans with SeaWiFS: a preliminary algorithm. Appl. Opt. 33, 443–452. doi:10.1364/AO.33.000443.

Grasshoff, K., Ehrhardt, M., Kremling, K., 1983. Methods of Seawater Analysis, 2nd ed. Verlag Chemie GmbH, Weinheim.

Graziano, L.M., Geider, R.J., Li, W.K.W., Olaizola, M., 1996. Nitrogen limitation of North Atlantic phytoplankton: Analysis of physiological condition in nutrient enrichment experiments. Aquat. Microb. Ecol. 11, 53–64.

Grob, C., Ulloa, O., Claustre, H., Huot, Y., Alarcon, G., Marie, D., others, 2007. Contribution of picoplankton to the total particulate organic carbon concentration in the eastern South Pacific. Biogeosciences 4, 837–852.

Gruber, N., Gloor, M., Fletcher, S.E.M., Doney, S.C., Dutkiewicz, S., Follows, M.J., Gerber, M., Jacobson, A.R., Joos, F., Lindsay, K., 2009. Oceanic sources, sinks, and transport of atmospheric CO_2. Global Biogeochem. Cycles 23, GB1005. doi:10.1029/2008GB003349.

Guay, C.K.H., Bishop, J.K.B., 2002. A rapid birefringence method for measuring suspended $CaCO_3$ concentrations in seawater. Deep Sea Res. Part I Oceanogr. Res. Pap. 49, 197–210.

Guidi, L., Jackson, G.A., Stemmann, L., Miquel, J.C., Picheral, M., Gorsky, G., 2008. Relationship between particle size distribution and flux in the mesopelagic zone. Deep Sea Res. Part I Oceanogr. Res. Pap. 55, 1364–1374.

Guo, L., Hung, C.C., Santschi, P.H., Walsh, I.D., 2002. ^{234}Th scavenging and its relationship to acid polysaccharide abundance in the Gulf of Mexico. Mar. Chem. 78, 103–119.

Gustafsson, Ö., Andersson, P., Roos, P., Kukulska, Z., Broman, D., Larsson, U., Hajdu, S., Ingri, J., 2004. Evaluation of the collection efficiency of upper ocean sub-photic-layer sediment traps: a 24-month in situ calibration in the open Baltic Sea using ^{234}Th. Limnol.Oceanogr.Methods 2, 62–74.

Gustafsson, Ö., Gschwend, P.M., Buesseler, K.O., 1997a. Settling removal rates of PCBs into the northwestern Atlantic derived from ^{238}U-^{234}Th disequilibria. Environ. Sci. Technol. 31, 3544–3550.

Gustafsson, Ö., Gschwend, P.M., Buesseler, K.O., 1997b. Using ^{234}Th disequilibria to estimate the vertical removal rates of polycyclic aromatic hydrocarbons from the surface ocean. Mar. Chem. 57, 11–23. doi:http://dx.doi.org/10.1016/S0304-4203(97)00011-X.

Gustafsson, Ö., Larsson, J., Andersson, P., Ingri, J., 2006. The POC/234Th ratio of settling particles isolated using split flow-thin cell fractionation (SPLITT). Mar. Chem. 100, 314–322.

Hansell, D.A., 2013. Recalcitrant dissolved organic carbon fractions. Mar. Sci. 5, 421–445. doi:10.1146/annurev-marine-120710-100757.

Hansell, D.A., Carlson, C.A., Schlitzer, R., 2012. Net removal of major marine dissolved organic carbon fractions in the subsurface ocean. Global Biogeochem. Cycles 26, GB1016. doi:10.1029/2011GB004069.

Hargrave, B.T., Burns, N.M., 1979. Assessment of sediment trap collection efficiency. Limnol. Oceanogr. 24, 1124–1135.

Hays, G.C., Richardson, A.J., Robinson, C., 2005. Climate change and marine plankton. Trends Ecol. Evol. 20, 337–344.

Heath, R.A., 1976. Models of the diffusive–advective balance at the subtropical convergence. Deep Sea Res. Oceanogr. Abstr. 23, 1153–1164. doi:http://dx.doi.org/10.1016/0011-7471(76)90891-3.

Hedges, J.I., Clark, W.A., Quay, P.D., Richey, J.E., Devol, A.H., Santos, U. de M., others, 1986. Compositions and fluxes of particulate organic material in the Amazon River. Limnol. Oceanogr. 31, 717–738.

Henson, S.A., Dunne, J.P., Sarmiento, J.L., 2009. Decadal variability in North Atlantic phytoplankton blooms. J. Geophys. Res. Ocean. 114. doi:10.1029/2008JC005139.

Henson, S.A., Painter, S.C., Penny Holliday, N., Stinchcombe, M.C., Giering, S.L.C., 2013. Unusual subpolar North Atlantic phytoplankton bloom in 2010: Volcanic fertilization or North Atlantic Oscillation? J. Geophys. Res. Ocean. 118, 4771–4780. doi:10.1002/jgrc.20363.

Henson, S.A., Sanders, R., Holeton, C., Allen, J.T., 2006. Timing of nutrient depletion, diatom dominance and a lower-boundary estimate of export production for Irminger Basin, North Atlantic. Mar. Ecol. Prog. Ser. 313, 73–84.

Henson, S.A., Sanders, R., Madsen, E., Morris, P.J., Le Moigne, F., Quartly, G.D., 2011. A reduced estimate of the strength of the ocean's biological carbon pump. Geophys. Res. Lett. 38, L04606. doi:10.1029/2011GL046735.

Hibbert, A., Leach, H., Strass, V., Cisewski, B., 2009. Mixing in cyclonic eddies in the Antarctic Circumpolar Current. J. Mar. Res. 67, 1–23.

Honjo, S., 1996. Fluxes of particles to the interior of the open oceans. SCOPE-SCIENTIFIC Comm. Probl. Environ. Int. Counc. Sci. UNIONS 57, 91–154.

Honjo, S., Doherty, K.W., Agrawal, Y.C., Asper, V.L., 1984. Direct optical assessment of large amorphous aggregates (marine snow) in the deep ocean. Deep Sea Res. Part A. Oceanogr. Res. Pap. 31, 67–76. doi:http://dx.doi.org/10.1016/0198-0149(84)90073-6.

Honjo, S., Eglinton, T.I., Taylor, C.D., Ulmer, K.M., Sievert, S.M., Bracher, A., German, C.R., Edgcomb, V., Francois, R., Inglesias-Rodriguez, M.D., others, 2014. Understanding the role of the Biological Pump in the Global Carbon Cycle: An imperative for Ocean Science. Oceanography 27, 10–16. doi:10.5670/oceanog.2014.78.

Honjo, S., Manganini, S.J., 1993. Annual biogenic particle fluxes to the interior of the North Atlantic Ocean; studied at 34°N 21°W and 48°N 21°W. Deep Sea Res. Part II Top. Stud. Oceanogr. 40, 587–607. doi:http://dx.doi.org/10.1016/0967-0645(93)90034-K.

Honjo, S., Manganini, S.J., Cole, J.J., 1982. Sedimentation of biogenic matter in the deep ocean. Deep Sea Res. Part A. Oceanogr. Res. Pap. 29, 609–625. doi:http://dx.doi.org/10.1016/0198-0149(82)90079-6.

Honjo, S., Manganini, S.J., Krishfield, R.A., Francois, R., 2008. Particulate organic carbon fluxes to the ocean interior and factors controlling the biological pump: A synthesis of global sediment trap programs since 1983. Prog. Oceanogr. 76, 217–285. doi:10.1016/j.pocean.2007.11.003.

Hoppe, C.J.M., Klaas, C., Ossebaar, S., Soppa Altenburg, M., Cheah, W., Laglera, L.M., Santos-Echeandia, J., Rost, B., Wolf-Gladrow, D.A., Bracher, A., Hoppema, M., Strass, V., Trimborn, S., 2016. Controls of primary production in two phytoplankton blooms in the Antarctic Circumpolar Current. Deep Sea Res. Part II Top. Stud. Oceanogr. doi:10.1016/j.dsr2.2015.10.005.

Hoppema, M., de Baar, H.J.W., Bellerby, R.G.J., Fahrbach, E., Bakker, K., 2002. Annual export production in the interior Weddell Gyre estimated from a chemical mass balance of nutrients. Deep Sea Res. Part II Top. Stud. Oceanogr. 49, 1675–1689.

Hoppema, M., Fahrbach, E., de Baar, H.J.W., 2000. Surface layer balance of the southern Antarctic Circumpolar Current (prime meridian) used to derive carbon and silicate consumptions and annual air-sea exchange for CO_2 and oxygen. J. Geophys. Res. Ocean. 105, 11359–11371.

Houghton, R.A., 2008. Carbon Flux to the Atmosphere from Land-Use Changes: 1850-2005. In TRENDS: A Compendium of Data on Global Change. Oak Ridge, Tenn., U.S.A.

Houghton, R.A., House, J.I., Pongratz, J., van der Werf, G.R., DeFries, R.S., Hansen, M.C., Le Quéré, C., Ramankutty, N., 2012. Carbon emissions from land use and land-cover change. Biogeosciences 9, 5125–5142. doi:10.5194/bg-9-5125-2012.

Hung, C.-C., Gong, G.-C., 2007. Export flux of POC in the main stream of the Kuroshio. Geophys. Res. Lett. 34, L18606. doi:10.1029/2007GL030236.

Hung, C.C., Gong, G.C., 2010. POC/^{234}Th ratios in particles collected in sediment traps in the northern South China Sea. Estuar. Coast. Shelf Sci. 88, 303–310.

Hung, C.C., Gong, G.C., Santschi, P.H., 2012. ^{234}Th in different size classes of sediment trap collected particles from the Northwestern Pacific Ocean. Geochim. Cosmochim. Acta 91, 60–74.

Hung, C.C., Guo, L., Roberts, K.A., Santschi, P.H., 2004. Upper ocean carbon flux determined by the 234Th approach and sediment traps using size-fractionated POC and ^{234}Th data from the Gulf of Mexico. Geochem. J. 38, 601–611.

Hung, C.C., Xu, C., Santschi, P.H., Zhang, S.J., Schwehr, K.A., Quigg, A., Guo, L., Gong, G.C., Pinckney, J.L., Long, R.A., 2010. Comparative evaluation of sediment trap and ^{234}Th-derived POC fluxes from the upper oligotrophic waters of the Gulf of Mexico and the subtropical northwestern Pacific Ocean. Mar. Chem. 121, 132–144.

Hunt, B.P. V, Hosie, G.W., 2005. Zonal structure of zooplankton communities in the Southern Ocean South of Australia: results from a 2150 km continuous plankton recorder transect. Deep Sea Res. Part I Oceanogr. Res. Pap. 52, 1241–1271. doi:http://dx.doi.org/10.1016/j.dsr.2004.11.019.

Hutchins, D.A., Fu, F.-X., Zhang, Y., Warner, M.E., Feng, Y., Portune, K., Bernhardt, P.W., Mulholland, M.R., 2007. CO_2 control of Trichodesmium N_2 fixation, photosynthesis, growth rates, and elemental ratios: Implications for past, present, and future ocean biogeochemistry. Limnol. Oceanogr. 52, 1293–1304. doi:10.4319/lo.2007.52.4.1293.

IAEA, 1985. Sediment Kd's and concentration factors for radionuclides in the marine enviroment. Technical Reports Series 247. Vienna, Austria.

IOCCG, 2010. Atmospheric Correction for Remotely-Sensed Ocean-Colour Products. Wang M. (ed.), Reports of the International Ocean-Colour Coordinating Group, No 10. IOCCG, Dartmouth, Canada.

IPCC, 2014. Climate Change 2014: Impacts, Adaptation, and Vulnerability. Part A: Global and Sectoral Aspects. Contribution of Working Group II to the Fifth Assessment Report of the Intergovernmental Panel on Climate Change. Cambridge University Press, Cambridge, United Kingdom and New York, NY, USA.

IPCC, 2013. IPCC, 2013: Climate Change 2013: The Physical Science Basis. Contribution of Working Group I to the Fifth Assessment Report of the Intergovernmental Panel on Climate Change. Cambridge University Press, Cambridge, Cambridge, United Kingdom and New York, NY, USA.

IPCC, 2007. Cambio climático 2007: Informe de síntesis. Contribución de los Grupos de trabajo I, II y III al Cuarto Informe de evaluación del Grupo Intergubernamental de Expertos sobre el Cambio Climático. Grupo Intergubernamental de Expertos sobre el Cambio Climático, Ginebra, Suiza.

IPCC, 2001. Climate Change 2001: The Scientific Basis is the most comprehensive and up-to-date scientific assessment of past, present and future climate change. Intergovernmental Panel on Climate Change, Cambridge University Press, Cambridge, United Kingdom and New York, NY, USA.

Iversen, M.H., Pakhomov, E.A., Hunt, B.P. V, Jagt, H. v, Wolf-Gladrow, D., Klaas, C., 2016. Sinkers or floaters? Contribution from salp pellets to the export flux during a large bloom event in the Southern Ocean. Deep Sea Res. Part II Top. Stud. Oceanogr.

Izquierdo, R., Benítez-Nelson, C.R., Masqué, P., Castillo, S., Alastuey, A., Àvila, A., 2012. Atmospheric phosphorus deposition in a near-coastal rural site in the NE Iberian Peninsula and its role in marine productivity. Atmos. Environ. 49, 361–370. doi:10.1016/j.atmosenv.2011.11.007.

Jacquet, S.H.M., Lam, P.J., Trull, T.W., Dehairs, F., 2011. Carbon export production in the subantarctic zone and polar front zone south of Tasmania. Deep Sea Res. Part II Top. Stud. Oceanogr. 58, 2277–2292. doi:/10.1016/j.dsr2.2011.05.035.

Jenkins, W.J., Wallace, D.W.R., 1992. Tracer based inferences of new primary production in the sea, in: Primary Productivity and Biogeochemical Cycles in the Sea. Springer, pp. 299–316. doi:10.1007/978-1-4899-0762-2_17.

Johnson, R., Strutton, P.G., Wright, S.W., McMinn, A., Meiners, K.M., 2013. Three improved satellite chlorophyll algorithms for the Southern Ocean. J. Geophys. Res. Ocean. 118, 3694–3703. doi:10.1002/jgrc.20270.

Joos, F., Plattner, G.-K., Stocker, T.F., Marchal, O., Schmittner, A., 1999. Global Warming and Marine Carbon Cycle Feedbacks on Future Atmospheric CO_2. Science. 284, 464–467. doi:10.1126/science.284.5413.464.

Joos, F., Spahni, R., 2008. Rates of change in natural and anthropogenic radiative forcing over the past 20,000 years. Proc. Natl. Acad. Sci. 105 , 1425–1430. doi:10.1073/pnas.0707386105

Karl, D., Michaels, A., Bergman, B., Capone, D., Carpenter, E., Letelier, R., Lipschultz, F., Paerl, H., Sigman, D., Stal, L., 2002. Dinitrogen fixation in the world's oceans. Springer.

Karl, D.M., 2002. Nutrient dynamics in the deep blue sea. Trends Microbiol. 10, 410–418.

Karl, T.R., Trenberth, K.E., 2003. Modern global climate change. Science. 302, 1719–1723. doi:10.1126/science.1090228.

Keeling, R.F., Körtzinger, A., Gruber, N., 2010. Ocean deoxygenation in a warming world. Ann. Rev. Mar. Sci. 2, 199–229.

Khatiwala, S., Primeau, F., Hall, T., 2009. Reconstruction of the history of anthropogenic CO_2 concentrations in the ocean. Nature 462, 346–349.

Kim, G., Hussain, N., Church, T.M., 2003. Tracing the advection of organic carbon into the subsurface Sargasso Sea using a $^{228}Ra/^{226}Ra$ tracer. Geophys. Res. Lett. 30. doi:10.1029/2003GL017565.

Klaas, C., Archer, D.E., 2002. Association of sinking organic matter with various types of mineral ballast in the deep sea: Implications for the rain ratio. Glob. Biogeochem.Cycles 16, 1116. doi:10.1029/2001GB001765.

Klunder, M.B., Laan, P., Middag, R., De Baar, H.J.W., van Ooijen, J.C., 2011. Dissolved iron in the Southern Ocean (Atlantic sector). Deep Sea Res. Part II Top. Stud. Oceanogr. 58, 2678–2694. doi:10.1016/j.dsr2.2010.10.042.

Knap, A.H., Michaels, A., Close, A.R., Ducklow, H., Dickson, A.G., 1996. Protocols for the joint global ocean flux study (JGOFS) core measurements. JGOFS, Repr. IOC Manuals Guid. No. 29, UNESCO 1994 19, 1–210.

Köhler, P., Fischer, H., Munhoven, G., Zeebe, R.E., 2005. Quantitative interpretation of atmospheric carbon records over the last glacial termination. Global Biogeochem. Cycles 19, GB4020. doi:10.1029/2004GB002345.

Korb, R.E., Whitehouse, M.J., Ward, P., Gordon, M., Venables, H.J., Poulton, A.J., 2012. Regional and seasonal differences in microplankton biomass, productivity, and structure across the Scotia Sea: Implications for the export of biogenic carbon. Deep Sea Res. Part II Top. Stud. Oceanogr. 59–60, 67–77. doi:http://dx.doi.org/10.1016/j.dsr2.2011.06.006.

Kostadinov, T.S., Siegel, D.A., Maritorena, S., 2010. Global variability of phytoplankton functional types from space: assessment via the particle size distribution. Biogeosciences (BG) 7, 3239–3257. doi:10.5194/bg-7-3239-2010.

Kostadinov, T.S., Siegel, D.A., Maritorena, S., 2009. Retrieval of the particle size distribution from satellite ocean color observations. J. Geophys. Res. Ocean. 114, 1–22. doi:10.1029/2009JC005303.

Kostadinov, T.S., Siegel, D.A., Maritorena, S., Guillocheau, N., 2012. Optical assessment of particle size and composition in the Santa Barbara Channel, California. Appl. Opt. 51, 3171–3189.

Kriest, I., Evans, G.T., 1999. Representing phytoplankton aggregates in biogeochemical models. Deep Sea Res. Part I Oceanogr. Res. Pap. 46, 1841–1859. doi:http://dx.doi.org/10.1016/S0967-0637(99)00032-1.

Kriest, I., Oschlies, A., 2011. Numerical effects on organic-matter sedimentation and remineralization in biogeochemical ocean models. Ocean Model. 39, 275–283. doi:http://dx.doi.org/10.1016/j.ocemod.2011.05.001.

Kumar, K., Dasgupta, C.N., Nayak, B., Lindblad, P., Das, D., 2011. Development of suitable photobioreactors for CO_2 sequestration addressing global warming using green algae and cyanobacteria. Bioresour. Technol. 102, 4945–4953.

Lacis, A.A., Schmidt, G.A., Rind, D., Ruedy, R.A., 2010. Atmospheric CO_2: Principal Control Knob Governing Earth's Temperature. Sci. 330 , 356–359. doi:10.1126/science.1190653.

Laglera, L.M., Santos-Echeandía, J., Caprara, S., Monticelli, D., 2013. Quantification of iron in seawater at the low picomolar range based on optimization of bromate-ammonia-dihydroxynaphtalene system by catalytic adsorptive cathodic stripping voltammetry. Anal. Chem. 85, 2486–92. doi:10.1021/ac303621q.

Lalande, C., Moran, S.B., Wassmann, P., Grebmeier, J.M., Cooper, L.W., 2008. ^{234}Th-derived particulate organic carbon fluxes in the northern Barents Sea with comparison to drifting sediment trap fluxes. J. Mar. Syst. 73, 103–113.

Lam, P.J., Bishop, J.K.B., 2007. High biomass, low export regimes in the Southern Ocean. Deep Sea Res. Part II Top. Stud. Oceanogr. 54, 601–638. doi:http://dx.doi.org/10.1016/j.dsr2.2007.01.013.

Lam, P.J., Doney, S.C., Bishop, J.K.B., 2011. The dynamic ocean biological pump: Insights from a global compilation of particulate organic carbon, $CaCO_3$, and opal concentration profiles from the mesopelagic. Global Biogeochem. Cycles 25, GB3009.

Lampitt, R.S., Boorman, B., Brown, L., Lucas, M., Salter, I., Sanders, R., Saw, K., Seeyave, S., Thomalla, S.J., Turnewitsch, R., 2008. Particle export from the euphotic zone: Estimates using a novel drifting sediment trap, ^{234}Th and new production. Deep Sea Res. Part I Oceanogr. Res. Pap. 55, 1484–1502. doi:10.1016/j.dsr.2008.07.002.

Landry, M.R., Selph, K.E., Taylor, A.G., Décima, M., Balch, W.M., Bidigare, R.R., 2011. Phytoplankton growth, grazing and production balances in the HNLC equatorial Pacific. Deep Sea Res. Part II Top. Stud. Oceanogr. 58, 524–535. doi:http://dx.doi.org/10.1016/j.dsr2.2010.08.011.

Landschützer, P., Gruber, N., Haumann, F.A., Rödenbeck, C., Bakker, D.C.E., van Heuven, S., Hoppema, M., Metzl, N., Sweeney, C., Takahashi, T., Tilbrook, B., Wanninkhof, R., 2015. The reinvigoration of the Southern Ocean carbon sink. Science. 349, 1221–1224. doi:10.1126/science.aab2620.

Latham, J., Rasch, P., Chen, C.-C., Kettles, L., Gadian, A., Gettelman, A., Morrison, H., Bower, K., Choularton, T., 2008. Global temperature stabilization via controlled albedo enhancement of low-level maritime clouds. Philos. Trans. R. Soc. A Math. Phys. Eng. Sci. 366, 3969–3987.

Latham, J., Rasch, P.J., Launder, B., 2014. Climate engineering: exploring nuances and consequences of deliberately altering the Earth's energy budget. Philos. Trans. R. Soc. A Math. Phys. Eng. Sci. 372 . doi:10.1098/rsta.2014.0050.

Laubscher, R.K., Perissinotto, R., McQuaid, C.D., 1993. Phytoplankton production and biomass at frontal zones in the Atlantic sector of the Southern Ocean. Polar Biol. 13, 471–481.

Laurenceau-Cornec, E.C., Trull, T.W., Davies, D.M., Bray, S.G., Doran, J., Planchon, F., Carlotti, F., Jouandet, M.-P., Cavagna, A.-J., Waite, A.M., Blain, S., 2015. The relative importance of phytoplankton aggregates and zooplankton fecal pellets to carbon export: insights from free-drifting sediment trap deployments in naturally iron-fertilised waters near the Kerguelen Plateau. Biogeosciences 12, 1007–1027. doi:10.5194/bg-12-1007-2015.

Law, C.S., Abraham, E.R., Watson, A.J., Liddicoat, M.I., 2003. Vertical eddy diffusion and nutrient supply to the surface mixed layer of the Antarctic Circumpolar Current. J. Geophys. Res. Ocean. 108, 3272. doi:10.1029/2002JC001604.

Laws, E.A., D'Sa, E., Naik, P., 2011. Simple equations to estimate ratios of new or export production to total production from satellite-derived estimates of sea surface temperature and primary production. Limnol. Oceanogr. Methods 9, 593–601. doi:10.4319/lom.2011.9.593.

Laws, E.A., Falkowski, P.G., Smith, W.O., Ducklow, H., McCarthy, J.J., 2000. Temperature effects on export production in the open ocean. Global Biogeochem. Cycles 14, 1231–1246.

Le Moigne, F.A.C., Boye, M., Masson, A., Corvaisier, R., Grossteffan, E., Guéneugues, A., Pondaven, P., 2013a. Description of the biogeochemical features of the subtropical southeastern Atlantic and the Southern Ocean south of South Africa during the austral summer of the International Polar Year. Biogeosciences 10, 281–295.

Le Moigne, F.A.C., Henson, S.A., Sanders, R.J., Madsen, E., 2013b. Global database of surface ocean particulate organic carbon export fluxes diagnosed from the ^{234}Th technique. Earth Syst. Sci. Data 5, 295–304. doi:10.5194/essd-5-295-2013.

Le Moigne, F.A.C., Sanders, R.J., Villa-Alfageme, M., Martin, A.P., Pabortsava, K., Planquette, H., Morris, P.J., Thomalla, S.J., 2012. On the proportion of ballast versus non-ballast associated carbon export in the surface ocean. Geophys. Res. Lett. 39, L15610. doi:10.1029/2012GL052980.

Le Quéré, C., Peters, G.P., Andres, R.J., Andrew, R.M., Boden, T., Ciais, P., Friedlingstein, P., Houghton, R.A., Marland, G., Moriarty, R., Others, 2014. Global carbon budget 2013. Earth Syst. Sci. Data 6, 235–263. doi:10.5194/essd-6-235-2014.

Lee, C., Hedges, J.I., Wakeham, S.G., Zhu, N., 1992. Effectiveness of various treatments in retarding microbial activity in sediment trap material and their effects on the collection of swimmers. Limnol. Oceanogr. 37, 117–130.

Lepore, K., Moran, S.B., Burd, A.B., Jackson, G.A., Smith, J.N., Kelly, R.P., Kaberi, H., Stavrakakis, S., Assimakopoulou, G., 2009. Sediment trap and in-situ pump size-fractionated POC/^{234}Th ratios in the Mediterranean Sea and Northwest Atlantic: Implications for POC export. Deep Sea Res. Part I Oceanogr. Res. Pap. 56, 599–613.

Liu, H.-S., 1992. Frequency variations of the Earth's obliquity and the 100-kyr ice-age cycles. Nature 358, 397–399.

Liu, K.-K., Kaplan, I.R., 1989. The eastern tropical Pacific as a source of ^{15}N-enriched nitrate in seawater off southern California. Limnol. Oceanogr. 34, 820–830.

Liu, Z., Cochran, J.K., Lee, C., Gasser, B., Miquel, J.C., Wakeham, S.G., 2009. Further investigations on why POC concentrations differ in samples collected by Niskin bottle and in situ pump. Deep Sea Res. Part II Top. Stud. Oceanogr. 56, 1558–1567. doi:10.1016/j.dsr2.2008.12.019.

Loisel, H., Nicolas, J.-M., Sciandra, A., Stramski, D., Poteau, A., 2006. Spectral dependency of optical backscattering by marine particles from satellite remote sensing of the global ocean. J. Geophys. Res. Ocean. 111, C09024. doi:10.1029/2005JC003367.

Lomas, M.W., Moran, S.B., 2011. Evidence for aggregation and export of cyanobacteria and nano-eukaryotes from the Sargasso Sea euphotic zone. Biogeosciences 8, 203–216. doi:10.5194/bg-8-203-2011.

Longhurst, A., 1995. Seasonal cycles of pelagic production and consumption. Prog. Oceanogr. 36, 77–167. doi:http://dx.doi.org/10.1016/0079-6611(95)00015-1.

Longhurst, A.R., 2010. Ecological geography of the sea, 2nd ed. Academic Press.

Luo, Y., 2013. Applications of U-decay series isotopes to studying the meridional overturning circulation and particle dynamics in the ocean. University of British Columbia.

Lynn, R.J., Simpson, J.J., 1987. The California Current System: The seasonal variability of its physical characteristics. J. Geophys. Res. 92, 12947–12966.

Lyons, G., Benitez-Nelson, C.R., Thunell, R.C., 2011. Phosphorus composition of sinking particles in the Guaymas Basin, Gulf of California. Limnol. Oceanogr. 56, 1093–1105.

MacMartin, D.G., Caldeira, K., Keith, D.W., 2014. Solar geoengineering to limit the rate of temperature change. Philos. Trans. R. Soc. A Math. Phys. Eng. Sci. 372 . doi:10.1098/rsta.2014.0134.

Madin, L.P., 1982. Production, composition and sedimentation of salp fecal pellets in oceanic waters. Mar. Biol. 67, 39–45.

Maiti, K., Benitez-Nelson, C.R., Buesseler, K.O., 2010. Insights into particle formation and remineralization using the short-lived radionuclide, Thoruim-234. Geophys. Res. Lett. 37, L15608. doi:10.1029/2010GL044063.

Maiti, K., Bosu, S., D'Sa, E.J., Adhikari, P.L., Sutor, M., Longnecker, K., 2016. Export fluxes in northern Gulf of Mexico - Comparative evaluation of direct, indirect and satellite-based estimates. Mar. Chem. 184, 60–77. doi:http://dx.doi.org/10.1016/j.marchem.2016.06.001.

Maiti, K., Buesseler, K.O., Pike, S.M., Benitez-Nelson, C., Cai, P., Chen, W., Cochran, K., Dai, M., Dehairs, F., Gasser, et al., 2012. Intercalibration studies of short-lived Thorium-234 in the water column and marine particles. Limnol. Ocean. Methods 10, 631–644. doi:10.4319/lom.2012.10.631.

Maiti, K., Charette, M.A., Buesseler, K.O., Kahru, M., 2013. An inverse relationship between production and export efficiency in the Southern Ocean. Geophys. Res. Lett. 40, 1557–1561. doi:doi:10.1002/grl.50219.

Manizza, M., Buitenhuis, E.T., Le Quéré, C., 2010. Sensitivity of global ocean biogeochemical dynamics to ecosystem structure in a future climate. Geophys. Res. Lett. 37.

Manno, C., Stowasser, G., Enderlein, P., Fielding, S., Tarling, G.A., 2015. The contribution of zooplankton faecal pellets to deep-carbon transport in the Scotia Sea (Southern Ocean). Biogeosciences 12, 1955–1965. doi:10.5194/bg-12-1955-2015.

Maritorena, S., Siegel, D.A., 2005. Consistent merging of satellite ocean color data sets using a bio-optical model. Remote Sens. Environ. 94, 429–440. doi:http://dx.doi.org/10.1016/j.rse.2004.08.014.

Maritorena, S., Siegel, D.A., Peterson, A.R., 2002. Optimization of a semianalytical ocean color model for global-scale applications. Appl. Opt. 41, 2705–2714. doi:10.1364/AO.41.002705.

Martin, J.H., Knauer, G.A., Karl, D.M., Broenkow, W.W., 1987. VERTEX: carbon cycling in the northeast Pacific. Deep Sea Res. Part A. Oceanogr. Res. Pap. 34, 267–285. doi:http://dx.doi.org/10.1016/0198-0149(87)90086-0.

Martin, P., Lampitt, R.S., Jane Perry, M., Sanders, R., Lee, C., D'Asaro, E., 2011. Export and mesopelagic particle flux during a North Atlantic spring diatom bloom. Deep Sea Res. Part I Oceanogr. Res. Pap. 58, 338–349. doi:10.1016/j.dsr.2011.01.006.

Matsumoto, K., Tokos, K.S., Chikamoto, M.O., Ridgwell, A., 2010. Characterizing post-industrial changes in the ocean carbon cycle in an Earth system model. Tellus B 62, 296–313. doi:10.1111/j.1600-0889.2010.00461.x.

Mawji, E., Schlitzer, R., Masferrer, E., Abadie, C., Abouchami, W., Anderson, R.F., Baars, O., Bakker, K., Baskaran, M., Bates, et al. The GEOTRACES Intermediate Data Product 2014. Mar. Chem. 1–8. doi:http://dx.doi.org/10.1016/j.marchem.2015.04.005.

Mayor, D.J., Sanders, R., Giering, S.L.C., Anderson, T.R., 2014. Microbial gardening in the ocean's twilight zone: Detritivorous metazoans benefit from fragmenting, rather than ingesting, sinking detritus. BioEssays. doi:10.1002/bies.201400100.

Michaels, A.F., Silver, M.W., 1988. Primary production, sinking fluxes and the microbial food web. Deep Sea Res. Part A.Oceanographic Res. Pap. 35, 473–490.

Middag, R., van Hulten, M.M.P., Van Aken, H.M., Rijkenberg, M.J.A., Gerringa, L.J.A., Laan, P., de Baar, H.J.W., 2015. Dissolved aluminium in the ocean conveyor of the West Atlantic Ocean: Effects of the biological cycle, scavenging, sediment resuspension and hydrography. Mar. Chem. 177, 69–86. doi:10.1016/j.marchem.2015.02.015.

Millero, F.J., Sotolongo, S., Izaguirre, M., 1987. The kinetics of oxidation of Fe(II) in seawater. Geochim. Cosmochim. Acta 51, 793–801. doi:10.1016/0016-7037(87)90093-7.

Mills, M.M., Ridame, C., Davey, M., La Roche, J., Geider, R.J., 2004. Iron and phosphorus co-limit nitrogen fixation in the eastern tropical North Atlantic. Nature 429, 292–294.

Mizdalski, E., 1988. Weight and length data of zooplankton in the Weddell Sea in austral spring 1986 (ANT V/3). Berichte zur Polarforsch. Reports Polar Res. 55.

Moore, C.M., Mills, M.M., Milne, A., Langlois, R., Achterberg, E.P., Lochte, K., Geider, R.J., La Roche, J., 2006. Iron limits primary productivity during spring bloom development in the central North Atlantic. Glob. Chang. Biol. 12, 626–634. doi:10.1111/j.1365-2486.2006.01122.x.

Moore, R.M., Hunter, K.A., 1985. Thorium adsorption in the ocean: reversibility and distribution amongst particle sizes. Geochim. Cosmochim. Acta 49, 2253–2257.

Moore, W.S., 2000. Determining coastal mixing rates using radium isotopes. Cont. Shelf Res. 20, 1993–2007. doi:10.1016/S0278-4343(00)00054-6.

Moran, B.S., Buesseler, K.O., 1993. Size-fractionated ^{234}Th in continental shelf waters off New England: Implications for the role of colloids in oceanic trace metal scavenging. J. Mar. Res. 51, 893–922.

Moran, S.B., Weinstein, S.E., Edmonds, H.N., Smith, J.N., Kelly, R.P., Pilson, M.E.Q., Harrison, W.G., 2003. Does ^{234}Th/^{238}U disequilibrium provide an accurate record of the export flux of particulate organic carbon from the upper ocean? Limnol. Oceanogr. 48, 1018–1029.

Morán, X.A.G., López- Urrutia, Á., Calvo- Díaz, A., Li, W.K.W., 2010. Increasing importance of small phytoplankton in a warmer ocean. Glob. Chang. Biol. 16, 1137–1144.

Morel, A., Berthon, J.-F., 1989. Surface pigments, algal biomass profiles, and potential production of the euphotic layer: Relationships reinvestigated in view of remote-sensing applications. Limnol. Oceanogr. 34, 1545–1562. doi:10.4319/lo.1989.34.8.1545.

Morel, A., Maritorena, S., 2001. Bio-optical properties of oceanic waters: A reappraisal. J. Geophys. Res. Ocean. 106, 7163–7180. doi:10.1029/2000JC000319.

Murphy, J., Riley, J.P., 1962. A modified single solution method for the determination of phosphate in natural waters. Anal. Chim. Acta 27, 31–36. doi:10.1016/S0003-2670(00)88444-5.

Murray, J.W., Downs, J.N., Strom, S., Wei, C.L., Jannasch, H.W., 1989. Nutrient assimilation, export production and ^{234}Th scavenging in the eastern equatorial Pacific. Deep Sea Res. Part A.Oceanographic Res. Pap. 36, 1471–1489.

Murray, J.W., Young, J., Newton, J., Dunne, J., Chapin, T., Paul, B., McCarthy, J.J., 1996. Export flux of particulate organic carbon from the central equatorial Pacific determined using a combined drifting trap-^{234}Th approach. Deep Sea Res. Part II Top. Stud. Oceanogr. 43, 1095–1132.

National Research Council, 2015. Climate Intervention: Carbon Dioxide Removal and Reliable Sequestration. The National Academies Press, Washington, DC.

Naveira Garabato, A.C., Leach, H., Allen, J.T., Pollard, R.T., Strass, V.H., 2001. Mesoscale Subduction at the Antarctic Polar Front Driven by Baroclinic Instability. J. Phys. Oceanogr. 31, 2087–2107. doi:10.1175/1520-0485(2001)031<2087:MSATAP>2.0.CO;2.

Naveira Garabato, A.C., Polzin, K.L., King, B.A., Heywood, K.J., Visbeck, M., 2004. Widespread intense turbulent mixing in the Southern Ocean. Science. 303, 210–213. doi:10.1126/science.1090929.

NOAA, 2016. Earth System Research Laboratory. Global Monitorin Division. http://www.esrl.noaa.gov/gmd/ccgg/trends/.

Nowlin, W.D., Klinck, J.M., 1986. The physics of the Antarctic circumpolar current. Rev. Geophys. 24, 469–491.

OC-CCI, 2015. Ocean Color Climate Change Initiative Product User Guide Version 2. Plymouth Marine Laboratory, Plymouth, UK.

Orlandini, K.A., Bowling, J.W., Pinder III, J.E., Penrose, W.R., 2003. ^{90}Y-^{90}Sr disequilibrium in surface waters: investigating short-term particle dynamics by using a novel isotope pair. Earth Planet. Sci. Lett. 207, 141–150.

Orsi, A.H., Whitworth, T., Nowlin, W.D., 1995. On the meridional extent and fronts of the Antarctic Circumpolar Current. Deep Sea Res. Part I Oceanogr. Res. Pap. 42, 641–673.

Owens, S.A., 2013. Advances in measurements of particle cycling and fluxes in the ocean. PhD thesis, Massachusetts Institute of Technology.

Owens, S.A., Buesseler, K.O., Lamborg, C.H., Valdes, J., Lomas, M.W., Johnson, R.J., Steinberg, D.K., D.A, S., 2013. A new time series of particle export from neutrally buoyant sediments traps at the Bermuda Atlantic Time-series Study site. Deep Sea Res. Part I Oceanogr. Res. Pap. 72, 34–47. doi:http://dx.doi.org/10.1016/j.dsr.2012.10.011.

Owens, S.A., Buesseler, K.O., Sims, K.W.W., 2011. Re-evaluating the ^{238}U-salinity relationship in seawater: Implications for the 238U-234Th disequilibrium method. Mar. Chem. 127, 31–39. doi:10.1016/j.marchem.2011.07.005.

Owens, S.A., Pike, S., Buesseler, K.O., 2015. Thorium-234 as a tracer of particle dynamics and upper ocean export in the Atlantic Ocean. Deep Sea Res. Part II Top. Stud. Oceanogr. 116, 42–59. doi:http://dx.doi.org/10.1016/j.dsr2.2014.11.010.

Pakhomov, E.A., McQuaid, C.D., 1996. Distribution of surface zooplankton and seabirds across the Southern Ocean. Polar Biol. 16, 271–286.

Parekh, P., Dutkiewicz, S., Follows, M.J., Ito, T., 2006. Atmospheric carbon dioxide in a less dusty world. Geophys. Res. Lett. 33, L03610. doi:10.1029/2005GL025098.

Passow, U., 2002. Transparent exopolymer particles (TEP) in aquatic environments. Prog. Oceanogr. 55, 287–333. doi:DOI: 10.1016/S0079-6611(02)00138-6.

Pates, J.M., Muir, G.K.P., 2007. U-salinity relationships in the Mediterranean: Implications for ^{234}Th: ^{238}U particle flux studies. Mar. Chem. 106, 530–545.

Paulmier, A., Ruiz-Pino, D., 2009. Oxygen minimum zones (OMZs) in the modern ocean. Prog. Oceanogr. 80, 113–128.

Pérez, F.F., Mercier, H., Vázquez-Rodríguez, M., Lherminier, P., Velo, A., Pardo, P.C., Rosón, G., Ríos, A.F., 2013. Atlantic Ocean CO2 uptake reduced by weakening of the meridional overturning circulation. Nat. Geosci. 6, 146–152.

Perissinotto, R., Pakhomov, E.A., 1998. Contribution of salps to carbon flux of marginal ice zone of the Lazarev Sea, Southern Ocean. Mar. Biol. 131, 25–32.

Peterson, B.J., Fry, B., 1987. Stable isotopes in ecosystem studies. Annu. Rev. Ecol. Syst. 293–320.

Phillips, B., Kremer, P., Madin, L.P., 2009. Defecation by Salpa thompsoni and its contribution to vertical flux in the Southern Ocean. Mar. Biol. 156, 455–467.

Pike, S.M., Buesseler, K.O., Andrews, J., Savoye, N., 2005. Quantification of Th-234 recovery in small volume seawater samples by inductively coupled plasma-mass spectrometry. Journal Radioanal. Nucl. Chem. 263, 355–360.

Planchon, F., Ballas, D., Cavagna, A.-J., Bowie, A.R., Davies, D., Trull, T., Laurenceau-Cornec, E.C., Van Der Merwe, P., Dehairs, F., 2015. Carbon export in the naturally iron-fertilized Kerguelen area of the Southern Ocean based on the ^{234}Th approach. Biogeosciences 12, 3831–3848. doi:10.5194/bg-12-3831-2015.

Planchon, F., Cavagna, A.-J., Cardinal, D., André, L., Dehairs, F., 2013. Late summer particulate organic carbon export and twilight zone remineralisation in the Atlantic sector of the Southern Ocean. Biogeosciences 10, 803–820. doi:10.5194/bg-10-803-2013.

Pollard, R.T., Bathmann, U., Dubischar, C., Read, J.F., Lucas, M., 2002a. Zooplankton distribution and behaviour in the Southern Ocean from surveys with a towed Optical Plankton Counter. Deep Sea Res. Part II Top. Stud. Oceanogr. 49, 3889–3915. doi:http://dx.doi.org/10.1016/S0967-0645(02)00116-9.

Pollard, R.T., Lucas, M.I., Read, J.F., 2002b. Physical controls on biogeochemical zonation in the Southern Ocean. Deep Sea Res. Part II Top. Stud. Oceanogr. 49, 3289–3305. doi:10.1016/S0967-0645(02)00084-X.

Prahl, F.G., Popp, B.N., Karl, D.M., Sparrow, M.A., 2005. Ecology and biogeochemistry of alkenone production at Station ALOHA. Deep Sea Res. Part I Oceanogr. Res. Pap. 52, 699–719. doi:http://dx.doi.org/10.1016/j.dsr.2004.12.001.

Puigcorbé, V., Benitez- Nelson, C.R., Masqué, P., Verdeny, E., White, A.E., Popp, B.N., Prahl, F.G., Lam, P.J., 2015. Small phytoplankton drive high summertime carbon and nutrient export in the Gulf of California and Eastern Tropical North Pacific. Global Biogeochem. Cycles 29, 1309–1332. doi:10.1002/ 2015GB005134.

Quéguiner, B., 2013. Iron fertilization and the structure of planktonic communities in high nutrient regions of the Southern Ocean. Deep. Res. Part II Top. Stud. Oceanogr. 90, 43–54. doi:10.1016/j.dsr2.2012.07.024.

Rasch, P.J., Tilmes, S., Turco, R.P., Robock, A., Oman, L., Chen, C.-C.J., Stenchikov, G.L., Garcia, R.R., 2008. An overview of geoengineering of climate using stratospheric sulphate aerosols. Philos. Trans. R. Soc. A Math. Phys. Eng. Sci. 366, 4007–4037.

Read, J.F., Pollard, R.T., Bathmann, U., 2002. Physical and biological patchiness of an upper ocean transect from South Africa to the ice edge near the Greenwich Meridian. Deep Sea Res. Part II Top. Stud. Oceanogr. 49, 3713–3733.

Rembauville, M., Blain, S., Armand, L., Quéguiner, B., Salter, I., 2015a. Export fluxes in a naturally iron-fertilized area of the Southern Ocean – Part 2: Importance of diatom resting spores and faecal pellets for export. Biogeosciences 12, 3171–3195. doi:10.5194/bg-12-3171-2015.

Rembauville, M., Salter, I., Leblond, N., Gueneugues, A., Blain, S., 2015b. Export fluxes in a naturally iron-fertilized area of the Southern Ocean – Part 1: Seasonal dynamics of particulate organic carbon export from a moored sediment trap. Biogeosciences 12, 3153–3170. doi:10.5194/bg-12-3153-2015.

Resplandy, L., Martin, A.P., Le Moigne, F., Martin, P., Aquilina, A., Mémery, L., Lévy, M., Sanders, R., 2012. How does dynamical spatial variability impact ^{234}Th-derived estimates of organic export? Deep Sea Res. Part I Oceanogr. Res. Pap. 68, 24–45. doi:http://dx.doi.org/10.1016/j.dsr.2012.05.015.

Reul, N., Fournier, S., Boutin, J., Hernandez, O., Maes, C., Chapron, B., Alory, G., Quilfen, Y., Tenerelli, J., Morisset, S., Kerr, Y., Mecklenburg, S., Delwart, S., 2014. Sea Surface Salinity Observations from Space with the SMOS Satellite: A New Means to Monitor the Marine Branch of the Water Cycle. Surv. Geophys. 35, 681–722. doi:10.1007/s10712-013-9244-0.

Richardson, A.J., Schoeman, D.S., 2004. Climate Impact on Plankton Ecosystems in the Northeast Atlantic. Science. 305, 1609–1612. doi:10.1126/science.1100958.

Richardson, T.L., Jackson, G.A., 2007. Small phytoplankton and carbon export from the surface ocean. Science. 315, 838–840.

Rijkenberg, M., 2010. Geotraces West Atlantic leg 2. Cruise report 64PE321 on RV Pelagia.

Rijkenberg, M.J.A., Middag, R., Laan, P., Gerringa, L.J.A., van Aken, H.M., Schoemann, V., de Jong, J.T.M., de Baar, H.J.W., 2014. The Distribution of Dissolved Iron in the West Atlantic Ocean. PLoS One 9, e101323. doi:10.1371/journal.pone.0101323.

Roca-Martí, M., Puigcorbé, V., Iversen, M.H., Rutgers van der Loeff, M., Klaas, C., Cheah, W., Bracher, A., Masqué, P., 2016. High particulate organic carbon export during the decline of a vast diatom bloom in the Atlantic sector of the Southern Ocean.

Roca-Martí, M., Puigcorbé, V., Iversen, M.H., van der Loeff, M.R., Klaas, C., Cheah, W., Bracher, A., Masqué, P., 2015. High particulate organic carbon export during the decline of a vast diatom bloom in the Atlantic sector of the Southern Ocean. Deep Sea Res. Part II Top. Stud. Oceanogr. -. doi:10.1016/j.dsr2.2015.12.007.

Rodellas, V., 2014. Evaluating submarine groundwater discharge to the Mediterranean Sea by using radium isotopes. PhD thesis, Universitat Autònoma de Barcelona.

Roden, G.I., 1958. Oceanographic and meteorological aspects of the Gulf of California. J. Mar. Res. 18, 10–35. doi:10125/7874.

Rosengard, S.Z., Lam, P.J., Balch, W.M., Auro, M.E., Pike, S., Drapeau, D., Bowler, B., 2015. Carbon export and transfer to depth across the Southern Ocean Great Calcite Belt. Biogeosciences 12, 3953–3971. doi:10.5194/bg-12-3953-2015.

Ruff, S.E., Probandt, D., Zinkann, A.-C., Iversen, M.H., Klaas, C., Würzberg, L., Krombholz, N., Wolf-Gladrow, D., Amann, R., Knittel, K., 2014. Indications for algae-degrading benthic microbial communities in deep-sea sediments along the Antarctic Polar Front. Deep Sea Res. Part II Top. Stud. Oceanogr. 108, 6–16. doi:http://dx.doi.org/10.1016/j.dsr2.2014.05.011.

Rutgers van der Loeff, M., Cai, P., Stimac, I., Bracher, A., Middag, R., Klunder, M., van Heuven, S., 2011. ^{234}Th in surface waters: distribution of particle export flux across the Antarctic Circumpolar Current and in the Weddell Sea during the GEOTRACES expedition ZERO and DRAKE. Deep Sea Res. Part II Top. Stud. Oceanogr. 58, 2749–2766. doi:10.1016/j.dsr2.2011.02.004.

Rutgers van der Loeff, M., Moore, W.S., 1999. Determination of natural radioactive tracers, in: Methods of Seawater Analysis. Verlag Chemie GmbH, Weinheim, pp. 365–397.

Rutgers van der Loeff, M.M., Buesseler, K., Bathmann, U., Hense, I., Andrews, J., 2002. Comparison of carbon and opal export rates between summer and spring bloom periods in the region of the Antarctic Polar Front, SE Atlantic. Deep Sea Res. Part II Top. Stud. Oceanogr. 49, 3849–3869. doi:10.1016/S0967-0645(02)00114-5.

Rutgers van der Loeff, M.M., Friedrich, J., Bathmann, U. V, 1997. Carbon export during the spring bloom at the Antarctic Polar Front, determined with the natural tracer ^{234}Th. Deep Sea Res. Part II Top. Stud. Oceanogr. 44, 457–478. doi:10.1016/S0967-0645(96)00067-7.

Saba, V.S., Friedrichs, M.A.M., Antoine, D., Armstrong, R.A., Asanuma, I., Behrenfeld, M.J., Ciotti, A.M., Dowell, M., Hoepffner, N., Hyde, K.J.W., et al., 2011. An evaluation of ocean color model estimates of marine primary productivity in coastal and pelagic regions across the globe. Biogeosciences 8, 489–503. doi:10.5194/bg-8-489-2011.

Sabine, C.L., Feely, R.A., Gruber, N., Key, R.M., Lee, K., Bullister, J.L., Wanninkhof, R., Wong, C.S., Wallace, D.W.R., Tilbrook, B., 2004. The oceanic sink for anthropogenic CO_2. Science. 305, 367. doi:10.1126/science.1097403.

Sallée, J.-B., Speer, K., Rintoul, S., Wijffels, S., 2010. Southern Ocean thermocline ventilation. J. Phys. Oceanogr. 40, 509–529. doi:*10.1175/2009JPO4291.1*.

Salter, I., Kemp, A.E.S., Moore, C.M., Lampitt, R.S., Wolff, G.A., Holtvoeth, J., 2012. Diatom resting spore ecology drives enhanced carbon export from a naturally iron-fertilized bloom in the Southern Ocean. Global Biogeochem. Cycles 26, GB1014. doi:10.1029/2010GB003977.

Sanders, R., Brown, L., Henson, S., Lucas, M., 2005. New production in the Irminger Basin during 2002. J. Mar. Syst. 55, 291–310. doi:http://dx.doi.org/10.1016/j.jmarsys.2004.09.002.

Sanders, R., Morris, P.J., Poulton, A.J., Stinchcombe, M.C., Charalampopoulou, A., Lucas, M.I., Thomalla, S.J., 2010. Does a ballast effect occur in the surface ocean? Geophys. Res. Lett. 37, L08602. doi:10.1029/2010GL042574.

Santamaría del Angel, E., Alvarez Borrego, S., Müller Karger, F.E., 1994. Gulf of California biogeographic regions based on coastal zone color scanner imagery. J. Geophys. Res. Ocean. 99, 7411–7421. doi:10.1029/93JC02154.

Santschi, P.H., Hung, C.C., Schultz, G., Alvarado-Quiroz, N., Guo, L., Pinckney, J., Walsh, I., 2003. Control of acid polysaccharide production and ^{234}Th and POC export fluxes by marine organisms. Geophys.Res.Lett 30, 1044. doi:10.1029/2002GL016046.

Santschi, P.H., Murray, J.W., Baskaran, M., Benitez-Nelson, C.R., Guo, L.D., Hung, C.C., Lamborg, C., Moran, S.B., Passow, U., Roy-Barman, M., 2006. Thorium speciation in seawater. Mar. Chem. 100, 250–268. doi: 10.1016/j.marchem.2005.10.024.

Sarmiento, J.L., Gruber, N., 2006. Ocean biogeochemical dynamics. Cambridge Univ Press.

Sarmiento, J.L., Gruber, N., Brzezinski, M.A., Dunne, J.P., 2004. High-latitude controls of thermocline nutrients and low latitude biological productivity. Nature 427, 56–60. doi:10.1038/nature02127.

Savoye, N., Benitez-Nelson, C., Burd, A.B., Cochran, J.K., Charette, M., Buesseler, K.O., Jackson, G.A., Roy-Barman, M., Schmidt, S., Elskens, M., 2006. ^{234}Th sorption and export models in the water column: a review. Mar. Chem. 100, 234–249. doi:10.1016/j.marchem.2005.10.014.

Savoye, N., Buesseler, K.O., Cardinal, D., Dehairs, F., 2004. ^{234}Th deficit and excess in the Southern Ocean during spring 2001: Particle export and remineralization. Geophys.Res.Lett 31, L12301. doi:10.1029/2004GL019744.

Savoye, N., Trull, T.W., Jacquet, S.H.M., Navez, J., Dehairs, F., 2008. ^{234}Th-based export fluxes during a natural iron fertilization experiment in the Southern Ocean (KEOPS). Deep Sea Res. Part II Top. Stud. Oceanogr. 55, 841–855. doi:doi:10.1016/j.dsr2.2007.12.036.

Scharek, R., Tupas, L.M., Karl, D.M., 1999. Diatom fluxes to the deep sea in the oligotrophic North Pacific gyre at Station ALOHA. Mar. Ecol. Prog. Ser. 182, 55–67. doi:10.3354/meps182055.

Schlitzer, R., 2002. Carbon export fluxes in the Southern Ocean: Results from inverse modeling and comparison with satellite-based estimates. Deep Sea Res. Part II Top. Stud. Oceanogr. 49, 1623–1644. doi: 10.1016/S0967-0645(02)00004-8.

Schmidt, S., Andersen, V., Belviso, S., Marty, J.-C., 2002. Strong seasonality in particle dynamics of north-western Mediterranean surface waters as revealed by ^{234}Th/^{238}U. Deep Sea Res. Part I Oceanogr. Res. Pap. 49, 1507–1518. doi:http://dx.doi.org/10.1016/S0967-0637(02)00039-0.

Schmittner, A., Brook, E.J., Ahn, J., 2007. Impact of the ocean's overturning circulation on atmospheric CO_2. Ocean Circ. Mech. Impacts-Past Futur. Chang. Merid. Overturning 315–334. doi: 10.1029/173GM20.

Schmittner, A., Latif, M., Schneider, B., 2005. Model projections of the North Atlantic thermohaline circulation for the 21st century assessed by observations. Geophys. Res. Lett. 32, L23710. doi:10.1029/2005GL024368.

Siegel, D.A., Buesseler, K.O., Behrenfeld, M.J., Benitez-Nelson, C.R., Boss, E., Brzezinski, M.A., Burd, A., Carlson, C.A., D'Asaro, E.A., Doney, S.C., Perry, M.J., Stanley, R.H.R., Steinberg, D.K., 2016. Prediction of the Export and Fate of Global Ocean Net Primary Production: The EXPORTS Science Plan. Front. Mar. Sci. 3. doi:10.3389/fmars.2016.00022.

Siegel, D.A., Buesseler, K.O., Doney, S.C., Sailley, S.F., Behrenfeld, M.J., Boyd, P.W., 2014. Global assessment of ocean carbon export by combining satellite observations and food-web models. Global Biogeochem. Cycles 28, 181–196. doi:10.1002/2013GB004743.

Smetacek, V., Klaas, C., Strass, V.H., Assmy, P., Montresor, M., Cisewski, B., Savoye, N., Webb, A., D'Ovidio, F., Arrieta, J.M., others, 2012. Deep carbon export from a Southern Ocean iron-fertilized diatom bloom. Nature 487, 313–319. doi:10.1038/nature11229.

Smetacek, V., Naqvi, S.W.A., 2008. The next generation of iron fertilization experiments in the Southern Ocean. Philos. Trans. R. Soc. A Math. Phys. Eng. Sci. 366, 3947–3967. doi:10.1098/rsta.2008.0144.

Smith, C.R., Leo, F.C. De, Bernardino, A.F., Sweetman, A.K., Arbizu, P.M., 2008. Abyssal food limitation, ecosystem structure and climate change. Trends Ecol. Evol. 23, 518–528. doi:http://dx.doi.org/10.1016/j.tree.2008.05.002.

Smith, K.L., Ruhl, H.A., Kahru, M., Huffard, C.L., Sherman, A.D., 2013. Deep ocean communities impacted by changing climate over 24 y in the abyssal northeast Pacific Ocean. Proc. Natl. Acad. Sci. 110, 19838–19841. doi:10.1073/pnas.1315447110.

Smoak, J.M., Moore, W.S., Thunell, R.C., Shaw, T.J., 1999. Comparison of ^{234}Th, ^{228}Th, and ^{210}Pb fluxes with fluxes of major sediment components in the Guaymas Basin, Gulf of California. Mar. Chem. 65, 177–194. doi: 10.1016/S0304-4203(98)00095-4.

Smythe-Wright, D., Chapman, P., Rae, C.D., Shannon, L. V, Boswell, S.M., 1998. Characteristics of the South Atlantic subtropical frontal zone between 15°W and 5°E. Deep Sea Res. Part I Oceanogr. Res. Pap. 45, 167–192. doi:http://dx.doi.org/10.1016/S0967-0637(97)00068-X.

Sokolov, S., Rintoul, S.R., 2007. On the relationship between fronts of the Antarctic Circumpolar Current and surface chlorophyll concentrations in the Southern Ocean. J. Geophys. Res. Ocean. 112, C07030. doi:10.1029/2006JC004072.

Speicher, E.A., Moran, S.B., Burd, A.B., Delfanti, R., Kaberi, H., Kelly, R.P., Papucci, C., Smith, J.N., Stavrakakis, S., Torricelli, L., 2006. Particulate organic carbon export fluxes and size-fractionated POC/^{234}Th ratios in the Ligurian, Tyrrhenian and Aegean Seas. Deep Sea Res. Part I Oceanogr. Res. Pap. 53, 1810–1830. doi: 10.1016/j.dsr.2006.08.005.

Steinberg, D.K., Carlson, C.A., Bates, N.R., Johnson, R.J., Michaels, A.F., Knap, A.H., 2001. Overview of the US JGOFS Bermuda Atlantic Time-series Study (BATS): a decade-scale look at ocean biology and biogeochemistry. Deep Sea Res. Part II Top. Stud. Oceanogr. 48, 1405–1447. doi10.1016/S0967-0645(00)00148-X.

Steinberg, D.K., Van Mooy, B.A.S., Buesseler, K.O., Boyd, P.W., Kobari, T., Karl, D.M., 2008. Bacterial vs. zooplankton control of sinking particle flux in the ocean's twilight zone. Limnol. Oceanogr. 53, 1327–1338.

Steinmetz, F., Deschamps, P.-Y., Ramon, D., 2011. Atmospheric correction in presence of sun glint: application to MERIS. Opt. Express 19, 9783–9800. doi:10.1364/OE.19.009783.

Stemmann, L., Jackson, G.A., Gorsky, G., 2004. A vertical model of particle size distributions and fluxes in the midwater column that includes biological and physical processes—Part II: application to a three year survey in the NW Mediterranean Sea. Deep Sea Res. Part I Oceanogr. Res. Pap. 51, 885–908. doi:10.1016/j.dsr.2004.03.002.

Stewart, G., Cochran, J.K., Miquel, J.C., Masqué, P., Szlosek, J., Rodriguez y Baena, A.M., Fowler, S.W., Gasser, B., Hirschberg, D.J., 2007. Comparing POC export from ^{234}Th/^{238}U and ^{210}Po/^{210}Pb disequilibria with estimates from sediment traps in the northwest Mediterranean. Deep Sea Res. Part I Oceanogr. Res. Pap. 54, 1549–1570. doi:10.1016/j.dsr.2007.06.005.

Stewart, G., Moran, S.B., Lomas, M.W., Kelly, R.P., 2011. Direct comparison of ^{210}Po, ^{234}Th and POC particle-size distributions and export fluxes at the Bermuda Atlantic Time-series Study (BATS) site. J. Environ. Radioact. 102, 479–489. doi:10.1016/j.jenvrad.2010.09.011.

Stewart, G.M., Bradley Moran, S., Lomas, M.W., 2010. Seasonal POC fluxes at BATS estimated from ^{210}Po deficits. Deep Sea Res. Part I Oceanogr. Res. Pap. 57, 113–124. doi: 10.1016/j.dsr.2009.09.007.

Strass, V.H., Garabato, A.C.N., Bracher, A.U., Pollard, R.T., Lucas, M.I., 2002a. A 3-D mesoscale map of primary production at the Antarctic Polar Front: results of a diagnostic model. Deep Sea Res. Part II Top. Stud. Oceanogr. 49, 3813–3834. doi:http://dx.doi.org/10.1016/S0967-0645(02)00112-1.

Strass, V.H., Leach, H., Prandke, H., Donnelly, M., Bracher, A.U., Wolf-Gladrow, D.A., 2016. The physical environmental conditions for biogeochemical differences along the Antarctic Circumpolar Current in the Atlantic Sector during late austral summer 2012. Deep Sea Res. Part II Top. Stud. Oceanogr. doi:10.1016/j.dsr2.2016.05.018.

Strass, V.H., Naveira Garabato, A.C., Pollard, R.T., Fischer, H.I., Hense, I., Allen, J.T., Read, J.F., Leach, H., Smetacek, V., 2002b. Mesoscale frontal dynamics: shaping the environment of primary production in the Antarctic Circumpolar Current. Deep Sea Res. Part II Top. Stud. Oceanogr. 49, 3735–3769. doi:10.1016/S0967-0645(02)00109-1.

Strickland, J.D.H., Parsons, T.R., 1968. A practical handbook of seawater analysis. Bull. Fish. Res. Board Canada 167, 1–310.

Stukel, M.R., Kahru, M., Benitez-Nelson, C.R., Décima, M., Goericke, R., Landry, M.R., Ohman, M.D., 2015. Using Lagrangian-based process studies to test satellite algorithms of vertical carbon flux in the eastern North Pacific Ocean. J. Geophys. Res. Ocean. 120, 7208–7222. doi:10.1002/2015JC011264.

Sverdrup, H.U., 1953. On conditions for the vernal blooming of phytoplankton. ICES J. Mar. Sci. 18, 287. doi: 10.1093/icesjms/18.3.287.

Sweeney, E.N., McGillicuddy, D.J., Buesseler, K.O., 2003. Biogeochemical impacts due to mesoscale eddy activity in the Sargasso Sea as measured at the Bermuda Atlantic Time-series Study (BATS). Deep Sea Res. Part II Top. Stud. Oceanogr. 50, 3017–3039. doi:10.1016/j.dsr2.2003.07.008.

Sydeman, W.., García-Reyes, M., Schoeman, D.S., Rykaczewski, R.R., Thompson, S.A., Black, B.A., Bograd, S.J., 2014. Climate change and wind intensification in coastal upwelling ecosystems. Science, 345, 77–80. doi:10.1126/science.1250830.

Szlosek, J., Cochran, J.K., Miquel, J.C., Masqué, P., Armstrong, R.A., Fowler, S.W., Gasser, B., Hirschberg, D.J., 2009. Particulate organic carbon–^{234}Th relationships in particles separated by settling velocity in the northwest Mediterranean Sea. Deep Sea Res. Part II Top. Stud. Oceanogr. 56, 1519–1532. doi:10.1016/j.dsr2.2008.12.017.

Takahashi, T., Sutherland, S.C., Wanninkhof, R., Sweeney, C., Feely, R.A., Chipman, D.W., Hales, B., Friederich, G., Chavez, F., Sabine, C., Watson, A., Bakker, D.C.E., Schuster, U., Metzl, N., Yoshikawa-Inoue, H., Ishii, M., Midorikawa, T., Nojiri, Y., Körtzinger, A., Steinhoff, T., Hoppema, M., Olafsson, J., Arnarson, T.S., Tilbrook, B., Johannessen, T., Olsen, A., Bellerby, R., Wong, C.S., Delille, B., Bates, N.R., de Baar, H.J.W., 2009. Climatological mean and decadal change in surface ocean pCO_2, and net sea–air CO_2 flux over the global oceans. Deep. Res. Part II 56, 554–577. doi: 10.1016/j.dsr2.2008.12.009.

Taylor, A.H., Harbour, D.S., Harris, R.P., Burkill, P.H., Edwards, E.S., 1993. Seasonal succession in the pelagic ecosystem of the North Atlantic and the utilization of nitrogen. J. Plankton Res. 15, 875–891. doi:10.1093/plankt/15.8.875.

Taylor, G.T., Muller-Karger, F.E., Thunell, R.C., Scranton, M.I., Astor, Y., Varela, R., Ghinaglia, L.T., Lorenzoni, L., Fanning, K.A., Hameed, S., 2012. Ecosystem responses in the southern Caribbean Sea to global climate change. Proc. Natl. Acad. Sci. 109, 19315–19320. doi:10.1073/pnas.1207514109/-/DCSupplemental.

Thomalla, S.J., Turnewitsch, R., Lucas, M., Poulton, A., 2006. Particulate organic carbon export from the North and South Atlantic gyres: The 234Th/238U disequilibrium approach. Deep Sea Res. Part II Top. Stud. Oceanogr. 53, 1629–1648. doi:10.1016/j.dsr2.2006.05.018.

Thunell, R., Pride, C., Ziveri, P., Muller-Karger, F., Sancetta, C., Murray, D., 1996. Plankton response to physical forcing in the Gulf of California. J. Plankton Res. 18, 2017–2026. doi:10.1093/plankt/18.11.2017.

Thunell, R.C., 1998. Seasonal and annual variability in particle fluxes in the Gulf of California: A response to climate forcing. Deep. Res. Part I 45, 2059–2083. doi:10.1016/S0967-0637(98)00053-3.

Toggweiler, J.R., Gnanadesikan, A., Carson, S., Murnane, R., Sarmiento, J.L., 2003. Representation of the carbon cycle in box models and GCMs: 1. Solubility pump. Global Biogeochem. Cycles 17. doi: 10.1029/2001GB001841.

Tomczak, M., Godfrey, J.S., 2001. Regional oceanography: an introduction. Pergamon, Oxford.

Tréguer, P.J., De La Rocha, C.L., 2013. The world ocean silica cycle. Ann. Rev. Mar. Sci. 5, 477–501. doi:10.1146/annurev-marine-121211-172346.

Trenberth, K.E., Stepaniak, D.P., 2004. The flow of energy through the earth's climate system. Q. J. R. Meteorol. Soc. 130, 2677–2701. doi:10.1256/qj.04.83.

Trent, J.D., Shanks, A.L., Silver, M.W., 1978. In situ and laboratory measurements on macroscopic aggregates in Monterey Bay, California. Limnol. Ocean. 23, 626–635.

Tsunogai, S., Minagawa, M., 1976. Vertical flux of organic materials estimated from Th-234 in the ocean, in: Joint Oceanographic Assembly. Edinburgh, UK, p. 156.

Turner, J.T., 2015. Zooplankton fecal pellets, marine snow, phytodetritus and the ocean's biological pump. Prog. Oceanogr. 130, 205–248. doi:http://dx.doi.org/10.1016/j.pocean.2014.08.005.

Turner, J.T., 2002. Zooplankton fecal pellets, marine snow and sinking phytoplankton blooms. Aquat. Microb. Ecol. 27, 57–102. doi:10.3354/ame027057.

Twardowski, M.S., Sullivan, J.M., Donaghay, P.L., Zaneveld, J.R. V, 1999. Microscale quantification of the absorption by dissolved and particulate material in coastal waters with an ac-9. J. Atmos. Ocean. Technol. 16, 691–707. doi: *10.1175/1520-0426(1999)016<0691:MQOTAB>2.0.CO;2*.

Uitz, J., Claustre, H., Griffiths, F.B., Ras, J., Garcia, N., Sandroni, V., 2009. A phytoplankton class-specific primary production model applied to the Kerguelen Islands region (Southern Ocean). Deep. Res. Part I Oceanogr. Res. Pap. 56, 541–560. doi:10.1016/j.dsr.2008.11.006.

Usbeck, R., Schlitzer, R., Fischer, G., Wefer, G., 2003. Particle fluxes in the ocean: comparison of sediment trap data with results from inverse modeling. J. Mar. Syst. 39, 167–183. doi:http://dx.doi.org/10.1016/S0924-7963(03)00029-0.

Valdes, J.R., Price, J.F., 2000. A neutrally buoyant, upper ocean sediment trap. J. Atmos. Ocean. Technol. 17, 62–68. doi:*10.1175/1520-0426(2000)017<0062:ANBUOS>2.0.CO;2*.

van Aken, H., 2011. GEOTRACES, the hydrography of the Western Atlantic Ocean.

Van Mooy, B.A.S., Keil, R.G., Devol, A.H., 2002. Impact of suboxia on sinking particulate organic carbon: Enhanced carbon flux and preferential degradation of amino acids via denitrification. Geochim. Cosmochim. Acta 66, 457–465. doi:10.1016/S0016-7037(01)00787-6.

Verdeny, E., Masqué, P., Garcia-Orellana, J., Hanfland, C., Kirk Cochran, J., Stewart, G.M., 2009. POC export from ocean surface waters by means of $^{234}Th/^{238}U$ and $^{210}Po/^{210}Pb$ disequilibria: A review of the use of two radiotracer pairs. Deep Sea Res. Part II Top. Stud. Oceanogr. 56, 1502–1518. doi:10.1016/j.dsr2.2008.12.018.

Verdugo, P., Alldredge, A.L., Azam, F., Kirchman, D.L., Passow, U., Santschi, P.H., 2004. The oceanic gel phase: a bridge in the DOM-POM continuum. Mar. Chem. 92, 67–85. doi: 10.1016/j.marchem.2004.06.017.

Volk, T., Hoffert, M.I., 1985. Ocean Carbon Pumps: Analysis of Relative Strengths and Efficiencies in Ocean-Driven Atmospheric CO_2 Changes, in: The Carbon Cycle and Atmospheric CO_2: Natural Variations Archean to Present. American Geophysical Union, pp. 99–110. doi:10.1029/GM032p0099.

Wafar, M.V.M., Corre, P. Le, L'Helguen, S., 1995. *f*-Ratios calculated with and without urea uptake in nitrogen uptake by phytoplankton. Deep Sea Res. Part I Oceanogr. Res. Pap. 42, 1669–1674. doi:http://dx.doi.org/10.1016/0967-0637(95)00066-F.

Wakeham, S.G., Canuel, E.A., 1988. Organic geochemistry of particulate matter in the eastern tropical North Pacific Ocean: Implications for particle dynamics. J. Mar. Res. 46, 183–213. doi: 10.1357/002224088785113748.

Waples, J.T., Benitez-Nelson, C., Savoye, N., Rutgers van der Loeff, M., Baskaran, M., Gustafsson, Ö., 2006. An introduction to the application and future use of ^{234}Th in aquatic systems. Mar. Chem. 100, 166–189. doi:10.1016/j.marchem.2005.10.011.

Ward, P., 1989. The distribution of zooplankton in an Antarctic fjord at South Georgia during summer and winter. Antarct. Sci. 1, 141–150. doi:10.1017/S0954102089000210.

Weinstein, S.E., Moran, S.B., 2005. Vertical flux of particulate Al, Fe, Pb, and Ba from the upper ocean estimated from $^{234}Th/^{238}U$ disequilibria. Deep Sea Res. Part I Oceanogr. Res. Pap. 52, 1477–1488. doi:http://dx.doi.org/10.1016/j.dsr.2005.03.008.

Westberry, T., Behrenfeld, M.J., Siegel, D.A., Boss, E., 2008. Carbon-based primary productivity modeling with vertically resolved photoacclimation. Global Biogeochem. Cycles 22, GB2024. doi:10.1029/2007GB003078.

White, A.E., Foster, R.A., Benitez-Nelson, C.R., Masqué, P., Verdeny, E., Popp, B.N., Arthur, K.E., Prahl, F.G., 2013. Nitrogen fixation in the Gulf of California and the Eastern Tropical North Pacific. Prog. Oceanogr. 109, 1–17. doi: 10.1016/j.pocean.2012.09.002.

White, A.E., Prahl, F.G., Letelier, R.M., Popp, B.N., 2007. Summer surface waters in the Gulf of California: Prime habitat for biological N_2 fixation. Global Biogeochem. Cycles 21, GB2017. doi: 10.1029/2006GB002779.

Whitworth, T., Nowlin, W.D., 1987. Water masses and currents of the Southern Ocean at the Greenwich Meridian. J. Geophys. Res. Ocean. 92, 6462–6476. doi:10.1029/JC092iC06p06462.

Wolf-Gladrow, D., 2013. The Expedition of the Research Vessel "Polarstern" to the Antarctic in 2012 (ANT-XXVIII/3). Reports on Polar and Marine Research 661. Bremerhaven, Germany.

Xu, C., Santschi, P.H., Hung, C.C., Zhang, S., Schwehr, K.A., Roberts, K.A., Guo, L., Gong, G.C., Quigg, A., Long, R.A., 2011. Controls of ^{234}Th removal from the oligotrophic ocean by polyuronic acids and modification by microbial activity. Mar. Chem., 123, 111-126 doi:10.1016/j.marchem.2010.10.005.

Yool, A., Martin, A.P., Fernández, C., Clark, D.R., 2007. The significance of nitrification for oceanic new production. Nature 447, 999–1002. doi:10.1038/nature05885.

Ziveri, P., Thunell, R.C., 2000. Coccolithophore export production in Guaymas Basin, Gulf of California: response to climate forcing. Deep Sea Res. Part II Top. Stud. Oceanogr. 47, 2073–2100. doi:10.1016/S0967-0645(00)00017-5.

Appendix A

Appendix A

A.1 Supplementary information for *Chapter 3*

Table A.1.1: Information about location and date of the sampled stations, mixed layer depth (MLD; determined through subjective analysis of temperature and density profiles, generally in good agreement with the 0.02 kg m^3 criterion from Cisewski et al., 2008), fluorescence maximum (Fluor max), satellite-derived NPP using the A&M96, the VGPM and the CbPM models (see text for details).

Cruise	Domain	Location	Date	Station	Lat	Long	MLD (m)		Fluor max	A&M96	VGPM	CbPM
				#	ºN	ºW	shallow	deep	m	mmol C m^{-2} d^{-1}		
64PE319	Sub-polar	Irminger Basin	2-May	PE2	64.00	34.25	17	235	26	44.5	35.0	0.004
		Irminger Basin	4-May	PE5	60.43	37.91	10	95	35	47.2	38.8	0.13
		Irminger Basin / Labrador Sea	5-May	PE6	58.60	39.71	25	77	32	51.0	34.3	0.006
		Labrador Sea	7-May	PE8	54.06	45.84	25	NA	31	44.5	32.0	7.2
	Temperate	Newfoundland Basin	11-May	PE11	47.80	39.40	NA	NA	21	98.6	163.9	56.7
		Newfoundland Basin	12-May	PE12	46.31	39.66	NA	NA	19	92.1	116.7	51.5
		Newfoundland Basin	13-May	PE13	44.84	42.53	17	NA	21	140.0	256.1	19.9
		Sohm Abyssal Plain	17-May	PE14	39.50	48.08	115	NA	30	76.8	118.9	45.5
		Sohm Abyssal Plain	19-May	PE15	37.52	50.76	70	NA	13	69.4	97.6	35.0
		Sohm Abyssal Plain	20-May	PE16	36.21	53.29	24	110	45	72.0	116.2	6.3
64PE321	Oligotrophic	Sohm Abyssal Plain	21-May	PE17	34.33	55.43	18	80	36	76.0	97.9	24.9
		Hatteras Plain	22-May	PE18	33.43	58.05	8	26	59	46.7	56.0	21.9
		Hatteras Plain	23-May	PE19	32.55	61.10	12	53	89	38.7	38.5	17.7
		BATS // Hatteras Plain	13-Jun	PE21	31.67	64.17	11	NA	78	39.5	27.5	19.2
		Hatteras Plain	14-Jun	PE22	29.62	66.53	7	NA	88	31.5	20.5	16.7
		Blake-Bahamas Basin	15-Jun	PE23	28.09	67.50	9	NA	135	28.7	14.8	12.6
		Blake-Bahamas Basin	16-Jun	PE24	26.24	67.80	9	NA	123	26.4	13.5	12.1
		Blake-Bahamas / Nares Basin	17-Jun	PE25	24.71	67.07	6	NA	129	25.9	14.9	16.8
		Nares Plain	18-Jun	PE26	23.27	65.64	16	NA	93	30.9	13.3	17.2
		Nares Plain	19-Jun	PE27	22.34	63.58	17	NA	126	26.4	12.8	15.1
		Nares Plain	20-Jun	PE28	21.78	61.84	23	NA	121	25.1	13.5	15.3
	Riverine	Barracuda Plain	21-Jun	PE29	20.46	59.53	33	NA	124	32.9	19.5	22.5
		Barracuda Plain	22-Jun	PE30	18.57	57.61	25	NA	32	89.4	31.7	41.6
		Barracuda Plain	24-Jun	PE31	16.83	56.27	24	NA	18	113.3	74.4	39.3
		Vidal Plain	25-Jun	PE32	14.88	54.80	16	NA	20	331.0	231.9	25.4
		Demerara Plain	26-Jun	PE33	13.16	53.42	NA	NA	26	242.2	105.5	71.2
		Demerara Plain	27-Jun	PE34	11.37	52.05	26	70	101	112.8	56.8	44.6
	Equatorial	Demerara Plain	28-Jun	PE35	9.55	50.47	54	NA	101	81.2	26.5	35.6
		Demerara Plain	30-Jun	PE36	7.76	48.88	7	NA	85	131.9	48.7	31.0
		Demerara Plain	1-Jul	PE37	5.98	46.42	8	NA	55	128.0	22.7	42.7
		Demerara Plain	2-Jul	PE38	3.97	43.75	8	NA	72	81.1	20.7	37.9
		Ceará Plain	3-Jul	PE39	2.54	41.70	28	63	69	44.4	19.3	41.8
		Ceará Plain	4-Jul	PE40	1.15	39.69	26	58	79	45.4	22.9	51.5

Table A.1.2: ^{234}Th fluxes at 100 m, at the PPZ and at the deficit depth at each station.

Cruise	Domain	Station	Lat	^{234}Th flux at 100m	Depth PPZ	^{234}Th flux at PPZ	Depth deficit	^{234}Th flux at deficit depth
		#	ºN	dpm m^{-2} d^{-1}	m	dpm m^{-2} d^{-1}	m	dpm m^{-2} d^{-1}
64PE319	Sub-polar	PE2	64,00	320 ± 190	255	-6 ± 390	150	420 ± 250
		PE5	60.43	1040 ± 160	129	1180 ± 190	200	1420 ± 300
		PE6	58.60	2740 ± 130	132	3620 ± 150	200	4810 ± 240
		PE8	54.06	280 ± 180	75	270 ± 150	50	270 ± 130
	Temperate	PE11	47.80	470 ± 180	67	360 ± 150	250	880 ± 340
		PE12	46.31	710 ± 170	60	560 ± 140	150	700 ± 220
		PE13	44.84	710 ± 180	65	470 ± 150	250	1870 ± 330
		PE14	39.50	1350 ± 200	153	1890 ± 270	250	2530 ± 400
		PE15	37.52	1740 ± 170	110	1860 ± 180	150	1970 ± 220
		PE16	36.21	1650 ± 170	157	1900 ± 250	150	1870 ± 230
	Oligotrophic	PE17	34.33	1170 ± 180	90	1080 ± 170	100	1170 ± 180
		PE18	33.43	1270 ± 180	102	1280 ± 190	75	1570 ± 280
		PE19	32.55	720 ± 200	163	840 ± 290	150	870 ± 270
64PE321		PE21	31.67	610 ± 160	135	650 ± 440	50	440 ± 170
		PE22	29.62	-250 ± 210	150	-810 ± 240	-	No deficit
		PE23	28.09	77 ± 200	301	310 ± 370	150	52 ± 520
		PE24	26.24	-620 ± 180	235	-1860 ± 340	-	No deficit
		PE25	24.71	320 ± 160	173	550 ± 220	175	550 ± 220
		PE26	23.27	-310 ± 180	150	-380 ± 210	-	No deficit
		PE27	22.34	140 ± 190	190	220 ± 290	100	140 ± 190
		PE28	21.78	510 ± 160	225	1200 ± 280	225	1200 ± 280
	Riverine	PE29	20.46	930 ± 110	220	420 ± 210	100	930 ± 110
		PE30	18.57	490 ± 220	185	800 ± 280	200	830 ± 300
		PE31	16.83	670 ± 150	31	540 ± 84	75	650 ± 130
		PE32	14.88	1020 ± 160	52	930 ± 110	50	920 ± 100
		PE33	13.16	1480 ± 140	84	1440 ± 120	100	1480 ± 140
		PE34	11.37	670 ± 160	180	1550 ± 250	200	1680 ± 280
	Equatorial	PE35	9.55	800 ± 170	174	1130 ± 240	150	1130 ± 210
		PE36	7.76	830 ± 110	140	830 ± 140	250	1490 ± 270
		PE37	5.98	630 ± 140	128	750 ± 160	250	1130 ± 370
		PE38	3.97	680 ± 130	135	340 ± 170	83	680 ± 110
		PE39	2.54	640 ± 130	151	550 ± 190	100	640 ± 130
		PE40	1.15	360 ± 150	140	440 ± 200	150	460 ± 200

Table A.1.3: C/^{234}Th ratios obtained during this study (numbers in italics indicate averaged values obtained for each domain), together with C fluxes at 100 m calculated using different C/^{234}Th ratios (see text for further details).

Cruise	Domain	Station #	Lat °N	C/^{234}Th from this study µmol C dpm^{-1}	C flux using C/^{234}Th ratios from this study mmol C m^{-2} d^{-1}	C flux using C/^{234}Th ratios from compilation mmol C m^{-2} d^{-1}	C flux using C/^{234}Th ratios from fitting curve mmol C m^{-2} d^{-1}
64PE319	Sub-polar	PE2	64,00	4.692 ± 0.064	1.48 ± 0.89	3.2 ± 2.6	0.9 ± 1.0
		PE5	60.43	*7.6 ± 7.1*	*7.8 ± 7.5*	10.5 ± 6.0	2.8 ± 3.4
		PE6	58.60	15.68 ± 0.22	43.0 ± 2.1	28 ± 15	7.5 ± 8.9
		PE8	54.06	2.323 ± 0.015	0.66 ± 0.41	2.9 ± 2.4	0.78 ± 0.92
	Temperate	PE11	47.80	8.02 ± 0.16	3.7 ± 1.4	2.6 ± 1.5	1.3 ± 1.5
		PE12	46.31	*6.7 ± 1.9*	*4.7 ± 1.8*	3.9 ± 2.0	2.0 ± 2.3
		PE13	44.84	5.306 ± 0.064	3.79 ± 0.95	3.9 ± 2.0	2.0 ± 2.3
		PE14	39.50	*6.7 ± 1,9*	*9.0 ± 2.9*	7.4 ± 3.4	3.7 ± 4.4
		PE15	37.52	*6.7 ± 1,9*	*11.6 ± 3.5*	9.5 ± 4.3	4.8 ± 5.7
		PE16	36.21	*6.7 ± 1,9*	*11.0 ± 3.3*	9.0 ± 4.1	4.5 ± 5.4
	Oligotrophic	PE17	34.33	*10.2 ± 5.4*	*11.9 ± 6.6*	4.3 ± 2.8	3.2 ± 3.8
		PE18	33.43	*10.2 ± 5.4*	*13.0 ± 7.1*	4.6 ± 3.0	3.5 ± 4.1
		PE19	32.55	*10.2 ± 5.4*	*7.3 ± 4.4*	2.6 ± 1.8	2.0 ± 2.3
64PE321		PE21	31.67	9.47 ± 0.56	5.8 ± 1.6	2.2 ± 1.5	1.7 ± 2.0
		PE22	29.62	*10.2 ± 5.4*	*-2.6 ± -2.5*	-0.92 ± -0.96	-0.69 ± -0.82
		PE23	28.09	16.1 ± 1.9	1.2 ± 3.3	0.28 ± 0.76	0.21 ± 0.25
		PE24	26.24	*10.2 ± 5.4*	*-6.3 ± -3.8*	-2.3 ± -1.6	-1.7 ± -2.0
		PE25	24.71	*10.2 ± 5.4*	*3.3 ± 2.4*	1.16 ± 0.95	0.9 ± 1.0
		PE26	23.27	5.231 ± 0.081	-1.63 ± -0.92	-1.14 ± -0.97	-0.9 ± -1.0
		PE27	22.34	*10.2 ± 5.4*	*1.4 ± 2.0*	0.50 ± 0.75	0.38 ± 0.45
		PE28	21.78	*10.2 ± 5.4*	*5.3 ± 3.2*	1.9 ± 1.3	1.4 ± 1.7
	Riverine	PE29	20.46	*7.47 ± 7.25*	*7.0 ± 6.8*	13.0 ± 8.7	2.6 ± 3.0
		PE30	18.57	12.56 ± 0.86	6.2 ± 2.8	6.9 ± 5.5	1.4 ± 1.6
		PE31	16.83	*7.47 ± 7.25*	*5.0 ± 5.0*	9.3 ± 6.5	1.8 ± 2.2
		PE32	14.88	*7.47 ± 7.25*	*7.7 ± 7.5*	14.3 ± 9.8	2.8 ± 3.3
		PE33	13.16	2.344 ± 0.057	3.46 ± 0.34	21 ± 13	4.1 ± 4.8
		PE34	11.37	*7.47 ± 7.25*	*5.0 ± 5.0*	9.4 ± 6.6	1.8 ± 2.2
	Equatorial	PE35	9.55	*4.14 ± 0.11*	*3.28 ± 0.69*	7.0 ± 6.5	2.2 ± 2.6
		PE36	7.76	4.14 ± 0.11	3.39 ± 0.45	7.2 ± 6.6	2.3 ± 2.7
		PE37	5.98	*4.14 ± 0.11*	*2.56 ± 0.57*	5.5 ± 5.1	1.7 ± 2.0
		PE38	3.97	*4.14 ± 0.11*	*2.78 ± 0.54*	5.9 ± 5.5	1.9 ± 2.2
		PE39	2.54	*4.14 ± 0.11*	*2.61 ± 0.54*	5.6 ± 5.2	1.8 ± 2.1
		PE40	1.15	*4.14 ± 0.11*	*1.48 ± 0.60*	3.2 ± 3.1	1.0 ± 1.2

A.2 Supplementary information for *Chapter 4*

Physical transport processes: effect on ^{234}Th export fluxes

In order to explore the influence of advective and diffusive fluxes on the ^{234}Th export fluxes, below we discuss the limitations to quantify such processes in the present work and provide an estimate of their magnitude with respect to the ^{234}Th downward export fluxes at 100 m.

The physical transport processes (V) can be expressed as the sum of the advective and diffusive components along the x, y and z direction as follows:

$$V = \pm u\frac{\partial A_{Th}}{\partial x} \pm v\frac{\partial A_{Th}}{\partial y} \pm w\frac{\partial A_{Th}}{\partial z} \pm K_x\frac{\partial^2 A_{Th}}{\partial x^2} \pm K_y\frac{\partial^2 A_{Th}}{\partial y^2} \pm K_z\frac{\partial^2 A_{Th}}{\partial z^2} \qquad (A.2.1)$$

Where the advection fluxes in the different directions are defined by u, v and w, which represent the velocities, multiplied by the respective ^{234}Th activity gradients, $\frac{\partial A_{Th}}{\partial x}$, $\frac{\partial A_{Th}}{\partial y}$ and $\frac{\partial A_{Th}}{\partial z}$, and the diffusivity fluxes are expressed by the multiplication between the different diffusivity coefficients, K_x, K_y and K_z and the respective second derivative of the ^{234}Th activity gradients, $\frac{\partial^2 A_{Th}}{\partial x^2}$, $\frac{\partial^2 A_{Th}}{\partial y^2}$ and $\frac{\partial^2 A_{Th}}{\partial z^2}$.

Advection

The main stream of the currents along the transect was eastward (see Strass et al., 2016), however, we do not have the ^{234}Th gradient in that direction to be able to calculate the zonal advection fluxes. Yet, considering that ^{234}Th profiles measured further west (51ºS, 12ºW) (Roca-Martí et al., 2016) were reasonably consistent with the ones measured along the 10ºE transect we assume that the horizontal gradient in ^{234}Th inventories is small, hence the lateral net flux, although we cannot provide a proper estimate.

Given that the ^{234}Th deficits represent a time integral over a few weeks, the meridional advection fluxes were calculated using the mean meridional velocities in the upper 100 m to be 0.025 m s^{-1} (Naveira Garabato et al., 2001). Thus, the meridional advective fluxes would represent <10% of the downward ^{234}Th flux.

Strass et al. (2002b) observed upwelling and downwelling mesoscale cells that, despite being rather weak, had effects on biological processes. However, ^{234}Th export fluxes from the same

expedition presented in Rutgers van der Loeff et al. (2002), remained constant in time and space. The ^{234}Th deficits examined here do not suggest strong upwelling or downwelling either. During Eddy-Pump mesoscale vertical velocities were however not determined. While measurements of horizontal currents by the ships acoustic Doppler current profiler (ADCP) revealed variations on the mesoscale (Strass et al., 2016) we do not have reason to assume that the associated vertical velocities exceeded those reported in previous studies. Averaged in time over periods longer than the timescale associated with the mesoscale dynamics (days to months) the eddy-driven meridional overturning will approximately compensate the wind-driven Ekman flow (Bryden, 1979; Strass et al., 2002b). In fact, buoy trajectories shown in Strass et al. (2016), do not give evidence for an Ekman or meridional flow in the mixed layer. Additionally, due to the integration time scale of the ^{234}Th proxy, temporal peaks of intense vertical advective flow lasting a few days typically could also be unnoticed. Thus, we neglect possible upwelling and downwelling fluxes linked to mesoscale dynamics due to their relative temporal nature regarding velocities and direction, since they might be masked by longer integration times on ^{234}Th export fluxes and by geostrophic flows.

Downwelling of surface waters occurs in the Antarctic Convergence, with average annual velocities up to 200 m y^{-1}, although in the transect covered during this study the maximum downwelling velocities are expected to be in the order of ~50 m y^{-1} (Sallée et al., 2010). Upwelling of deep-water masses occurs further south, in the Antarctic Divergence (average latitude 65ºS; Gordon, 1971), thus it is considered to play a minimal role compared to the ^{234}Th downward flux in our study area. However, assuming a typical annual average upwelling velocity of 0.1 m d^{-1}, reported by Buesseler et al. (2001) based on the mean climatological winds, and similar to that reported earlier by Gordon et al. (1977) (15 x 10^{-5} cm s^{-1}) that were used in previous studies taken place in the same region (i.e., Friedrich and Rutgers van der Loeff, 2002; Klunder et al., 2011), and downwelling velocities reported in Sallée et al. (2010), the vertical advective fluxes in the upper 100 m would represent <10% of the estimated export fluxes, except for the southernmost stations where this percentage would increase to 13% and 15% at 52ºS and 53ºS, respectively.

Diffusion

Although generally small compared to advection fluxes in the open ocean, diffusion fluxes can also be considered when estimating ^{234}Th fluxes. However, due to the scarce spatial coverage, as well as the lack of horizontal diffusion coefficients, only the vertical diffusion could be calculated. Strass et al., (2016) provide vertical diffusivity values, based on the Thorpe scale (K_T), ranging from 10^{-4} to 10^{-3} m^2 s^{-1}, and derived from a free-falling microstructure profiler (MSS) of 4 x 10^{-5} m^2

s^{-1}. These diffusion coefficients were obtained during the expedition but at different locations, however, they are in agreement with previous reported values for the ACC (Cisewski et al., 2005; Naveira Garabato et al., 2004).

Here the $\frac{\partial^2 A_{Th}}{\partial z^2}$ is defined as the activity gradient between 100 ± 20 m depth and we consider a K_z value of 10^{-4} m^2 s^{-1}, the mean of the K_z values reported Strass et al. (2016) and of the same order of magnitude that the K_z reported by Law et al. (2003) and Hibbert et al. (2009) for the ACC. The vertical diffusivity flux would represent <10% of the ^{234}Th export flux, similar to the meridional advective fluxes.

Overall, the advective and diffusive fluxes estimated would represent 7-17% of the ^{234}Th export fluxes at 100 m contributing to increase the ^{234}Th flux uncertainties from 6-12% to 10-21%.

A.3 Supplementary information for *Chapter 5*

Table A.3.1: Concentration profiles of ^{234}Th, C and N and stable isotopic composition for particulate samples[a]

		Large particles						Small particles						Sediment traps		
Sta.	Depth (m)	^{234}Th (dpm/L)	PC (µmol/L)	PN (µmol/L)	PC/PN	δ^{15}N ‰	δ^{13}C ‰	^{234}Th (dpm/L)	PC (umol/L)	PN (umol/L)	PC/PN	δ^{15}N ‰	δ^{13}C ‰	PC/PN	δ^{15}N ‰	δ^{13}C ‰
GC4-1	30	0.041 ± 0.002	0.38	0.046	8	9.9	-20.3	0.12 ± 0.01	1.30	0.21	6	9.2	-21.8			
	50	0.083 ± 0.005	0.72	0.097	7	12.3	-21.1	0.16 ± 0.01	3.29	0.55	6	11.1	-22.5			
	70	0.155 ± 0.014	0.39	0.048	8	12.4	-20.4	0.24 ± 0.01	1.15	0.18	6	12.5	-21.3			
	115	0.194 ± 0.005	0.31	0.035	9	13.1	-19.7	0.25 ± 0.02	0.59	0.09	6	14.2	-21.5	8	11.5	-21.5
	130	0.140 ± 0.006	0.22	0.026	9	13.7	-20.3	0.30 ± 0.02	0.65	0.10	6	14.2	-21.6			
	199	0.107 ± 0.007	0.17	0.019	9	13.2	-20.7	0.33 ± 0.02	0.51	0.08	6	14.6	-21.2			
	300	0.131 ± 0.012	0.16	0.014	11	13.1	-20.0	0.36 ± 0.02	0.48	0.07	7	15.0	-20.5			
	476	0.102 ± 0.009	0.12	NA	NA	NA	-19.5	0.34 ± 0.02	0.40	0.05	7	14.6	-20.9			
GC4-2	10	0.024 ± 0.002	0.17	0.018	10	7.9	-19.1	0.18 ± 0.01	1.68	0.24	7	7.1	-21.8			
	20	0.028 ± 0.001	0.18	0.018	10	8.4	-18.6	0.24 ± 0.02	2.14	0.18	6	12.3	-21.7			
	30	0.055 ± 0.003	0.26	0.021	12	8.6	-19.3	0.40 ± 0.03	3.14	0.42	8	9.5	-21.7			
	40	0.091 ± 0.006	0.38	0.034	11	8.3	-19.6	0.12 ± 0.01	2.01	0.27	7	9.2	-22.3			
	55	0.083 ± 0.008	0.22	0.026	9	10.1	-20.2	0.24 ± 0.02	1.40	0.24	6	11.6	-22.1			
	80	0.051 ± 0.002	0.13	0.015	8	7.4	-20.2	0.23 ± 0.02	1.10	0.35	6	7.1	-21.2	8	10.0	-22.0
	85	0.090 ± 0.006	0.25	0.023	11	9.2	-19.2	0.22 ± 0.01	1.32	0.24	6	10.4	-22.0			
	108	0.142 ± 0.013	0.20	0.021	10	10.6	-19.7	0.34 ± 0.03	1.06	0.17	6	14.5	-20.9			
	147	0.302 ± 0.019	0.25	0.024	10	10.5	-20.0	0.40 ± 0.04	0.98	0.15	6	11.0	-21.9			
	155	0.291 ± 0.027	0.23	0.021	11	10.4	-19.8	0.52 ± 0.04	1.66	0.25	7	13.2	-21.7			
	237	0.188 ± 0.017	0.16	0.014	12	9.4	-20.4	0.62 ± 0.04	1.10	0.16	7	10.0	-22.0			
	277	0.122 ± 0.011	0.12	0.009	13	10.2	-20.7	NA	NA	NA	NA	NA	NA			
GC4-2b	10	0.020 ± 0.001	0.09	0.009	10	7.6	-19.5	0.14 ± 0.01	0.90	0.12	7	6.7	-22.4	7	11.2	-19.6
	20	0.008 ± 0.001	0.07	0.007	11	8.0	-18.8	0.17 ± 0.01	1.06	0.15	7	8.3	-22.0			
	30	0.040 ± 0.003	0.20	0.023	9	8.1	-19.5	0.25 ± 0.03	2.12	0.29	7	8.2	-21.5			
	40	0.085 ± 0.008	0.30	0.035	9	8.4	-20.0	0.21 ± 0.02	2.16	0.35	6	8.7	-21.9			
	60	0.105 ± 0.003	0.35	0.040	9	8.4	-19.8	0.14 ± 0.01	1.69	0.26	6	7.6	-23.4			
	80	0.098 ± 0.004	0.18	0.020	9	9.1	-19.9	0.27 ± 0.02	1.26	0.23	5	9.6	-21.8			
	100	0.079 ± 0.005	0.18	0.021	9	9.3	-20.1	0.23 ± 0.02	1.15	0.19	6	10.0	-20.8			
	125	0.105 ± 0.010	0.14	0.017	8	11.2	-20.4	0.32 ± 0.02	0.67	0.11	6	13.1	-22.0			
	150	0.141 ± 0.013	0.10	0.010	9	10.6	-21.0	0.36 ± 0.03	0.48	0.07	7	13.7	-21.6			
	200	0.212 ± 0.006	0.13	0.014	9	10.9	-21.1	0.34 ± 0.02	0.49	0.08	6	13.1	-21.2			
	250	0.134 ± 0.006	0.09	0.011	9	11.5	-20.7	0.38 ± 0.03	0.50	0.08	6	14.6	-20.8			

(continues)

(Table A.3.1 continued)

Sta.	Depth (m)	Large particles ^{234}Th (dpm/L)	PC (µmol/L)	PN (µmol/L)	PC/PN	δ^{15}N ‰	δ^{13}C ‰	Small particles ^{234}Th (dpm/L)	PC (umol/L)	PN (umol/L)	PC/PN	δ^{15}N ‰	δ^{13}C ‰	Sediment traps PC/PN	δ^{15}N ‰	δ^{13}C ‰
GC4-8	10	0.007 ± 0.001	0.07	0.006	10	6.8	-19.4	0.10 ± 0.01	0.76	0.12	6	7.6	-21.3			
	20	0.044 ± 0.001	0.24	0.021	11	7.4	-18.5	0.43 ± 0.02	2.65	0.36	7	10.1	-21.7			
	35	0.058 ± 0.003	0.17	0.014	12	8.7	-18.1	0.38 ± 0.03	1.55	0.21	8	8.5	-21.6			
	57	0.168 ± 0.007	0.24	0.025	9	8.9	-19.9	0.44 ± 0.03	2.03	0.33	6	8.8	-22.1			
	80	0.055 ± 0.004	0.08	0.009	9	8.9	-20.4	0.30 ± 0.03	1.13	0.21	6	9.4	-21.9			
	100	0.041 ± 0.004	0.08	0.009	8	9.3	-21.0	0.16 ± 0.01	0.63	0.13	5	14.3	-22.2	7	11.6	-21.0
	120	0.054 ± 0.005	0.07	0.007	9	10.3	-20.8	0.22 ± 0.02	0.45	0.08	6	13.1	-22.2			
	150	0.109 ± 0.007	0.09	0.010	10	9.1	-21.3	0.70 ± 0.07	1.17	0.17	7	11.2	-21.6			
	200	0.101 ± 0.009	0.06	0.007	8	6.5	NA	0.49 ± 0.03	0.73	0.10	7	11.5	-21.2			
	250	0.121 ± 0.011	0.09	0.009	10	8.8	-20.9	0.50 ± 0.03	0.70	0.09	7	11.4	-21.5			
	298	0.069 ± 0.002	0.08	0.007	11	7.8	-19.5	0.27 ± 0.01	0.50	0.07	7	11.4	-21.7			
GC4-9	10	0.025 ± 0.002	0.15	0.015	10	9.7	-19.3	0.24 ± 0.02	1.58	0.22	7	8.9	-21.7			
	25	0.047 ± 0.003	0.35	0.039	9	10.6	-19.4	0.18 ± 0.02	1.25	0.19	6	9.9	-21.3			
	40	0.065 ± 0.006	0.36	0.041	9	11.1	-19.9	0.21 ± 0.02	2.05	0.33	6	10.0	-21.6			
	50	0.096 ± 0.009	0.50	0.062	8	10.8	-20.5	0.19 ± 0.01	1.66	0.29	6	7.8	-23.6			
	56	0.050 ± 0.002	0.14	0.017	8	11.1	-21.0	0.21 ± 0.01	1.47	0.25	6	10.4	-24.3			
	63	0.054 ± 0.003	0.11	0.014	8	10.7	-20.0	0.19 ± 0.01	0.72	0.12	6	10.3	-24.0	8	10.8	-22.4
	73	0.059 ± 0.004	0.12	0.013	9	10.3	-20.5	0.25 ± 0.02	0.54	0.09	6	11.6	NA			
	100	0.058 ± 0.006	0.06	0.006	9	10.9	-20.1	0.26 ± 0.02	0.34	0.06	6	13.5	-22.7			
	125	0.057 ± 0.004	0.08	0.008	11	10.5	-19.9	0.23 ± 0.02	0.27	0.05	6	13.1	-22.3			
	144	0.052 ± 0.003	0.07	0.007	10	8.6	-18.9	0.19 ± 0.01	0.25	0.05	5	9.7	-21.8			
	200	NA	NA	NA	NA	NA	NA	0.26 ± 0.01	0.35	0.05	7	10.2	-21.2			
	251	0.064 ± 0.006	0.07	0.006	11	9.2	-19.4	0.18 ± 0.01	0.16	0.03	5	11.1	-21.1			
GC4-10	10	0.062 ± 0.003	0.23	0.024	10	9.5	-20.2	0.22 ± 0.01	NA	NA	NA	NA	NA			
	25	0.086 ± 0.008	0.31	0.036	9	8.4	-20.5	0.13 ± 0.01	1.51	0.22	7	8.6	-21.8			
	40	0.080 ± 0.008	0.22	0.026	9	8.4	-21.2	0.24 ± 0.02	2.50	0.38	7	8.5	-22.4			
	51	0.142 ± 0.004	0.44	0.049	9	8.4	-20.3	0.18 ± 0.01	2.50	0.41	6	7.6	-23.6			
	60	0.338 ± 0.014	1.03	0.111	9	8.3	-20.2	0.22 ± 0.02	2.54	0.41	6	6.9	-23.1			
	70	0.256 ± 0.016	NA	NA	NA	NA	NA	0.18 ± 0.01	1.73	0.29	6	8.5	-23.6	7	9.3	-22.5
	80	0.174 ± 0.016	0.36	0.042	9	8.7	-20.7	0.30 ± 0.02	1.67	0.26	7	8.9	-23.4			
	101	0.037 ± 0.004	0.06	0.006	11	9.6	-20.0	0.25 ± 0.02	0.58	0.07	8	13.3	-21.8			
	120	0.050 ± 0.005	0.07	0.006	11	9.2	-18.8	0.25 ± 0.02	0.37	0.05	7	12.6	-20.6			
	150	0.043 ± 0.002	0.04	0.004	11	7.7	-18.5	0.23 ± 0.01	0.36	0.04	8	11.8	-21.2			
	200	0.058 ± 0.003	0.07	0.005	13	8.6	-18.1	0.24 ± 0.02	0.32	0.04	9	12.6	-21.6			
	247	0.028 ± 0.002	0.03	0.003	10	7.6	-20.7	0.27 ± 0.03	0.35	0.04	9	12.7	-21.2			

(continues)

(Table A.3.1 continued)

Sta.	Depth (m)	Large particles ^{234}Th (dpm/L)	PC (µmol/L)	PN (µmol/L)	PC/PN	δ^{15}N ‰	δ^{13}C ‰	Small particles ^{234}Th (dpm/L)	PC (umol/L)	PN (umol/L)	PC/PN	δ^{15}N ‰	δ^{13}C ‰	Sediment traps PC/PN	δ^{15}N ‰	δ^{13}C ‰
GC4-11	10	0.032 ± 0.002	0.18	0.021	9	8.1	-21.6	0.21 ± 0.02	1.71	0.23	7	7.2	-22.4			
	25	0.063 ± 0.005	0.25	0.024	10	9.2	-21.4	0.23 ± 0.02	1.63	0.20	8	8.6	-22.5			
	40	0.059 ± 0.006	0.17	0.019	9	8.4	-21.7	0.28 ± 0.02	2.47	0.35	7	8.5	-22.5			
	49	0.032 ± 0.003	0.16	0.018	8	9.6	-20.8	0.24 ± 0.02	2.62	0.40	6	8.9	-22.7			
	59	0.032 ± 0.003	0.10	0.012	9	9.0	-21.2	0.15 ± 0.01	1.51	0.26	6	7.8	-23.0	10	8.3	-24.0
	75	0.035 ± 0.002	0.07	0.007	10	8.0	-21.7	0.19 ± 0.02	1.36	0.21	6	8.2	-23.4			
	123	0.049 ± 0.005	0.05	0.006	9	12.1	-19.6	0.31 ± 0.02	0.84	0.14	6	12.9	-19.8			
	150	0.062 ± 0.002	0.08	0.008	9	11.1	NA	0.21 ± 0.02	0.43	0.06	7	12.2	-20.1			
	200	0.079 ± 0.004	0.09	0.009	10	10.5	-19.3	0.27 ± 0.02	0.35	0.05	7	13.1	-20.3			
	248	0.090 ± 0.006	0.09	0.008	12	9.4	-19.2	0.42 ± 0.03	0.52	0.07	7	11.8	-19.7			
GC4-12	10	0.178 ± 0.016	1.30	0.338	4	11.9	-19.6	0.05 ± 0.01	0.94	0.14	7	14.2	-21.5			
	25	0.162 ± 0.015	0.99	0.262	4	11.8	-19.2	0.13 ± 0.01	3.42	0.53	6	NA	-21.2			
	40	0.163 ± 0.005	0.39	0.052	8	10.1	-19.6	0.09 ± 0.01	2.20	0.38	6	8.6	-22.7			
	80	0.040 ± 0.002	0.08	0.007	10	10.1	-21.1	0.33 ± 0.02	0.78	0.12	7	11.1	-20.7			
	145	0.065 ± 0.003	0.08	0.008	10	NA	-20.4	0.31 ± 0.02	0.62	0.09	7	12.0	-20.3	8	9.2	21.2
	190	0.086 ± 0.004	0.05	0.005	9	9.4	-21.1	0.36 ± 0.02	0.60	0.09	7	12.1	-19.8			
	241	0.047 ± 0.003	0.07	0.007	9	9.3	-19.9	0.30 ± 0.02	0.47	0.07	7	11.3	-20.0			
	325	0.041 ± 0.003	0.05	0.004	12	8.0	-20.5	0.21 ± 0.01	0.30	0.05	6	12.3	-20.9			
	448	0.028 ± 0.003	0.03	0.002	12	9.6	-21.2	0.21 ± 0.02	0.21	0.03	7	11.8	NA			
Avg					10						7			8		
Std					2						1			1		
Min					4						5			7		
Max					13						9			10		

[a]Small and large particles collected with *in situ* pumps at different depths and sediment trap material collected at 100 m. NA is noted when samples were not available or the parameter was not possible to measure or calculate due to low concentrations or because one of the parameters needed was not available.

Appendix B

B.1 Raw data for *Chapter 3*

Data presented in *Chapter 3* was included in the GEOTRACES Intermediate Data Product 2014 and is available for download from the GEOTRACES Data Management Committee website (http://www.bodc.ac.uk/geotraces/data/idp2014/)

B.2 Raw data for *Chapter 4*

Data presented in *Chapter 4* is available for download from the PANGAEA (http://dx.doi.org/10.1594/PANGAEA.848823)

B.3 Raw data for *Chapter 5*

Table B.3.1: Station location, sampling date, concentration profiles of ^{234}Th and ^{238}U (dpm L^{-1}) and salinity.

Station	Latitude (°N)	Longitude (°E)	Sampling date	Depth (m)	^{234}Th (dpm L^{-1})	^{238}U (dpm L^{-1})	Salinity
GC4-1	26.31	-110.17	13/jul/2008	5	1.58 ± 0.13	2.51 ± 0.04	35.23
GC4-1	26.31	-110.17	13/jul/2008	25	1.52 ± 0.16	2.49 ± 0.04	34.93
GC4-1	26.31	-110.17	13/jul/2008	50	1.83 ± 0.19	2.48 ± 0.04	34.71
GC4-1	26.31	-110.17	13/jul/2008	75	1.44 ± 0.08	2.48 ± 0.04	34.77
GC4-1	26.31	-110.17	13/jul/2008	100	1.56 ± 0.10	2.49 ± 0.04	34.99
GC4-1	26.31	-110.17	13/jul/2008	125	1.74 ± 0.13	2.49 ± 0.04	34.96
GC4-1	26.31	-110.17	13/jul/2008	150	1.99 ± 0.20	2.49 ± 0.04	34.93
GC4-1	26.31	-110.17	13/jul/2008	175	2.15 ± 0.22	2.49 ± 0.04	34.93
GC4-1	26.31	-110.17	13/jul/2008	200	1.85 ± 0.09	2.48 ± 0.04	34.84
GC4-1	26.31	-110.17	13/jul/2008	225	2.18 ± 0.13	2.49 ± 0.04	34.89
GC4-1	26.31	-110.17	13/jul/2008	250	1.93 ± 0.15	2.49 ± 0.04	34.86
GC4-1	26.31	-110.17	13/jul/2008	275	2.15 ± 0.22	2.49 ± 0.04	34.86
GC4-1	26.31	-110.17	13/jul/2008	300	2.17 ± 0.23	2.48 ± 0.04	34.83
GC4-1	26.31	-110.17	13/jul/2008	350	1.95 ± 0.10	2.48 ± 0.04	34.80
GC4-1	26.31	-110.17	13/jul/2008	400	2.16 ± 0.13	2.48 ± 0.04	34.74
GC4-1	26.31	-110.17	13/jul/2008	450	2.21 ± 0.17	2.47 ± 0.04	34.70
GC4-1	26.31	-110.17	13/jul/2008	500	2.28 ± 0.24	2.47 ± 0.04	34.65
GC4-1	26.31	-110.17	13/jul/2008	550	2.10 ± 0.22	2.47 ± 0.04	34.63
GC4-1	26.31	-110.17	13/jul/2008	600	2.17 ± 0.12	2.47 ± 0.04	34.59
GC4-1	26.31	-110.17	13/jul/2008	650	2.23 ± 0.14	2.47 ± 0.04	34.58
GC4-1	26.31	-110.17	13/jul/2008	700	2.22 ± 0.17	2.46 ± 0.04	34.56
GC4-1	26.31	-110.17	13/jul/2008	800	2.51 ± 0.26	2.46 ± 0.04	34.54
GC4-1	26.31	-110.17	13/jul/2008	900	2.42 ± 0.26	2.46 ± 0.04	34.53
GC4-1	26.31	-110.17	13/jul/2008	1000	2.20 ± 0.11	2.46 ± 0.04	34.54

Station	Latitude (°N)	Longitude (°E)	Sampling date	Depth (m)	^{234}Th (dpm L^{-1})	^{238}U (dpm L^{-1})	Salinity
GC4-2	24.40	-109.02	16/jul/2008	5	1.63 ± 0.10	2.48 ± 0.04	34.84
GC4-2	24.40	-109.02	16/jul/2008	20	1.51 ± 0.11	2.49 ± 0.04	34.92
GC4-2	24.40	-109.02	16/jul/2008	40	1.65 ± 0.17	2.48 ± 0.04	34.81
GC4-2	24.40	-109.02	16/jul/2008	60	0.78 ± 0.08	2.47 ± 0.04	34.66
GC4-2	24.40	-109.02	16/jul/2008	80	1.14 ± 0.06	2.47 ± 0.04	34.64
GC4-2	24.40	-109.02	16/jul/2008	100	1.04 ± 0.06	2.47 ± 0.04	34.66
GC4-2	24.40	-109.02	16/jul/2008	125	1.48 ± 0.12	2.47 ± 0.04	34.69
GC4-2	24.40	-109.02	16/jul/2008	150	1.80 ± 0.18	2.47 ± 0.04	34.71
GC4-2	24.40	-109.02	16/jul/2008	175	1.92 ± 0.20	2.48 ± 0.04	34.72
GC4-2	24.40	-109.02	16/jul/2008	200	2.10 ± 0.10	2.48 ± 0.04	34.77
GC4-2	24.40	-109.02	16/jul/2008	220	2.23 ± 0.13	2.48 ± 0.04	34.78
GC4-2	24.40	-109.02	16/jul/2008	227	2.10 ± 0.16	2.49 ± 0.04	34.86
GC4-2	24.40	-109.02	16/jul/2008	255	2.43 ± 0.25	2.48 ± 0.04	34.80
GC4-2	24.40	-109.02	16/jul/2008	275	2.45 ± 0.25	2.48 ± 0.04	34.77
GC4-2	24.40	-109.02	16/jul/2008	300	2.44 ± 0.12	2.48 ± 0.04	34.76
GC4-2	24.40	-109.02	16/jul/2008	400	2.24 ± 0.18	2.47 ± 0.04	34.67
GC4-2	24.40	-109.02	16/jul/2008	450	2.70 ± 0.28	2.47 ± 0.04	34.63
GC4-2	24.40	-109.02	16/jul/2008	500	2.42 ± 0.25	2.47 ± 0.04	34.59
GC4-2	24.40	-109.02	16/jul/2008	600	2.41 ± 0.12	2.47 ± 0.04	34.57
GC4-2	24.40	-109.02	16/jul/2008	700	2.32 ± 0.14	2.46 ± 0.04	34.55
GC4-2	24.40	-109.02	16/jul/2008	800	2.24 ± 0.17	2.46 ± 0.04	34.53
GC4-2	24.40	-109.02	16/jul/2008	900	2.27 ± 0.23	2.46 ± 0.04	34.54
GC4-2	24.40	-109.02	16/jul/2008	1000	2.29 ± 0.18	2.46 ± 0.04	34.55
GC4-8	20.50	-106.50	20/jul/2008	5	1.77 ± 0.19	2.45 ± 0.04	34.36
GC4-8	20.50	-106.50	20/jul/2008	20	1.77 ± 0.19	2.46 ± 0.04	34.48
GC4-8	20.50	-106.50	20/jul/2008	60	1.65 ± 0.11	2.48 ± 0.04	34.81
GC4-8	20.50	-106.50	20/jul/2008	80	1.99 ± 0.12	2.47 ± 0.04	34.66
GC4-8	20.50	-106.50	20/jul/2008	100	2.37 ± 0.25	2.46 ± 0.04	34.53
GC4-8	20.50	-106.50	20/jul/2008	120	2.65 ± 0.28	2.47 ± 0.04	34.61
GC4-8	20.50	-106.50	20/jul/2008	140	2.21 ± 0.12	2.48 ± 0.04	34.79
GC4-8	20.50	-106.50	20/jul/2008	160	2.49 ± 0.16	2.48 ± 0.04	34.81
GC4-8	20.50	-106.50	20/jul/2008	180	2.22 ± 0.18	2.48 ± 0.04	34.81
GC4-8	20.50	-106.50	20/jul/2008	200	2.55 ± 0.27	2.48 ± 0.04	34.80
GC4-8	20.50	-106.50	20/jul/2008	225	2.62 ± 0.28	2.48 ± 0.04	34.80
GC4-8	20.50	-106.50	20/jul/2008	250	2.38 ± 0.13	2.48 ± 0.04	34.78
GC4-8	20.50	-106.50	20/jul/2008	300	2.54 ± 0.16	2.48 ± 0.04	34.72
GC4-8	20.50	-106.50	20/jul/2008	350	2.40 ± 0.19	2.47 ± 0.04	34.67
GC4-8	20.50	-106.50	20/jul/2008	400	2.54 ± 0.27	2.47 ± 0.04	34.65
GC4-8	20.50	-106.50	20/jul/2008	450	2.59 ± 0.28	2.47 ± 0.04	34.61
GC4-8	20.50	-106.50	20/jul/2008	500	2.44 ± 0.14	2.46 ± 0.04	34.57
GC4-8	20.50	-106.50	20/jul/2008	550	2.52 ± 0.16	2.46 ± 0.04	34.54
GC4-8	20.50	-106.50	20/jul/2008	600	2.36 ± 0.19	2.46 ± 0.04	34.53
GC4-8	20.50	-106.50	20/jul/2008	700	2.71 ± 0.28	2.46 ± 0.04	34.52
GC4-8	20.50	-106.50	20/jul/2008	800	2.45 ± 0.26	2.46 ± 0.04	34.52
GC4-8	20.50	-106.50	20/jul/2008	900	2.42 ± 0.14	2.46 ± 0.04	34.52
GC4-8	20.50	-106.50	20/jul/2008	1000	2.48 ± 0.16	2.46 ± 0.04	34.54
GC4-9	21.48	-109.50	25/jul/2008	5	1.54 ± 0.13	2.49 ± 0.04	34.98
GC4-9	21.48	-109.50	25/jul/2008	20	1.57 ± 0.17	2.49 ± 0.04	34.87
GC4-9	21.48	-109.50	25/jul/2008	40	1.81 ± 0.20	2.47 ± 0.04	34.65
GC4-9	21.48	-109.50	25/jul/2008	60	2.36 ± 0.13	2.46 ± 0.04	34.44
GC4-9	21.48	-109.50	25/jul/2008	80	2.69 ± 0.17	2.46 ± 0.04	34.47
GC4-9	21.48	-109.50	25/jul/2008	100	2.35 ± 0.19	2.46 ± 0.04	34.50

Station	Latitude (°N)	Longitude (°E)	Sampling date	Depth (m)	^{234}Th (dpm L^{-1})	^{238}U (dpm L^{-1})	Salinity
GC4-9	21.48	-109.50	25/jul/2008	120	2.63 ± 0.28	2.47 ± 0.04	34.59
GC4-9	21.48	-109.50	25/jul/2008	140	2.69 ± 0.29	2.47 ± 0.04	34.68
GC4-9	21.48	-109.50	25/jul/2008	160	2.72 ± 0.16	2.48 ± 0.04	34.72
GC4-9	21.48	-109.50	25/jul/2008	180	2.60 ± 0.18	2.48 ± 0.04	34.73
GC4-9	21.48	-109.50	25/jul/2008	200	2.43 ± 0.19	2.48 ± 0.04	34.73
GC4-9	21.48	-109.50	25/jul/2008	225	2.72 ± 0.29	2.47 ± 0.04	34.71
GC4-9	21.48	-109.50	25/jul/2008	250	2.54 ± 0.27	2.47 ± 0.04	34.69
GC4-9	21.48	-109.50	25/jul/2008	300	2.57 ± 0.14	2.47 ± 0.04	34.64
GC4-9	21.48	-109.50	25/jul/2008	350	2.70 ± 0.17	2.47 ± 0.04	34.59
GC4-9	21.48	-109.50	25/jul/2008	400	2.41 ± 0.20	2.46 ± 0.04	34.57
GC4-9	21.48	-109.50	25/jul/2008	450	2.62 ± 0.31	2.46 ± 0.04	34.55
GC4-9	21.48	-109.50	25/jul/2008	500	2.61 ± 0.31	2.46 ± 0.04	34.54
GC4-9	21.48	-109.50	25/jul/2008	550	2.56 ± 0.16	2.46 ± 0.04	34.53
GC4-9	21.48	-109.50	25/jul/2008	600	2.38 ± 0.18	2.46 ± 0.04	34.53
GC4-9	21.48	-109.50	25/jul/2008	700	2.21 ± 0.20	2.46 ± 0.04	34.52
GC4-9	21.48	-109.50	25/jul/2008	800	2.40 ± 0.25	2.46 ± 0.04	34.52
GC4-9	21.48	-109.50	25/jul/2008	900	2.58 ± 0.28	2.46 ± 0.04	34.52
GC4-9	21.48	-109.50	25/jul/2008	1000	2.36 ± 0.13	2.46 ± 0.04	34.53
GC4-10	24.67	-113.36	29/jul/2008	5	1.45 ± 0.11	2.41 ± 0.04	33.86
GC4-10	24.67	-113.36	29/jul/2008	20	1.76 ± 0.10	2.41 ± 0.04	33.75
GC4-10	24.67	-113.36	29/jul/2008	40	2.12 ± 0.19	2.40 ± 0.04	33.69
GC4-10	24.67	-113.36	29/jul/2008	60	2.26 ± 0.12	2.40 ± 0.04	33.69
GC4-10	24.67	-113.36	29/jul/2008	80	2.38 ± 0.25	2.40 ± 0.04	33.72
GC4-10	24.67	-113.36	29/jul/2008	100	2.58 ± 0.22	2.43 ± 0.04	34.07
GC4-10	24.67	-113.36	29/jul/2008	125	2.33 ± 0.12	2.44 ± 0.04	34.27
GC4-10	24.67	-113.36	29/jul/2008	150	2.26 ± 0.20	2.46 ± 0.04	34.45
GC4-10	24.67	-113.36	29/jul/2008	175	2.48 ± 0.13	2.47 ± 0.04	34.67
GC4-10	24.67	-113.36	29/jul/2008	200	2.39 ± 0.25	2.47 ± 0.04	34.63
GC4-10	24.67	-113.36	29/jul/2008	225	2.31 ± 0.21	2.47 ± 0.04	34.68
GC4-10	24.67	-113.36	29/jul/2008	250	2.30 ± 0.11	2.47 ± 0.04	34.60
GC4-10	24.67	-113.36	29/jul/2008	275	2.18 ± 0.18	2.47 ± 0.04	34.59
GC4-10	24.67	-113.36	29/jul/2008	300	2.54 ± 0.12	2.47 ± 0.04	34.61
GC4-10	24.67	-113.36	29/jul/2008	350	2.63 ± 0.27	2.47 ± 0.04	34.58
GC4-10	24.67	-113.36	29/jul/2008	400	2.44 ± 0.21	2.46 ± 0.04	34.49
GC4-10	24.67	-113.36	29/jul/2008	450	2.40 ± 0.12	2.46 ± 0.04	34.47
GC4-10	24.67	-113.36	29/jul/2008	500	2.38 ± 0.21	2.46 ± 0.04	34.50
GC4-10	24.67	-113.36	29/jul/2008	550	2.47 ± 0.13	2.46 ± 0.04	34.47
GC4-10	24.67	-113.36	29/jul/2008	600	2.41 ± 0.26	2.46 ± 0.04	34.48
GC4-10	24.67	-113.36	29/jul/2008	700	2.49 ± 0.22	2.46 ± 0.04	34.47
GC4-10	24.67	-113.36	29/jul/2008	800	2.50 ± 0.15	2.46 ± 0.04	34.47
GC4-10	24.67	-113.36	29/jul/2008	900	2.64 ± 0.24	2.46 ± 0.04	34.49
GC4-10	24.67	-113.36	29/jul/2008	1000	2.48 ± 0.16	2.46 ± 0.04	34.50
GC4-11	27.53	-117.57	01/ago/2008	5	1.54 ± 0.18	2.40 ± 0.04	33.64
GC4-11	27.53	-117.57	01/ago/2008	20	1.77 ± 0.18	2.39 ± 0.04	33.56
GC4-11	27.53	-117.57	01/ago/2008	40	1.62 ± 0.10	2.37 ± 0.04	33.22
GC4-11	27.53	-117.57	01/ago/2008	60	1.63 ± 0.15	2.38 ± 0.04	33.41
GC4-11	27.53	-117.57	01/ago/2008	80	2.09 ± 0.12	2.39 ± 0.04	33.59
GC4-11	27.53	-117.57	01/ago/2008	100	2.38 ± 0.26	2.40 ± 0.04	33.66
GC4-11	27.53	-117.57	01/ago/2008	125	2.38 ± 0.21	2.43 ± 0.04	34.01
GC4-11	27.53	-117.57	01/ago/2008	150	2.17 ± 0.14	2.44 ± 0.04	34.29
GC4-11	27.53	-117.57	01/ago/2008	175	2.41 ± 0.22	2.45 ± 0.04	34.31
GC4-11	27.53	-117.57	01/ago/2008	200	2.61 ± 0.16	2.46 ± 0.04	34.43

Station	Latitude (°N)	Longitude (°E)	Sampling date	Depth (m)	^{234}Th (dpm L^{-1})	^{238}U (dpm L^{-1})	Salinity
GC4-11	27.53	-117.57	01/ago/2008	225	2.45 ± 0.27	2.45 ± 0.04	34.31
GC4-11	27.53	-117.57	01/ago/2008	250	2.42 ± 0.23	2.45 ± 0.04	34.35
GC4-11	27.53	-117.57	01/ago/2008	275	2.36 ± 0.13	2.45 ± 0.04	34.38
GC4-11	27.53	-117.57	01/ago/2008	300	2.33 ± 0.21	2.45 ± 0.04	34.40
GC4-11	27.53	-117.57	01/ago/2008	350	2.41 ± 0.14	2.46 ± 0.04	34.55
GC4-11	27.53	-117.57	01/ago/2008	400	2.56 ± 0.28	2.46 ± 0.04	34.48
GC4-11	27.53	-117.57	01/ago/2008	500	2.41 ± 0.15	2.46 ± 0.04	34.46
GC4-11	27.53	-117.57	01/ago/2008	550	2.23 ± 0.22	2.45 ± 0.04	34.40
GC4-11	27.53	-117.57	01/ago/2008	600	2.44 ± 0.17	2.45 ± 0.04	34.42
GC4-11	27.53	-117.57	01/ago/2008	700	2.18 ± 0.26	2.45 ± 0.04	34.41
GC4-11	27.53	-117.57	01/ago/2008	800	2.21 ± 0.22	2.46 ± 0.04	34.43
GC4-11	27.53	-117.57	01/ago/2008	900	2.45 ± 0.15	2.46 ± 0.04	34.46
GC4-11	27.53	-117.57	01/ago/2008	1000	2.37 ± 0.22	2.46 ± 0.04	34.49
GC4-12	32.52	-120.57	04/ago/2008	5	1.20 ± 0.11	2.39 ± 0.04	33.56
GC4-12	32.52	-120.57	04/ago/2008	20	1.32 ± 0.17	2.39 ± 0.04	33.56
GC4-12	32.52	-120.57	04/ago/2008	40	0.99 ± 0.13	2.40 ± 0.04	33.69
GC4-12	32.52	-120.57	04/ago/2008	60	2.03 ± 0.16	2.40 ± 0.04	33.72
GC4-12	32.52	-120.57	04/ago/2008	80	2.46 ± 0.24	2.41 ± 0.04	33.81
GC4-12	32.52	-120.57	04/ago/2008	100	2.70 ± 0.18	2.42 ± 0.04	33.89
GC4-12	32.52	-120.57	04/ago/2008	125	2.65 ± 0.31	2.42 ± 0.04	33.93
GC4-12	32.52	-120.57	04/ago/2008	150	2.70 ± 0.27	2.43 ± 0.04	34.03
GC4-12	32.52	-120.57	04/ago/2008	175	2.74 ± 0.16	2.43 ± 0.04	34.10
GC4-12	32.52	-120.57	04/ago/2008	200	2.62 ± 0.24	2.43 ± 0.04	34.12
GC4-12	32.52	-120.57	04/ago/2008	225	2.63 ± 0.17	2.43 ± 0.04	34.15
GC4-12	32.52	-120.57	04/ago/2008	250	2.45 ± 0.28	2.44 ± 0.04	34.16
GC4-12	32.52	-120.57	04/ago/2008	275	2.43 ± 0.23	2.44 ± 0.04	34.18
GC4-12	32.52	-120.57	04/ago/2008	300	2.33 ± 0.18	2.44 ± 0.04	34.17
GC4-12	32.52	-120.57	04/ago/2008	350	2.51 ± 0.25	2.44 ± 0.04	34.18
GC4-12	32.52	-120.57	04/ago/2008	400	2.34 ± 0.19	2.44 ± 0.04	34.21
GC4-12	32.52	-120.57	04/ago/2008	450	2.64 ± 0.31	2.44 ± 0.04	34.23
GC4-12	32.52	-120.57	04/ago/2008	500	2.44 ± 0.25	2.44 ± 0.04	34.26
GC4-12	32.52	-120.57	04/ago/2008	550	2.48 ± 0.17	2.44 ± 0.04	34.29
GC4-12	32.52	-120.57	04/ago/2008	600	2.67 ± 0.25	2.45 ± 0.04	34.34
GC4-12	32.52	-120.57	04/ago/2008	700	2.47 ± 0.17	2.45 ± 0.04	34.39
GC4-12	32.52	-120.57	04/ago/2008	800	2.80 ± 0.32	2.45 ± 0.04	34.42
GC4-12	32.52	-120.57	04/ago/2008	900	2.70 ± 0.26	2.46 ± 0.04	34.45
GC4-12	32.52	-120.57	04/ago/2008	1000	2.46 ± 0.18	2.46 ± 0.04	34.47